2809645234

REFERENCE ONLY

UNIVERSITY OF LONDON THESIS

Degree PhD Year 2007 Name of Author NG, Keat-Eng

COPYRIGHT
This is a thesis accepted for a Higher Degree of the University of London. It is an unpublished typescript and the copyright is held by the author. All persons consulting this thesis must read and abide by the Copyright Declaration below.

COPYRIGHT DECLARATION
I recognise that the copyright of the above-described thesis rests with the author and that no quotation from it or information derived from it may be published without the prior written consent of the author.

LOANS
Theses may not be lent to individuals, but the Senate House Library may lend a copy to approved libraries within the United Kingdom, for consultation solely on the premises of those libraries. Application should be made to: Inter-Library Loans, Senate House Library, Senate House, Malet Street, London WC1E 7HU.

REPRODUCTION
University of London theses may not be reproduced without explicit written permission from the Senate House Library. Enquiries should be addressed to the Theses Section of the Library. Regulations concerning reproduction vary according to the date of acceptance of the thesis and are listed below as guidelines.

A. Before 1962. Permission granted only upon the prior written consent of the author. (The Senate House Library will provide addresses where possible).

B. 1962-1974. In many cases the author has agreed to permit copying upon completion of a Copyright Declaration.

C. 1975-1988. Most theses may be copied upon completion of a Copyright Declaration.

D. 1989 onwards. Most theses may be copied.

This thesis comes within category D.

☑ This copy has been deposited in the Library of UCL

☐ This copy has been deposited in the Senate House Library, Senate House, Malet Street, London WC1E 7HU.

THE DISTRIBUTION AND FUNCTION OF THE ATP-SENSITIVE POTASSIUM CHANNEL SUBUNIT KIR6.1 IN CARDIAC AND SKELETAL MUSCLE CELL LINES

A thesis submitted to University College London, University of London in part fulfilment of the requirement for the degree of;

DOCTOR OF PHILOSOPY

by

Keat-Eng Ng

Department of Medicine
Rayne Institute
UCL
2007

UMI Number: U592198

All rights reserved

INFORMATION TO ALL USERS
The quality of this reproduction is dependent upon the quality of the copy submitted.

In the unlikely event that the author did not send a complete manuscript
and there are missing pages, these will be noted. Also, if material had to be removed,
a note will indicate the deletion.

UMI U592198
Published by ProQuest LLC 2013. Copyright in the Dissertation held by the Author.
Microform Edition © ProQuest LLC.
All rights reserved. This work is protected against
unauthorized copying under Title 17, United States Code.

ProQuest LLC
789 East Eisenhower Parkway
P.O. Box 1346
Ann Arbor, MI 48106-1346

Abstract

ATP-sensitive potassium channels (K_{ATP}) are present in the plasma membrane of a number of tissues but are also present on endomembranes such as the endoplasmic reticulum (ER) and mitochondria. They are involved in a number of physiological and pathophysiological processes and form a link between cellular metabolism and membrane excitability. Ischaemic preconditioning describes the phenomenon in which a short period of ischaemia protects against a more prolonged one. The ability of potassium channel openers such as pinacidil and nicorandil can mimic this phenomenon, with inhibitors such as glibenclamide to abolish this response, led to the suggestion that the final effector in this process was the sarcolemmal K_{ATP} channel as it was able to shorten the cardiac action potential reducing the energy requirements of the cell. However, a number of pharmacological observations were not compatible with this hypothesis as diazoxide, which does not activate the sarcolemmal channel, was able to mimic preconditioning. The focus of research then turned to the potential involvement of a K_{ATP} channel present in the mitochondrial inner membrane called the mitoK_{ATP} channel.

The molecular identification of this channel would be important and there is controversial evidence to suggest that Kir6.1 may be a major component of the mitoK_{ATP} channel. I examined the hypothesis that the localisation of Kir6.1 is functionally significant in cardiac and skeletal muscle because it generates important K^+ flux in intracellular membranes such as the ER and perhaps mitochondria. Colocalisation studies showed that transfected Kir6.1 was located in the ER with a small but significant proportion in mitochondria. However, Kir6.1 was ER retained and not trafficked to the plasma membrane when co-expressed with its regulatory subunit, the sulphonylurea receptor SUR1. Immunofluorescent staining also detected the presence of endogenous Kir6.1 in these cell lines using antibodies specific to Kir6.1. The distribution of Kir6.1 suggests that it may play a role in reactive oxygen species (ROS) production, calcium (Ca^{2+}) handling in the ER and perhaps cellular respiration in mitochondria.

ROS production is often associated with K_{ATP} channel opening and protection against cell death at reperfusion. My results showed that diazoxide induced ROS production in C2C12, HepG2 and HEK293 cell lines with glibenclamide abolishing this effect. However, in the absence of Kir6.1, the same response was still observed. This suggests that Kir6.1 is not involved in the mechanism that is responsible for ROS production. The functional role of K_{ATP} channels were also examined in mitochondria by measuring flavoprotein and NADH autofluorescence, an index of mitochondrial redox state and mitochondrial membrane potential ($\Delta\psi_m$) in C2C12 cells and rat ventricular myocytes. In myocytes, flavoprotein oxidation increased when cells were treated with 3-nitroproprionic acid (3-NPA) and diazoxide. Glibenclamide did not reverse this effect. However, this phenomenon was absent in C2C12 cells. Given these observations, 3-NPA and diazoxide did not affect the $\Delta\psi_m$ in C2C12 cells whereas glibenclamide caused mitochondrial depolarisation. The $\Delta\psi_m$ could not be measured in myocytes. A large proportion of Kir6.1 resides in the ER and I examined whether Kir6.1 would alter ATP-induced Ca^{2+} transients. Upon ATP stimulation, C2C12 cells released Ca^{2+} from internal stores via the P2Y purinergic signalling pathway. The use of dominant negatives (DN) for Kir6.1 showed that ATP-induced Ca^{2+} transients were affected by the absence of Kir6.1. However, on closer inspection; it was revealed that the presence of eGFP to identify transfected cells seriously perturbed the Fura-2 signal.

In conclusion, the K_{ATP} sensitive channel subunit Kir6.1 is predominantly distributed in the ER with a small but significant proportion in mitochondria. I also report that pharmacological compounds such as diazoxide and glibenclamide are not always truly 'selective' for the activation and inhibition of K_{ATP} channels. I have not identified a specific role for Kir6.1 but my data suggests that Kir6.1 is not part of the mitoK_{ATP} channel and Kir6.1 is not involved in ROS production and mitochondrial function but it may still have a role in Ca^{2+} handling.

Acknowledgements

I would like to take the opportunity to thank everyone who has supported me throughout my PhD. I have thoroughly enjoyed my studies and am grateful for the assistance I have received from my friends and colleagues.

I am grateful to my supervisors Professor Andrew Tinker and Professor Michael Duchen for their help and guidance and their constructive comments of this thesis.

My thesis is dedicated to my dear father and mother, my sisters Hwei Min and Ying Jun and my brother Liang Hui for their love and guidance. I would like to thank all my friends for their continuous support and encouragement. I thank them from the bottom of my heart.

List of abbreviations

A^-	Anion
K^+	Potassium
Na^+	Sodium
Cl^-	Chloride
Ca^{2+}	Calcium
K_{IR}	Potassium inwardly rectifying
SUR	Sulphonylurea receptor
ABC	ATP-binding cassette
KCO	Potassium channel opener
NBD	Nucleotide binding domain
ATP	Adenosine triphosphate
NDP	Nucleotide diphosphate
IPC	Ischaemic preconditioning
APD	Action potential duration
PKC	Protein kinase C
PIP_2	Phosphatidylinositol (4,5) bisphosphate
PIP_3	Phosphatidylinositol (3,4,5) triphosphate
DAG	Diacylglycerol
IP_3	Inositol triphosphate
PLC	Phospholipase C
PI3K	Phosphatidylinositol-3-kinase
NCX	Na^+/Ca^{2+} exchanger
sarcK_{ATP}	Sarcolemmal K_{ATP}
mitoK_{ATP}	Mitochondrial K_{ATP}
SDH	Succinate dehydrogenase
5-HD	5-Hydroxydecanoate
ANT	Adenine nucleotide translocator
PIC	Phosphate carrier
3-NPA	3- Nitroproprionic acid
ROS	Reactive oxygen species
KO	Knock out
GFP	Green fluorescent protein
ER	Endoplasmic reticulum
SR	Sarcoplasmic reticulum
siRNA	Small interfering RNA
DN	Dominant negative
MBP	Maltose binding protein
FCCP	Carbonyl cyanide 4-(trifluoromethoxy) phenylhydrazone
NaCN	Sodium cyanide
$\Delta\psi_m$	Mitochondrial membrane potential
TMRE	Tetramethylrhodamine ethyl ester, perchlorate
TMRM	Tetramethylrhodamine methyl ester, perchlorate
CCD	Charged-coupled device
$[Ca^{2+}]_i$	Intracellular Ca^{2+} concentration

Contents

List of tables and figures

Tables

Figures

Figure 3.50. An experiment to show the changes in mitochondrial redox state in rat ventricular myocytes treated with 1 mM 3-NPA, 100 μM diazoxide followed by 20 mM NaCN and 1 μM FCCP.
Figure 3.51. An experiment to show the changes in $\Delta\psi_m$ in C2C12 cells loaded with 20 nM TMRM. The cells were treated with 100 μM diazoxide, 10 μM glibenclamide and 1 μM FCCP.
Figure 3.52. An experiment to show the changes in $\Delta\psi_m$ in C2C12 cells loaded with 20nM TMRM. The cells were treated with 1 mM 3-NPA, 100 μM diazoxide, 10 μM glibenclamide and 1 μM FCCP.
Figure 3.53. An experiment to show the changes in $\Delta\psi_m$ in C2C12 cells loaded with 400 nM TMRM. The cells were treated with 1 mM 3-NPA, 100 μM diazoxide, 10 μM glibenclamide and 1 μM FCCP.

Figure 3.54. A graph to show the Ca^{2+} transients in C2C12 cells stimulated with just 10 μM ATP (n=26).
Figure 3.55. A graph to show the Ca^{2+} transients in C2C12 cells stimulated with 1 mM caffeine and 10 μM ATP (n= 20).
Figure 3.56. A graph to show the Ca^{2+} transients in differentiated C2C12 cells (48 hours). The cells were stimulated with 1 mM caffeine and 10 μM ATP (n= 40).
Figure 3.57. A graph to show the Ca^{2+} transients in differentiated C2C12 cells (96 hours). The cells were stimulated with 1 mM caffeine followed by 10 μM ATP (n= 22).
Figure 3.58. The Ca^{2+} transients in figure 3.57 were separated according to their response. A. A graph to show the Ca^{2+} transients in C2C12 cells in response to 10 μM ATP (n= 9). B. A graph to show the Ca^{2+} transients in C2C12 cells response to 1 mM caffeine and 10 μM ATP (n= 13).
Figure 3.59. A graph to show the Ca^{2+} transients in rat ventricular myocytes in response to 1 mM caffeine (n= 7).
Figure 3.60. A graph to show the Ca^{2+} transients in C2C12 cells transfected with DNG→A, these were stimulated with 1 mM caffeine and 10 μM ATP. (Non transfected cells = 7, transfected cells = 6).
Figure 3.61. A graph to show the Ca^{2+} transients in C2C12 cells transfected with DNG→S, these were stimulated with 1 mM caffeine and 10 μM ATP. (Transfected cells = 9, non transfected cells = 11).
Figure 3.62. A graph to show the Ca^{2+} transients in C2C12 cells transfected with eGFP these were stimulated with 1 mM caffeine and 10 μM ATP. (Transfected cells = 9, non transfected cells = 13).

1.0 INTRODUCTION

1.1 Transport through cellular membranes and membrane potentials

Each cell is highly compartmentalised by the plasma membrane and intracellular membranes. The plasma membrane is composed of a phospholipid bilayer. This is impermeable to most ionic and polar substances and the specific transport of ions and solutes is achieved through an array of channel and receptor proteins that are embedded in the membrane. Two transport processes; facilitated diffusion and active transport control the movement of ions. Facilitated diffusion is a passive process by which molecules or ions will equilibrate in their environment by flowing down their concentration gradient. Active transport involves the specific action of carrier proteins where molecules or ions are transported against their concentration gradient, using energy from the hydrolysis of adenosine triphosphate (ATP).

The semi-permeability property of cell membranes allows charged ions such as potassium (K^+) and chloride (Cl^-) to cross easily whereas sodium (Na^+) do not. The intracellular compartment also has a high protein content, phosphate groups from ATP and organic molecules which, at physiological pH, are negatively charged and contribute to the intracellular anion (A^-) pool. The presence of anions in the intracellular compartment will upset transmembrane osmolarity, but a balance is maintained by the action of the Na^+/K^+ ATPase. The high intracellular content of impermeant anions produces an unequal charge distribution across the membrane with excess negative charge on the inner surface of the membrane compared to the outer face. This difference in charge is known as the membrane potential. The ionic composition of extracellular ($_1$) and intracellular ($_2$) compartments is determined by two principles:

1. Electroneutrality in bulk solutions where:

   $[K^+]_1 = [Cl^-]_1$ Equation 1 $[K^+]_2 = [Cl^-]_2 + [A^-]_2$ Equation 2

2. The Donnan equilibrium where the product of permeable ions in one compartment is equal to the second:

$[K^+]_1 [Cl^-]_1 = [K^+]_2 [Cl^-]_2$ Equation 3

The net result of these forces determined by equations 1-3 is that the concentration of permeable cations (e.g. K^+) is greater in compartment 2 and the concentration of permeable anions (e.g. Cl^-) is greater in compartment 1. Furthermore, these forces yield a greater solute concentration in compartment 2 compared to compartment 1. Osmotic balance is achieved by the accumulation of an impermeable ion (e.g. Na^+). Thus, there will be equal anion and cation concentrations in both compartments. This is an important condition because the two solutions must have the same tonicity to maintain the cell volume so that there is no net movement of water across the membrane. Na^+ cannot leave the cell passively but is actively pumped out of cells through the action of the Na-pump, which is often referred to as the Na^+/K^+ ATPase. The Na-pump moves three Na^+ out of the cell in exchange for two K^+.

At equilibrium, the inside of the cell membrane is more negative then the outside of the membrane. The asymmetry of permeable ions such as K^+ leads to the difference in charge or potential difference across the membrane which is also known as the membrane potential. This can be summarised by the Nernst equation. The Nernst equation allows the theoretical equilibrium potential to be calculated for a particular permeable ion when its transmembrane concentration gradient is known. Below, is the simplified equation at a temperature of 37 °C:

$$E_m = \frac{61}{z} \log_{10} \frac{[X_0]}{[X_1]}$$

E_m = equillibrium potential in millivolts (mV) for ion X

X_0 = concentration of ion outside cell

X_1 = concentration of ion inside cell

Z = valency of ion (+1 for Na^+ or K^+)

If the membrane is permeable to a single ionic species, the membrane potential can be calculated from the Nernst equation. The concentration of K^+ is higher inside that cell than outside for example, if it is 150 mM inside compared to 5 mM on the outside, the equilibrium potential for K^+ is -90 mV. For Na^+ because the concentration inside the cell is for example is 10 mM compared to 144 mM on the outside. The equilibrium potential for Na^+ is thus calculated to be + 70 mV. The resting membrane potential of most cells in the body lies between -65 mV to -85 mV. This value is near to the E_K value because the membrane is much more permeable to K^+.

1.2 Potassium channels

Ion channels regulate a number of functions. These include electrical excitability, ionic homeostasis, control of neurotransmission and hormone secretions (*Hille 1992*). Ion channels can be in open or closed conformation and the equilibrium is determined by voltage and concentration, depending on the channel. The physiological role of potassium (K^+) channels is largely based on their ability to stabilise the plasma membrane potential. The action of Na^+/K^+ ATPase maintains a high K^+ concentration inside the cell relative to the outside. When potassium channels open, the membrane is hyperpolarised (the membrane potential becomes more negative than the resting potential) and this decreases excitability in cells. The potassium channel family contains a variety of diverse proteins that can be classified into particular subfamilies depending on their structure and functional properties. The types of K^+ current can be classified by their electrophysiological properties *(Fujita & Kurachi 2000)*. Potassium channel families include the six transmembrane domain voltage gated potassium channel (K_v family), two transmembrane domain inwardly rectifying (K_{IR} family) and four transmembrane domain two-pore channel ('Twin pore' channels). K_v and K_{IR} channels exist as tetramers whereas twin pore channels are dimers. There is also the calcium (Ca^{2+}) activated or dependent channel (K_{ca} family) and tandem pore region potassium channels.

1.2.1 Inwardly rectifying potassium channels

Inwardly rectifying K^+ channels are so called because they allow more inward flux of K^+ ions than outward flux with the same driving force but it is the small amount of outward current that is important physiologically because it causes membrane hyperpolarisation. Inward rectification was first demonstrated in K^+ depolarised muscle by Katz in 1949 and subsequent studies have identified potassium channels in different cell types such as starfish egg cells and neurones (*Katz 1949*). The first members of this potassium channel family were initially discovered by cloning mRNAs from rat kidney (ATP dependent $K_{IR}1.1$/ROMK) and from mouse macrophage cell line (Classical K_{IR} channel IRK/$K_{IR}2.1$) (*Ho et al. 1993; Kubo et al. 1993*). Several members of the K_{IR} channel family have been identified and named as K_{IR} subfamily (K_{IR} 1.0 - 6.0) based on unifying nomenclature (*Chandy & Gutman 1993*). The inwardly rectifying K^+ channel family (K_{IR}) contains seven family members, these are characterised by the degree of their inward rectification in response to extracellular stimuli, see Table 1.1

Table 1.1. A table to show examples of native inwardly rectifying K^+ channels.

K_{IR} Channels	Name	Original name	Nomenclature
I_{K1} channel	Classically inwardly rectifying K^+ channel	IRK1 IRK2 IRK3 IRK4	Kir2.1 Kir2.2 Kir2.3 Kir2.4
K_G Channel	G protein activated K^+ channel	GIRK1 GIRK2 GIRK3 GIRK4	Kir3.1 Kir3.2 Kir3.3 Kir3.4
K_{ATP} channel	ATP-sensitive K^+ channel	uK_{ATP}-1 BIR	Kir6.1 Kir6.2
ATP-dependent K^+ channels	K^+ transport channels	ROMK1 K_{AB}-2 BIR9	Kir1.1a Kir4.1 Kir5.1

The K_{IR} channel is made up of tetrameric subunits, each K_{IR} subunit contains two transmembrane domains called M1 and M2 with a pore forming loop (p) in the middle of the H5 pore region. This is responsible for conferring K^+ selectivity and the amino and carboxylic termini are located on the cytoplasmic side. Please refer to figure 1.1. Two thirds of the K_{IR} channel amino acid sequence forms an intracellular domain, which

forms the pore that regulates channel activity and inward rectification (*Ashcroft & Ashcroft 1990*). Magnesium (Mg^{2+}) and other cations interact with negatively charged amino acids in transmembrane domain 2 (TM2) at the C terminal end of the K_{IR} subunit that induces rectification. The majority of the K_{IR} channels identified are eukaryotic but the 3D structure of the first prokaryotic K_{IR} channel called KirBac1.1 was determined in 2003 using high resolution X-ray crystallography *(Kuo et al. 2003; Bicher et al. 2003)*. $K_{IR}1.0$ family members are important in transepithelial membrane transport. $K_{IR}1.1$ (ROMK1) is inhibited by acidification for example; H^+ can bind to the channel and cause inhibition. The $K_{IR}2.0$ family are responsible for controlling the excitability in the heart and brain. The $K_{IR}3.0$ family are known as the G protein inwardly rectifying K^+ channel family (GIRK) as the channel activity is regulated by the G protein $G\beta\gamma$ subunit. In general, the K_{IR} 2.0 and 3.0 family members are strong inward rectifiers whereas K_{IR} 1.0 and K_{IR} 6.0 members are weak rectifiers (*Reinmann & Ashcroft 1999*).

1.3 ATP-sensitive potassium channels (K_{ATP})

1.3.1 The molecular structure and basic properties of K_{ATP} channels

K_{ATP} channels were originally discovered in the heart by Noma (*Noma 1983*). K_{ATP} channels are present in many tissue types with a variety of important functions and they respond to intracellular levels of ATP thus coupling cell metabolism to the electrical activity of the cell (*Rodrigo & Standen 2005*). They are inhibited by non hydrolysable forms of ATP and activated by nucleotide diphosphates (NDPs). The K_{ATP} channels can also be activated by potassium channel openers (KCO) and inhibited by sulphonylureas. The K_{ATP} channel is an octameric complex comprised of four Kir 6.0 subunits from the inward rectifier family of potassium channels and four sulfonylurea receptors (SUR), a member of the ATP-binding cassette (ABC) family of proteins. The SUR is the site of action for antidiabetic drugs such as glibenclamide used in the treatment of type 2 diabetes mellitus (*Szewcyk & Marban 2003; Aguilar-Bryan & Bryan 1999; Ashcroft & Gribble 1998*). The structure of a K_{ATP} channel is shown in figure 1.1.

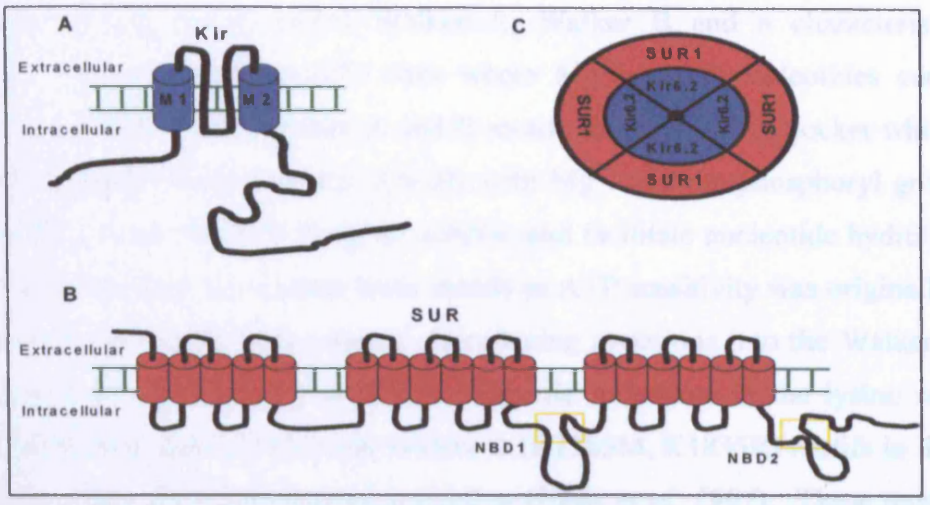

Figure 1.1. A diagram to show the topology of a K_{ATP} channel. **A**. The K_{IR} subunit **B**. The SUR subunit **C**. The pancreatic K_{ATP} channel is composed of Kir6.2 and SUR1 subunit.

The pore forming subunit Kir6.0 has two different members called Kir6.1 and Kir6.2 that share 70 % amino acid identity. Recently, a new member of the K_{IR} subfamily has been identified and characterised in zebrafish called Kir6.3 (*Zhang et al. 2006*). The regulatory subunit, SUR is encoded by two distinct genes, SUR1 and SUR2 (*Aguilar-Bryan & Bryan 1999; Bryan & Aguilar-Bryan 2003; Higgins, 1992*). The SUR1 protein was first cloned in 1995 in protein purification studies and expressed in pancreatic β cells, the SUR1 cDNA sequence encoded a protein of 1582 amino acids with a molecular mass of 177 kDa (*Aguilar-Bryan et al 1995*). A few years later, the SUR2 gene was identified with two splice variants named SUR2A and SUR2B, these differ by 42 amino acids in the C terminus (*Chutkow et al. 1996*; *Inagaki et al. 1996; Isomoto et al. 1996*).

The SUR regulatory subunit contains three main transmembrane domains, TMD0, TMD1 and TMD2 which are composed of five, six and six transmembrane regions respectively. The topology of the complete full-length SUR1 was predicted using membrane impermeable biotinylating reagent called biotin malemide (*Conti et al. 2001*). The SUR subunit contains 17 transmembrane domains in total with an extracellular N-terminus and intracellular C terminus. There are two nucleotide binding domains (NBD) which are located between TMD1 and TMD2 in the C terminus (*Grover & Garlid 2000; Bryan & Aguilar-Bryan 2003; Aguilar-Bryan et al 1998).* The NBD contains three consensus

nucleotide binding motifs called Walker A, Walker B and a characteristic linker sequence. These contain specific sites where Mg^{2+} bound nucleotides can bind to (*Walker et al. 1982*). The Walker A and B motifs form a binding pocket which houses the MgATP complex and interacts directly with Mg^{2+} and the phosphoryl group whilst the role of the linker motif is likely to stabilise and facilitate nucleotide hydrolysis. The Kir6.0 subfamily does not contain these motifs so ATP sensitivity was originally thought to be determined by the SUR subunit. Introducing mutations into the Walker A and B motifs can alter ATP binding to SUR1. Specific mutations of the lysine residues in Walker A (K719R and K719M) and Walker B (K1385M, K1835R) motifs in the NBD-1 of hamster SUR1 abolished channel activation (*Ueda et al. 1997*). These mutations are not vital for K_{ATP} channel inhibition but NBDs are responsible for MgADP activation.

The stoichiometry of K_{ATP} channels has been determined by using cDNAs encoding tandem dimers of SUR1 and Kir6.2 (*Clement et al. 1997*). This group demonstrated that the Kir6.2 and SUR1 tandem dimer exhibited electrophysiological properties similar to native pancreatic ß-cell K_{ATP} channel where a 1:1 stoichiometry was sufficient to generate functional channels. However, the triple fusion protein consisting of Kir6.2, Kir6.2 and SUR1 did not produce functional channels. Our laboratory have carried out biochemical and functional experiments with these subunits and found that K_{ATP} channel complexes containing SUR1, SUR2 and Kir6.2 could not form, even after overexpression in HEK293 cells (*Giblin et al. 2002*). However, SUR2A and SUR2B are C-terminal splice variants and differ by about 40 amino acids there is a possibility that these channels can still form and possess channel activity. The glycosylated form of Kir6.2/SUR1 channel was reported to be a protein complex of 950 kDa suggesting that the K_{ATP} channel was an octameric protein with 4:4 stoichiometry (*Inagaki et al. 1997).* Shyng and Nichols confirmed that the K_{ATP} channel pore consisted of four Kir6.2 subunits and each Kir6.2 subunit required an SUR1 subunit to form a functional channel in an octameric or tetradimeric structure *(Shyng & Nichols 1997; Shyng et al. 1997*).

1.3.2 Chromosomal localisation of SUR and Kir6.0 genes

The human Kir6.2 and SUR1 genes are clustered at 11p15.1 where the Kir6.2 gene is approximately 4.5 kb downstream of SUR1. There is about 71 % amino acid identity between Kir6.1 and Kir6.2 (*Inagaki et al. 1995a*). The SUR1 gene contains 39 exons and is more than 100 kbp in length (*Aguilar-Bryan et al 1998; 1995*). The human Kir6.1 and SUR2 genes are also close together with Kir6.1 gene at 12p11.23 and SUR2 gene located at 12p11.12 (*Chutkow et al. 1996*). The proximity of the Kir6.0 and SUR genes (Kir6.2 and SUR1, Kir6.1 and SUR2) suggests that each gene pair may have derived from the same loci but during the course of evolution they duplicated and diverged to different positions on the chromosome. In the rat heart, the mRNA level of SUR1 was expressed at low levels indicating another isoform was also present. This was later confirmed to be SUR2A. SUR2A is expressed at high levels in rat and mouse hearts and has 68 % amino acid identity to SUR1. The other isoform of SUR2, SUR2B is composed of 1546 amino acids and only has 67 % similarity to SUR1 but 97 % identity to SUR2A; the differences exist in the C terminal part of the protein (*Chutkow et al. 1996*; *Inagaki et al. 1995a*).

1.3.3 K_{ATP} channel isoforms

Different combinations of Kir6.0 and SUR genes can create various K_{ATP} channels with distinct electrophysiological and pharmacological properties (*Seino & Miki 2003a; Yokoshiki et al. 1998*). The different types of channels are displayed in table 1.2.

Table 1.2. A table to show different combinations of Kir6.0 and SUR genes create distinct K_{ATP} channels in various tissues.

Channel Type	**Tissue**	**References**
Kir6.2/SUR1	Pancreas/Brain	*Inagaki et al, 1995a; Sakura et al. 1999*
Kir6.2/SUR2A	Cardiac muscle	*Inagaki et al 1996*
Kir6.2/SUR2B	Smooth muscle	*Isomoto et al 1996*
Kir6.1/SUR2B	Vascular smooth muscle	*Yamada et al 1997*

The Kir6.2/SUR1 isoform is present in pancreatic ß cells and has been studied extensively by many groups (*Ashcroft & Gribble 1998; Inagaki et al. 1995b*). The Kir6.2/SUR2A isoform forms the cardiac sarcolemmal channel and is mainly expressed in heart and skeletal muscle (*Babenko et al 1998a; Inagaki et al 1996*). The Kir6.1/SUR2B isoform constitutes the channel found in vascular smooth muscle and K_{ATP} channels in non-vascular smooth muscle are predominantly composed of Kir6.2/SUR2B and Kir6.1/SUR2B channels. It is vital that functional K_{ATP} channels are trafficked to the plasma membrane. For example, the Kir6.2 contains an ER retention motif at the C terminus which is composed of three amino acids, arginine-lysine-arginine (RKR). SUR1 also contains an RKR sequence in the intracellular loop between TMD0 and NBD1. This mechanism prevents SUR1 surface expression in the absence of Kir6.1 or Kir6.2 (*Zerangue et al. 1999*). When K_{ATP} channel subunits coassemble to form the octameric protein, the ER retention motif is masked, allowing the complex to exit the ER. The truncation of the C terminus of Kir6.2 (Kir6.2ΔC) eliminated the ER retention motif allowing channels to form in the absence of SUR (*Tucker et al. 1997*). The authors found that the channel was inhibited through Kir6.2, which contains the ATP binding site and not SUR. Furthermore, deleting seven amino acid residues from the C terminus of SUR1 clearly reduced the surface expression of K_{ATP} channels (*Babenko et al. 1998b*). The trafficking of K_{ATP} channels to the cell surface is a complex process because in contrast, the deletion of the furthest amino acid sequences at the C terminus of SUR1 allowed K_{ATP} channels to be expressed at the cell surface (*Sakura et al. 1999*).

1.3.4 Biophysical properties of K_{ATP} channels

Single channel conductance measured in the inside out configuration in pancreatic ß cells recorded inward current from 50 to 75 pS whereas cardiac cells measured 70-90 pS in 140 mM K^+ recording solution (*Nichols & Lederer 1991*). A characteristic of K_{ATP} channels is that channel openings occurred in bursts with relatively long closed periods in between (*Trube et al. 1984*). A study investigating single channel recordings made from ventricular cells isolated enzymatically from guinea-pig heart showed that the channel was inhibited in the presence of ATP (*Kakei et al. 1985*). More importantly, the results

showed that when ATP concentrations increased, the number of openings decreased whereas the duration of the closed-intervals increased, resulting in the overall decrease of the open-state probability.

1.3.5 K_{ATP} channel regulation by ATP and nucleotide diphosphates

The expression of Kir6.0 and SUR subunits in different combinations reconstitutes K_{ATP} channels with distinct electrophysiological properties and characteristics in native tissues (*Seino & Miki 2003a*). One of the characteristic properties K_{ATP} channels possess is the dose dependent inhibition by ATP. This inhibitory effect can be mimicked by non-hydrolysable analogues of ATP and also ATP in the absence of Mg^{2+} i.e. channel inhibition does not depend on ATP hydrolysis. ATP sensitivity varies in different tissues but channels are usually inhibited in the micromolar range. For example, in pancreatic cells, the K_i is ~ 30 μM. The other factors that regulate K_{ATP} channels include intracellular nucleotides, phospholipids, protein kinases and phosphatases. It was originally thought that the SUR subunit mediated the direct hydrolysis of ATP and this was a required element for channel inhibition (*Kakei et al. 1985; Cook & Hales. 1984*).

One study showed that the truncation of the C terminal (26-36 amino acids) of Kir6.2 (Kir6.2ΔC) without the SUR subunit generated K^+ currents which were inhibited by ATP but not activated by MgADP, this suggested that the Kir6.2 subunit does not confer ATP sensitivity (*Tucker et al. 1997*). Other studies showed that equivalent mutations of the Walker A and B motifs of rat SUR1 when heterologously expressed with Kir6.2 did not affect the inhibitory effect of ATP on channel activity (*Gribble et al. 1997*). When the last 36 amino acids from the C-terminus were deleted from Kir6.2, MgADP, KCOs and sulphonylureas of low concentration had no effect on channel activity, suggesting that the SUR subunit was the site of drug action (*Reinmann & Ashcroft 1999*). COS cells expressing Kir6.2 and SUR2A have a conductance of ~80 pS and like cardiac and skeletal cells, they are generally less sensitive to intracellular levels of ATP compared to the Kir6.2/SUR1 type channel (*Inagaki et al. 1996*).

NDPs such as ADP, UDP and GDP, in the presence of Mg^{2+} stimulate channel opening and reduce the inhibitory effect of ATP. In the absence of NDPs, the maximal block in β-cell K_{ATP} channels is around 60-80 %, suggesting that sulphonylureas such as glibenclamide can act as partial antagonists. Intracellular MgADP will modulate sulphonylurea block and enhance the inhibition of Kir6.2/SUR1 (β-cell) channel but decrease the inhibition of Kir6.2/SUR2A (cardiac-type) channels (*Reinmann et al. 2003*). The NBDs in SUR1 in particular are responsible for channel activation; MgADP will activate the K_{ATP} channel by interacting with the NBDs in the SUR subunit (*Gribble et al. 1997; Shyng et al 1997*). In SUR1, there is strong ATP Mg^{2+} independent high affinity binding at NBD1 which is antagonised by MgADP at NBD2 (*Ueda et al. 1997*). The SUR subunit has other important regulatory roles apart from NDP activation. For example, the energy status of mitochondria may be linked to K_{ATP} channel activity and during metabolic stress; adenylate kinase may transport ADP from the mitochondria via a phosphorelay network linking mitochondria to K_{ATP} channels on the plasma membrane (*Carrasco et al. 2003*).

1.3.6 K_{ATP} channel regulation by potassium channel openers and inhibitors

The SUR subunits are so called because they form the crucial target for the interaction of therapeutic drugs such as sulphonylureas but they also confer sensitivity to activation by a group of potent channel activating drugs called potassium channel openers (KCOs). Examples include diazoxide, pinacidil, cromakalim and nicorandil, these are known as pyridines the latter, nicorandil is an antianginal agent and can be used as a vasodilator to lower blood pressure. KCOs are a diverse group of drugs and will stimulate K_{ATP} channel opening which generates an outward current that changes the membrane potential. This is important because it modulates cellular function by reducing the electrical activity of a cell (*Seino & Miki 2003a; Ashcroft & Gribble, 2000).* KCOs can have different effects on various tissues, as the different SUR subunits will confer varying sensitivities to KCOs. Diazoxide is used in some hypoglycaemic conditions for its hyperglycaemic actions by strongly activating K^+ currents in pancreatic cells whereas pinacidil have no major effect on β cells (*Gribble et al. 1998; Inagaki et al. 1995b;*

Garrino et al. 1989). Other sulphonylureas such as glibenclamide and tolbutamide are hypoglycaemic agents that stimulate insulin secretion by closing the K_{ATP} channel (*Tucker et al. 1997*). Glibenclamide can inhibit the channel by binding directly to the SUR subunit and block K_{ATP} channels resulting in membrane depolarisation and Ca^{2+} influx (*Koster et al. 1999*).

1.3.7 K_{ATP} channel regulation by other factors

K_{ATP} channel activity can also be closely modulated by other intracellular factors. Protein kinase A (PKA) has been shown to stimulate K_{ATP} channel activity in native tissues such as rabbit arterial smooth muscle (*Wellman et al. 1998; Quayle et al. 1994; Beech et al. 1993; Ribalet et al. 1989*). In pancreatic ß-cells, Kir6.2 can also be phosphorylated by PKA (*Yamada et al. 1997*). Phosphatidylinositol (4,5) bisphosphate (PIP_2) and phosphatidylinositol (3,4,5) trisphosphate (PIP_3) are membrane phospholipids and have been shown to modulate the ATP sensitivity of K_{ATP} channels. PIP_2 in particular decreased the ATP-sensitivity of K_{ATP} channels and it prevents the inhibition of the channel in the presence of tolbulamide by stabilising the open state of the channel (*Koster et al. 1999*). Finally, K_{ATP} channel activity can also be modulated by GTP binding proteins ($G\alpha_i$), pH, or protein kinase C (PKC) and cytosolic factors such as Cl^- (*Hu et al. 1996; Kayano et al. 1993; Kirsch et al. 1990*).

PKC can activate K_{ATP} channels in rabbit and human myocytes by decreasing sensitivity to intracellular ATP (*Hu et al. 1996*). Rat ventricular myocytes with tolbutamide sensitive K_{ATP} currents were studied and purinergic receptors were shown to be coupled to K_{ATP} channels via G proteins with three different types of $G\alpha_i$ protein reducing channel sensitivity to ATP (*Kirsch et al. 1990*). Furthermore, $G\alpha_{i1}$ could stimulate both Kir6.2/SUR1 and Kir6.2/SUR2A channels whereas $G\alpha_{i2}$ stimulated Kir6.2/SUR2A but not Kir6.1/SUR2B channels (*Sanchez et al. 1998*). K_{ATP} channels in guinea pig cardiac ventricular myocytes were closed by internal ATP and activated by lowering the pH (7.6-6.0) in a dose dependent manner. This is due to the decrease in sensitivity of the channel to ATP (*Kayano et al. 1993*).

1.4 The physiological roles of K_{ATP} channels

K_{ATP} channels have many important physiological roles and have been identified in tissues such as the kidney, brain and skeletal muscle and pancreatic β cells (*Inagaki et al. 1995c*). For example, when K_{ATP} channels in β cells are closed, cell depolarisation stimulates insulin and growth hormone secretion (*Bernardi et al. 1993*). In resting β cells, blood glucose is 2-3 mM (fasting period) and the role of the K_{ATP} channel is to set the membrane potential close to the K^+ equilibrium potential reducing excitability which inhibits insulin secretion. After a meal, blood glucose increases and is transported to the ß-cells via the glucose transporter (*Seino & Miki 2003b*). The increase in intracellular glucose stimulates glycolysis and subsequently ATP production. This increase in intracellular ATP closes the K_{ATP} channel followed by depolarisation of the plasma membrane. There is an increase in intracellular Ca^{2+} mainly through the activation of L-type voltage gated Ca^{2+} channels. Rapid cytoplasmic Ca^{2+} in turn stimulates the release of insulin from insulin containing vesicles via exocytosis. Insulin stimulates the uptake of glucose from the blood to the tissue causing plasma glucose levels to fall. The adenine nucleotide levels normalise allowing membrane repolarisation therefore inhibiting insulin release. In Kir6.2 knockout mice, the membrane potential of ß-cells has been reported to be permanently depolarised at approximately ~ 40 mV (*Miki et al. 1998a*).

1.4.1 Genetic mutations affecting K_{ATP} channel subunits

Familial persistent hyperinsulinaemic hypoglycaemia of infancy (PHHI) is characterised by persistent insulin secretion in newborns despite severe hypoglycaemia (*Kane et al. 1996; Thomas et al. 1995*). This can be caused by a mutation in the gene encoding SUR1 or in rare cases in the pore-forming subunit, Kir6.2. Thomas et al originally identified three mutations in SUR1 gene in patients with PHHI and later studies identified further mutations in Kir6.2 (*Nestorowicz et al. 1997; Thomas et al. 1996*). Although these mutations have been identified in K_{ATP} channel subunits, mutations in the glucokinase gene and glutamate dehydrogenase gene can also cause PHHI (*Glaser et al. 1998; Stanley et al. 1998*). Dilated cardiomyopathy is a disease of the heart muscle that causes

the heart to become enlarged. The muscle becomes weak and the heart cannot pump blood efficiently around the body. Two mutations in ABCC9 gene, which encodes the regulatory SUR2A subunit of the cardiac K_{ATP} channel have been linked to dilated cardiomyopathy (*Bienengraeber et al. 2004*).

1.4.2 The physiological roles of K_{ATP} channels in other tissues

K_{ATP} channels also play important physiological roles in tissues such as non vascular smooth muscle, neurons, endocrine cells, renal cells, vascular, endothelial and follicular cells of the ovary (*Seino & Miki 2003b*). For example, cromakalim induced K_{ATP} channel opening and hyperpolarisation in rat juxtaglomerular cells of the *vas afferens* in the kidney which increased renin secretion (*Ferrier et al. 1989*). Diazoxide, unlike cromakalim and pinacidil cannot activate cardiac sarcolemmal K_{ATP} channels but has cardioprotective properties (*Babenko et al 1998b; Nakayama et al. 1990*). Some studies have demonstrated that glibenclamide reduced basal coronary blood flow in anesthetised dogs, suggesting that K_{ATP} channels may act to regulate background K^+ conductance and therefore vascular tone (*Imamura et al. 1992*; *Samaha et al. 1992*). K_{ATP} channels also have vital roles in smooth muscle. For example, glibenclamide can cause vasoconstriction in arteries, which supports the fact that K_{ATP} channels are important in regulating resting membrane potentials and vascular tone (*Samaha et al. 1992; Clapp & Gurney 1992*). In vivo studies conducted by Quayle et al also reported that diazoxide and pinacidil promoted vasodilation through K_{ATP} channel opening with glibenclamide affecting smooth muscle membrane potential by significantly increasing vascular resistance and arterial diameter (*Quayle et al. 1997*).

The exact role of K_{ATP} channels in skeletal muscle has not been clearly defined but the opening of K_{ATP} channels in isolated fibre bundles from myotonic human skeletal muscle prevented after-contractions and spontaneous mechanical activity, which would otherwise happen in myotonia congentia (*Quasthoff et al. 1990*). In the brain, hypoglycaemia or local hypoxia opens neuronal K_{ATP} channels. This reduces the firing rate of a subset of neurons that express K_{ATP} channels, for example in the hypothalamus,

nuclei of the vagus nerve and dopaminergic neurons (*Miki et al. 2002; Muller et al. 2001; Liss & Roeper 2001a and b).* Finally, K_{ATP} channels also play a protective role in the heart during metabolic stress. K_{ATP} channels were initially discovered in the cardiac sarcolemma where they were expressed at high density and opened in the presence of cyanide or under hypoxic conditions (*Noma et al. 1983*). The cardiac action potential is the electrical activity of individual cells in the electrical conduction system of the heart.

The cardiac action potential has five phases (0-4); phase 4 is the resting membrane potential and is the period where the cell is not stimulated. Once the cell is electrically stimulated, usually by an electric current from an adjacent cell, it begins a sequence of actions involving the influx and efflux of multiple cations and anions that together produce the action potential of the cell. See figure 1.2. Phase 0 is a rapid depolarisation stage where Na^+ channels opens resulting in a rapid influx of Na^+ ions into the cell. Phase 1 of the action potential occurs with the inactivation of the fast Na^+ channels. The transient net outward current causing the small downward deflection of the action potential is due to the movement of K^+ and Cl^- ions. Phase 2, the plateau stage is mostly maintained by the influx of Ca^{2+} ions through the L-type Ca^{2+} channel and the outward movement of K^+ ions via the slow delayed rectifier K^+ channels I_{Ks}. During phase 3 of the action potential, the L-type Ca^{2+} channels close, while the slow delayed rectifier K^+ channels remain open. This outward flow of K^+ ions promote other types of K^+ channels to open such as the rapid delayed rectifier K^+ channels (I_{Kr}) and the inwardly rectifiying K^+ current, I_{K1}. This causes the cell to repolarise. The delayed rectifier K^+ channels close when the membrane potential is restored to -80 to -85 mV, while I_{K1} remains conducting throughout phase 4 to set the resting membrane potential. K_{ATP} channels were recognised to have a cardioprotective role by shortening the cardiac action potential duration (APD) and preventing Ca^{2+} influx in the cytosol to reduce muscle contraction and conserve cellular ATP. This is thought to act as a protective mechanism that adapts local energy expenditure to local energy supply in cardiac muscle cells during periods of interrupted blood supply (*Suzuki et al. 2001, Flagg & Nichols 2001).*

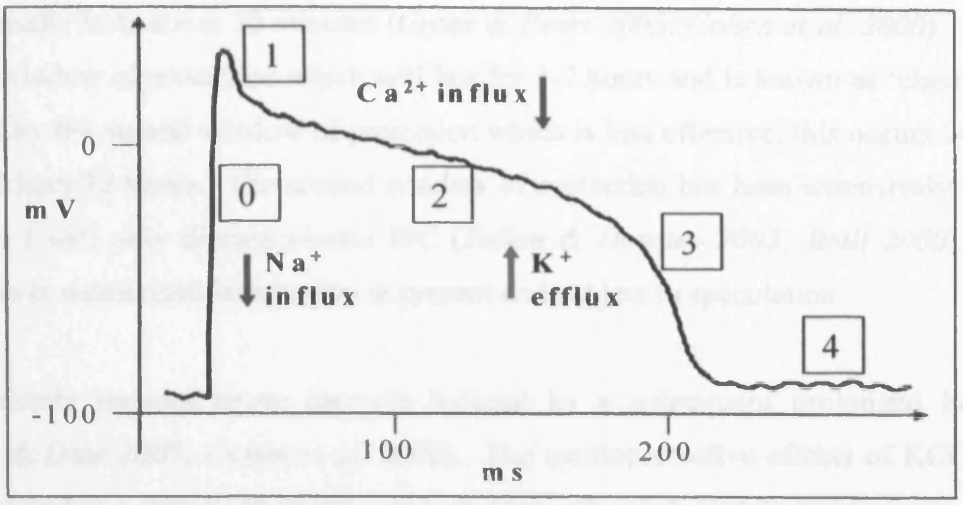

Figure 1.2. The cardiac action potential may be divided into a number of phases: Phase 0 - rapid depolarisation. Phase1 - early repolarisation. Phase 2 - plateau phase. Phase 3 - late repolarisation and phase 4 - diastolic phase.

1.5 The phenomenon of ischaemic preconditioning

Ischaemia results from a situation in which tissue is deprived of blood leading to tissue damage and irreversible necrosis. Myocardial ischaemia affects the heart muscle and can be caused by a number of factors such as atherosclerosis, thromboembolism and surgical interventions; these include heart bypass operation, percutaneous transluminal coronary angioplasty (PTCA) and heart transplants. Ischaemic preconditioning (IPC) was first described by Murry in 1986 where brief ischaemic episodes would protect the heart from a subsequent lethal ischaemic insult (*Murry et al. 1986*). This original study examined dog hearts which were subjected to four to five minute episodes of ischaemia and these were reported to have less necrosis from a sustained 40 minute coronary occlusion when compared to control hearts. In Murry's study, it was also noted that preconditioning delayed cell injury by slowing the rate of ATP depletion therefore limiting the accumulation of harmful catabolites such as lactate during reperfusion.

Other groups have used this protocol to investigate how IPC can delay cell injury and death in ischaemic myocardium. For example, hearts can be protected from ischaemic and or reperfusion injury by subjecting the organ to one or more short ischaemic periods (usually 3-5 minutes) with regular recovery phases before prolonged index ischaemia,

which usually lasts about 30 minutes (*Gross & Peart 2003; Cohen et al. 2000*). This is the first window of protection which will last for 1-2 hours and is known as 'classic IPC' followed by the second window of protection which is less effective; this occurs 24 hours later and lasts 72 hours. The second window of protection has been extensively studied however; I will only discuss classic IPC (*Yellon & Downey 2003; Bolli 2000*). How protection is memorised is unknown at present and subject to speculation.

IPC evidently reduces tissue necrosis induced by a subsequent prolonged ischemia (*Hanley & Daut 2005; Cohen et al. 2000*). The cardioprotective effects of KCOs have been reported in a variety of species such as dogs, rat, mice, rabbits and humans *(Yellon & Downey 2003; Cohen et al. 2000; Yao & Gross 1994a, 1994b; Grover et al. 1992*). It is widely accepted that preconditioning activates intracellular signalling mechanisms that increase tolerance to injury (*Yellon & Downey 2003; Dzeja et al. 2001*). These signalling mechanisms are complex and are linked to a variety of factors such as mitochondrial function, cellular metabolism and electrical activity of the cell (*Wang et al. 2005; Dzeja et al. 2001*). Although preconditioning studies predominantly focus on the heart, this protective mechanism has also been studied in the brain, skeletal muscle, kidney and liver (*Jaeschke 2003; Cochrane et al. 1999; Pang et al. 1997*).

1.5.1 Ischaemic preconditioning: The events that occur

In a normal cell, K_{ATP} channels are inhibited by high intracellular concentration of ATP in the μM range but open when ATP levels are low. In ischaemic myocardium, firstly, the lack of oxygen cannot support oxidative phosphorylation so pyruvate is converted into lactic acid. The anaerobic generation of ATP is not sufficient to keep up with the requirements of the heart and eventually ATP levels fall. Anoxic mitochondria may consume ATP to maintain their membrane potential. The ischemic cell will become acidotic as lactic acid is increasingly formed in the hypoxic, ATP-starved cell (*Cohen 2004*). There are three main steps in preconditioning which are hypothesised to lead to the activation of K_{ATP} channels. The first in the sequence is the trigger, which activates

the second, the mediator that initiates a series of signal transduction pathways before it activates the end effector. Ischaemic myocardium will rapidly consume ATP to form the trigger adenosine. Other triggers include bradykinin, opioids, reactive oxygen species, Ca^{2+} and acetylcholine which also confer cardioprotection (*Cohen et al. 2000; Thornton et al. 1993*). The consensus is that these triggers activate intracellular mediators such as PKC, receptor tyrosine kinases (RTK) and mitogen activated protein kinase (MAPK) signalling cascades. The final effectors in ischaemic preconditioning include the mitochondrial K_{ATP} channel (mitoK_{ATP} channel) and or mitochondrial permeability transition pore (mPTP) (*Ardehali & O'Rourke 2005; Javadov et al 2003, Cohen et al. 2000; Garlid et al 1996*). Whether the K_{ATP} channel is the end-effector or is simply another element in a complex signalling pathway remains debatable. The protective effects of exposing the myocardium to brief periods of ischaemia can also be mimicked by a variety of drugs in a phenomenon known as pharmacological conditioning. These agents include diazoxide, volatile anaesthetics such as isoflurane and agonists of G(i)-coupled receptors such as adenosine and opioids (*Riess et al. 2004*; *Patel et al. 2002; Cohen et al. 2001).*

1.5.2 *The receptors and intracellular messengers involved in ischaemic preconditioning*

During ischaemia, ATP is metabolised to AMP and subsequently converted to adenosine. Adenosine and other triggers will bind to and activate their appropriate receptors which couple to mediator phospholipase C (PLC) (*Simkhovich et al. 1998*). For example, at the cellular level, the release of adenosine will bind to the A1 receptor and activate a G protein. The G protein is composed of three subunits ($\alpha\beta\gamma$) and upon activation, the α_i subunit will dissociate from the complex and activate PLC (PLCβ subtype). PLC catalyses the hydrolysis of PIP_2, generating secondary messengers inositol (3,4,5) triphosphate (IP_3) and diacylglycerol (DAG). The latter, DAG will activate its target PKC. PKC is a serine/threonine kinase which can be categorised into three groups. The conventional or classical PKCs ($\alpha\beta_I, \beta_{II}, \gamma$) require Ca^{2+}, DAG and phospholipids for their activation. The novel PKC isoforms (δ, ε, η, θ) are not dependent on Ca^{2+} as they lack

the Ca^{2+} binding domains. Finally, the atypical group (ζ, ι, λ, μ) do not bind to Ca^{2+}, DAG or phorbol esters because they lack the Zn^{2+} finger motif needed to bind to DAG and phorbol esters so instead, they may be activated by 3'phosphoinositides (*Cohen et al. 2000*). There is substantial evidence in the literature to show that PKC is a key mediator in preconditioning (*Miki et al. 1998b; Ytrehus et al. 1994*). The mechanism may be by the direct phosphorylation of effector molecules or the activation of kinase cascades (*Hudman & Standen 2004; Baines et al. 2002*). There is no doubt that PKC is an essential trigger of preconditioning and it has been shown that specific isoforms of PKC do exist and will act at different points during preconditioning (*Simkhovich et al. 1998*). For example, the Ca^{2+} independent novel isoform of PKC (PKCε) is activated during ischaemic injury (*Gray et al. 1997*). Despite this, some studies have shown that the involvement of other intracellular messengers such as PKA and its mode of action may be through the inhibition of Rho-kinase (*Sanada et al. 2004*). This observation is supported by the fact that protection can be mediated through β-adrenergic receptor agonists to PKA (*Lochner et al. 1999*).

The signalling mechanism that leads to protection also involves MAPKs and phosphatidylinositol-3-kinase (PI3K) (*Armstrong 2004; Fryer et al. 2001a; Tong et al. 2000*). In quiescent myocytes, the majority of PKC is present in the cytosol and the activation of cytosolic PKC by lipid cofactors has been shown to be accompanied by its translocation and kinase activity to the membrane cytoskeleton (*Liu et al. 1994, Yuan et al. 1987*). More importantly, upon activation, PKC is translocated to membranes such as the plasma membrane or mitochondria where it can initiate signalling cascades and many groups believe is an important downstream event that leads to the activation of mitoK_{ATP} channels and ROS production (*Armstrong et al. 1996; Yoshida et al. 1996; Ping et al. 1997; Liu et al. 1999; Albert & Ford 1999; Fryer et al. 2001a*). However, glibenclamide and K_{ATP} channel blocker 5-hydroxydecanoate (5-HD) application during diazoxide pre-treatment or preconditioning period can block the cardioprotective effects of IPC (*Pain et al. 2000*). Using these results, they concluded that the timing of mitoK_{ATP} channel opening was more compatible with the channel performing as trigger rather than an end-effector role. In contrast, a study by Fryer et al suggested that the mitoK_{ATP} channel

acted as a trigger and downstream effector (*Fryer et al. 2001a*). At present, both views remain controversial. A schematic diagram to show the pathways involved in the mechanism of preconditioning is shown in figure 1.3.

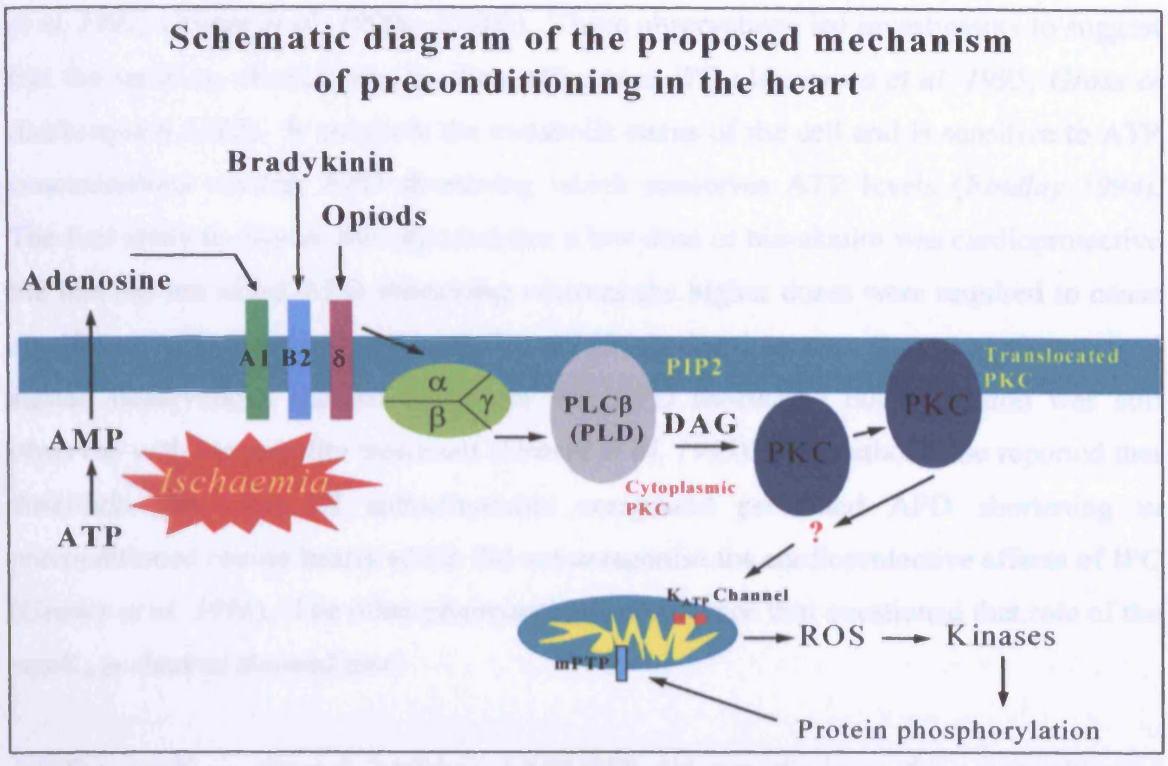

Figure 1.3. A diagram to show the proposed events which occur during ischaemic preconditioning. It is clear that K_{ATP} channels, whether as end effectors or signalling elements, are originally important in the cardioprotective mechanism.

1.6 The evidence for K_{ATP} channels in preconditioning

1.6.1 The sarcolemmal and mitochondrial K_{ATP} channel: The story so far

It has been more than 23 years since the sarcolemmal K_{ATP} channel ($sarcK_{ATP}$) was first discovered by Noma in cardiac myocytes (*Noma 1983*). The role of K_{ATP} channels in the heart has not been clearly defined but pharmacological evidence has shown that the opening of these channels protects the heart against ischaemic injury. KCOs such as nicorandil and pinacidil mimicked IPC with inhibitors such as glibenclamide abolishing this effect. The protective effects of KCOs exerted during ischaemia in rat hearts following recovery of contractile function during reperfusion is accompanied by

conservation of ATP (*Baird et al. 1996; McPherson et al. 1993*). However, it is not certain if protection exerted during ischaemia is a direct effect on reperfusion injury because KCOs such as aprikalim and cromakalim did not confer protection (*Auchampach et al. 1991; Grover et al. 1990a; 1990b*). These observations led investigators to suggest that the sarcK_{ATP} channel was the final effector in IPC (*Mizumura et al. 1995; Gross & Auchampach 1992*). It monitors the metabolic status of the cell and is sensitive to ATP concentrations causing APD shortening which conserves ATP levels (*Findlay 1994*). The first study to dispute this reported that a low dose of bimakalim was cardioprotective but this did not affect APD shortening whereas the higher doses were required to cause significant APD shortening (*Yao & Gross 1994a*). Furthermore, Grover et al described similar observations showed that there was APD shortening but protection was still observed with cromakalim treatment (*Grover et al. 1995*). The authors also reported that dofetilide, the class III antiarrhythmic compound prevented APD shortening in preconditioned canine hearts which did not antagonise the cardioprotective effects of IPC (*Grover et al. 1996*). The other pharmacological evidence that questioned that role of the sarcK_{ATP} channel showed that:

1.) The sarcK_{ATP} channel inhibitor, HMR1098 did not eliminate the preconditioning response induced by KCOs (*Sato et al. 2000*).
2.) The specific mitoK_{ATP} channel inhibitor 5-HD could block the anti-infarct effect of diazoxide and IPC (*Hu et al. 1999*).
3.) Diazoxide protected hearts from reperfusion injury without causing APD shortening.

These observations lead to the alternative hypothesis that the K_{ATP} channel involved in cardioprotection was mitochondrial (mitoK_{ATP}). This channel was first identified in the inner mitochondrial membrane by Inoue in 1991 but research turned a new corner when influential papers from Garlid's and Marban's groups were published (*Garlid et al. 1997a and b; Inoue et al. 1991*). Since its discovery, pharmacological studies have reported that activation by diazoxide and inhibition by 5-HD are the hallmarks of mitoK_{ATP} channel. For example, mitoK_{ATP} channel activity was assayed by measuring the changes in flavoprotein autofluorescence in rabbit ventricular myocytes where

diazoxide selectively opened and 5-HD inhibited the channel (*Liu et al. 1998*). Later studies conducted by Garlid's and by Grover's groups showed that diazoxide, nicorandil, and BMS-191095 activated the mitoK$_{ATP}$ channel in perfused rat hearts and were protective with little effect on cardiac or smooth muscle sarcK$_{ATP}$ channels (*Garlid et al. 2003*; *Grover et al. 2001*). These studies support the notion that mitoK$_{ATP}$ channel opening is an important event that confers protection. However, there is much debate on the precise role and existence of mitoK$_{ATP}$ channel opening as it has been suggested that channel opening may act as a trigger but it also has a prominent role as an effector after index ischaemia (*O'Rourke 2004; Liu & O'Rourke 2003; Gross & Fryer 1999*).

1.6.2 Basic principles of mitochondrial function

Mitochondria are responsible for generating cellular ATP and are involved in a number of important intracellular signalling processes such as the modulation of intracellular Ca^{2+} levels (*Jacobson & Duchen 2004*). During aerobic respiration, glucose is broken down into pyruvate via glycolysis which occurs in the cytoplasm. Pyruvate is taken up into mitochondria and converted into acetyl CoA and fed into the Kreb's cycle. During of breakdown of acetyl CoA into other substrates, decarboxylation reactions occur and the reaction generates a supply of reduced nicotinamide adenine dinucleotide (NADH) and flavin adenine dinucleotide ($FADH_2$) from oxidised forms NAD^+ and FAD^{2+}. ATP is also formed during these steps but the majority of ATP is formed in the final step called oxidative phosphorylation (*Mitchell 1967*). See figure 1.4.

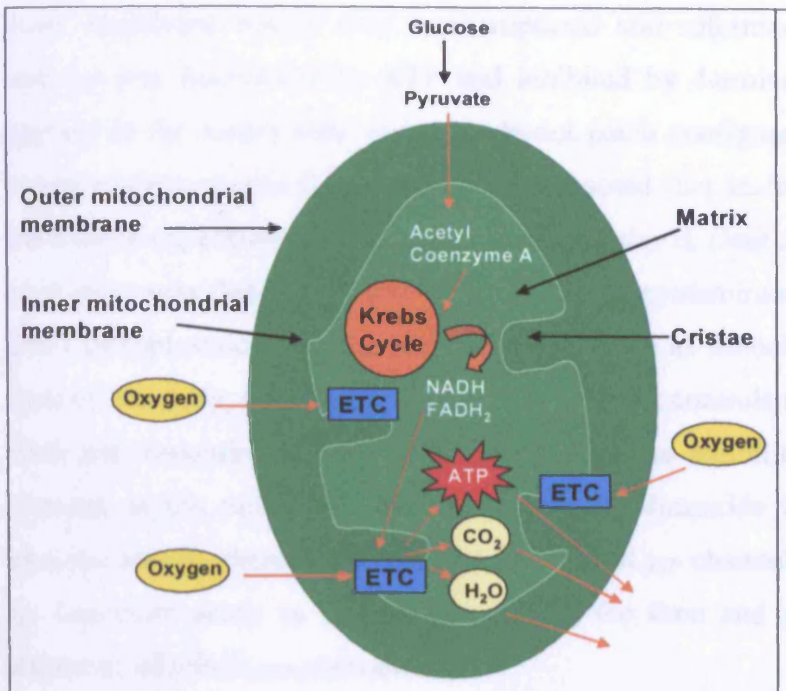

Figure 1.4.

A diagram to illustrate the structure of mitochondria and the reactions that occur within.

The mitoK$_{ATP}$ channel is located on the inner mitochondrial membrane. (ETC – electron transport chain)

During oxidative phosphorylation, oxygen is required by the electron transport chain to reduce oxygen to water. The electron transport chain translocates H^+ across the membrane to set up the mitochondrial membrane potential ($\Delta\psi_m$) which usually lies between -150 to -200 mV. It is the $\Delta\psi_m$ which provides the driving force for proton influx across the inner mitochondrial membrane through the ATPase; this energy is used to generate ATP. Mitochondria can sequester excess Ca^{2+} ions and the driving force for mitochondrial Ca^{2+} uptake is dependent on $\Delta\psi_m$, but the route of entry is mostly through the uniporter (*Jacobson & Duchen 2004*). Ca^{2+} is then redistributed between the mitochondria and cytosol through the action of Na^+/Ca^{2+} (NCX) exchanger.

1.6.3 Evidence for the existence of mitoK$_{ATP}$ channels

The study which discovered mitoK$_{ATP}$ channels was first published in 1991 by Inoue et al where they identified K^+ specific currents with a conductance of 10 pS from giant mitoplasts prepared from rat liver mitochondria (*Inoue et al. 1991*). The mitoplasts were prepared by homogenising the tissue and chemically dissociating mitochondria from their

outer membrane before they were ruptured and reformed into mitoplasts. Channel activity was inactivated by ATP and inhibited by 4-aminopyridine and glibenclamide applied to the matrix side under inside-out patch configuration. In Hanley and Daut's recent review on mitoK$_{ATP}$ channels, they noted that in Inoue's study there may have been some experimental flaws to the work (*Hanley & Daut 2005*). The problem with this procedure was that the sample may have been contaminated with other K$_{ATP}$ channels from sarcoplasmic, endoplasmic reticular as well as mitochondrial membranes. At the time of the study, the authors did not employ strict controls to ensure that their mitoplasts were not contaminated but the block by 5-HD and inhibition by ATP characterised this channel as the mitoK$_{ATP}$ channel. However, diazoxide had no significant effect on channel activity therefore it may not be a mitoK$_{ATP}$ channel but in fairness, this remains an important study as it was advanced at the time and provided an insight into the existence of mitoK$_{ATP}$ channels.

1.6.4 Studies investigating the mitoK$_{ATP}$ channel in liposomes and lipid bilayers

After single channel studies in mitoplasts, the majority of research on mitoK$_{ATP}$ channels focused on the technique of channel reconstitution in liposomes and lipid bilayers. A high $\Delta\psi_m$ is essential for oxidative phosphorylation and it is the influx of K^+ ('leak') that uncouples the respiratory chain causing changes in mitochondrial matrix volume. The $\Delta\psi_m$ is maintained by the ejection of H^+ across the inner membrane through the K^+/H^+ antiporter. Paucek and colleagues provided further insight for the existence of this channel designed to facilitate the uptake of K^+ into mitochondria (*Paucek et al. 1992*). A highly purified inner membrane fraction of isolated rat liver and beef heart mitochondria was reconstituted into liposomes or lipid bilayers and exhibited channel activity with a conductance of around 30 pS. This channel was purified using DEAE cellulose column, the main protein in this fraction had a molecular mass of 54 kDa which was a similar size to the mitochondrial Ca^{2+} activated K^+ channel identified in cardiac muscle with a molecular mass of 55 kDa (*Xu et al. 2002; Paucek et al. 1992*).

The liposomes in Paucek's study containing this reconstituted protein were loaded with the fluorescent K^+ indicator PBFI to measure CCCP dependent electropheretic K^+ uptake. In comparison, Inoue et al reported ATP inhibition from mitoplasts in Mg^{2+} free medium and that a high concentration of glibenclamide (5 μM) was required to inhibit the channel electrophysiologically (*Inoue et al. 1991*). On the other hand, Paucek et al found that K^+ influx was inhibited by a much lower concentration of glibenclamide with an IC_{50} value of ~50 nM (*Paucek et al 1992*). Although the majority of this work was carried out using rat liver mitochondrial preparations, the studies using the beef heart mitochondria were virtually identical with respect to K^+ specificity and inhibition by ATP and glibenclamide. Paucek argued that this variation in the data may be due to the presence of Ca^{2+} in the solutions used by Inoue et al as their preliminary studies indicated that the presence of such divalent cations will lead to a high binding affinity for the K_{ATP} channel and slow dissociation constant.

The effects of several factors such as diazoxide, glibenclamide, 5-HD, MgATP and ROS were examined on mitoK_{ATP} channels from bovine ventricular myocardium reconstituted in planar lipid bilayers (*Zhang et al. 2001*). The channel had a unitary conductance of 56 pS with symmetrical 150 mM KCl; this was substantially inhibited by 1 mM MgATP applied to the *trans* (matrix) side of the bilayer. Diazoxide (10 μM) increased channel activity and 5-HD (10-100 μM) reduced the open state probability in a dose dependent manner but HMR1098, the specific inhibitor for sarcK_{ATP} channel did not inhibit activity of the reconstituted channels. However, MgATP had no effect on the cytosolic side despite the fact that Yarov-Yarovoy et al reported that the regulatory sites on mitoK_{ATP} channel faced the cytosol (*Yarov-Yarovoy et al. 1997*). Garlid's group reported that the proteoliposomes containing the mitoK_{ATP} channel was tightly regulated by KCOs and inhibitors as well as nucleotides and Mg^{2+} (*Paucek et al. 1996*). These channels were reactivated by cytosolic GTP and long-chain acyl-CoA esters inhibited K^+ flux. The authors noted that channel inhibition may depend on how it was activated and experimental conditions used. In contrast, the mitoK_{ATP} channel from active respiring mitochondria was entirely insensitive to glibenclamide and 5-HD under experimental conditions in which the open state of the channel was stimulated by the absence of ATP

and Mg^{2+} *(Jaburek et al. 1998)*. However, K^+ influx was inhibited by glibenclamide and 5-HD when the open state was induced by either diazoxide, ATP, Mg^{2+} or GTP.

Biological membranes are not just physical barriers but are rather complex and dynamic environments and K_{ATP} channels residing within these environments control the flux of ions across the membrane through conformational changes through the pore (*Tillman & Cascio 2003)*. Any changes caused to these membranes may directly affect the behaviour and activity of the ion channel in question. The studies investigating the characterisation of mitoK_{ATP} channels have provided valuable insight into mitoK_{ATP} channel activity. However, there is variation in the data when one considers the parameters that were investigated such as molecular mass, drug sensitivity, ion selectivity and channel conductance because the various purification methods and techniques may have influenced the results. The methods for isolating and reconstituting native or cloned channels into these lipid bilayers are technically difficult (*Favre et al. 1999*).

1.6.5 Studies investigating mitochondrial matrix volume in isolated mitochondria

There is evidence to show that mitoK_{ATP} channel opening facilitates changes in mitochondrial bioenergetics (*Kowaltowski et al. 2001*). Many groups agree that mitoK_{ATP} channel opening is accompanied by an increase in matrix volume which will activate components of the respiratory chain (*O'Rourke 2004; Garlid 2000*). However, there is much debate to what occurs in the mitochondrial matrix as a consequence of mitoK_{ATP} channel opening. Garlid and co-workers focused their work on the changes in light scattering where an increase in K^+ influx and mitochondrial matrix volume was observed as a decrease in light scattering (*Garlid et al. 1996, Beavis et al. 1985*). They reported that mitochondrial swelling was inhibited by adenine nucleotides ATP, ADP or AMP and KCOs such as diazoxide and cromakalim increased light scattering; this effect was inhibited by both glibenclamide and 5-HD (*Jaburek et al.1998; Garlid et al 1996*).

These experiments were conducted in K^+ and not tetraethylammonium medium, which selectively blocks voltage gated K^+ channels therefore the changes observed were due to

K^+ influx through the mitoK_{ATP} channel. However, Halestrap's group were unable to reproduce the same changes in light scattering by administering KCO such as diazoxide and pinacidil and blockers such as glibenclamide and 5-HD (*Das et al. 2003; Lim et al. 2002*). They reported no increase in light scattering in response to ATP and ADP, which disagrees with the original results obtained by Beavis et al providing evidence that a putative K_{ATP} channel does exist in the mitochondrial inner membrane (*Beavis et al. 1993*). Guanine nucleotides such as GTP and GDP had no effect on matrix volume whereas carboxyatractyloside, an inhibitor of adenine nucleotide translocator (ANT) was found to inhibit K^+ influx. Whilst Garlid and Paucek's work showed that the changes in light scattering were due to changes in the mitochondrial matrix volume, Halestrap's group disputed this theory as the changes observed in Garlid's studies were probably due to the physical changes in the morphology or shape of mitochondria (*Garlid & Paucek 2003; Das et al. 2003*).

More recently, other aspects of mitochondrial function such as oxygen consumption, $\Delta\psi_m$ and ATP synthesis have been examined in isolated heart mitochondria under ischaemic conditions with the build up of ADP causing transient depolarisation. This was followed by an increase in oxygen consumption and light scattering, an index of matrix shrinkage (*Korge et al. 2005*). Furthermore, Korge et al found that mitochondria under metabolic stress had a decreased ability to maintain $\Delta\psi_m$ but this was rescued by ions such as K^+, Na^+ and Li^+. The application of valinomyocin and diazoxide also improved the recovery of $\Delta\psi_m$ and promoted matrix shrinkage. In conclusion, K^+ influx controlled matrix volume and swelling with external factors becoming more significant when mitochondria become under stress such as under high ADP load. The authors noted that caution must be taken with respect to light scattering measurements as mitochondrial swelling and conformational changes of the ANT have been postulated to be responsible for the published changes in mitochondrial matrix volume.

1.6.6 Other mitochondrial channels

The mitoK$_{ATP}$ channel opening is a important event in protection against necrotic and apoptotic cell injury after ischaemia but many other mitochondrial channels exist for example, large-conductance Ca^{2+}-activated K^+ channels (BK$_{ca}$) were discovered in the inner membrane of mitochondria (mitoK$_{ca}$) of guinea pig ventricular myocytes (*Xu et al. 2002*). Mitoplasts prepared from isolated cardiac myocytes were patch clamped and this channel was shown to contribute to background K^+ conductance. The BK$_{ca}$ channel opener NS1619 also protected hearts against infarction and the protective effects abolished by BK$_{ca}$ channel blocker paxilline. The mitoK$_{ca}$ channel may be the primary target of BK$_{ca}$ channel selective agents but these agents can also affect the sarcolemmal BK$_{ca}$ channel. However, this channel has not been identified in ventricular myocytes (*Gribkoff et al. 1996*; *Kenyon et al. 1995*). More recently, Sato and co-workers reported that mitoK$_{ca}$ opening will confer protection which is independent of mitoK$_{ATP}$ channel activity. They demonstrated that cAMP-dependent protein kinase induced mitoK$_{ca}$ opening which in turn depolarised the $\Delta\psi_m$ preventing mitochondrial Ca^{2+} overload (*Sato et al. 2005*).

Finally, Ardehali et al recently produced highly controversial work on reconstituted mitoK$_{ATP}$ channels in proteoliposomes. They identified a highly purified fraction of the mitochondrial inner membrane that formed part of a multiprotein complex containing SDH (complex II) and four other proteins including the mitochondrial ATP-binding cassette protein 1 (mABC1), phosphate carrier (PIC), ANT and ATP synthase (*Ardehali et al. 2004*). This was shown to have similar properties of a mitoK$_{ATP}$ channel as it was sensitive to KCOs and inhibitors as well as SDH inhibitors such as 3-nitroproprionic acid (3-NPA). Their data suggested that 3-NPA increased K^+ transport activity as well as 100 μM diazoxide in proteoliposomes, this was reversed by 500 μM 5-HD, 10 μM glibenclamide or 2 mM ATP suggesting that SDH has a regulatory role in mitoK$_{ATP}$ channel activation. .

1.7 The pharmacology of K_{ATP} channels

1.7.1 The pharmacology of sarcK_{ATP} and mitoK_{ATP} channels

To date, there are many pharmacological agonists that act on the sarcK_{ATP} and mitoK_{ATP} channel. See table 1.3 for the list of KCO and inhibitors. The list of KCO is extensive, these also include: P1060, P1075 (pinacidil derivatives), minoxidil, KRN2391, sidenafil, desflurane, isoflurane, aprikalim and levosimendan (*O'Rourke 2004; Oldenburg et al. 2003a; Gross 2003; Toller et al. 2000a; 2000b*). The non-selective KCOs include pinacidil and cromakalim which will activate both the sarcK_{ATP} and mitoK_{ATP} channel. However, there are exceptions such as diazoxide and nicorandil which can be used selectively to activate mitoK_{ATP} channels. Glibenclamide is a strong inhibitor that binds to K_{ATP} channels with high affinity however, it is non-selective and will block both sarcK_{ATP} and mitoK_{ATP} channels. The sarcK_{ATP} and mitoK_{ATP} channels have different responses to pharmacological agents. The cardiac sarcK_{ATP} channel cannot be activated by diazoxide unless at high concentrations. Garlid's early work reported that diazoxide opened the mitoK_{ATP} channel with a $K_{1/2}$ of 0.8 mmol/L whereas 800 mmol/L was required to activate the sarcK_{ATP} channel (*Garlid et al. 1997b*).

Table 1.3. A table to show the various compounds that activate or inhibit K_{ATP} channels. * Diazoxide will activate sarcK_{ATP} channels at high concentration or when the concentration of ADP is high. ** Nicorandil activates sarcK_{ATP} channels at high concentrations.

K^+ channel openers and inhibitors	**Selectivity of K^+ channel Openers/inhibitors**
K^+ channel openers	
Diazoxide	SarcK_{ATP} *, MitoK_{ATP}
Cromakalim	SarcK_{ATP} , MitoK_{ATP}
Nicorandil	SarcK_{ATP} **, MitoK_{ATP}
Pinacidil (P-1075)	SarcK_{ATP} , MitoK_{ATP}
BMS -191095	MitoK_{ATP}
K^+ channel inhibitors	
Glibenclamide	SarcK_{ATP}. MitoK_{ATP}
5 Hydroxydecanoate	MitoK_{ATP}
HMR1089	SarcK_{ATP}

One study showed that mitoK$_{ATP}$ channel opener diazoxide increased flavoprotein autofluorescence, an index of mitoK$_{ATP}$ channel activity with an EC_{50} of 27 μmol/L. Interestingly, at this concentration, diazoxide did not affect sarcK$_{ATP}$ channel activity (*Liu et al. 1998)*. Furthermore, the protective effects of diazoxide and cromakalim were both abolished by glibenclamide and 5-HD suggesting a role for the mitoK$_{ATP}$ channel. In cellular models of simulated ischemia, 50 μM diazoxide decreased cell death by 50 % when compared to controls. These results are agreement with Garlid's findings which suggest that the mitoK$_{ATP}$ channel is involved in cardioprotection (*Garlid et al 1997b, Garlid et al 1996*). Sato et al subsequently showed that 100 μM diazoxide increased flavoprotein autofluorescence in isolated rabbit ventricular myocytes without affecting sarcK$_{ATP}$ channel activity (*Sato et al. 1998*). The myocytes were also exposed to 100 nM phorbol ester phorbol 12-myristate 13-acetate (PMA) which potentiated and accelerated the effect of diazoxide to activate the mitoK$_{ATP}$ channel. The effects of PMA and diazoxide were blocked effectively by 5-HD.

Sato et al later examined the effects of KCO P-1075 and K$_{ATP}$ channel blocker HMR1098 on sarcK$_{ATP}$ and mitoK$_{ATP}$ channels in rabbit ventricular myocytes (*Sato et al. 2000*). SarcK$_{ATP}$ channels were activated in the presence of 30 μM P-1075 with no increase in flavoprotein autofluorescence. SarcK$_{ATP}$ channel activity was completely inhibited by 30 μM HMR1098. HMR1098 also inhibited sarcK$_{ATP}$ currents activated by metabolic inhibition however, it did not abolish diazoxide (100 μM) induced flavoprotein oxidation. The cardioprotective effects of diazoxide was abolished by 500 μM 5-HD but not by 30 μM HMR1098. These results suggest that P-1075 selectively activates sarcK$_{ATP}$ channels (without altering flavoprotein oxidation) and HMR1098 selectively inhibits sarcK$_{ATP}$ channels. 5-HD is regarded as a specific inhibitor of mitoK$_{ATP}$ channels because it can abolish the protective effects of ischaemic and pharmacological preconditioning in studies where infarct size was used as an indicator of tissue damage. The specificity of 5-HD for the mitoK$_{ATP}$ channel was confirmed by Jaburek et al where mitochondrial matrix swelling was used as an indicator of K^+ influx. They reported that 5-HD inhibited diazoxide induced K^+ flux (in the presence of 0.2 mM ATP) in isolated rat hearts

(*Jaburek et al. 1998*). In contrast, Tschida et al reported that nicorandil induced protection was abolished by HMR1098 and the authors also showed that PKC inhibitor calphostin C did not affect nicorandil induced protection suggesting that both sarcK_{ATP} and mitoK_{ATP} channels may contribute to protection (*Tsuchida et al. 2002*). BMS-191095 is a benzopyran derivative and is a less effective vasodilator than compounds such as cromakalim but still retains its cardioprotective properties by activating mitoK_{ATP} channels without affecting vascular smooth muscle sarcK_{ATP} channels (*Grover et al. 2001*). The cardioprotective effect of BMS-191095 was demonstrated in isolated rat hearts and protection was abolished by glibenclamide and 5-HD (*Grover & Atwal 2002*).

1.7.2 The non specific effects of K_{ATP} channel openers and inhibitors

There is an increasing list of pharmacological agents that offer cardioprotection. These compounds are structurally diverse but have the ability to partially impair the respiratory chain, which suggests that pharmacological inhibition of the respiratory chain may trigger cardioprotection (*Garlid et al. 2003*). For example, pinacidil and volatile anaesthetics can inhibit NADH dehydrogenase (complex I) and nicorandil can inhibit complex IV (*Tanaka et al. 2004*). Diazoxide is routinely used at low concentration (30-100μM) to precondition hearts, it can also influence mitochondrial metabolism which is independent of its K_{ATP} channel channel opening abilities (*Grimmsmann & Rustenbeck 1998*). The cardioprotective effects of diazoxide have been postulated to result from inhibition of SDH and a decrease in respiration. SDH inhibitors such as malonate and 3-nitroproprionic acid (3-NPA) have been shown to induce cardioprotection (*Lim et al. 2002; Hanley et al 2002*; *Ockaili et al. 2001*). Diazoxide can inhibit SDH at high concentrations (150 μM) and inhibit succinate oxidation in single cardiac myocytes (*Lim et al. 2002*; *Ovide Bordeaux et al. 2000; Schafer et al. 1969*). Ovide-Bordeaux concluded that diazoxide and glibenclamide at high concentrations (100 μM) did not modulate mitochondrial functional or K_{ATP} channel activity (*Ovide Bordeaux et al. 2000*). Furthermore, diazoxide has also been reported to act as a protonophoric uncoupler (*Holmuhamedov et al. 2004*). The authors stated that the functional effect of diazoxide depends on respiratory substrates and do not appear to be related to K_{ATP} channel activity.

5-HD is widely recognised as a mitoK$_{ATP}$ channel inhibitor but it also possesses indirect effects. For example, Notsu et al showed that 5-HD was able block the sarcK$_{ATP}$ channel under ischaemic conditions (*Notsu et al. 1992a, 1992b*). This compound can also be readily converted to 5-HD-acetyl CoA by enzymes residing in the mitochondrial matrix, this has been confirmed recently by Hanley et al (*O'Rourke 2004, Hanley et al. 2002*). In agreement with this, some groups have shown that 5-HD could block both Kir6.1/SUR1 and Kir6.2/SUR2 surface channels implying that it has poor mitochondrial specificity (*Liu et al. 2001; Sato et al. 1998; McCullough et al. 1991*). Low concentrations of 5-HD did not affect matrix volume but higher concentrations of 5-HD (100 or 300 μM) produced an increase in matrix volume (*Das et al. 2003; Lim et al. 2002*).

1.8 The role of mitoK$_{ATP}$ channels in preconditioning

1.8.1 The consequences of mitoK$_{ATP}$ channel opening

At present, the consequences of mitoK$_{ATP}$ channel opening and its protective mechanism is unclear. However, there is a general consensus that mitoK$_{ATP}$ channel opening plays a key role in preconditioning. It has been shown that ischaemic and pharmacological preconditioning is linked to mitochondrial depolarisation (*Minners et al. 2001*). K$_{ATP}$ channel opening may uncouple mitochondria as a direct result of K^+ influx and through the action of the K^+/H^+ exchanger; K$_{ATP}$ channel opening will tend to cause the mitochondrial membrane potential ($\Delta\Psi_m$) to dissipate. Without a proton gradient, there is an increase in electron transfer which decreases the driving force for ATP synthesis, producing an uncoupling effect (*Liu et al. 1998*). This hypothesis is in agreement with several observations. For example, KCO can induce membrane depolarisation in rat liver mitochondria (*Szeweczyk et al. 1995*). Furthermore, in isolated mitochondria and myocytes, mitochondrial depolarisation has been suggested to be an important event to decrease the driving force for Ca^{2+} influx and prevent Ca^{2+} overload (*Holmuhamedov et al. 1998, 1999*). The opening of mitoK$_{ATP}$ channels may also activate protective mechanisms by increasing reactive oxygen species (ROS) production (*Das et al 1999*).

Garlid and colleagues opposed the original hypothesis and stated that the uncoupling effects of diazoxide and other KCOs were independent of K_{ATP} channels because the same response was observed in Li^+ medium. They reported that pharmacological doses of diazoxide and pinacidil (<50 μM) could open mitoK_{ATP} channels, which resulted in a decrease in $\Delta\psi_m$ but the magnitude of K^+ influx (24-30 nmol K^+ min^{-1} mg^{-1}) was only enough to depolarise the $\Delta\psi_m$ by 1-2 mV (*Kowaltowski et al. 2001*). The data also suggested that mitoK_{ATP} channel opening had little effect on respiration, $\Delta\psi_m$ and Ca^{2+} uptake but K^+ influx had important effects on the regulation of matrix and intermembrane space volumes. K^+ influx will increase matrix volume and mitochondrial swelling by shifting the balance between K^+ uniport and K^+/H^+ antiport, causing transient net K^+ uptake and matrix swelling due to a higher steady-state volume (*Yellon & Downey 2003; Garlid 1988*). This is followed immediately by uptake of phosphate via the phosphate/OH^- exchange carrier because K^+ uptake is always accompanied by anions and movement of water via osmosis. Another study confirmed that K^+ influx was insufficient to depolarise the $\Delta\psi_m$ and making mitochondria resistant to Ca^{2+} entry (*Terzic et al. 2000*). Garlid also suggested that perhaps the effects on mitochondria may be associated with the toxic effects of diazoxide because high concentrations of diazoxide will inhibit respiration and SDH (*Schafer et al. 1969*). Hanley recently confirmed the toxic and non-specific effects of diazoxide (*Hanley et al. 2002*).

Recent studies have been conducted to demonstrate the significance of mitochondrial uncoupling in the mechanism of protection (*Brennan et al 2006a and b*). The authors reported that the low dose of mitochondrial protonophore FCCP (100 nM) was cardioprotective whereas higher concentrations (300 nM) would cause mitochondrial depolarisation and exacerbate injury. Protection was observed with mitochondrial oxidation but this was not accompanied with mitochondrial depolarisation and sarcK_{ATP} channel activity. FCCP will induce mild uncoupling and activate protective mechanisms that lead to protection. However, in their hands, diazoxide (30 μM) did not alter mitochondrial function and the authors concluded that it must elicit protection via a different mechanism. These studies are of significant importance because they are in

agreement with Garlid's work that perhaps protection is associated with mitochondrial function and signalling pathways rather than regulating K_{ATP} channel activity.

MitoK_{ATP} channel opening may also facilitate the physical contact of proteins in the mitochondrial inner and outer membrane which was first described by Brierley (*Brierley 1974*). This interaction of proteins would promote ATP synthesis and this hypothesis is supported by recent data by Ardehali et al where the authors proposed that SDH is a structural and functional component of a multiprotein complex that exhibited mitoK_{ATP} channel activity (*Ardehali et al. 2004*). The authors proposed that SDH regulated the mitoK_{ATP} channel by means of its physical interactions without affecting oxidative phosphorylation. It has been proposed that the cardioprotective effect of diazoxide results from inhibition of SDH and a decrease in respiration, rather than opening of mitoK_{ATP} channels (*Lim et al. 2002; Hanley et al. 2002*).

In the high energy state, such as in the case of ischaemia, mitoK_{ATP} channel opening prevents matrix contraction. This is a protective mechanism because there is no matrix swelling and contraction which prevents the rupture of the mitochondrial inner membrane. Maintaining a constant volume is important so that the rate of substrate oxidation is regulated preventing energy wastage and this in turn facilitates efficient energy transfer to synthesise ATP (*Halestrap 1989*). Recently, Halestrap's group showed that 50 μM diazoxide and two cycles of preconditioning increased mitochondrial matrix volume in isolated mitochondria by 88 % and 58 %. IPC increased the rate of ADP-stimulated respiration by 2-oxoglutarate and succinate oxidation whereas diazoxide caused a similar increase in matrix volume but inhibited succinate and 2-oxoglutarate oxidation however, 5-HD did not reverse this process but instead promoted further matrix swelling (*Lim et al. 2002*). The authors suggested that the changes in matrix volume and respiratory chain activity might not be linked with protection.

1.8.2 MitoK_{ATP} channel opening and reactive oxygen species

ROS are group of messengers that are also known as free radicals. A free radical is a cluster of atoms that contains an unpaired electron in its outermost shell of electrons. This configuration is extremely unstable therefore making the radical react quickly with other molecules or radicals to achieve a more stable configuration. ROS are formed by several mechanisms, such as the interaction of ionising radiation with biological molecules, from enzymes such as NADPH oxidase in activated leukocytes, xanthine oxidase and as a by-product of cellular respiration from the mitochondrial electron transport chain. During cellular respiration, electrons are fed into the individual complexes of the respiratory chain and a very small percentage of these electrons that 'leak' are used to generate superoxide ions at complex I and III from the reduction of molecular oxygen (*Turrens 1997*). Ischaemia often results in an increase in ROS levels upon reperfusion and recent studies have shown ROS to cause significant damage to the respiratory chain (*Lesnefsky et al. 2004; Petrosillo et al. 2003*).

The ROS generated from mitoK_{ATP} channel opening can play either a protective or detrimental role. The ROS that are generated during the preconditioning phase are protective, supporting a role for ROS in triggering protection (*Forbes et al. 2001; Pain et al. 2000; Vanden Hoek et al. 1998*). However, the ROS produced upon reperfusion have detrimental effects which can lead to irreversible cell injury and cell death (*Dröge et al. 2002; Ozcan et al. 2002; Vanden Hoek et al. 2000, Zweier et al. 1987*). This burst of ROS can be prevented by the cardioprotective mechanism of mitoK_{ATP} openers at reoxygenation (*Ozcan et al. 2002*). The role of ROS has been confirmed in ischaemic and pharmacological preconditioning studies by the use of ROS scavengers and PKC inhibitors before index ischaemia (*Novalija et al. 2003; Forbes et al. 2001; Baines et al. 1997; Chen et al. 1995; Ytrehus et al. 1994*). Hence, the consensus is that mitoK_{ATP} opening facilitates the production of protective ROS during preconditioning but decreases detrimental post ischaemic ROS production. At present, the link between ROS and mitoK_{ATP} opening has not been fully elucidated.

Oldenburg et al proposed that K_{ATP} channel opening was the first step in preconditioning and the ROS produced act as an upstream trigger (*Oldenburg et al. 2003b; Yao et al. 1999*). This conclusion was solely based on the assumption that diazoxide and 5-HD act selectively on mitoK_{ATP} channels. Despite this hypothesis, Lebuffe et al postulated that the ROS generated during the trigger phase could in turn activate and open the mitoK_{ATP} channel (*Lebuffe et al. 2003*). Based on these studies, some authors believe that there is sufficient evidence to show that K_{ATP} channels act both as a trigger and as a 'distal' end effector in IPC (*Gross & Peart 2003; Gross & Fryer 1999*). The focus of research turned to mitoK_{ATP} channel activation and ROS generation. K_{ATP} channel opening was proposed to occur during index ischaemia and one group showed that exogenous H_2O_2 and ROS derived from mitochondria both induced preconditioning in cardiomyocytes triggered by hypoxia (*Vanden Hoek et al. 1998*). Recently, the opening of the mitoK_{ATP} channel can lead to partial mitochondrial depolarisation which can reduce Ca^{2+} entry and mitochondrial Ca^{2+} overload or alternatively increase the production of mitochondrial ROS (*Holmuhamedov et al. 1999; Das et al. 1999*).

Although mitoK_{ATP} channel opening is often associated with an increase in ROS production, the link between the degree of mitochondrial depolarisation and ROS production is not clear. In addition to this, diazoxide induced mitoK_{ATP} channel opening depolarised the mitochondria by 1-2 mV but these changes were too small to affect mitochondrial function (*Kowaltowski et al. 2001*). The use of FCCP to collapse the proton gradient will reduce the drive for ATP synthesis. At low concentrations (100 nM), FCCP can bypass the mitoK_{ATP} channel and induce partial depolarisation in mitochondria (*Brennan et al. 2006a*). The authors found that protection associated with FCCP was by dependent on ROS but independent of K_{ATP} channels because protection was abolished by antioxidants but not by glibenclamide or 5-HD. FCCP-induced mitochondrial flavoprotein oxidation without activating the sarcK_{ATP} channel (*Brennan et al. 2006b*). This recent study provides further evidence that ROS have an important role in cardioprotection.

1.8.3 The sarcK$_{ATP}$ channel and ischaemic preconditioning

The current literature suggests that the mitoK$_{ATP}$ channel is involved is preconditioning. However, there is also solid evidence to support the protective role of the sarcK$_{ATP}$ channel. Jovanovic and co-workers reported that COS-7 cells co-transfected with Kir6.2/SUR2A had channel activity when they were stimulated with pinacidil (*Jovanovic et al. 1998*). In addition to this, later experiments showed that these cells survived metabolic stress such as hypoxia-reoxygenation because Ca^{2+} overload was inhibited (*Jovanovic et al. 1999*). The main finding from Suzuki's study using Kir6.2 knock out mice was that IPC offered protection and shortened the APD duration in ventricular cells isolated from wild-type (WT) but not KO mice (*Suzuki et al. 2002*). However, the authors noted that the importance of sarcK$_{ATP}$ channels may have been amplified due to the fast heart beat in the murine model. In another study, transgenic mice expressing mutant Kir6.2 did not respond to IPC with reduced ATP sensitivity suggesting that the sarcK$_{ATP}$ may play a role in the mechanism leading to protection (*Rajashree et al. 2002*). The mechanism by which sarcK$_{ATP}$ channel confers protection still remains elusive. It has been suggested to participate in preconditioning by acting as a 'trigger' by some groups whilst the majority of evidence has confirmed a role for the channel as a 'distal' effector, summarised in a review by Peart and Gross (*Peart & Gross 2002*). PKC is a key secondary messenger involved in IPC and its activation and translocation is reported to couple to the sarcK$_{ATP}$ channel (*Light et al. 2001*). This field is still controversial with strong evidence for both sarcK$_{ATP}$ and mitoK$_{ATP}$ channels as the possible candidates involved in the mechanism that confers cardioprotection.

1.9 The molecular structure of the mitoK$_{ATP}$ channel

1.9.1 The evidence for and against Kir6.1 as a component of the mitoK$_{ATP}$

The structure of mitoK$_{ATP}$ channel is unknown. Controversially, it has been suggested that Kir6.1 may be a major component of the mitoK$_{ATP}$ channel (*Suzuki et al. 1997*). In this particular study, Suzuki et al identified a 51 kDa protein with a Kir6.1 antibody in a

mitochondrial preparation. The pharmacology of native mitoK$_{ATP}$ channels isolated from rabbit ventricular myocytes were compared with molecularly defined sarcK$_{ATP}$ channels expressed heterologously in HEK293 cells (*Liu et al. 2001*). Using flavoprotein autofluorescence as an index of mitoK$_{ATP}$ channel activity and electrophysiological recordings of currents from rabbit ventricular myocytes, Liu et al reported that HEK293 cells expressing Kir6.1/SUR1 subunits had a similar pharmacological profile to the native mitoK$_{ATP}$ channel. Pinacidil and diazoxide (100 μM) opened the Kir6.1/SUR1 type channel, while P-1075 activated most of the heterologously expressed K$_{ATP}$ channels but it had no effect on Kir6.1/SUR1 or native mitoK$_{ATP}$ channels. Glibenclamide (10 μM) blocked all channels whereas the mitoK$_{ATP}$ channel blocker 5-HD (200 μM) inhibited the native mitoK$_{ATP}$ and Kir6.1/SUR1 channel. The sarcK$_{ATP}$ channel inhibitor HMR1098 had no effect on these channels and P-1075 could not open native mitoK$_{ATP}$ channels either. The data showed that the native mitoK$_{ATP}$ channel closely resembled the Kir6.1/SUR1 channel expressed in HEK293 cells.

The immunogold labelling work by Suzuki suggested that Kir6.1 was a possible candidate of the mitoK$_{ATP}$ channel (*Suzuki et al. 1997).* However, recent work by Ardehali et al did not detect Kir6.1 in highly purified mitochondrial fractions (*Ardehali et al. 2004*). Similarly, Hambrock and co-workers showed that Kir6.1 tagged to GFP alone or co-expressed with the SUR subunit did not translocate to mitochondria (*Hambrock et al. 2002*). Furthermore, Kir6.1 and Kir6.2 have been shown to be expressed at high levels in rabbit ventricular myocytes but one study showed that the overexpression of Kir6.1 (and Kir6.2) dominant negatives (DN) did not block diazoxide induced flavoprotein autofluorescence in these cells, suggesting that neither Kir6.1 and Kir6.2 are part of the mitoK$_{ATP}$ channel (*Seharaseyon et al. 2000*). Subsequently, studies probing for the roles of Kir6.1 and Kir6.2 demonstrated that diazoxide induced flavoprotein oxidation in Kir6.1 and Kir6.2 deficient mice (*Miki et al. 2002; Suzuki et al 2002*).

1.9.2 Knockout mice studies

In the last year, research in this field has been focusing on the potential role of the sarcK_{ATP} channel in IPC because a number of studies have questioned the role and existence of mitoK_{ATP} channels. Studies conducted by Miki et al examine the importance of Kir6.x genes in different tissues by generating Kir6.1 and Kir6.2 null mice (*Miki et al. 2002; 1998a*). Both genes have vital physiological roles because functional K_{ATP} channels protect the cells against acute metabolic stress such as hyperglycaemia, hypoglycaemia, hypoxia and ischaemia (*Seino & Miki. 2003b*). Miki et al found that Kir6.1 knockout mice were susceptible to spontaneous ST elevation and atrioventricular block followed by sudden premature death. *In situ* hybridisation detected Kir6.1 mRNA in the hearts of wild type mice but none was detected in the Kir6.1 knockout mice. Kir6.1 mRNA and protein are up-regulated during myocardial infarction (*Akao et al. 1997*). Cardiomyocytes from wild type mice showed significant K^+ current when stimulated with pinacidil, this was blocked with glibenclamide but cardiomyocytes from Kir6.1 knockout mice had no response. See table 1.4 for knockout (KO) mice studies.

Table 1.4. A table to show knockout mice studies investigating the roles of Kir6.x and SUR subunits with the relevant references.

Knockout mice	**Reference**
Kir6.2 $^{-/-}$	*Miki et al 1998*
Kir6.1 $^{-/-}$	*Miki et al 2002*
SUR1 $^{-/-}$	*Seghers et al 2000*
SUR2 $^{-/-}$	*Chutkow et al 2001*

Suzuki and others showed that the infarct size in wild type mice with IPC was significantly less than wild type mice without IPC, however, there were no differences in infarct sizes between wild type and Kir6.2 KO mice with IPC (*Suzuki et al. 2002*). *In vitro* experiments using Langendorff perfused hearts. The hearts from Kir6.2 KO mice did not recover from an ischaemic insult whereas wild type mice do recover from ischaemia. Wild type mice pre-treated with HMR1098 (sarcK_{ATP} blocker) were susceptible to metabolic stress, similar to the observations seen in Kir6.2 KO mice. If the

hearts of wild type mice were preconditioned (with their mitoK$_{ATP}$ channels still intact), this suggests that Kir6.2 and sarcK$_{ATP}$ channel and not the mitoK$_{ATP}$ channel may be important in preconditioning (*Suzuki et al. 2002; 2003*). In addition to this, the absence of Kir6.2 in KO mice was found to negate protection of myocardium. After ischemia-reperfusion, IPC-induced energetic and functional improvements occurred in wild type but not Kir6.2 KO hearts (*Gumina et al. 2003*).

1.10 Hypothesis and aims

This study aims to test the hypothesis that:

The intracellular localisation of Kir6.1 is functionally significant in cardiac and skeletal muscle because it generates important K^+ flux in intracellular membranes such as the endoplasmic reticulum, sarcoplasmic reticulum and perhaps the mitochondria. The study will specifically examine the role of the channel in ROS production, mitochondrial function and Ca^{2+} handling. The aims are:

1. To examine the endogenous expression and subcellular distribution of natively expressed Kir6.1 and the subcellular distribution of heterologously expressed Kir6.1-GFP in HepG2, C2C12, HL-1 and HEK-293 cell lines.

2. To examine the functional role of Kir6.1 in the regulation of free radical generation, mitochondrial redox state and Ca^{2+} handling by overexpressing Kir6.1 or by knocking out Kir6.1 using siRNA or dominant negative forms of Kir6.1.

2.0 MATERIALS AND METHODS

2.1 General molecular biology

Common molecular biology techniques were used in this project. The data presented in this study required these techniques because K_{ATP} channel subunits and other plasmid DNA were manipulated or reproduced for specific experiments or in conjunction with other experiments.

2.1.1 Restriction digest of DNA molecules

Restriction enzymes hydrolyse double stranded DNA molecules at specific palindromic nucleotide sequences. These sequences are palindromes because they exhibit two fold rotational symmetry. Some enzymes cut the two strands of DNA in a staggered manner creating 'sticky' or cohesive ends (e.g. *Bam HI* and *Apa I*) with protruding 5' and 3' ends, *Bam HI* cuts at the 5' end of the axis whereas *Apa I* cuts at the 3'. Other endonulceases such as *Hae III* cleave in the middle of their recognition sequence at the axis of symmetry and produce blunt ends. The enzymes were stored on ice and added to the reaction mix last to avoid enzyme degradation and loss of activity. The buffers for the restriction enzymes were supplied as 10x stock and BSA as 100x stock (10x BSA was used so pipetting small volumes was avoided). The samples were mixed thoroughly and incubated for 1 hour generally at 37 °C. In some cases, two restriction enzymes were used to cut the DNA so a compatible buffer was used where both enzymes have greater than 50 % of their maximal activity. Restriction digests were set up as follows:

2 µl DNA (20-100 µg)
2 µl 10x BSA stock concentration (final concentration used 100 µg/ml)
2 µl enzyme buffer (10x)
1 µl restriction enzyme (2-10 units)
16 µl Sigma grade molecular biology water

2.1.2 Agarose gel electrophoresis

Gel electrophoresis separates DNA molecules of different sizes. Each nucleotide in the DNA molecule contains a phosphate group; therefore it is negatively charged and will migrate in the presence of an electrical field. Agarose gels are used to separate DNA fragments over a broad size range however; its resolving power is not as accurate as polyacrylamide gels which are used to separate smaller DNA fragments. DNA exists in three different forms: linear, supercoiled and nicked so its conformation is important because it would influence its migration rate in the gel. In most cases, a 0.7 % (w/v) agarose gel was made in 1x TAE buffer. A 50x TAE stock solution was made using 2 M Tris Base (*Sigma Aldrich, UK*), 50 mM EDTA pH8.0 and 5.71 % (v/v) glacial acetic acid (*BDH, UK*) and (0.7 g of electrophoresis grade agarose (*Invitrogen, UK*) was added to 100 ml 1x TAE.) This was microwaved until the agarose had completely dissolved. The mixture was left for a minute before ethidium bromide (*Sigma Aldrich, UK*) was added to give a final concentration of 0.5 μg/ml. This is an intercalating dye that binds between base pairs so that DNA bands can be visualised under ultra violet light. The agarose-TAE mixture was poured into a plastic gel tray sealed securely at the sides with autoclave tape and plastic combs were placed at the appropriate slots. The gel was left to set for an hour at room temperature.

After the restriction enzyme digest had been incubated at 37 °C, 2 μl 10x gel loading buffer was added to each sample. The buffer was made from 0.25 % (w/v) bromophenol blue, 0.25 % (v/v) xylene cyanol FF, 30 % glycerol (*all supplied from Sigma Aldrich, UK*). The samples were mixed thoroughly and 20 μl was loaded into its designated well along with a standard DNA molecular weight marker VII (*Roche Labs, UK*) as this was used to determine the size of the DNA fragments. The gel was set to run at 100 V for an hour before it was viewed under the ultra-violet (UV) light at 312 nm wavelength in a UVP dual intensity transilluminator connected to a camera, monitor and printer. Photographs were printed and DNA fragments were sized according to the DNA standard marker.

2.1.3 Extraction and purification of fragments/plasmid DNA from agarose gels

The DNA fragments separated by agarose gel electrophoresis was extracted and purified using a commercially available kit from Qiagen (*QiaEx II agarose gel extraction kit*). Silica gel particles bind DNA fragments under high salt conditions and contaminants were removed by a series of washes before the purified DNA was eluted with distilled water. The DNA fragment of interest was excised with a clean scalpel from the gel and weighed in an eppendorf tube to which three volumes of buffer QX1 was added to one volume of DNA fragment 100 bp-4 kb. This was resuspended in Qiagen II by vortexing for 30 seconds and for 2 µg DNA, 10 µl QiaEx II or for 2-10 µg DNA 30 µl QiaEx II was required to dissolve the gel. The DNA fragment was incubated at 50 °C for 10 minutes to solubilise the agarose and bind the DNA. The mixture was vortexed every two minutes to keep QIAEX II in suspension before the sample was centrifuged for 30 seconds and supernatant discarded. The pellet was washed with 500 µl of buffer QX1 before it was centrifuged for 30 seconds and it was washed twice with 500 µl wash buffer PE. This was followed by centrifugation for 30 seconds; the pellet was air-dried for 10-15 minutes. The sample was centrifuged with 20 µl of distilled water and the eluted DNA collected into a clean tube. This step was repeated so that approximately 40 µl was collected in total, this second elution step should in theory increase the yield by 10-15 %. The purified plasmid DNA/DNA fragment would be used in subsequent ligation reactions.

2.1.4 Ligation of DNA fragments

DNA fragments can be inserted into a vector in a ligation reaction. Whether a specific DNA fragment can be spliced into a vector is dependent on the termini produced by the restriction enzyme digest. The DNA fragment and vector are usually digested with restriction enzymes that have compatible cohesive ends. The enzyme DNA ligase is used during the ligation reaction to form new phosphodiester bonds between the phosphate residues located at the 5' terminus and hydroxyl group at the 3' terminus. Calf intestinal phosphatase (CIP) *(New England Labs, UK)* was used to remove the 5'phosphate group of the vector because the restriction enzymes producing identical cohesive ends may

religate especially if once partially digested by one of the enzymes. Ten units of CIP was added to the digested product and incubated at 37 °C for 1 hour. The reaction was set up and incubated at 16 °C overnight. The ligated DNA was then introduced into competent *E.coli* by transformation. The ligation reaction was set up as follows:

5 µl CIP-treated digested vector
12 µl digested DNA fragment
2 µl 10x ligation buffer
1 µl T4 DNA ligase (1 unit) (*Roche Diagnostics, UK*) Total volume 20 µl

2.1.5 Procedure for making competent *E.Coli* for transformation

Transformation is the process of introducing foreign DNA into bacteria. When bacteria are treated they are made 'competent', meaning they can readily take up foreign DNA. Foreign DNA can be introduced into bacteria by two main methods; the first is by electroporation and the second is by chemical transformation. In the case of electroporation, an electrical pulse permeabilises the cell membrane allowing DNA to be introduced into the cell. For chemical transformation, the bacteria were made competent by treating them in a variety of ice-cold buffers containing mostly $CaCl_2$ or RbCl. In this study, chemical transformation was used as it was efficient and reliable method. The Top10 strain of *E.Coli* was used for transformations as this particular strain is able to replicate steadily. The original Top10 stock was obtained from Invitrogen (*Groningen, Netherlands*). The Top10 *E.coli* competent cell stocks were replenished regularly. Using a sterile inoculating loop, cells from a glycerol stock were streaked onto Luria-Bertani (LB broth) agar plates. This was left to incubate at 37 °C overnight and stored at 4 °C for 1 week. LB broth (*Sigma Aldrich, UK*) is used as a growth medium for *E. Coli* (1 litre: 10 g Tryptone, 5 g yeast extract and 5 g NaCl). The agar plates were made using 1.5 g agar (*Sigma, Aldrich, UK*) for 100 ml LB broth. The agar was heated in the microwave until it had completely dissolved and cooled down before they were poured into 90 mm Petri dishes (*VWR, Merck house, UK*). Plates were left to set at room temperature and stored at 4°C until required.

One or two individual colonies were picked using a sterile pipette tip and placed into a falcon tube containing 3 ml of LB broth and left on a shaking incubator (225 rpm) at 37 °C for 7-9 hours. A sterile 2-litre flask containing 200 ml LB broth was inoculated with 1 ml of the starter culture and grown at 37 °C until the OD_{550nm} was between 0.450 and 0.550 nm. The cells were transferred into sterile centrifuge bottles and allowed to cool on ice for 30 minutes before centrifuging cells at 2500 rpm for 15 minutes. After this, the supernatant was discarded and the pellet was resuspended with 25 ml of ice-cold RF1 buffer (100 mM RbCl, 50 mM $MnCl_2.4H_20$, 30 mM potassium acetate, 10 mM $CaCl_2.2H_20$, 15 % (w/v) glycerol, pH adjusted to 5.8 with 0.2 M acetic acid and filter sterilised). Cells were incubated on ice for 15 minutes before centrifugation at 2500 rpm for 9 minutes. The supernatant was poured off and the pelleted cells were resuspended with 4.2 ml of ice-cold RF2 buffer (10 mM RbCl, 10 mM MOPS, 75 mM $CaCl_2.2H_2O$, 15 % glycerol, pH adjusted to 6.8 with 0.2 M NaOH- Filter sterilised) before they were kept on ice for 15 minutes. The competent bacteria were aliquoted into sterile eppendorf tubes and flash frozen using liquid nitrogen before they were stored in the -80 °C freezer. They were left in the freezer for at least 24 hours before use.

2.1.6 Transformation of plasmid DNA

Top10 *E.Coli* cells were slowly thawed out on ice before use. About 100 µl *E.Coli* Top10 cells were used for each transformation and mixed with 1 µl DNA in an eppendorf tube. They were left on ice for 30 minutes before they were heat shocked at 42 °C for 90 seconds to introduce the DNA into the bacteria. The tubes were cooled on ice for 2 minutes before 800 µl prewarmed LB broth was added to each sample. This gave the cells time to express the antibiotic resistance gene encoded by the plasmid DNA. Approximately 100 µl of the mixture was added to LB agar plates containing antibiotic; this was either with carbenicillin (100 µg/ml) or kanamycin (25 µg/ml) which was evenly distributed using a sterile spreader. (Frozen stocks of the antibiotics were added to the LB agar mixture when the temperature was less than 50 °C). The plates were left in the incubator overnight at 37 °C to allow the formation of discrete colonies.

2.1.7 Procedure for plasmid DNA purification (Midi preparation)

Plasmids are used extensively in DNA cloning. They are small double stranded circular DNA molecules that replicate independently of the host genome. However, plasmids do require the transcription and translation machinery of the host cell to replicate. The plasmid DNA with the correct sequence was identified before it could be retransformed and produced in larger quantities. Qiagen supplied the DNA purification kit and the method was followed according to manufacturer's instructions. The kit purifies the plasmids on a DEAE anion exchange column and plasmid DNA were produced according to how much DNA was needed for experiments. The DNA could be purified using either the midi or maxi preparation depending on the DNA yield that was required. The midi preparation was employed because 20-100 μg of DNA was generally required for subsequent experiments.

2.1.8 Subcloning K_{ATP} subunits into specific vectors

The K_{ATP} channel cDNA constructs were previously generated in the laboratory but it is important to understand how these constructs were made and the methods employed (*Cui et al. 2001*). The majority of the colocalisation work investigated the distribution of Kir6.1 using a cDNA construct called Kir6.1-GFP where the C terminus of Kir6.1 was fused to GFP (eGFP-N1 vector) (*Rizzuto et al. 1995*). In chapter 3.1, I will describe how this was made because elucidating the distribution of Kir6.1 with this fluorescent marker was a major focus of this thesis. The cDNA of Kir6.1 was originally identified in rat pancreatic islet cells (*Inagaki et al. 1995c*), Kir6.2 was also discovered by the same group, this was expressed in rat pancreatic islets and glucose-responsive insulin-secreting cell lines (*Inagaki et al. 1995a*). SUR1 was cloned from hamster cDNA (*Aguilar-Bryan et al. 1995*) and SUR2B was identified from mouse heart cDNA library (*Isomoto et al. 1996*). All the K_{ATP} channel subunits were expressed in pcDNA3 family of vectors. The dominant negatives for Kir6.1 (DNKir6.1), SUR1 and SUR2B were expressed in pcDNA3 and Kir6.1, Kir6.2 in pcDNA3.1/Zeo (*both vectors were from Invitrogen, UK*). The endoplasmic reticulum marker, DsRed2-ER was bought commercially (*Clonetech,*

UK). Figure 2.1 shows the restriction maps for the vectors used to subclone our K_{ATP} channel subunits. Please refer to table 3.1 in the results section for the complete list of plasmid cDNAs used throughout this thesis.

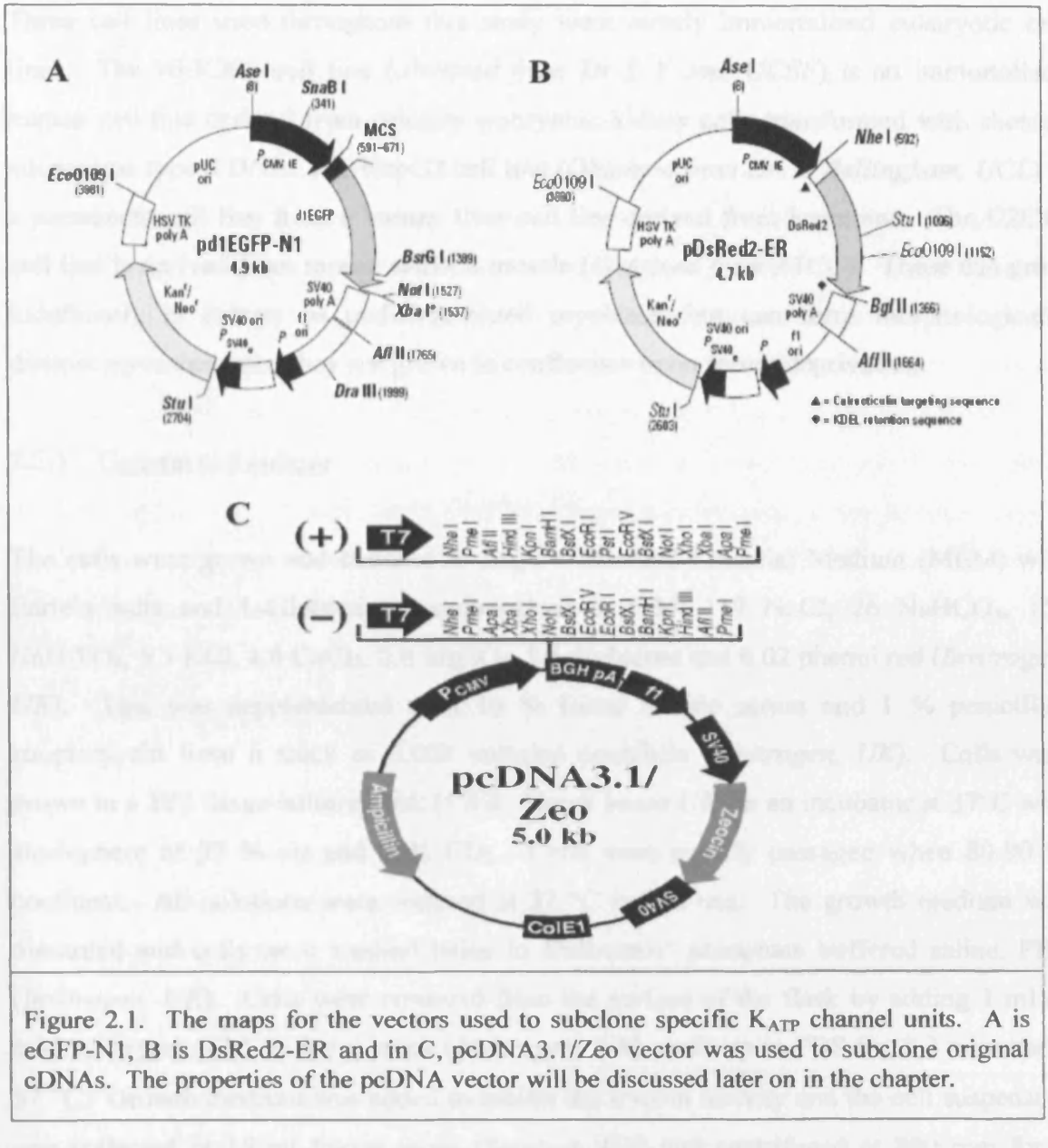

Figure 2.1. The maps for the vectors used to subclone specific K_{ATP} channel units. A is eGFP-N1, B is DsRed2-ER and in C, pcDNA3.1/Zeo vector was used to subclone original cDNAs. The properties of the pcDNA vector will be discussed later on in the chapter.

2.2 Cell culture

HEK293, HepG2 and C2C12 cell line

Three cell lines used throughout this study were mostly immortalised eukaryotic cell lines. The HEK293 cell line (*obtained from Dr L Y Jan, UCSF*) is an immortalised human cell line derived from primary embryonic kidney cells transformed with sheared adenovirus type 5 DNA. The HepG2 cell line (*Obtained from Dr. G Bellingham, UCL*) is a permanent cell line from a human liver cell line derived from hepatoma. The C2C12 cell line is derived from mouse skeletal muscle (*Obtained from ATCC*). These can grow indefinitely in culture as undifferentiated myoblasts but can form morphologically distinct myotubes once they are grown to confluence upon serum deprivation.

2.2.1 General cell culture

The cells were grown and cultured in Eagle's Minimal Essential Medium (MEM) with Earle's salts and L-Glutamine (composition) in mM: 117 NaCl, 26 $NaHCO_3$, 158 NaH_2PO_4, 5.3 KCl, 1.8 $CaCl_2$, 0.8 $MgSO_4$, 5.5 d-glucose and 0.02 phenol red (*Invitrogen, UK*). This was supplemented with 10 % foetal bovine serum and 1 % penicillin-streptomycin from a stock of 5,000 units/ml penicillin (*Invitrogen, UK*). Cells were grown in a T75 tissue culture flask (*VWR, Merck house UK*) in an incubator at 37°C with atmosphere of 95 % air and 5 % CO_2. Cells were usually passaged when 80-90 % confluent. All solutions were warmed at 37 °C before use. The growth medium was discarded and cells were washed twice in Dulbeccos' phosphate buffered saline, PBS (*Invitrogen, UK*). Cells were removed from the surface of the flask by adding 1 ml of 0.25 % Trypsin (2.5 % (w/v) stock (*Invitrogen, UK*) made up in PBS for 2-3 minutes at 37 °C. Growth medium was added to inhibit the trypsin activity and the cell suspension was collected in 15 ml falcon tubes (*Sarstedt, UK*) and centrifuged at 800 rpm for 5 minutes. The medium was discarded and pelleted cells were resuspended in 10 ml of fresh medium. One ml of resuspended HEK293 cells was used to seed a new T75 flask.

For HepG2 and C2C12 cell lines, 0.5 ml was used to seed a T75 flask. Cells were cultured twice weekly and the growth medium was changed every 2-3 days.

2.2.2 Production and revival of frozen stocks

In order to obtain frozen stocks of cells, they were only passaged when 80-100 % confluent. After centrifugation, the cell pellet was resuspended in 5 ml growth medium and 5 ml 10 % dimethyl sulfoxide DMSO (*Sigma Aldrich, UK*) before they were aliquoted (1 ml) into cryogenic vials (*VWR, Merck house, UK*). These were frozen down using a Nalgene freezing jar containing room temperature isopropanol (*VWR, Merck house, UK*). The jar with the cryovials were placed into the -80 °C freezer for approximately 6-12 hours before the vials were transferred to a liquid nitrogen container for long-term storage. The cells were revived by placing the vial in the waterbath set at 37 °C for 2-3 minutes. The whole aliquot was added to a flask containing pre-warmed growth medium. The cells were left to adhere to the flask under normal growth conditions. After 6-18 hours the culture medium containing DMSO was removed as DMSO becomes toxic to the cells. This was replaced with fresh growth medium.

2.2.3 Selection and maintenance of stably transfected cell lines

The stable cell lines HEK Kir6.1/SUR2B and Kir6.2/SUR2B which I have used in this thesis were originally generated in the lab. Although I did not generate these, it is important to fully understand and appreciate the process. This section will explain how the stable cells expressing the K_{ATP} channel subunits were isolated. When plasmid DNA enters the cell, it is trafficked to the nucleus where the DNA encoded proteins can be expressed. In transient transfections, most plasmids will replicate using the host DNA replication machinery but this process cannot continue indefinitely as the plasmid is eventually lost. With a stable transfection, the plasmid can either replicate independently of host cell and pass its DNA on to daughter cells during division or alternatively, the plasmid can be randomly integrated into the host cell, replicate and pass on from one generation to the next. The plasmid usually contains a gene when expressed confers

resistance to a specific antibiotic. The stably transfected cells were selected in this way. The K_{ATP} channel subunits of interest intended for the generation of stable cell lines were subcloned into one of two mammalian vectors; pcDNA3 and pcDNA3.1/zeo (*Invitrogen, UK*). These vectors have been genetically manipulated to make them efficient in introducing the genes of interest into my cell lines. The K_{ATP} subunits were co-transfected simultaneously and cells co-expressing both constructs were selected using media containing 727 μg/ml Geneticin and 344 μg/ml Zeocin (Tranfections will be discussed in the next section). The pcDNA3 and pcDNA3.1/zeo vectors contain genes encoding for resistance to Neomycin (Geneticin) and Zeocin respectively.

Cells containing pcDNA3 vector were selected using Geneticin, a glycoside which inhibits protein synthesis and causes cell death by affecting ribosome function. Cells expressing the Neomycin resistance gene, encodes for proteins with aminoglycoside phosphotransferase activity, which makes cells resistant to Geneticin. Cells containing the pcDNA3.1 vector were selected with Zeocin, this causes cell death by DNA cleavage. Cells expressing the Zeocin resistance gene encode a protein which binds to Zeocin directly preventing DNA cleavage. All pcDNA vectors also contain an ampicillin resistance gene that permits selection of transformed bacteria. The structure of the vectors is shown in figure 2.2 with notes on its important features. Therefore cells expressing these plasmids were selected using their relevant antibiotics.

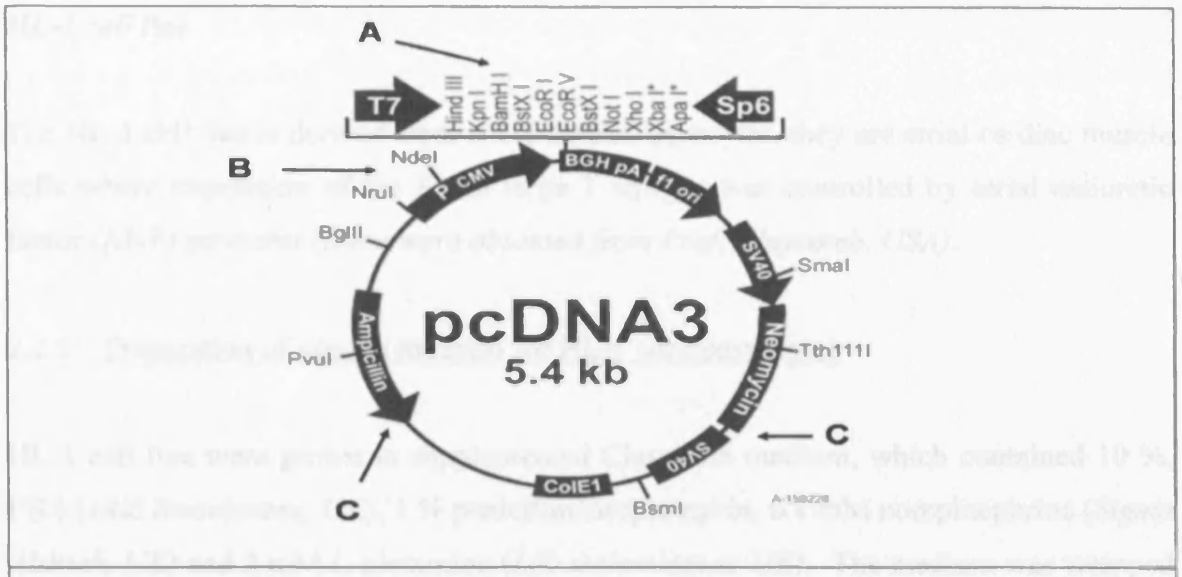

Figure 2.2. PcDNA3 vector restriction map.

A is the multiples cloning site (MCS), this is a synthetic DNA sequence which encodes a variety of unique restriction endonuclease recognition sites. This permits the insertion of the gene of interest and facilitates cloning.

B is known as the promoter sequence, this contains a viral human CMV immediate-early promoter (from Cytomegalovirus) for high level of expression in mammalian cells. The T7 promoter contains a binding site for RNA polymerase II which also binds with transcription factors. Expression is driven by the CMV immediate early promoter, the powerful CMV promoter (and SV40 polyadenylation site contains a sequence that provides signals required for termination of mammalian transcription and translation).

C encodes for specific genes that encode for drug resistance. This allows cells to synthesise an essential component in deficient media. What makes the pcDNA3 vectors so useful is that there are selectable markers for prokaryotic (amplicillin) and eukaryotic systems (Neomycin and Zeocin). E.g. the neomycin resistance gene is used for the selection of stable cell lines.

2.2.4 General cell culture for K_{ATP} channel stable cell lines

The stable cell lines HEK Kir6.1/SUR2B and Kir6.2/SUR2A were cultured in the same way as described with the other cell lines. These cell lines grew more slowly than wild type HEK293 so were only cultured every 7-10 days but the media was changed twice a week. MEM was supplemented with FBS, 344 µg/ml Zeocin (*Invitrogen, UK*) and 727 µg/ml Geneticin or G418 (*Life Technologies, UK*).

HL-1 cell line

The HL-1 cell line is derived from AT-1 cardiac myocytes, they are atrial cardiac muscle cells where expression of the SV40 large T antigen was controlled by atrial natiuretic factor (ANF) promoter (*these were obtained from Prof. Claycomb, USA).*

2.2.5 Preparation of growth medium for HL-1 cardiomyocytes

HL-1 cell line were grown in supplemented Claycomb medium, which contained 10 %, FBS (*JRH Biosciences, UK*), 1 % penicillin/streptomycin, 0.1 mM norepinephrine (*Sigma Aldrich, UK*) and 2 mM L-glutamine (*Life technologies, UK).* The medium was wrapped in foil as it was light sensitive and was replaced after two weeks because L-glutamine had to be replenished. Norepinephrine was made up in 30 mM L-ascorbic acid (*Sigma Aldrich, UK)* and filter sterilised using a 0.2 μm syringe filter (*VWR, Merck house, UK*) and stored at -20 °C for a month. L-glutamine (100x) solution was also stored at -20 °C. Soybean trypsin inhibitor (12.5 mg) was dissolved in 50 ml of PBS (*both supplied by Invitrogen, UK*). This was filter sterilised and stored at 4 °C for a week. HL-1 cardiomyocytes were cultured on a gelatine (0.02 % [wt/vol])/fibronectin (10 μg/ml) matrix. Tissue culture flasks were coated with this the day before cells were passaged. To obtain stocks, 0.1 g gelatin (*BD Biosciences, UK*) was added to 500 ml of distilled water (0.02 % gelatin) and this was autoclaved and 1 ml of fibronectin (*Sigma Aldrich, UK*) was diluted in 199 ml of 0.02 % gelatin. This was mixed and aliquoted before they were frozen at -20 °C.

2.2.6 Maintaining and culturing HL-1 cell line

HL-1 cardiomyocytes were grown in supplemented Claycomb medium every weekday and were passaged only at full confluence. A T75 flask was rinsed with 5 ml 0.05 % trypsin/EDTA and aspirated. Another 5 ml of trypsin/EDTA was added and left to incubate at 37°C for 2 minutes. This was removed and replaced with fresh trypsin/EDTA and incubated for an additional 5-8 minutes. Five ml of soybean trypsin inhibitor was

used to inhibit trypsin activity before cells were collected in a falcon tube. Five ml of Claycomb wash media (without FBS) was added to the flask to collect remaining cells and these were centrifuged at 800 rpm for 5 minutes. The gelatin/fibronectin solution was removed from flasks and replaced with 10 ml of supplemented Claycomb media. The pelleted cells were gently resuspended in 4-5 ml of fresh Claycomb medium. One ml of the cells was used to seed the new flask.

2.2.7 Production/revival HL-1 cell line frozen stocks

In order to obtain stocks of HL-1 cell line, cells from a confluent T75 flask were frozen into one cryovial. The cells were trypsinised and collected as before but were centrifuged at 1000 rpm for 5 minutes. Each cell pellet was resuspended in 1.5 ml of freezing medium (95 % FBS and 5 % DMSO). Cryovials were frozen down using the same method as described for the other cell lines. Before reviving the cells, a T75 flask was coated with gelatin/fibronectin the day before and frozen stocks were thawed for 2-3 minutes at 37 °C before centrifugation at 1000 rpm for 5 minutes. The pellet was resuspended in 5 ml of supplemented Claycomb medium and transferred to a T75 flask already containing prewarmed Claycomb media. The medium was replaced with fresh medium after 4 hours when the cells had attached.

2.2.8 Counting viable cells using Trypan Blue exclusion assay

The majority of cells cultured throughout this study were healthy but a minority of cells did not grow as expected, in order to determine if a new aliquot of cells (frozen) were required, counting the number of viable cells in existing tissue culture stocks was necessary. Trypan Blue (*Sigma Aldrich, UK*) is a dye that is used routinely to determine the viability of cell lines. Living cells exclude the dye, whereas dead cells will take up the blue dye. This is because the plasma membrane is damaged therefore facilitates the uptake of the dye to which the cell is normally impermeable. The blue stain is easily visible, and cells can be placed into a haemocytometer and counted using a light microscope. A 200 µl aliquot of cell suspension was mixed with equal volume of 0.4 %

(w/v) Trypan Blue staining solution. A coverslip was placed on top of the grid on the haemocytometer (Neubauer 0.100 mm depth) (*Invitrogen, UK*). A small drop of the cell suspension was applied at the edge of the coverslip because the two chambers filled by capillary action). The number of viable cells in each 1 mm square was counted and results were averaged. The number of cells per ml was calculated using the expression: *No. of cells/ml = Mean count/mm^2 x 10,000 x 2.* The volume of the 1 mm square is 0.1 mm^3 (as the depth is 0.1 mm) and volume conversion factor for 1 mm^2. The calculated value was multiplied by two to take into account the dilution factor of the cell suspension in Trypan Blue solution.

2.3 Transfection

Transfection is the process of introducing foreign DNA into a eukaryotic cell. Once in the cytoplasm, DNA is transported to the nucleus whereby the proteins encoded by the DNA is expressed by using the host cell's transcriptional and translational machinery. Transfected DNA is maintained transiently in many cells but only stably integrated in a few. There are many known methods for introducing plasmid DNA into a eukaryotic cell. There are numerous non-viral transfection techniques, the DEAE-dextran method was discovered by Pagano and McCutchan in 1969 and calcium phosphate co-precipitation by Graham and Van der Eb in 1972 (*Graham & Van der Eb 1973; Pagano & McCutchan 1969*). Liposome mediated gene transfer was pioneered in the late 1980's by Itani et al, this was a useful method because it provided high efficiency of gene transfer and DNA could be integrated transiently or stably integrated into a cell line. There are other methods for introducing DNA into a cell without forming a DNA-mediator complex; these include electroporation and direct microinjection. The best method of transfection would allow high transfer of DNA into the cell with minimal interference to the cell's physiology, low toxicity, reproducibility and ease of use. For the transfection experiments in this study, the liposome based transfection was employed.

2.3.1 Liposome based transfection

Cells were passaged the day before transfection into 6 well tissue culture dishes (*Triple Red, UK*) so that they reached 60-70 % confluency the next day. Cells were transfected with no more than 2 μg DNA because overloading the cells with DNA would cause cell death. For each transfection, 5 μl of 2 mg/ml Lipofectamine was diluted in 100 μl of Opti-MEM reduced serum medium (*both obtained from Invitrogen, UK*). Opti-MEM is a modification of Eagle's Minimal Essential Medium (MEM) buffered which contains L-glutamine, 2400 mg/L sodium bicarbonate, HEPES, sodium pyruvate, hypoxanthine, thymidine, trace elements, growth factors and 1.1 mg/L Phenol Red. A 100 μl aliquot of Opti-MEM was added to eppendorf tubes containing 0.8-2 μg DNA (depending on the amount of DNA used).

The mixtures were incubated for 15 minutes before 100 μl of lipofectamine-optimem mixture was added to DNA and left to incubate for 30 minutes to allow DNA-lipid complexes to form. After this, 800 μl of optimem was added and mixed (final volume of 1ml). Cells were washed briefly with optimem before the ml of transfection mixture was added to appropriate wells. The cells were incubated with the transfection mixture under normal growth conditions for 10-15 hours before it was removed and replaced with fresh medium. This allowed transfected cells to recover and to express the DNA. With the cell lines used, cells were transfected up to 15 hours because it produced higher transfection efficiencies. This gave cells sufficient time to take up the DNA, any longer than 15 hours would result in cell death.

2.3.2 Transfecting siRNA using liposome based transfection method

Lipofectamine 2000 reagent (*Invitrogen, UK*) facilitates high transfection efficiency of small interfering RNA (siRNA) to mammalian cells with effective knockdown of a gene (see 2.4). Some factors can affect the degree of gene expression and this can be reduced, for example when siRNA are used. The factors to consider are transfection efficiency, the transcription rate of the gene of interest, protein stability (and its degradation) and the

actual efficacy of the siRNA duplex used in the experiment. Cells were passaged and cultured the day before transfection into 6 well tissue culture dishes. After centrifugation, the pelleted cells were resuspended and plated in MEM media containing only 10 % FBS but with no P/S as it would affect the transfection efficiency and was reported to cause cell death. The cells were incubated overnight under normal growth conditions so that they would be 30-50 % confluent the next day, in order to minimise the loss of cell viability due to cell overgrowth. The procedure for transfecting siRNA is the same method used in 2.3.1. The only differences are that the first incubation period with lipofectamine 2000 and the DNA with Opti-MEM is 5 minutes. The DNA-lipofectamine complexes are allowed to form in 20 minutes and the mixture is added directly to cells still in growth media. The plates were mixed gently by rocking them back and forth before they were incubated at 37 °C for 24-72 hours until cells were ready to be analysed for gene knockdown or used in subsequent experiments. The growth media could be removed after 4-6 hours without loss in transfection activity.

2.4 Small interfering RNA (siRNA)

2.4.1 2-for- Silencing siRNA Duplexes

Small interfering RNAs are a useful new tool in molecular biology as they have the ability to suppress gene expression. The siRNA kit used throughout this study was custom made by Qiagen. The first siRNA kit previously used in the first year of my PhD was a kit provided by *Imgenex* which was based on the short hairpin approach. However the siRNA did not show any positive results in gene knockdown so it was not possible to move onto functional work. Recently, Qiagen provided a service to design and make the siRNA duplexes and 2-for silencing siRNA duplexes were guaranteed to have 100 % effect in gene silencing. The entire mRNA coding sequence for the gene of interest was scanned for all possible 21 base pair primers of this gene and analysed for potential siRNA activity using the highly accurate Hiperformance design algorithm. Stringent homology analysis was used and high-scoring candidates were ranked by their uniqueness using a sensitive alignment tool and a non-redundant sequence database.

Two siRNA that combine optimal potential activity and high specificity were chosen and used as the duplexes. Two high performance purity (HPP) grade siRNAs (20 nmol) for Kir6.1 were custom designed by Qiagen. The siRNA were synthesised so that they were specific to rat, mouse and human Kir6.1. The HPP process yielded > 90 % purity with the quality checked by ion-exchange high performance liquid chromatography (IE-HPLC) analysis. The sequence and identity of each siRNA was confirmed using MALDI-TOF spectrometry analysis. The target sequences used for siRNA duplexes for the specific species are as follows.

61siRNA Duplex 1 (Rat and Mouse)	61siRNA Duplex 2 (Rat and Mouse)
5' CAC CAC CTT GGT AGA CCT GAA 3'	5' CAG GAA GAG CAT CAT CCC GGA 3'

61siRNA Duplex 1 (Human only)

5' GAG GTG GTT CCT ATT CAC CAA 3'

The siRNA was prepared in RNAse free environment. A ml of siRNA suspension buffer was added to the lyophilised siRNA to obtain a 20 μM solution. The tubes (Duplex 1 and 2) were heated for 1 minute at 95 °C before they were incubated at 37 °C for an hour. The duplexes were stored at -20 °C until required. The method for transfecting siRNA into eukaryotic cells is described in section 2.3. The transfection efficiency was observed under a fluorescent microscope (after co-transfection with eGFP) and images were taken in the eGFP field and brightfield. However, the rat and human DNA sequence had 89 % homology therefore the presence of mismatched pairs in the siRNA would not be effective (see chapter 3.1). Therefore, separate human siRNA was acquired for the functional studies. These siRNA in conjunction with the dominant negatives are vital in this project for determining the possible functions of Kir6.1 in immortalised cell lines. This will be discussed in chapter 3.1.

2.5 Confocal microscopy

The confocal microscope is an advanced and powerful tool compared to the conventional fluorescent microscope. In contrast, the limitations of the fluorescent microscope are the resolution, depth of focus (magnification) and contrast. The image produced from the fluorescent microscope is obtained by illuminating the sample with a light source. The fluorescent light source is usually either from a Xenon lamp, mercury bulb or a laser. A monochromator or filter transmits a selectable narrow band of wavelengths of light filtered from the light source. The directed light is then passed through a condenser lens and imaged with an objective lens before the image is viewed through the eyepiece. The resolution of the image is predominantly dependent on the objective lens.

2.5.1 The basic principles of fluorescence

Fluorescence microscopy analyses fluorescence from a sample by using a beam of light, often UV light to excite the electrons in the sample to emit light of a lower energy, usually in the visible range. The compound being examined will have a ground electronic state or low energy state and an excited electronic state of higher energy. Photons of high frequency have a greater energy than those of low frequency. The compound absorbs a photon of light from its ground state to various vibrational states in the excited electronic state. The excited compound reaches the lowest vibrational state thus emitting a photon with energy equivalent to the difference of these states.

2.5.2 The basic principles of confocal microscopy

In confocal microscopy the light source is provided by a laser. The principle of the confocal microscope is to direct the laser beam to a focal point as it scans over the specimen. A detector collects the light emitted from the point of focus while out of focus light is excluded. Confocal microscopy removes out of focus light by passing the light through one or more small apertures (pinhole), leaving only a thin, highly focused plane. The thickness of the focal plane depends on the pinhole aperture and is placed in front of

the detector to eliminate out-of-focus information. Only the light within the focal plane can be detected, so the image quality is better and gives a higher resolution image than that of wide-field images. Scanning mirrors then use the focused laser light to scan different parts of the specimen until an entire field is obtained.

The light emitted from the specimen is detected by photomultiplier tubes (PMT) which generates a current that is proportional to the light intensity. PMTs are constructed from a glass vacuum tube which houses a photocathode, several dynodes to amplify the signal and an anode. The light (photons) excites electrons in the tube wall and the electrons are accelerated by the electric field towards the first dynode. The high energy electrons strike the first dynode and emit low energy electrons which in turn are accelerated towards the second dynode. This cascade increases the number of electrons produced at each stage before it reaches the anode where the accumulation of charge results in a sharp current that generates a voltage across a resistor. The signal is converted into a digital mode by an A-D convertor which can be displayed on a computer as an image, see figure 2.3. For the study of the distribution of Kir6.1, the Bio-Rad Radiance 2000 laser scanning confocal microscope (*Bio-Rad, Hemel Hampstead, UK*) was used to investigate the localisation of Kir6.1 whereas the Zeiss laser scanning LSM 510 confocal microscope (*Zeiss, UK*) was used to study the changes in mitochondrial redox state and mitochondrial membrane potential in cultured and primary cell lines.

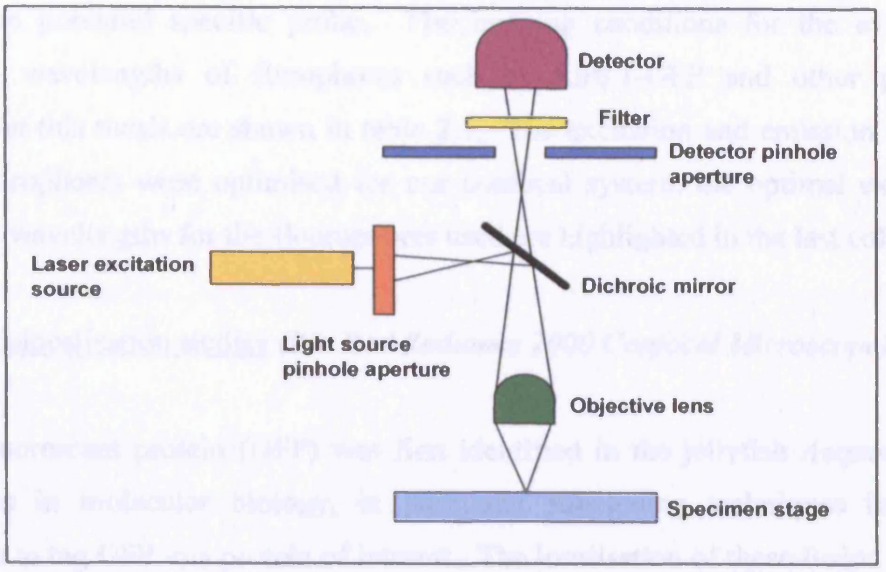

Figure 2.3. A diagram to show the main components of a confocal microscope.

Table 2.1. The excitation and emission wavelengths of Kir6.1-GFP and DsRed2-ER are shown with other fluorescent probes used throughout this study. * TMRM was used to measure changes in mitochondrial membrane potential using the Zeiss laser scanning LSM 510 confocal system.

Fluorophores	**Excitation wavelength used (nm)**	**Emission filter used (nm)**	**Maximum excitation and emission wavelength (nm)**
Kir6.1-GFP	488	510-530	Ex: 488 Em: 509
DsRed2-ER	543	LP>560	Ex: 563 Em: 582
tetramethylrhodamine, ethyl ester, perchlorate (TMRE)	543	LP>560	Ex: 549 Em: 573
tetramethylrhodamine, methyl ester, perchlorate (TMRM)*	543	LP>560	Ex: 549 EM: 573
MitoTracker Red	543	LP>560	Ex: 579 EM: 599
Mito-Ds Red	543	LP>560	Ex: 563 Em: 582
Concanavalin A-FITC	488	510-530	Ex: 506 Em: 529
Rhodamine conjugated goat α rabbit antibody	543	LP>560	Ex: 560 Em: 584

For colocalisation studies, live cells were transfected with fluorescently labelled probes such as Kir6.1-GFP and DsRed2-ER and cells that were stained using specific antibodies and markers were imaged using the Bio Rad radiance 2000 confocal microscope. In some cases, cells were first transfected before they were loaded with a mitochondrial

membrane potential specific probe. The imaging conditions for the excitation and emission wavelengths of flurophores such as Kir6.1-GFP and other probes used throughout this thesis are shown in table 2.1. The excitation and emission wavelengths used fluorophores were optimised for our confocal system, the optimal excitation and emission wavelengths for the fluorophores used are highlighted in the last column.

2.5.3 Colocalisation studies *(Bio Rad Radiance 2000 Confocal Microscope)*

Green fluorescent protein (GFP) was first identified in the jellyfish *Aequorea victoria.* Advances in molecular biology, in particular subcloning techniques have enabled scientists to tag GFP to a protein of interest. The localisation of these fusion proteins can be studied using fluorescent or confocal microscopy. There are also spectral variants of GFP such as YFP (yellow) and CFP (cyan). The aim of the project was to investigate the distribution of Kir6.1 in the different cell lines. Cells were transfected with Kir6.1 (in eEGP-N1 vector) where the C terminus of Kir6.1 was tagged to GFP called Kir6.1-GFP and the endoplasmic reticulum marker called DsRed2-ER (in pDsRed2-ER vector). Cells were also transfected with the sulphonylurea receptor, SUR1 (in pcDNA3 vector). The cells transfected with Kir6.1-GFP, DsRed2-ER and or SUR1 were left for approximately 24-48 hours before they were analysed and used in subsequent experiments. Transfected cells were removed using 500 µl trypsin and cells were collected by adding 500 µl growth medium. The dislodged cells were evenly distributed into a 6 well plate already prepared with 25 mm coverslips (*VWR, Merck house, UK*). These were left to grow at 37 °C for 24-48 hours before they were imaged on the confocal microscope. In some cases, cells were transfected directly on the coverslips.

The 543 nm and 488 nm argon laser, fluorescent lamp and Bio Rad TE300 Software were switched on first before the cells were handled. The confocal microscope was also fixed to a brightfield light source and a mercury bulb. The image resolution was set to 1024 x 1024 pixels and the 25 mm coverslips containing the cells were removed carefully using fine forceps and placed in an imaging dish (*Harvard apparatus, USA*). The cells were washed briefly with Opti-MEM without phenol red (This contains a HEPES buffer, 2,400

mg/L sodium bicarbonate, hypoxanthine, thymidine, sodium pyruvate, L-glutamine, trace elements, and growth factors, but no phenol red) (*Invitrogen, UK*) before it was replaced with 1ml of the same solution. This was placed on the microscope stage and viewed using an x60 oil objective. The cells were positioned carefully using the brightfield before they were checked for red (DsRed2-ER) fluorescence then the field of cells was positioned and zoomed in accordingly in the green channel. Scanning was then set to the Kalman configuration taking three scans in total so that the final colocalised image taken would be an average. The Kir6.1-GFP signal was excited by the 488 nm argon laser with a 500-530 nm emission filter. The laser gain was set to 50 % and laser power ranged from 20-40 % depending on the intensity of the green fluorescence. This laser was switched off before the DsRed2-ER was excited with 543 nm laser with 560-630 nm emission filter; the signal was much weaker in comparison to GFP because the 543 nm laser is a weaker laser than the 488 nm argon laser. Good signals were obtained which did not saturate before the final images (Kir6.1-GFP and DsRed2-ER) were taken sequentially producing a composite image that is a superimposition of the two.

MitoTracker Red compounds and Tetramethylrhodamine, ethyl ester, perchlorate (TMRE) (*Invitrogen, UK*) are red-fluorescent dyes that stain mitochondria in live cells and their accumulation is dependent upon the mitochondrial membrane potential ($\Delta\psi_m$). Mitotracker dyes can diffuse passively across the plasma membrane and concentrate in respiring mitochondria. The probe contains a mildly thiol-reactive choromethyl moiety that is oxidised in mitochondria and this will react with thiols on proteins to form an aldehyde fixable conjugate. The probe was supplied in a vial containing 50 μg of lyophilised solid for reconstitution in high quality DMSO to a make a 1 mM stock solution. TMRE was also supplied as a powder and a 1 mM stock solution was prepared in HEPES-buffered salt solution (physiological solution) composed of (in mM): 156 NaCl, 3 KCl, 2 $MgSO_4$, 1.25 KH_2PO_4, 2 $CaCl_2$, 10 glucose, and 10 HEPES, pH 7.35. The mitochondrial dyes were prepared from stocks stored at -20°C. The 1 mM stock solution of MitoTracker Red was diluted in OptiMEM-1(without phenol red) to a final concentration of 150 nM whereas 1 mM TMRE was diluted to a final concentration of 20 nM in OptiMEM-1. Cells on 25 mm coverslips were first transfected with Kir6.1-GFP

and after the transfection period, the transfection mixture was replaced with cell culture media and cells were left for 24-36 hours before loading with MitoTracker Red for 30 minutes at 37 °C. The Kir6.1-GFP fluorophore was excited with 488 nm laser and the emitted light was collected between 510-530 nm whereas MitoTracker Red was excited using the 543 nm laser and emitted light was detected using long pass filter for fluorescence above 560 nm. Please refer to table 2.1.

2.5.4 Analysing colocalisation and statistical analyses

The images were analysed individually using the Laserpix program. This was able to examine the red, green and merged images separately, cells could be sized individually and thresholds for the red and green pixels were set accordingly. The proportion of colocalisation was measured in each cell and the numbers were given as percentages. The software measured e.g. the total number of existing green pixels (Kir6.1-GFP) which also contained red pixels (DsRed2-ER) and vice versa, see figure 2.4.

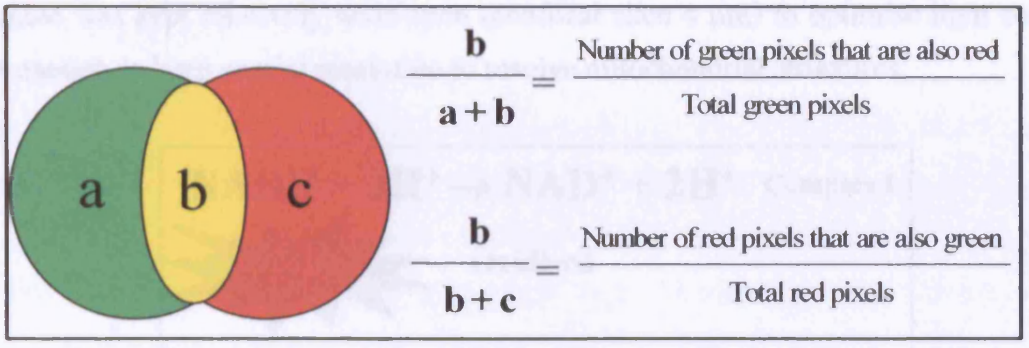

Figure 2.4. A Venn diagram to show how colocalisation is analysed. These pixels represent Kir6.1-GFP (a) and the pixels that represent DsRed2-ER (c) and (b) is the total number of pixels which colocalise.

Approximately 15 good images with at least two to three cells in each field were used in analysing the proportion of colocalisation between Kir6.1-GFP and DsRed2-ER signals. The results (in percentages) were put into a table and analysed using the statistical package Prism 4.0. The Mann Whitney test (rank scoring) was used to compare the proportion of colocalisation between Kir6.1-GFP and DsRed2-ER signals against a theoretical value of zero. The null hypothesis (H_o) where '*There is no colocalisation*

between Kir6.1-GFP and DsRed2-ER signals'. The probability value (p-value) was compared to a significance level and if it was smaller, the null hypothesis was rejected. For example, the null hypothesis was rejected at the 5 % significance level, this was reported as "$p < 0.05$". The results are presented as medians and interquartile ranges.

2.5.5 Investigating changes in mitochondrial redox state and mitochondrial membrane potential (Zeiss LSM 510 Confocal Microscope)

Mitochondrial redox state was monitored by measuring NADH (nicotinamide adenine dinucleotide) and FAD^{2+} (flavin adenine dinucleotide) autofluorescence. These two variables were measured nearly simultaneously on the Zeiss 510 CLSM confocal microscope switching between excitation at 364 nm measuring fluorescence at 435-485 nm for NADH, to excitation at 458 nm measuring fluorescence at >505 nm for FAD^{2+}. See figure 2.5. This is a good system as it minimises photo bleaching and produces good image with minimal background noise by using a high numeric aperture objective. The pinhole was kept relatively wide open (confocal slice 4 μm) to optimise light collection but enough to keep spatial resolution to resolve mitochondrial structures.

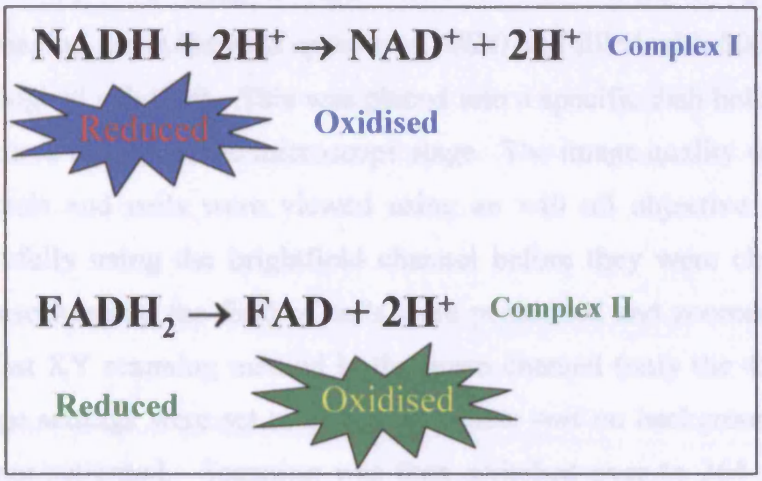

Diagram 2.5. A diagram to show the oxidised and reduced forms of redox agents in the mitochondria. The reduced form of NAD, NADH is fluorescent whereas the oxidised form of FAD^{2+} is the fluorescent form.

2.5.6 Preparation of cells and physiological solution

The immortalised skeletal muscle cell line C2C12s were cultured for 1-2 days before they used for taking mitochondrial redox state and mitochondrial membrane potential measurements. After the centrifugation step, the cells were evenly distributed evenly into a 6 well plate already prepared with 22 mm coverslips (*VWR, UK*). The cells were left to grow at 37°C for 24-48 hours before they were used. The rat primary ventricular myocytes were grown on laminin coverslips in M199 medium. These cells were used a few hours after isolation or the day after (*These were generously provided by Dr. Sean Davidson, Hatter institute, UCL*). The cells were studied using physiological HEPES-buffered salt (HBSS) solution composed of (in mM): 156 NaCl, 3 KCl, 2 $MgSO_4$, 1.25 KH_2PO_4, 2 $CaCl_2$, 10 glucose, and 10 HEPES, pH 7.35.

2.5.7 Procedure for imaging cells

The 22 mm coverslips containing the cells were removed carefully using fine forceps and placed in an imaging dish (*Harvard apparatus, USA*) and filled with 500 µl of recording media (physiological solution). This was placed into a specific dish holder before it was placed and secured tightly on the microscope stage. The image quality was set to at least 512 x 512 pixels and cells were viewed using an x40 oil objective. The cells were positioned carefully using the brightfield channel before they were checked for green (FAD^{2+}) fluorescence and the field of cells were positioned and zoomed in accordingly by using the fast XY scanning method in the green channel (only the 458 nm laser was on). The image settings were set to ensure that there was no background noise and the signals were not saturated. Scanning was then switched over to 364 nm UV laser to measure NAD fluorescence in the blue channel. Both lasers were turned on before the experiment was started on the time series mode. The images were taken every 5 seconds with the final image being an average of two images because this would produce a high quality image with little background noise. Each drug such as diazoxide was applied and

mixed carefully with a Gilson pipette and the times were noted using the markers on the Zeiss software. To ensure that the cells were viable, the 'resting levels' of fluorescence in each population were calibrated to the maximally oxidised and maximally reduced states as an index of the resting redox state. A fully reduced state is induced by sodium cyanide (NaCN). After washing off NaCN a fully oxidised state by Carbonyl cyanide 4-(trifluoromethoxy) phenylhydrazone (FCCP). Both NaCN and FCCP were purchased from *Sigma Aldrich, UK*. It is the reduced NADH that is the fluorescent form, observed as blue autofluorescence whereas oxidised FAD is observed as green autofluorescence.

To measure the changes in mitochondrial membrane potential ($\Delta\psi_m$), there are many types of commercial mitochondrial dyes available that will label live mitochondria. The commonly used compounds are Tetramethylrhodamine methyl ester perchlorate (TMRM) and Tetramethylrhodamine ethyl ester perchlorate (TMRE). These dyes are use for the quantitative measurements of the mitochondrial membrane potential ($\Delta\psi_m$) based on the Nernst equation. The advantage with these dyes is that they do not form aggregates in cell membranes and interact with membrane proteins minimally. The transmembrane distribution of the dyes is directly related to the membrane potential via Nernst equation. The C2C12 cell line was loaded with 20 nM TMRM (made up in physiological solution) for 30 minutes at 37 °C before imaging. In the case of the rat primary ventricular myocytes, these were loaded with 20 nM TMRM for approximately 1 hour to allow full equilibration of the dye before confocal analysis. The 543 nm laser was used to excite TMRM and images were taken every second in order to observe the changes in $\Delta\psi_m$.

2.5.8 Analysing the changes in mitochondrial redox state and $\Delta\psi_m$

The images were saved as LSM image files. For each experiment, regions of interest (ROI) were selected from each cell in the field and the measurements for the changes in NADH and FAD^{2+} or TMRM fluorescence were saved as text files. These text files were imported into Origin 6.0 for further analysis where the data were normalised using a macro. The data were averaged and presented as means $\pm$ SEM (arbitrary units) so that any changes in signal observed would be observed as a percentage change (increase or

decrease when compared to the basal level). The data for changes in TMRM fluorescence were presented as individual traces so that changes such as mitochondrial depolarisation in response to the drugs could be observed. One-way ANOVA with Dunnett's post test was carried out on NADH, FAD^{2+} or TMRM measurements to compare the control value with the values taken in response to each drug application.

2.6 Procedure for SDS polyacrylamide gel electrophoresis (PAGE)

The methods listed in 2.6 were taken from protocols for SDS PAGE and Western blotting The apparatus for pouring the gels were set up as described in the BioRad manual (*BioRad Laboratories, Hemel Hempstead, UK*). All gels were prepared with a thickness of 1.5 mm. The resolving gel was prepared and polymerisation was initiated with 100 µl 10% Ammonium persulfate (APS) and 20 µl N, N, N', N'-Tetramethylethlyenediamine (TEMED) (*Sigma Aldrich, UK*). APS was made up in 1ml distilled water and stored at 4 °C. The gel mixture was mixed gently by inverting the tube before it was poured between two glass plates. A small volume of distilled water or room temperature isopropanol was added to the top of the gel to prevent it from being exposed to the air. This was left for an hour to polymerise and the water/isopropanol was removed carefully using filter paper. The stacking gel was prepared and mixed carefully before it was poured on top of the resolving gel. A 10 well plastic comb was inserted in between the plates to form wells where samples would be loaded. The stacking gel was left for 30 minutes for it to set. The components for the resolving and stacking gel are listed in table 2.2.

Table 2.2. A table to show the materials required to make the resolving and stacking gels.

Materials Required	**10 % Resolving Gel**	**4 % Stacking Gel**
30 % solution of 29:1 acrylamide: Bisacrylamide	6.6 ml	1.3 ml
0.5 M TrisHCl, pH 6.8	-	2.5 ml
1.5 M TrisHCl, pH 8.8	5 ml	-
10 % SDS (w/v)	0.1 ml	0.1 ml
10 % APS	100 µl	50 µl
TEMED	20 µl	13 µl
dH_20	8 ml	6.1 ml
Final volume	20 ml	10 ml

2.6.1 Preparation of samples and running SDS PAGE

The cells required were grown in T25 flasks until they were 80-90 % confluent before they were washed twice with PBS. One ml of PBS was used, along with a cell scraper (*VWR, Merck house, UK*) to dislodge the cells from the flask and they were collected in eppendorf tubes. The samples were centrifuged at 14,000 rpm for 5 minutes. The supernatant was removed and the cell pellet was resuspended in 300 µl of PBS and 300 µl of 6x gel loading buffer containing 200 mM dithiothreitol (DTT) (*Sigma Aldrich, UK*). The samples were heated at 95 °C for 5 minutes and sonicated for about 5 seconds using a Soniprep 150 probe sonicator (MSE). The denatured samples were kept on ice or stored at -20 °C until required. The gel plates were fixed onto the SDS PAGE apparatus as per instructions and placed into a tank filled with fresh running buffer (this was made from 25 mM Tris, 250 mM glycine, 0.1 % SDS, pH 8.3).

Prior to loading, the combs were removed and each well was washed with running buffer using a 5 ml syringe and needle. Five µl of pre-stained broad range molecular weight marker (*BioRad Laboratories, Hemel Hempstead, UK)* was loaded in the first lane of the gel, followed by 25 µl of each samples. The maximum volume for each well is 40 µl. The gel tank lid was assembled and voltage was supplied using a power pack at a constant voltage of 40 V for 20 minutes through the stacking gel. It was increased to 120 V for 1.5 hours until the dye from the marker had reached the bottom of the glass plate.

2.6.2 Transferring proteins onto nitrocellulose and immunoblotting

In order to transfer protein onto nitrocellulose for western blotting, a cassette was prepared and the gel was cut and placed in transfer buffer. The cassette had a layer of sponge, 2x filter paper, SDS gel, followed by nitrocellulose (*Hybond ECL, Amersham-Pharmcia Biotech, UK*) cut to size and then another layer of 2x filter followed by another sponge. This was assembled tightly, removing any air bubbles and secured into the cassette. The cassette was placed into its holder and placed into a tank containing transfer buffer (48 mM tris, 39 mM glycine, 0.03 % (w/v) SDS, 20 % (w/v) methanol, pH

8.3). The tank was connected to the power supply and the transfer was carried out at 250 mA for 2 hours at 4°C to prevent the apparatus from overheating because it could cause air bubbles to form and disrupt the transfer of proteins from gel to nitrocellulose. After the transfer, the nitrocellulose membranes were removed from the cassettes (the appearance of the prestained marker indicated a successful transfer). These were cut to size and placed into appropriate chambers with labels.

Membranes were first incubated in blocking solution containing 5 % (w/v) Non-fat milk (*Marvel, Premier brands, UK*) in PBS + 0.1 % Tween-20 (*Sigma Aldrich, UK*) (PBST) on a shaker for 1 hour at room temperature. The primary antibody was added to the membranes at typical dilution of 1:500 and 1:2000 in blocking solution and left on a shaker at 4 °C overnight. After incubation with the primary antibody, the membranes were washed three times in PBST for 15 minutes followed by two quick washes. The secondary antibody used was Horseradish peroxidase linked anti-rabbit IgG (supplied in ECL kit) used at a dilution of 1:5000 and this was applied to membranes for 1 hour at room temperature (on shaker). After incubation with horse radish peroxidase (HRP) antibody, the membranes were washed five times in PBST for 15 minutes then followed by four quick washes before they were visualised using ECL reagents and film (Hyperfilm ECL) (*Amersham-Pharmcia Biotech, UK*). Both short and long exposures were obtained.

2.7 Production of polyclonal antibodies

Polyclonal antibodies were synthesised to aid the study of K_{ATP} sensitive potassium channels. The polyclonal antibodies to Kir6.1 were raised using two methods; one using a rat peptide sequence to generate antibodies against Kir6.1C (78A), this was already purified and characterised by our group. The second method chosen employed a maltose binding protein (MBP) fusion protein to generate Kir6.1 antibodies. My contribution to this part of the study was to purify and characterise a MBP Kir6.1C fusion antibody called MBP-Kir6.1C (93A). For this antibody, the first step was to express the MBP-Kir6.1C protein in *E.coli* competent cells followed by the purification of the expressed

protein. This protein was subsequently injected into a rabbit to allow the production of MBP-Kir6.1C antibodies. The rabbit would produce antibodies to both MBP and Kir6.1C therefore when the animal was culled the serum collected at the end of the study was affinity purified to obtain Kir6.1C antibodies.

2.7.1 The expression and purification of MBP Kir6.1C fusion protein

The plasmid DNA, pMALc2x + Kir61C terminus (a/a 179-424) was transformed into *E.Coli* BL21 (DE3) competent cells and plated on LB agar plates containing carbenicillin. A single colony was picked and placed into 10 ml of rich broth media (RB) and carbenicillin (RB composed of 10 g tryptone, 5 g yeast extract, 5 g NaCl and 2 g glucose (*all from Sigma Aldrich, UK)* dissolved in 1 litre of distilled water and autoclaved). This starter culture was placed in a shaking incubator for 12-16 hours before 5 ml was used to inoculate 2x 500 ml flasks containing RB media with 100 μg/ml carbenicillin. The cells were grown for a further 2-3 hours until the OD at 600 nm had reached 0.6 to 0.8 absorbance units. A 1ml sample was taken for analysis and the resulting cell pellet was resuspended in SDS loading buffer and stored at -20 °C. Once the cells had reached 0.6 to 0.8 nm, the fusion protein was induced with 0.3 mM iso-propylthiogalactosidase IPTG (*Promega, UK*) and the cells were grown for a further 12-16 hours, shaking at 25 °C. Before centrifugation, 1 ml supernatant was centrifuged and processed as before. The contents of the flasks were centrifuged at 6,000 rpm for 30 minutes at 4 °C. After centrifugation, the supernatant was discarded and the pellet was resuspended in 25 ml of PBS + 5 mM EDTA + 1 mM DTT and subsequently stored at -20 °C. The pellet was thawed in a waterbath for 10 minutes then sonicated for 5 x 60 seconds. The pellet was centrifuged at 12,000 rpm at 4 °C for 30 minutes before the supernatant was removed and kept on ice. The pellet was resuspended in 8 ml MBP column buffer (PBS + 5 mM EDTA + 1 mM DTT) and was centrifuged and sonicated again to ensure all of the protein was collected. The supernatant from both samples were pooled and stored on ice and a sample was taken for analysis.

The MBP fusion protein was affinity purified using an amylose resin. The amylose resin was supplied as a slurry in ethanol (*New England Labs, UK*), it was mixed gently before 10ml was applied to a Poly-Prep chromatography column (*BioRad Laboratories, UK*). The slurry was left to settle in the column before it was equilibrated using 8-10 column volumes (CV) of MBP column buffer. The supernatant containing MBP-Kir6.1C protein was diluted in the buffer 1:4 before loading onto the column. It was washed with 12 CVs of MBP column buffer. The packed amylose-protein mixture was resuspended with PBS + 5 mM EDTA in a 1:1 ratio and a sample was taken for analysis. The column was stored at 4°C until it was required. The coupling efficiency was checked by taking a small sample (20 µl) before and after the protein was coupled to the amylose resin by using the Bradford assay and SDS PAGE. The samples collected were subjected to SDS PAGE analysis to determine whether the fusion protein had been produced efficiently. Finally, the MBP-Kir6.1C protein was eluted by washing the column with 10 mM maltose in PBS buffer. A sample of this MBP-Kir6.1C protein was sent to *Eurogentec, Belgium* where it was used to invoke an immune response of a susceptible animal. The pre-immune serum was taken before the MBP Kir6.1C protein was injected into the rabbit. The serum was collected at the peak of antibody production at 17 weeks where the rabbit was culled and the terminal bleed stored at -80 °C.

2.7.2 Coupling MBP to amylose resin: Depleting MBP antibodies

The MBP-Kir6.1C fusion protein would evoke the rabbit to produce antibodies to MBP and Kir6.1C therefore the contaminating antibodies to MBP were first removed by affinity chromatography. The terminal bleed (serum) was thawed out on ice before it was applied to the column. The terminal bleed (~150 ml) was centrifuged at 2,000 G at 4 °C for 15 minutes. This step was essential because it removed red blood cells and general cell debris. A MBP affinity resin was prepared by coupling purified MBP (5 mg/ml) to the amylose resin, as described by the manufacturer (*Bio-Rad Laboratories, UK*). The serum was then applied to the equilibrated amylose column and the flowthrough containing the Kir6.1C antibodies were collected and stored on ice. The MBP antibodies will bind to the MBP-amylose resin, and therefore is not present in the flowthrough.

2.7.3 Affinity purification of Kir6.1 antiserum on affi-gel/protein column

Affi-Gel 10 is an N-hydroxysuccinimide ester of agarose gel beads supplied in 1:1 slurry in isopropanol. The total concentration of MBP-Kir6.1C fusion protein used in the coupling reaction was 1.5mg/ml which was prepared in a solution of 100mM HEPES pH 7.4 (*Sigma Aldrich, UK*). One ml of Affi-Gel 10 was transferred into a Buchner funnel, washed twice with cold distilled water before the protein was placed into the funnel. The affi-gel/protein mixture was transferred to eppendorf tubes and placed on a rotating wheel for 1 hour at room temperature before it was left rotating overnight at 4 °C. The mixture was then centrifuged at 16,000 g for 1 minute at 4 °C. The gel was resuspended in an equal volume of Tris Buffered Saline, TBS (50 mM Tris base, 150 mM NaCl, 5 mM KCL, pH 7.4) which contained 0.01 % (w/v %) sodium azide (*All supplied by Sigma Aldrich, UK).* This affi-gel/protein mixture was transferred to a new column and prepared with a series of washes: Five CVs of $NaCHCO_3$, two CVs of Na_2CO_3, two CV of distilled water, two CV of 0.3 M Glycine HCL at pH2 and three CVs of TBS.

The flowthrough was placed into the column and collected before it was applied straight into the affi-gel/protein resin for a second time to ensure the maximum yield of the antibody was collected. This was followed by a series of washes in the following order: 5 CV of TBS, 10 CV of TBS + 0.2 % Triton-X-100 followed by another five CV of TBS. The antibody acid fractions were eluted using 5 ml acidic buffer (0.2 M NaCl, 0.2 M Glycine HCl, pH 2.5) and collected in 1 ml fractions in tubes already containing 100 µl 2 M Tris HCL, pH 8.5. The absorbance of these fractions were measured at 280 nm using a spectrophotometer and fractions with an absorbance between 0.04 to 0.1 nm were pooled together. In most cases, three to four acid fractions were pooled together and stored on ice. The column was washed with ten CV of TBS before the antibody containing fractions were eluted by collection of 1 ml aliquots with 5 ml Guanidine HCL, 0.1 M TrisCl pH 8. The antibody was located in the acid fraction but guanidine fractions were kept in case acid fractions were low, the guanidine fractions could be used less sparingly. The column was washed with TBS and stored in TBS + 0.01 % NaN_3. The pooled acid and guanidine fractions were dialysed with 500 ml TBS + 0.01 % sodium

azide in a beaker with a stirring bar overnight at 4 °C. The samples were then placed into centrifuge tubes and spun at 100,00 g at 4 °C to remove excess aggregated substances. The purified antibody was aliquoted and stored at -80 °C until required. See figure 2.6.

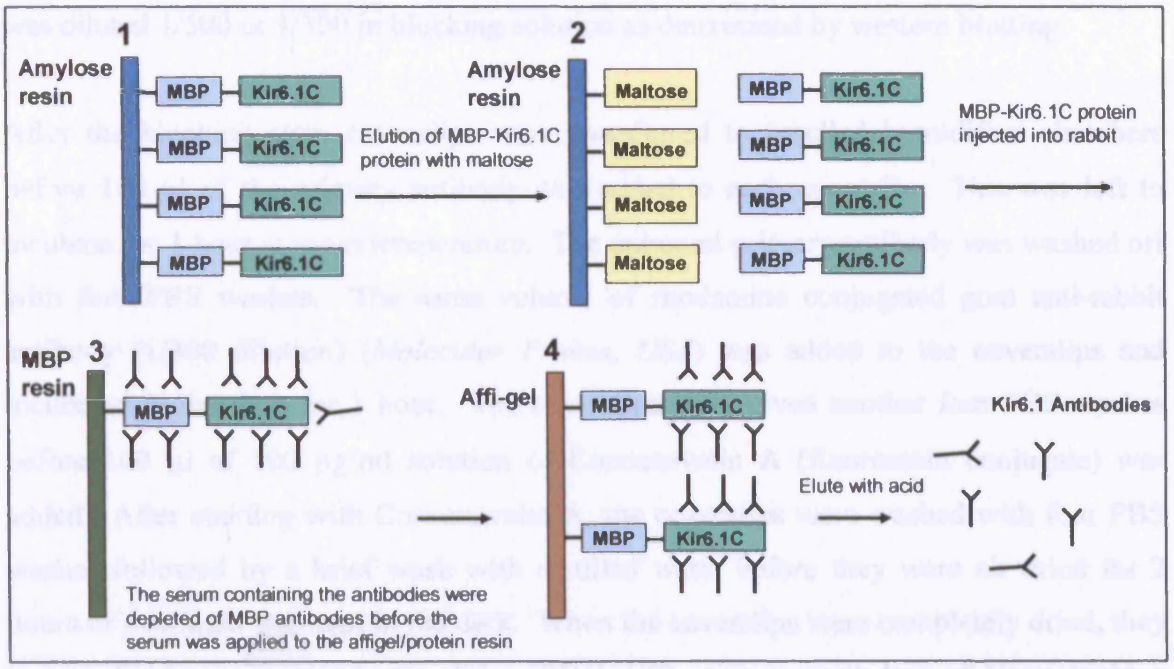

Figure 2.6. A schematic diagram to show the various steps during the production of our MBP-Kir6.1C antibody.

2.8 Immunofluorescent staining

2.8.1 Procedure for immunofluorescent staining

Cells were co stained with K_{ATP} channel subunits Kir6.1 specific antibodies and reagents that specifically stain the endoplasmic reticulum. The endoplasmic reticulum was stained using a fluorescein conjugate of Concanavalin A (*Molecular Probes, USA).* The cells were grown in 6 well dishes with five 13 mm coverslips (*VWR, Merck house, UK*) in each well. The cells were at least 60-70 % confluent before staining. The cells were washed twice with phosphate buffered saline, PBS, before they were fixed for 20 minutes at 4 °C with 4 % (vol/vol) paraformaldehyde (PFA). The cells were washed twice for 10 minutes with PBS before they were incubated for 20 minutes with PBS + 0.2 % Triton X-100 (*Sigma Aldrich, UK*) to permeabilise the cells. After this step, the solution was aspirated and cells were washed twice with PBS before they were incubated at 4 °C for 1

hour with blocking solution containing 2 % BSA, 5 % goat serum, and 0.1 % triton X-100 in PBS. During the blocking step, the appropriate primary antibodies were prepared in blocking solution and stored on ice. The affinity purified primary antibody, for Kir6.1 was diluted 1/500 or 1/300 in blocking solution as determined by western blotting.

After the blocking step, coverslips were transferred to labelled humidified chambers before 100 µl of the primary antibody was added to each coverslip. This was left to incubate for 1 hour at room temperature. The unbound primary antibody was washed off with four PBS washes. The same volume of rhodamine conjugated goat anti-rabbit antibody (1/300 dilution) (*Molecular Probes, USA*) was added to the coverslips and incubated in the dark for 1 hour. The coverslips were given another four PBS washes before 100 µl of 100 µg/ml solution of Concanavalin A (fluorescein conjugate) was added. After staining with Concanavalin A, the coverslips were washed with four PBS washes followed by a brief wash with distilled water before they were air dried for 2 hours or overnight and kept in the dark. When the coverslips were completely dried, they were individually mounted onto slides (*BDH, UK*) using a small drop of Vectashield, a non-fluorescent anti-fade specialised mounting medium (*Vector Laboratories, USA*) and fixed into position with clear nail varnish. The slides were stored at 4 °C before analysis.

The slides were analysed using a BioRad Confocal imaging system. Controls were also used to ensure that the fluorescent signals visualised were from the purified antibody for Kir6.1 and the antibody was not bound to any endogenous protein in the cell. The controls used were the pre immune serum samples before rabbits were immunised with the antigen and a fusion protein bound onto the antibody of interest. The fusion protein was used at 1mg/ml for immunoflourescence and depending on the protein concentration, the correct volume of the fusion protein (1 mg/ml) was taken and spun at 14,000 rpm at 4 °C for 5 minutes. The supernatant was removed and 1 ml blocking solution + 10 mM Maltose was added to the pellet, this was spun again for 15 minutes. The supernatant was discarded and the antibody at the correct dilution (1:500) was added to the sample and put onto a rotating wheel for 1 hour before it was used. In some experiments, we stained

for mitochondria using cytochrome C oxidase antibody therefore I used two different fluorescently tagged (Rhodamine or FITC) secondary antibodies to identify the proteins.

2.8.2 Analysing fluorescently labelled cells

The cells were visualised using 60x water objective and the image quality was set to 1024 x 1024 pixels. The Kalman scan was set to three so that the final image taken would be an average. The Kir6.1 antibody (using a rhodamine conjugated secondary) was excited by the 543 nm laser, the laser powers used were similar to DsRed2-ER analysis. Concanavalin A staining was excited by the argon 488 nm laser, the staining of the endoplasmic reticulum was high so very low laser power was required to see where it localised. The degree of colocalisation between the antibody for Kir6.1 and Concanavalin A was measured using Laserpix as described in section 2.4.

2.9 FLIPR experiments– Investigating the changes in ROS production

The FLIPR Flurometric imaging plate reader system (*Bucher Biotech, Switzerland*) is able to perform high throughput screening in kinetic cellular (adherent and non-adherent cells) assays in 96 well plate format. The argon-ion laser excites a fluorescent indicator dye and the CCD camera images the plate. The laser illumination and cooled CCD optical detection is fast and sensitive with data points taken at each second if required. Sensitivity is further enhanced by the proprietary cell-layer isolation optics that allows signal discrimination on a cell monolayer; this eliminates the extracellullar background fluorescence in the assay. Cells were grown in T75 flasks and passaged 24 hours before the experiment. The cells were counted using a haemocytometer so that approximately 10^6 to 10^7 cells were plated into each of the appropriate wells using a black wall, clear bottom 96 well plates (*Marathon lab supplies, London*). Cells were placed in the incubator overnight at 37 °C to allow them to adhere to the plate surface. The dyes used for measuring changes in ROS are susceptible to photo-oxidation therefore these black, wall, clear bottom plates were used to minimise their exposure to light. By reducing scattered light of all wavelengths, this limits any background artefacts.

2.9.1 Preparation of cells, fluorescent indicator dye and drug plates

There are reactive oxygen species (ROS) detection reagents such as 2'7' dichlorofluorescein (DCF) which is a cell-permanent indicator. The chemically reduced and acetylated forms of DCF are non fluorescent until the acetate groups are removed by esterases and oxidation in the cell. The oxidation of DCF can be detected by measuring the increase in fluorescence using a microplate reader, fluorescent microscope, flurometer or other excitation sources with the appropriate filter for fluorescein (FITC).

DCF-DA (*Invitrogen, UK*) is a light sensitive compound. It was stored at -20 °C and only dissolved immediately prior to use. A 30 μM stock DCF-DA (*Invitrogen, UK*) was prepared by weighing out 15 mg in an eppendorf tube which was dissolved immediately in 1 ml of 100 % ethanol. The final concentration used for the assay was 15 μg/ml which was prepared in PBS. The dye was loaded into each well and placed in the incubator at 37 °C for 1 hour. The cells were then washed twice with PBS and loaded with fresh PBS before the cells were imaged. The drug plates were prepared and loaded in clear 96 well plates (*VWR, UK*) after the cells were loaded with dye. Diazoxide and glibenclamide were prepared as 10x stocks so that when the FLIPR machine transferred the drugs to the cell plate, the final concentrations were correct. The agonist plate contained diazoxide (plate 1) and the antagonist plate contained glibenclamide (plate 2). The final concentration of DMSO in each well was 0.02 % (2.6 mM). Equivalent experiments using DMSO in PBS omitting the pharmacological agents were used as controls.

2.9.2 ROS production assay

The plates were loaded onto the FLIPR system in the order as shown in figure 2.7. The fluorescence was measured first to ensure that the signal was not saturated. The laser power was lowered and adjusted accordingly so that there was room for an increase in fluorescence. The FLIPR system includes an integrated state of the art 96 well pipettor. This was used to aspirate, dispense, and mix precise volumes of fluid from microplates containing the test compounds and the microplate containing cells. The fluorescence

(arbitrary units) was measured and recorded every second with interventions applied at 1, 2 and 3 minutes. The cells were illuminated for a minute before 20 µl of the agonist (diazoxide or PBS+ DMSO) was administered into the cell plate. At 3 minutes, 20 µl of the antagonist (glibenclamide or PBS + DMSO) was applied into the same wells already containing the agonist or control buffer. The conditions investigated were:

1. Control (using control buffer consisting of DMSO and PBS 1:5)
2. 50 µM diazoxide and 10 µM glibenclamide
3. 100 µM diazoxide and 10 µM glibenclamide

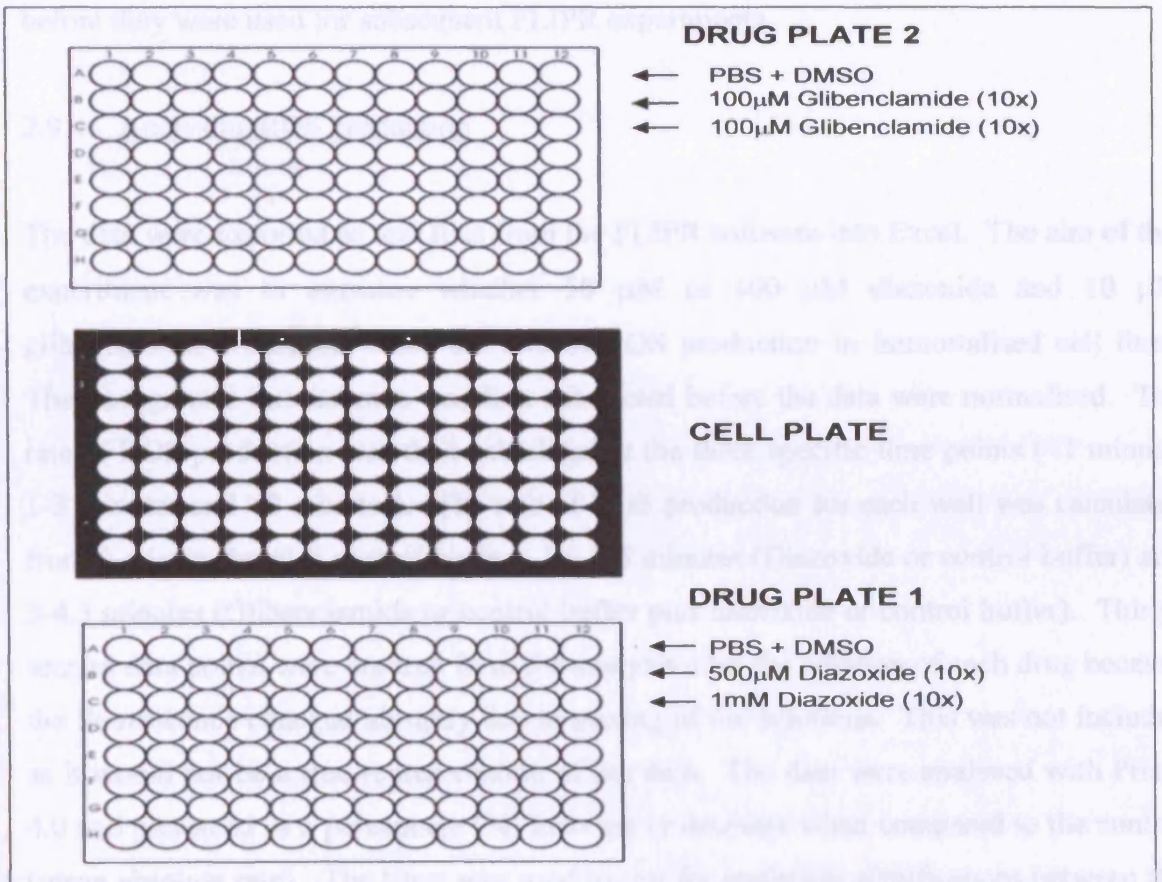

Figure 2.7. A figure to illustrate how the experiment was set up in the FLIPR system.

Drug plate 1 contained the agonist, diazoxide and drug plate 2 contained the antagonist glibenclamide.

2.9.3 Using SiRNA to suppress the expression of Kir6.1

To investigate whether the K_{ATP} channel subunit Kir6.1 was responsible for the potential changes in ROS production, siRNA for Kir6.1 was transfected into the cell lines and the experiment was repeated with the protocol. The siRNA for Kir6.1 was transfected with some eGFP and the mixture was loaded equally into the wells (approximately 100 µl), see section 2.3. A parallel plate was prepared with just siRNA as this plate would be used for the actual assay as eGFP would interfere with the fluorescence measurements. After transfection, the cells were placed in the incubator at 37 °C for at least 12-24 hours before they were used for subsequent FLIPR experiments.

2.9.4 Analysing ROS production

The data were exported as text files from the FLIPR software into Excel. The aim of this experiment was to examine whether 50 µM or 100 µM diazoxide and 10 µM glibenclamide would influence the rate of ROS production in immortalised cell lines. The background fluorescence was first subtracted before the data were normalised. The rate of ROS production was then calculated at the three specific time points (<1 minute, 1-3 minutes and >3 minutes). The rate of ROS production for each well was calculated from 0-<1min (basal + control buffer), 1.5-2.5 minutes (Diazoxide or control buffer) and 3-4.5 minutes (Glibenclamide or control buffer plus diazoxide or control buffer). Thirty-second data points were omitted from the analysis after the addition of each drug because the fluorescence changed abruptly due to mixing of the solutions. This was not included as it would not be a true representation of the data. The data were analysed with Prism 4.0 and presented as a percentage (%) increase or decrease when compared to the control (mean absolute rate). The t-test was used to test for statistical significances between the control and treated groups and for differences, if any, between transfected and non transfected cells, see 2.9.4. The data was significant when $p<0.05$ (*). The data from each cell line and condition were obtained from at least three different preparations.

2.10 Measuring changes in intracellular calcium (Ca^{2+})

2.10.1 The basic principles of Fura-2 AM

Fluorescent Ca^{2+} indicators such as Fura-2 AM are useful tools and provide insight into cell physiology since their manufacture by Roger Tsien in 1980 (*Grynkiewicz et al. 1985, Tsien 1980*). Fura-2 AM is an acetoxymethyl ester that forms a high affinity, intracellular Ca^{2+} indicator that is ratiometric and UV light excitable. AM esters are lipophilic molecules that freely pass through the lipid bilayer. Inside the cell, the ester is cleaved by esterases to form the hydrophilic acid and the indicator becomes localised inside the cell. Two wavelengths were used to excite Fura-2, 340 and 380 nm and the fluorescent emission were monitored > 515 nm. On binding Ca^{2+}, the emission spectrum shifts so that when Fura-2 binds Ca^{2+} as it will increase when excited at 340 nm and decrease when excited at 380 nm. The ratio of emission at 340 and 380 nm was used as an indicator of intracellular Ca^{2+} concentration, $[Ca^{2+}]_i$. Using this ratiometric method for measuring $[Ca^{2+}]_i$ has distinct advantages: for example, the absolute magnitude of the signal is not affected by changes such as dye leakage, which contributes to increased efficiency at measuring changes in $[Ca^{2+}]_i$. See figure 2.8.

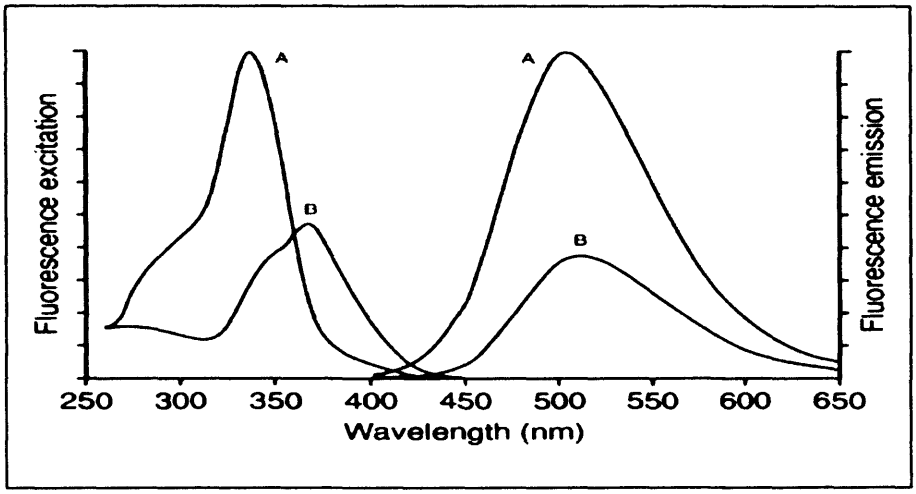

Figure 2.8. Diagram to show the fluorescence excitation (detected at 510 nm) and emission (excited at 340 nm) spectra of Ca^{2+}-saturated (A) and Ca^{2+}-free (B) Fura-2 in pH 7.2 buffer. (The Information was obtained from the Invitrogen website)

2.10.2 Protocol for Ca^{2+} assay and analysing data

Cells were passaged and plated into 6 well plates containing 25 mm coverslips 24 to 48 hours before the experiment. For $[Ca^{2+}]_c$ measurements, cells were loaded for 30 minutes at room temperature with 5 μM fura-2 AM (*Molecular Probes, UK*) and 0.005 % Pluronic (*Sigma Aldrich, UK*) in a HEPES-buffered salt (HBSS) solution composed of (in mM): 156 NaCl, 3 KCl, 2 $MgSO_4$, 1.25 KH_2PO_4, 2 $CaCl_2$, 10 glucose, and 10 HEPES, pH 7.35. This medium was removed and replaced with the same solution without $CaCl_2$ and 0.5 mM EGTA. The cells were left for 15 minutes to de-esterify.

Fluorescence measurements were obtained using a Nikon epifluorescence inverted microscope with a 20x fluorite objective (*Tokyo, Japan*). The excitation light from a Xenon arc lamp was selected using 10 nm bandpass filters centred at 340, 360, and 380 nm housed in a computer-controlled filter wheel (*Cairn Research, Faversham, UK*). The emitted light passed through a long-pass filter to a cooled charged-coupled device (CCD) camera (*Orca ER; Hamamatsu, Welwyn Garden City, UK*). The cells were protected from phototoxicity by interposing a shutter in the light path to limit exposure between the acquisitions of successive images. All imaging data were collected at intervals of 5-10 seconds before they were digitised and analysed using Origin 7.0. The traces were obtained using the cooled CCD imaging system and are presented as ratios of excitation at 340 and 380 nm, both with emission at > 515 nm. All presented data were obtained from at least five coverslips using two to three different cell preparations.

2.11 General statistical analysis

All data in this thesis are presented as mean ± S.E.M (Standard mean of error). The N value indicates the number of cells where the measurements were taken from or the number of times an experiment was carried out. The mean value (μ) is the sum of all the values (x) divided by N, the size of the sample.

$$\bar{X} = \frac{\sum_{n} x_{n}}{n}$$

The sample standard deviation S, is a measure of dispersion, that is to say, a measure of how widely the values in a distribution are spread. The standard deviation of a probability distribution is defined as the square root of the variance S^2. The formula for standard deviation is given below:

$$s = \sqrt{\frac{\sum_{n}(\bar{x}-x_{n})^2}{n-1}}$$

The standard error of a sample of sample size N is the sample's standard deviation is divided by $\sqrt{n-1}$. It therefore estimates the standard deviation of the sample mean based on the population mean. The standard error of the mean is given by:

$$SEM = \frac{s}{\sqrt{n-1}}$$

The data obtained throughout this thesis was analysed using the statistical methods in GraphPad Prism (version 4.0 for Windows) (*Graphpad Software, San Diego California, USA*). For example, the colocalisation experiments examined the distribution of Kir6.1 in the ER. The proportion of colocalisation was measured in each cell and the numbers were given as percentages. The software measured e.g. the total number of existing green pixels (Kir6.1-GFP) which also contained red pixels (DsRed2-ER) (Vice versa). The results were compared against a theoretical value of zero and the null hypothesis where 'There is no colocalisation between Kir6.1 and ER pixels' was rejected when $p<0.05$. From my observations, every cell had some colocalisation therefore I carried out

a rank scoring test (Mann-Whitney) to show the degree of colocalisation was significant. The data were presented as medians with the 25 % and 75 % interquartile ranges.

The Student's t-Test was carried out to assess for statistical differences between two sets of data and to determine if two sample means were equal. For example, to test if a new treatment is significantly different to the previous (control) treatment. In chapter 3.4, ROS production was measured in the presence of diazoxide and glibenclamide. The means of the control and the treatment groups were compared and the null hypothesis (H_o) was rejected if the means were significantly different. The formula for the t-Test is given by:

$$t = \frac{\bar{x}_1 - \bar{x}_2}{\sqrt{\frac{s_1^2}{n_1} + \frac{s_2^2}{n_2}}}$$

The probability value (p-value) of a statistical hypothesis test is the probability of getting a value of the test statistic as extreme as or more extreme from the parameter specified in the null hypothesis H_o. The p-value was compared to a significance level and if it was smaller, the null hypothesis was rejected. For example, if the null hypothesis were to be rejected at the 5% significance level, this would be reported as "$p < 0.05$". The use of this test requires non random sampling and assumes that the two populations have the same variances. Therefore the unpaired t test should not be used if there is a significant difference between the variances of the two samples.

The one-way ANOVA (ANalysis Of VAriance) with a Bonferonni post-test was employed to test for significant differences in data with three or more groups. ANOVA allows us to compare several groups of observations, all of which are independent but possibly with a different mean for each group. The ANOVA method relies heavily on the assumption that the populations have equal variances, independent errors and a normal distribution. The Dunnett's test is a specialised multiple comparison test that compares a single control group to all other groups several dependent or independent statistical tests are being performed simultaneously. Significant differences between data are indicated as follows: NS $p \geq 0.05$, significant * $p \leq 0.05$, ** $p \leq 0.01$ and *** $p \leq 0.001$.

3.0 RESULTS

3.1 Characterising K_{ATP} subunit DNA constructs, Kir6.1 antibodies and small interfering RNA (siRNA) for Kir6.1 for colocalisation and functional studies

In this chapter I will discuss how molecular tools such as K_{ATP} channel subunit cDNA constructs, antibodies and siRNA for Kir6.1 were characterised. It is important that these tools were characterised first because they were essential for investigating the distribution and function of Kir6.1 in subsequent colocalisation and functional studies.

3.1.1 *Characterising K_{ATP} channel subunit cDNA constructs*

The first aim of this project was to investigate the distribution of the ATP sensitive potassium channel subunit Kir6.1 in cardiac and skeletal muscle cell lines. K_{ATP} channel subunits were subcloned into the pcDNA family of vectors (see methods and materials). Although the K_{ATP} channel cDNA constructs were previously generated in the laboratory (*Cui et al. 2001*). The K_{ATP} channel cDNA constructs were used in colocalisation studies whilst other cDNAs such as dominant negatives were used in functional studies which will be discussed in detail in the relevant chapters.

3.1.1.1 K_{ATP} channel cDNA constructs

The majority of the cDNA constructs were provided to our laboratory as gifts, whereas the DsRed-2 ER vector was purchased commercially from *Clontech, UK*. Rat Kir6.1 and mouse Kir6.2 cDNAs were kind gifts from Professor S. Seino (*Chiba University, Japan*). Hamster SUR1 cDNA was kindly donated by Dr. J. Bryan (*Bayor College of Medicine, Houston, USA*) and mouse SUR2B cDNA was kindly provided by Professor Y. Kurachi (*Osaka University, Japan*). The species the original cDNA K_{ATP} subunit clones were derived from, along with the Genbank accession number are listed in table 3.1. The majority of the colocalisation work in this chapter investigated the distribution of Kir6.1 using a cDNA construct called Kir6.1-GFP where the C terminus of Kir6.1 was fused to

GFP (eGFP-N1 vector, see 2.1.8). The subcloning of Kir6.1 to the eGFP-N1 vector was carried out in two parts, firstly, inserting part of Kir6.1 sequence into eGFP-N1 vector before amplifying the rest of the Kir6.1 sequence by PCR. These different strategies were employed to reduce the possibility of introducing mutations into Kir6.1-GFP. This is because mismatched pairs can occur during the amplification process which may result in the miscorporation of nucleotides during PCR.

Table 3.1. A table to show vector and species details of cDNA constructs used throughout this thesis.

cDNA construct (species)	**Vector**	**Genbank accession number**
Kir6.1 (Rat)	pcDNA3.1/Zeo	NM_017099
Kir6.2 (mouse)	pcDNA3.1/Zeo	NM_010602
SUR1 (Hamster)	pcDNA3	L40623
SUR2B (Mouse)	pcDNA3	D86038

The tetrameric nature of K_{ATP} channels is significant as one gene product can co-assemble with others to form heteromultimeric channels. It is this distinct characteristic of K_{ATP} channels which allows us to explore protein function by using dominant negatives (DN) for Kir6.1 (*Tinker et al. 1996*). A DN contains a genetic mutation where the gene encodes mutant polypeptides that when overexpressed will interfere with the activity of the wild-type gene (*Herskowirz 1987*). The DNs for Kir6.1 were generated using site directed mutagenesis and were previously used in earlier studies to examine the heteromultimerisation of the Kir6.0 family (*Cui et al. 2001*). The mutations were introduced to the highly conserved pore regions of Kir6.1. The DN were named Kir6.1DN G→S (GFG to SFG) and Kir6.1DN G→A (GFG to AFA). The K_{ATP} channel cDNA constructs used throughout this study were used to either create stable cell lines or in transfection experiments. At the start of my PhD, the original cDNAs were already available in the laboratory but these were re-transformed and plasmid DNA was purified by standard midi or maxi preparation. Table 3.2 lists the vectors the cDNAs were cloned into and the specific restriction enzymes used for diagnostic digest to excise specific DNA fragments expected from their restriction maps.

Table 3.2. A table to show the cDNAs used throughout this thesis.

The cDNAs samples were digested with their specific enzymes for approximately one hour at 37°C. Some samples were double digests e.g. Kir6.1 with *BamHI/Not I*, this sample was first digested with *Apa I* and incubated at 25°C for one hour before the second enzyme was added.

cDNA construct	**Vector**	**Restriction digest**	**DNA fragment/s**
Kir6.1	pcDNA3.1/Zeo	*Bam HI/Not I*	5 kb & 2 kb
Kir6.2	pcDNA3.1/Zeo	*Bam HI/Xba I*	5 kb & 1.6 kb
Kir6.1-GFP	eGFP-N1	*Not I*	6.2 kb
Kir6.2-GFP	eGFP-N1	*Not I*	5.6 kb
Kir6.1 DN G → A	pcDNA3	*Bam HI/Apa I*	5.4 kb & 2 kb
Kir6.1 DN G → S	pcDNA3	*Bam HI/Apa I*	5.4 kb & 2 kb
SUR1	pcDNA3	*Not I*	5.4 kb & 4.5 kb
SUR2B	pcDNA3	*Not I*	5.4 kb & 5 kb
DsRed2-ER	DsRed-2 ER	*Xho I*	4.7 kb

Figure 3.1 shows the restriction digests of the cDNAs (Maxi preparations) used throughout this thesis. The DNA molecular weight marker VII (*Roche Diagnostics, Germany*) was used to determine the fragment size of the samples in all the restriction digests (lane 1). The *BamHI* enzyme was used to digest both Kir6.1 and Kir6.2 cDNAs as this would completely linearise the plasmids, if this was a single digest, this would produce a characteristic 7.0 kb fragment. For Kir6.1, *Not I* would cut that linear fragment giving the exact size of the Kir6.1 insert which is about 2.0 kb; there is also a larger 5.0 kb fragment which is the pcDNA3.1/Zeo vector as shown in lane 2. The Kir6.2 insert was smaller in size compared to Kir6.1; therefore *Xba I* was used to cut the 7.0 kb DNA fragment, giving a 1.6 kb fragment in lane 3 which migrated further down the agarose gel. There is also a 5.0 kb fragment for the pcDNA3.1/Zeo vector as in the Kir6.1 digest. Both Kir6.1 and Kir6.2 were fused to GFP via their C terminus. The original eGFP-N1 vector is 4.9 kb in size, together with the Kir6.1 insert (1.3 kb) the total size of Kir6.1-GFP would be about 6.2 kb as shown in lane 4. The digest for Kir6.1-GFP was cut once with *Not I* enzyme which linearised the plasmid producing a large fragment at the 6.0 kb mark. A linear fragment in lane 5 was also achieved with Kir6.2-GFP and *Not I*, the only difference is that the size as the Kir6.2 insert is smaller than Kir6.1 so the total fragment size shown in the gel in lane 5 is approximately 5.6 kb. A *Bam HI/Apa* I digest was set

up for both Kir6.1 DN samples in lanes 6 and 7. These enzymes were used to clone Kir6.1 into pcDNA3.0 therefore after restriction digest, two bands corresponding to the insert and the vector would be expected. The pcDNA3 vector is slightly larger in size (5.4 kb) compared to its family member pcDNA3.1/Zeo (5.0 kb) but the insert would be 2.0 kb in size, exactly the same as the original Kir6.1 insert. The gel shows that more DNA was digested in the Kir6.1G→A sample.

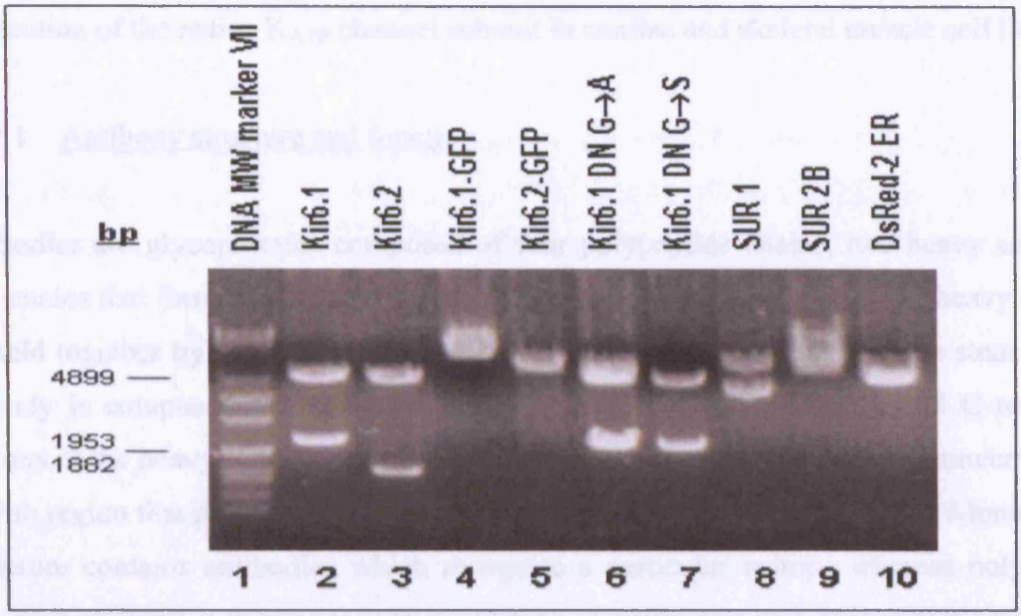

Figure 3.1. Restriction digests of cDNAs containing specific K_{ATP} subunits, their fluorescently tagged equivalents, dominant negatives and DsRed2-ER vector on a 0.8% agarose gel.

Both SUR1 and SUR2B samples were digested with *Not I* enzyme which cuts the plasmid DNA twice to produce two characteristic fragments. Firstly in lane 8 (SUR1), one fragment is 5.4 kb belonging to linearised pcDNA3 with another fragment at 4.5 kb which is the size of the SUR1 insert. The SUR protein is much larger in than inward rectifying (K_{IR}) proteins; this is reflected in the size of the insert. The SUR2B digest in lane 9 has what appears to be a large fragment of DNA at around the 5-5.0 kb mark. This is probably the combination of the pcDNA3 vector and the SUR2B insert as they migrate to a similar position on the gel because they are so similar in size. Finally, the DsRed2-ER vector which was bought commercially was digested with *Xho I* as this was sufficient to linearise the plasmid DNA producing a large fragment at 4.7 kb in lane 10.

3.1.1 *The characterisation of Kir6.1 antibodies using cloned subunits in stably transfected HEK293 cells*

The production of Kir6.1 channel subunit antisera and its characterisation using cloned K_{ATP} channel subunits stably expressed in HEK293 cells will be discussed in this chapter. This is of importance because these antibodies will be used to investigate the endogenous distribution of the native K_{ATP} channel subunit in cardiac and skeletal muscle cell lines.

3.1.2.1 Antibody structure and function

Antibodies are glycoproteins composed of four polypeptide chains, two heavy and two light chains that form a Y-shaped structure. The light and N terminus of the heavy chains are held together by disulphide linkages that form the arms of the Y and the stem of the antibody is composed of the C terminus of the heavy chain. The N and C terminal portions of the heavy chains are stabilised by a flexible region which allows movement of the Fab region that allows the antibody to bind to antigens in different ways. Monoclonal antiserum contains antibodies which recognise a particular epitope whereas polyclonal antiserum contains a heterogeneous population of antibodies that recognise a variety of epitopes. Polyclonal antibodies obtained from affinity purification will recognise epitopes on the antigen used to illicit the immune response but they will not all recognise the same epitope on the antigen.

The Kir6.1 antibodies I have used throughout my studies were affinity purified from polyclonal antiserum and protein-containing fractions were pooled and dialyzed against the column buffer before the acid fractions were stored at -80°C (see methods and materials 2.7). Two Kir6.1 antibodies were purified and characterised for this study, one was raised against a C terminal peptide sequence of rat Kir6.1 called Kir6.1C (78A) corresponding to amino acids 399 to 420, a terminal cysteine was added for coupling purposes (RRNNSSLMVPKVQFMTPEGNQC). This antibody had been previously purified and characterised by our group (*Cui et al. 2001*). My main contribution was the purification of an antibody which was raised against a fusion protein consisting of

maltose-binding protein with the C terminus of rat Kir6.1 (amino acids 179–424) called MBP-Kir6.1C (93A) (*Quinn et al. 2003*).

3.1.2.2 Antibody characterisation

I performed Western blotting to determine the specificity of the Kir6.1 antibodies before they were used to stain for endogenous Kir6.1 in immortalised cell lines. The antibodies were characterised using cell lysates from HepG2, HEK293 and stable lines Kir6.1/SUR2B and Kir6.2/SUR2B, see figure 3.2. The anti-Kir6.1 antibodies (78A and 93A) both detect a band of approximately 48 kDa in the Kir6.1/SUR2B stable cell line. In figure 3.2A, the Kir6.1C (78A) antibody used at 1:5000 detected a single band at 48 kDa in the Kir6.1/SUR2B stable cell line. I tested the same antibody at a higher concentration (1:100) and detected the same band in my stable cell line but the antibody also recognised other proteins of higher molecular weight in the samples, see figure 3.2B. In figure 3.2C, I tested the MBP-Kir6.1C (93A) antibody at 1:1000 with my cell lysates. This antibody detected a strong band in the stable cell line Kir6.1/SUR2B with a molecular weight of 48 kDa. It also detected other proteins in stable cell line Kir6.2/SUR2B, this may be due to the fact that there is some overlap between the C terminus sequence of Kir6.1 and Kir6.2 so my antibody detected other proteins in the lysates. HEK293 cells were used as a control because they do not appear to express native Kir6.1 (or Kir6.2) (*Cui et al.2001*).

Antibodies that are sensitive in immunofluorescent staining may not necessary be sensitive in immunoblot analysis. The cell lysates used were stained with Coomassie blue for all proteins present in the sample as shown in D. Our group had limited aliquots of the affinity purified Kir6.1C antibody (78A) so this was used sparingly for immunofluorescent staining. This was very sensitive and only detected a specific band (48 kDa) corresponding to Kir6.1. However, the results showed that the MBP-Kir6.1C (93A) antibody detected Kir6.1 as well as perhaps Kir6.2 and other non specific proteins.

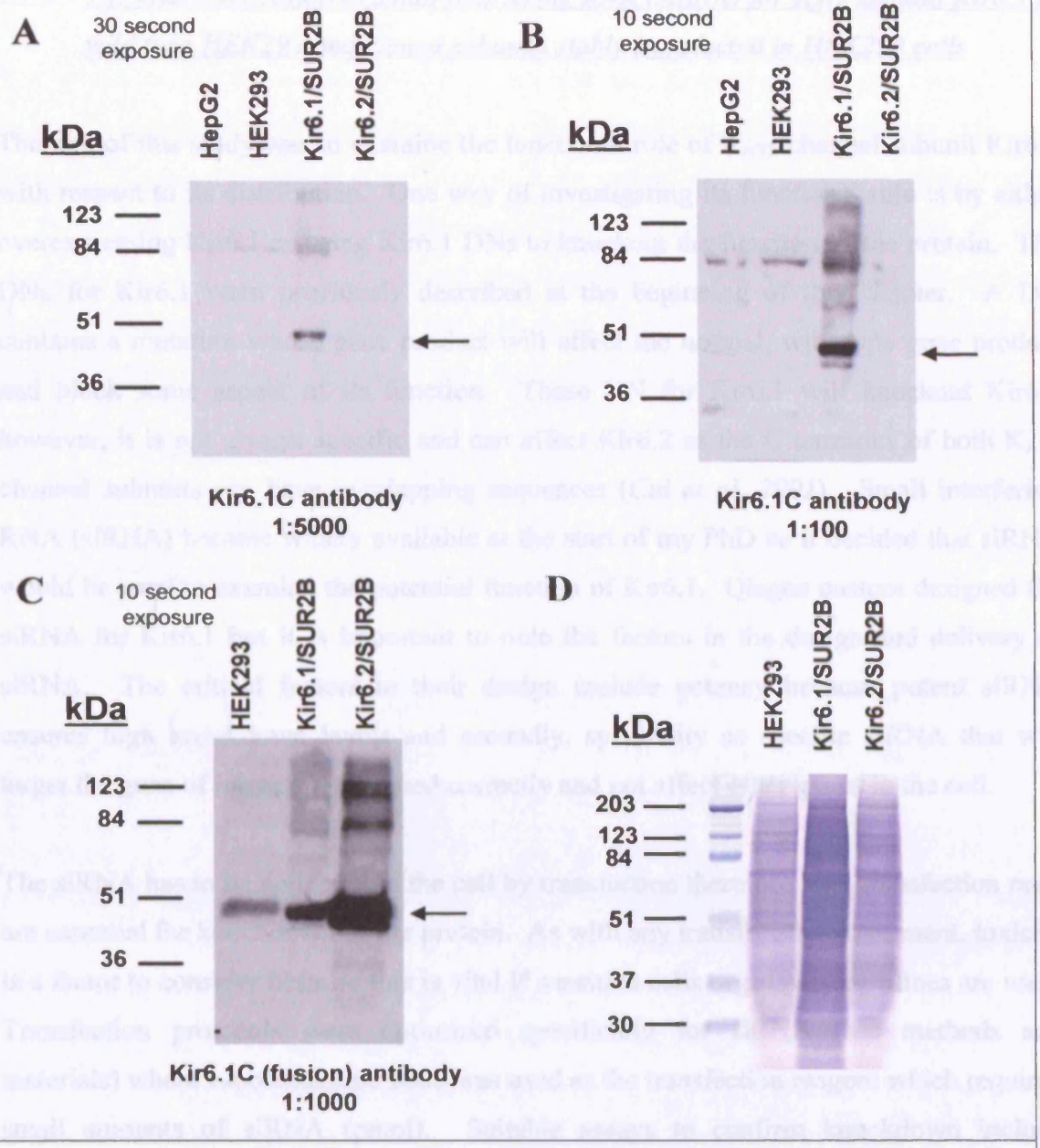

Figure 3.2. Characterisation of Kir6.1 antibody by SDS-PAGE and Western blotting.

A. Kir6.1C (78A) antibody at 1:5000 detected a band at 48 kDa in HEK Kir6.1/SUR2B.
B. Kir6.1C (78A) antibody at 1:1000 detected the same band at 48 kDa in HEK Kir6.1/SUR2B cell lysate. Non specific proteins were also detected.
C. MBP-Kir6.1 (93A) antibody at 1:1000 detected Kir6.1 as 48 kDa band in Kir6.1/SUR2B cell lysate but also detected other proteins in the other samples.
D. Coomassie staining of cell lysates

3.1.3 *The characterisation of small interfering RNA (siRNA) for K_{ATP} subunit Kir6.1 in wild type HEK293 and cloned subunits stably transfected in HEK293 cells*

The aim of this study was to examine the functional role of K_{ATP} channel subunit Kir6.1 with respect to its distribution. One way of investigating its functional role is by either overexpressing Kir6.1 or using Kir6.1 DNs to knockout the function of the protein. The DNs for Kir6.1 were previously described at the beginning of this chapter. A DN contains a mutation whose gene product will affect the normal, wild-type gene product and block some aspect of its function. These DN for Kir6.1 will knockout Kir6.1 however, it is not always specific and can affect Kir6.2 as the C terminus of both K_{ATP} channel subunits can have overlapping sequences (*Cui et al. 2001*). Small interfering RNA (siRNA) became widely available at the start of my PhD so it decided that siRNA would be used to examine the potential function of Kir6.1. Qiagen custom designed the siRNA for Kir6.1 but it is important to note the factors in the design and delivery of siRNA. The critical factors in their design include potency because potent siRNA ensures high knockdown levels and secondly, specificity as specific siRNA that will target the gene of interest if designed correctly and not affect other genes in the cell.

The siRNA has to be delivered to the cell by transfection therefore high transfection rates are essential for knockdown of the protein. As with any transfection experiment, toxicity is a factor to consider because this is vital if sensitive cells or primary cell lines are used. Transfection protocols were optimized specifically for siRNA (see methods and materials) where Lipofectamine 2000 was used as the transfection reagent which required small amounts of siRNA (pmol). Suitable assays to confirm knockdown include quantitative real-time RT-PCR which confirms knockdown and confirmation at the mRNA level and Western blot analysis and other methods of protein expression which shows knockdown at the protein level. The latter method was used in this study to analyse Kir6.1 protein knockdown.

3.1.3.1 Synthesising siRNA for Kir6.1

The whole nucleotide sequences for Kir6.1 for rat, mouse and human species with accession numbers were first located using Genbank nucleotide database, see table 3.3. The siRNA target sequences were located in the mouse, rat and human genome. using NCBI BLAST (*Basic Local Alignment Search Tool*) which finds regions of local similarity between sequences. The program compares nucleotide or protein sequences to sequence databases and calculates the statistical significance of matches. BLAST can also be used to identify members of gene families or similar genes in different species.

Table 3.3. The accession number and name of Kir6.1 gene in rat, mouse and human.

Species	Accession Number	Name
Rat	NM_017099	Rattus norvegicus potassium inwardly-rectifying channel, subfamily J, member 8 (Kcnj8)
Mouse	NM_008428	Mus musculus potassium inwardly-rectifying channel, subfamily J, member 8 (Kcnj8),
Human	NM_004982	Homo- sapiens potassium inwardly-rectifying channel, subfamily J, member 8 (KCNJ8)

Preliminary experiments characterising the silencing effects of siRNA (duplex 1 and 2 known as 61siRNA duplex 1 or 2) for Kir6.1 showed that duplex 2 was far more effective because it knocked down protein expression by 95 % (see results). BLAST was used to find out where the target sequence was located in the gene in each species. The 61siRNA duplex 2 target sequence was located in mouse and rat Kir6.1 DNA sequence with 100 % match but there were two mismatched base pairs in the human sequence so duplex 2 would not work in my human cell lines. The target sequences were present both in mouse and rat because the two species have 95 % homology between them whereas there is 89 % homology between rat and human so there is more chance that mismatched pairs would occur. However, the 61siRNA duplex was only specific to rat and mouse Kir6.1 gene so could only be used to knockdown native Kir6.1. For example, this was used in the C2C12 skeletal muscle cells as the original Kir6.1 gene which was subcloned

into the eGFP-N1 vector was derived from rat DNA. The table 3.4 shows the exact sequences in the siRNA duplexes.

Table 3.4. A table to show the DNA sequence of the siRNA for Kir6.1. The siRNA are compatible in both rat and mouse.

61siRNA data	**Duplex 1 (Rat and Mouse)**	**Duplex 2 (Rat and Mouse)**
Target name	61siRNA duplex 1	61siRNA duplex 2
Target sequence	5' CAC CAC CTT GGT AGA CCT GAA 3'	5' CAG GAA GAG CAT CAT CCC GGA 3'
Sense	r(CCA CCU UGG UAG ACC UGA A)dTdT	r(GGA AGA GCA UCA UCC CGG A)dTdT
Antisense	r(UCC AGG UCU ACC AAG GUG G)dTdG	r(UCC GGG AUG AUG CUC UUC C)dTdG
nmol/Tube	20 nmol	20 nmol

To perform functional studies, separate siRNA for human Kir6.1 gene was synthesised to accommodate later functional studies using human HepG2 and HEK293 cell lines. (The original siRNA for Kir6.1 for rat and mouse were synthesised as HiPerformance 2-For-Silencing siRNA Duplexes so came at 20 nmol whereas the siRNA for human Kir6.1 was synthesised individually at 5 nmol). See table 3.5 for the target sequence.

Table 3.5. A table to show the DNA sequence of siRNA for Kir6.1. This siRNA is specific for human Kir6.1 gene.

61siRNA data	**Duplex 1 (Human)**
Target name	61siRNA
Target sequence	5' GAG GTG GTT CCT ATT CAC CAA 3'
Sense	r(GGU GGU UCC UAU UCA CCA A)dTdT
Antisense	r(UUG GUG AAU AGG AAC CAC C)dTdC
nmol/Tube	5 nmol

From the nucleotide database, the human Kir6.1 gene is 2381 base pairs long. Part of the human sequence is shown below with the target sequence in table 3.4 highlighted. This is the target sequence for siRNA for human Kir6.1.

Homo-sapiens potassium inwardly-rectifying channel (KCNJ8) *NM_004982*

961	TCATGTTCCG	AGTGGGTGAC	CTGAGGAAAA	GCATGATCAT
	TAGTGCCTCT	GTGCGCATCC		
1021	AGGTGGTCAA	GAAAACAACT	ACACCTGAAG	**GGGAGGTGGT**
	TCCTATTCAC	**CAA**CTGGACA		
1081	TTCCTGTTGA	TAACCCAATC	GAGAGCAATA	ACATTTTTCT
	GGTGGCCCCT	TTGATCATCT		

3.1.3.2 How does siRNA target genes?

In eukaryotes, protein coding genes are transcribed from the DNA template by RNA polymerase II enzyme. The pre-mRNAs are processed to form mature mRNAs which are transported from the nucleus where the mRNA code is translated on the ribosome to a specific amino acid sequence encoding a protein. RNA interference (RNAi) occurs in a wide variety of eukaryotic organisms and regulates endogenous gene expression. It is a form of post-transcriptional gene silencing where double stranded RNA (dsRNA) causes the degradation of endogenous mRNA transcripts resulting in the reduction or loss of gene activity. RNA interference was initially discovered in the nematode *Caenorhabditis elegans* where long double stranded RNA sequences were injected into the worm's gonad (a standard procedure used to introduce transgenes into worms) and these were found to inhibit protein translation by targeting genes partially complementary to the 3' untranslated region of the mRNAs. Gene silencing is triggered by the presence of dsRNAs, these can vary in length and origin can arise in the cell from a variety of sources, including virus replication and hybridization of homologous transcripts from repetitive DNA sequences (transposons). There are three main steps in the mechanism of gene silencing by double stranded RNA: The first step involves processing the double stranded RNA to form siRNA, followed by the formation of the RNA-induced silencing complex (RISC). Finally, the RISC complex prevents protein synthesis because it cleaves the target mRNA sequence. This is outlined in figure 3.3.

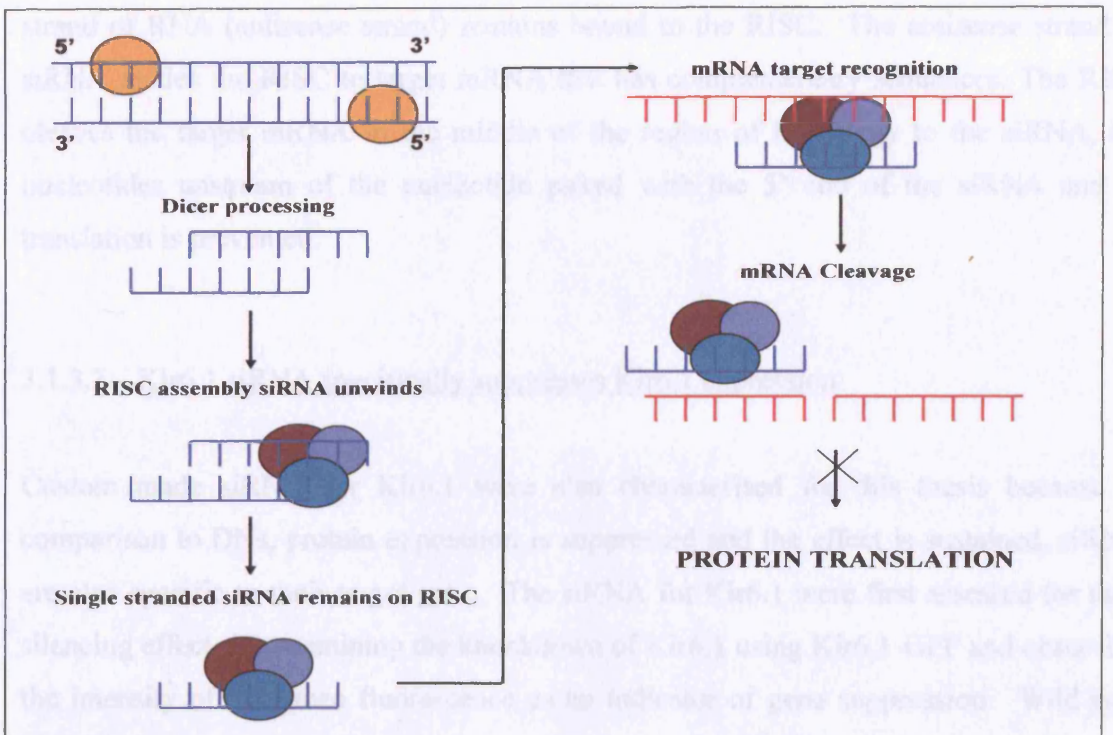

Figure 3.3. A diagram to show the steps involved in the mechanism of gene silencing.

Small double-stranded RNAs arise in the cell from a variety of sources, including virus replication, hybridisation of homologous transcripts from repetitive DNA sequences such as transposons, and introduction of synthetic siRNA into the cell in an experiment. Double stranded RNAs are first processed to form siRNAs, after processing the RISC complex is assembled. This causes siRNA to unwind and binds to a single strand. Finally this complex targets complementary mRNAs which are cleaved therefore preventing protein translation. (*This information was obtained from the Qiagen website*).

The first step of gene silencing is the processing of longer dsRNAs into siRNAs of characteristic size and structure. Long dsRNA is recognized and processed by a member of the RNase-III family of endonuleases called Dicer which contains catalytic RNAse III and dsRNA-binding proteins (dsRBDs). Processing of dsRNAs by Dicer yields RNA duplexes of approximately 21 nucleotides and 2-nucleotide 3'-end overhangs (siRNAs). After processing, a ribonucleoprotein complex called RISC (RNA-induced silencing complex) is assembled. There are many components of the RNA silencing machinery that have not been identified yet but there is an unidentified nuclease called 'Slicer' that is part of this protein complex. During RISC assembly, siRNAs unwind and a single

strand of RNA (antisense strand) remains bound to the RISC. The antisense strand of siRNA guides the RISC to target mRNA that has complementary sequences. The RISC cleaves the target mRNA in the middle of the region of homology to the siRNA, ten nucleotides upstream of the nucleotide paired with the 5' end of the siRNA and so translation is prevented.

3.1.3.3 Kir6.1 siRNA specifically suppresses Kir6.1 expression

Custom made siRNA for Kir6.1 were also characterised for this thesis because in comparison to DNs, protein expression is suppressed and the effect is sustained, siRNA are also specific to their target gene. The siRNA for Kir6.1 were first assessed for their silencing effects by examining the knockdown of Kir6.1 using Kir6.1-GFP and observing the intensity of the green fluorescence as an indicator of gene suppression. Wild type HEK293 cells were transiently transfected with Kir6.1-GFP with SUR2B in the presence of siRNA for Kir6.1 duplex 1 or 2. These cells were chosen because they contain very little or no Kir6.1 so that the effect of siRNA could be quantified. Cells were imaged about 36 hours after transfection. Separate images were captured, one for green fluorescence (Kir6.1-GFP) and one for brightfield. Cells were healthy after transfection with cell populations at similar confluence. This experiment was repeated at least three times.

The result for this experiment is displayed in figure 3.4. The control cells in A were transfected at high efficiency with Kir6.1-GFP and SUR2B. In the second experiment cells were also co-transfected with siRNA for Kir6.1 (duplex 1), see figure 3.4B. There is a substantial knockdown of Kir6.1 of 50 % in comparison to the control cells. In the presence of 61siRNA duplex 2, the expression of Kir6.1 was also suppressed, refer to figure 3.4C. However, this is more significant then the first duplex as there is about 95 % knockdown of Kir6.1-GFP fluorescence. The brightfield image show that the cells are clearly visible and healthy therefore the decrease in fluorescence is due to the presence of 61siRNA.

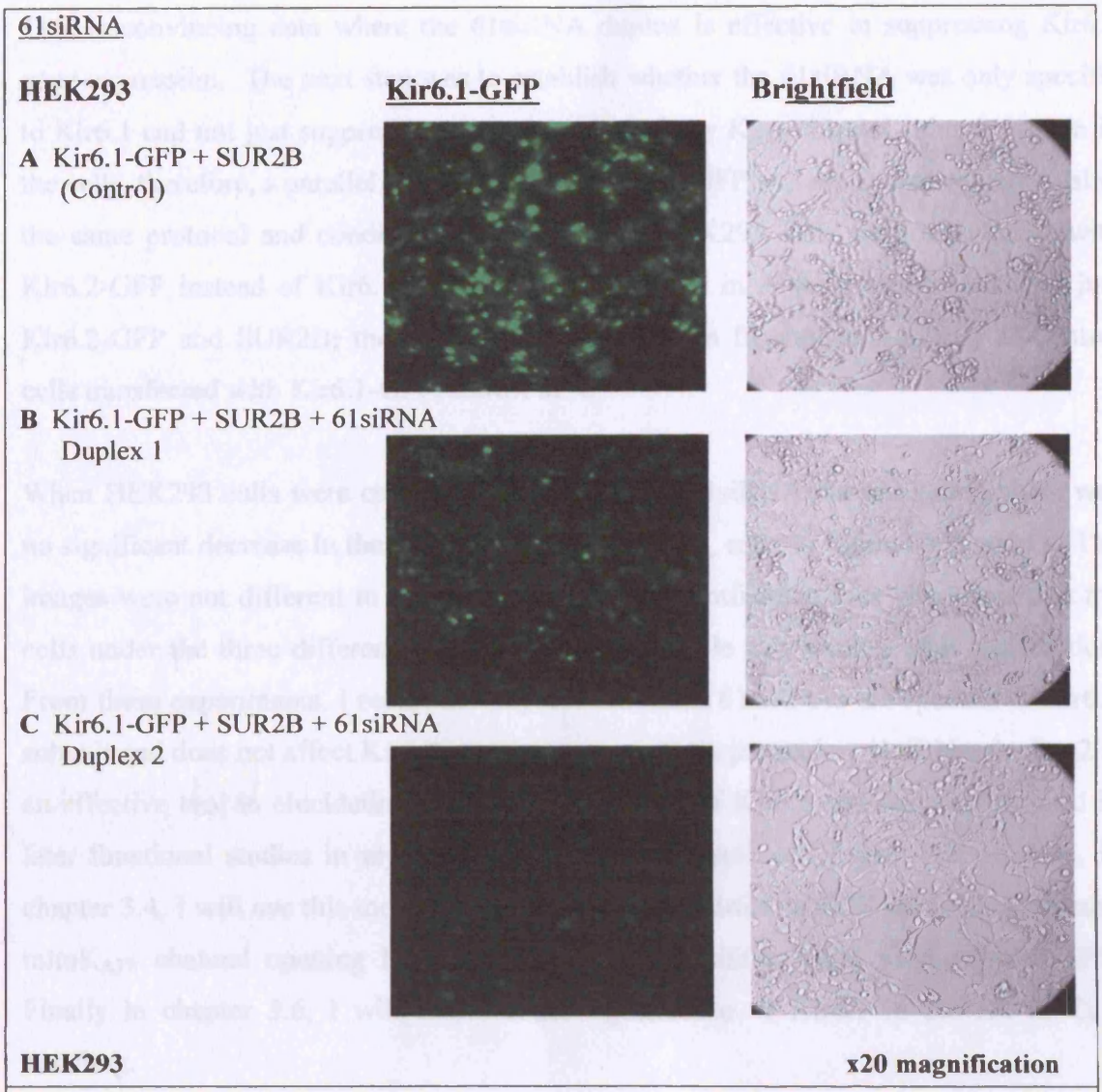

Figure 3.4. 61siRNA duplex 1 and 2 and gene silencing in HEK293 cells.

Images to show the silencing effect of siRNA for potassium channel subunit Kir6.1. HEK293 cells were cultured into 6 well plates with MEM containing only 10 % FBS and were 40-50 % confluent on the day of transfection. The cells were transfected using Lipofectamine 2000 with Kir6.1-GFP, sulfonylurea subunit SUR2B and siRNA for Kir6.1 (Duplex 1 or 2) at a concentration of 20 pmol/µl. The cells were left to incubate for approximately 36 hours before they were imaged.

A. The control cells were transfected with Kir6.1-GFP and SUR2B (without siRNA).
B. Cells transfected with 61siRNA duplex 1 show a decrease in Kir6.1-GFP expression.
C. Cells transfected with 61siRNA duplex 2 had pronounced knockdown of Kir6.1-GFP (95 %). The brightfield images in all cases show that cells are healthy and not affected by the transfection process.

This is convincing data where the 61siRNA duplex is effective in suppressing Kir6.1 gene expression. The next step was to establish whether the 61siRNA was only specific to Kir6.1 and not just suppressing the expression of any K_{ATP} channel subunit protein in the cells, therefore, a parallel experiment using Kir6.2-GFP was set up and repeated using the same protocol and conditions. In figure 3.5, HEK293 cells were transfected with Kir6.2-GFP instead of Kir6.1-GFP. The control cells in A were transfected with just Kir6.2-GFP and SUR2B; these cells have bright green fluorescence similar to control cells transfected with Kir6.1-GFP, shown in A.

When HEK293 cells were co-transfected with either 61siRNA duplex 1 or 2, there was no significant decrease in the expression of Kir6.2-GFP, refer to figure3.5 B and C. The images were not different to the control cells; the brightfield images also show that the cells under the three different conditions were all viable and healthy after transfection. From these experiments, I report that my custom made 61siRNAs are specific to Kir6.1 subunit and does not affect Kir6.2 protein expression. In particular, 61siRNA duplex 2 is an effective tool in elucidating the potential function of Kir6.1 and this will be used in later functional studies in my cardiac and smooth muscle cell lines. For example, in chapter 3.4, I will use this tool to examine the role of Kir6.1 in ROS production because mitoK_{ATP} channel opening has been proposed to facilitate ROS production in IPC. Finally in chapter 3.6, I will examine the significance of Kir6.1 in the ER in Ca^{2+} handling.

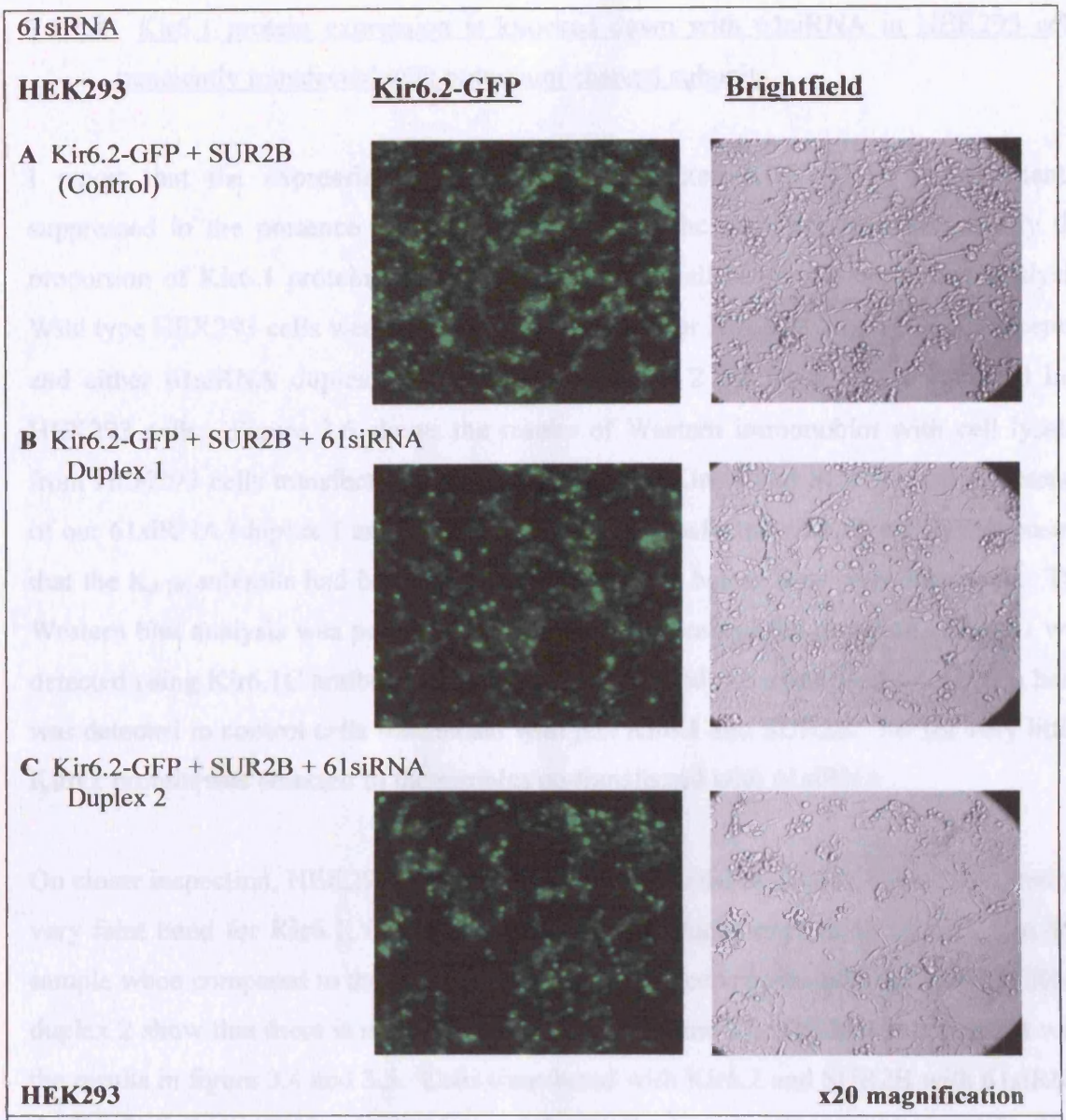

Figure 3.5. 61siRNA duplex 1 and 2 and gene silencing in HEK293 cells.

Images to show the effect of siRNA for potassium channel subunit Kir6.1. HEK293 cells were cultured as described in Figure 5.2. This is to show that the siRNA for Kir6.1 was only specific to the Kir6.1 subunit and not Kir6.2.

A. The control cells transfected with Kir6.2-GFP and SUR2B (without 61siRNA).

B. Cells transfected were with 61siRNA duplex 1 show green fluorescence (therefore expression of Kir6.2). The number of transfected cells is the same as in a.).

C. Cells transfected with 61siRNA duplex 2. Again, the siRNA had no effect on the expression of Kir6.2.

3.1.3.4 Kir6.1 protein expression is knocked down with 61siRNA in HEK293 cells transiently transfected with potassium channel subunits

I report that the expression of transiently transfected Kir6.1-GFP is significantly suppressed in the presence of siRNA for Kir6.1. The next step was to quantify the proportion of Kir6.1 protein knockdown using our 61siRNA by Western blot analysis. Wild type HEK293 cells were transfected with Kir6.1 or Kir6.2 subunit, SUR2B receptor and either 61siRNA duplex 1 or 2. No more than 2 μg DNA was transfected into HEK293 cells. Figure 3.6 shows the results of Western immunoblot with cell lysates from HEK293 cells transfected with either Kir6.1 or Kir6.2 and SUR2B in the presence of our 61siRNA (duplex 1 and 2). Cells were also transfected with 50 ng GFP to ensure that the K_{ATP} subunits had been transfected efficiently before they were harvested. The Western blot analysis was performed with these samples and the presence of Kir6.1 was detected using Kir6.1C antibody (78A) which was already characterised. A 48 kDa band was detected in control cells transfected with just Kir6.1 and SUR2B. No (or very little) Kir6.1 protein was detected in the samples co-transfected with 61siRNA.

On closer inspection, HEK293 cells transfected with 61siRNA duplex 1 (lane 2) contain a very faint band for Kir6.1, indicating that there is reduced expression of Kir6.1 in that sample when compared to the control in lane 1. Those cells co-transfected with 61siRNA duplex 2 show that there is no Kir6.1 in that sample (lane 3). The blot is consistent with the results in figure 3.4 and 3.5. Cells transfected with Kir6.2 and SUR2B with 61siRNA duplex 2 do not contain any Kir6.1 protein at all so no bands were detected in these samples (lanes 4-6). As shown in figure 3.4, 61siRNA does not affect theKir6.2 expression because it is specific to Kir6.1, therefore my Kir6.1 antibody did not detect any bands in these samples.

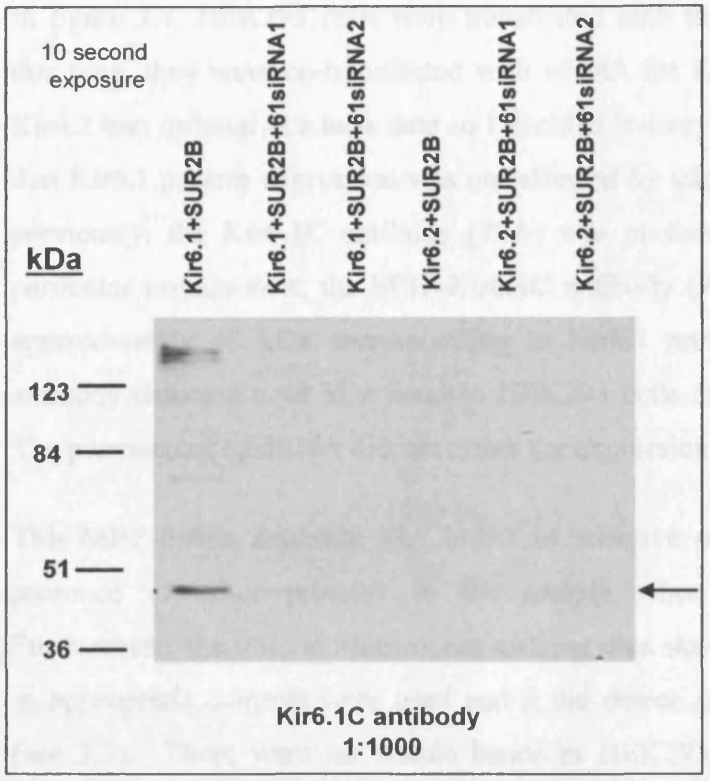

Figure 3.6. The effect of 61siRNA duplex 1 and 2 on Kir6.1 protein expression.

Western blot of HEK293 lysates, these were transiently transfected with Kir6.1/Kir6.2 with SUR2B and 61siRNA (Duplex 1 or 2). The molecular weight of the marker is shown on the left (kDa). The Kir6.1C antibody (78A) was used to detect Kir6.1 (1:1000). A band at 48 kDa is detected in samples transfected with Kir6.1 and SUR2B

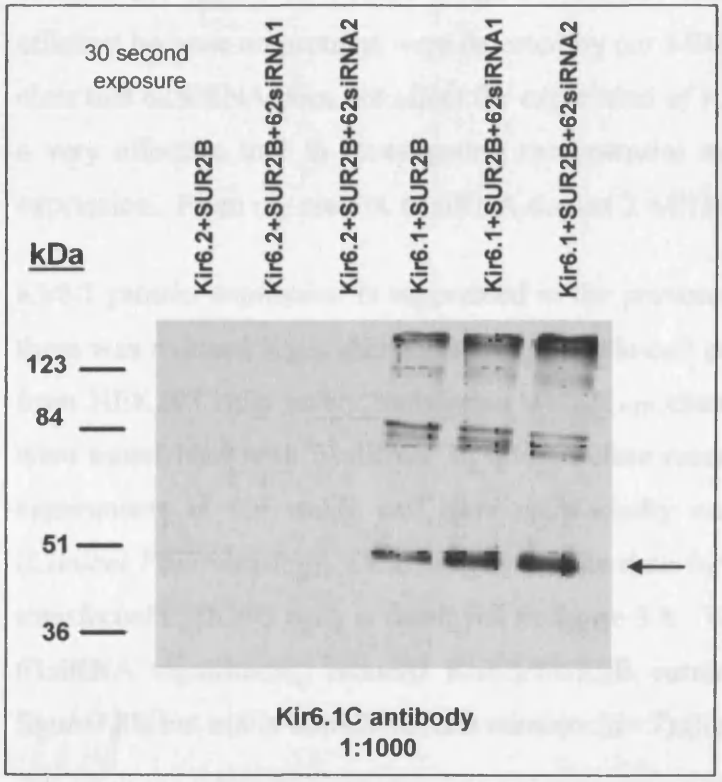

Figure 3.7. The effect of 62siRNA duplex 1 and 2 on Kir6.1 protein expression.

Western blot of HEK293 lysates, these were transiently transfected with Kir6.1/Kir6.2 with SUR2B and 62siRNA (Duplex 1 or 2). The molecular weight of the marker is shown on the left (kDa). The Kir6.1C antibody (93A) was used to detect Kir6.1 (1:1000). The antibody detected a band at 48 kDas which is consistent for Kir6.1.

In figure 3.7, HEK293 cells were transfected with the same K_{ATP} channel subunits but this time, they were co-transfected with siRNA for Kir6.2 (62siRNA). The siRNA for Kir6.2 was ordered at a later date so I decided to carry out a parallel experiment to prove that Kir6.1 protein expression was not affected by silencing Kir6.2 gene. As mentioned previously, the Kir6.1C antibody (78A) was in short supply at this time so for this particular immunoblot, the MBP-Kir6.1C antibody (93A) was used to detect a band of approximately 48 kDa corresponding to Kir6.1 protein. According to the blot, the antibody detected a 48 kDa band in HEK293 cells transfected with Kir6.1 (lanes 4-6). The presence of 62siRNA did not affect the expression of Kir6.1.

This MBP-fusion antibody 93A is not as selective as the 78A because it detected the presence of other proteins in the sample when used at higher concentrations. Furthermore, the immunofluorescent staining data showed that this antibody was reliable as appropriate controls were used and it did detect endogenous Kir6.1 in my cell lines (see 3.3). There were no visible bands in HEK293 cells transfected with the Kir6.2 subunit, see lanes 1-3. These samples were not contaminated and transfections were efficient because no proteins were detected by our MBP-Kir6.1C antibody (93A) and it is clear that 62SiRNA does not affect the expression of Kir6.1. To summarise, 61SiRNA is a very effective tool in investigating the potential role of Kir6.1 by knocking out its expression. From my results, 61siRNA duplex 2 will be used for functional assays.

Kir6.1 protein expression is suppressed in the presence of 61siRNA but to confirm that there was reduced K_{ATP} channel activity, whole-cell patch clamp recordings were taken from HEK293 cells stably transfected with K_{ATP} channel subunits (control). The cells were transfected with 61siRNA 36 hours before recordings were taken. The patching experiments in our stable cell lines were kindly carried out by Dr. Kathryn Quinn (*Clinical Pharmacology, UCL, London*). The data for Kir6.1/SUR2B currents in stably transfected HEK293 cells is displayed in figure 3.8. Whole cell currents were taken and 61siRNA significantly reduced Kir6.1/SUR2B currents (n= 8), see figure 3.8A and figure3.8B but not in Kir6.2/SUR2B currents (n= 7) (figure 3.8C and figure 3.8D).

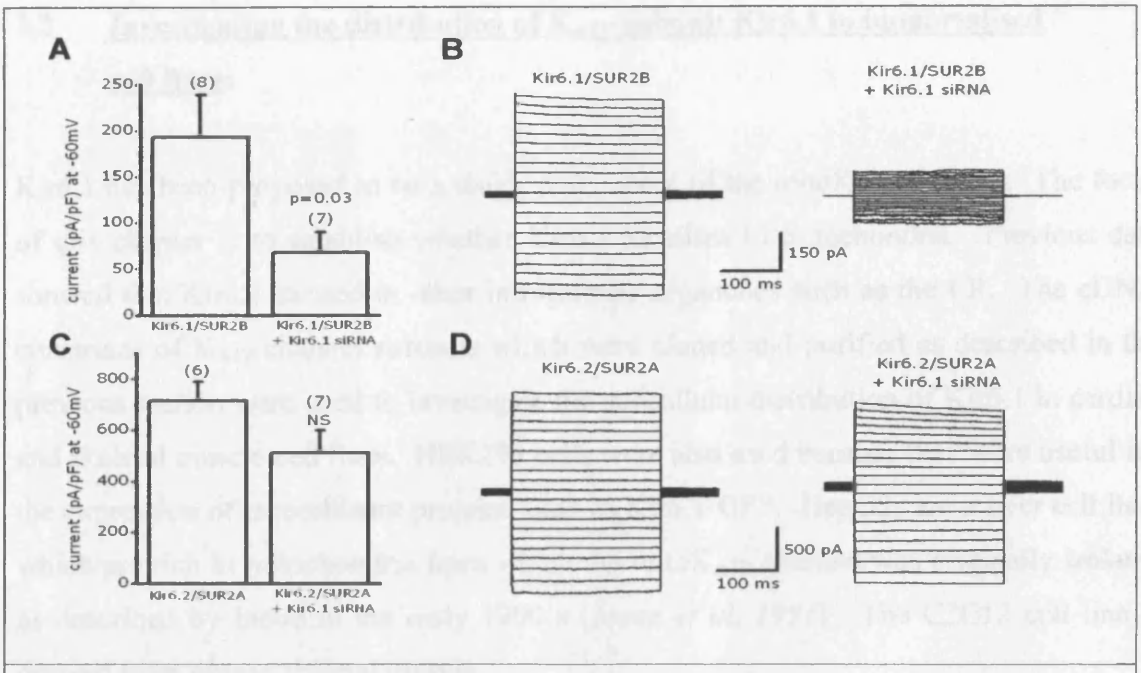

Figure 3.8. Whole cell patch recordings of single-channel currents from HEK293 cells stably transfected with K_{ATP} channel subunits. The Kir6.1 siRNA was transiently transfected into these stable cell lines along with eGFPN1 to allow transiently transfected cells to be identified using epifluorescence. Control recordings were made from cells which had gone through the transfection process but which had not taken up the GFP cDNA (and thus assumed had not been co-transfected with Kir6.1 siRNA). Patch pipette solutions were supplemented with nucleotide phosphates and diphosphates and recordings were made in a symmetrical K^+ gradient (140 mM). Under these conditions, the Kir6.1/SUR2B and Kir6.2/SUR2A currents were activated without use of levcromakalim or similar KCO but gradually reached steady state around 5 minutes after breaking through to whole-cell. At this point, steady-state currents were recorded by applying 250 ms voltage steps from a holding potential of 0 mV between -100 mV and +100 mV. Glibenclamide (10 μM) was applied at the end of the experiment to ensure that the current was abolished. Kir6.1/SUR2B channel activity is significantly reduced in the presence of 61siRNA when $p<0.03$ (A and B). Kir6.2/SUR2A currents were not affected by the presence of 61siRNA $p>0.05$ (C and D).

The basal current density at -50 mV was < 25 pA/pF in untransfected HEK293 cells (*Giblin et al 1999*). Application of 10 μM glibenclamide in the Kir6.1\SUR2B stable line reduces the current density to <20 pA\pF (*Quinn et al 2003*). Therefore the effect of the siRNA are significant but not complete i.e subtracting the background current would go from ~175 pA\pF (control) to ~40 pA\pF (+ siRNA to Kir6.1) ~ 80 % reduction.

The characterisation of siRNA is an important step in determining the function of K_{ATP} channel subunit, Kir6.1 in cardiac and skeletal muscle cell lines. 61siRNA duplex 2 will be used in functional studies so that the importance of Kir6.1 (channel) in ROS production, mitochondrial function and Ca^{2+} handling could be determined.

3.2 Investigating the distribution of K_{ATP} subunit Kir6.1 in immortalised cell lines:

Kir6.1 has been proposed to be a major component of the mitoK_{ATP} channel. The focus of this chapter is to establish whether Kir6.1 localises to mitochondria. Previous data showed that Kir6.1 existed in other intracellular organelles such as the ER. The cDNA constructs of K_{ATP} channel subunits which were cloned and purified as described in the previous section were used to investigate the subcellular distribution of Kir6.1 in cardiac and skeletal muscle cell lines. HEK293 cells were also used because they were useful for the expression of recombinant proteins such as Kir6.1-GFP. HepG2s are a liver cell line, which are rich in mitochondria from which the mitoK_{ATP} channel was originally isolated as described by Inoue in the early 1990's (*Inoue et al. 1991*). The C2C12 cell line is derived from mouse skeletal muscle.

3.2.1 Kir6.1 primarily localises to the ER

The subcellular distribution of Kir6.1 was investigated using transient transfections and cells were cultured so that they were 50-70 % confluent, ready for transfection 24 hours later. HEK293, C2C12 and HepG2 cells lines were transiently transfected with Kir6.1-GFP and with a specific ER marker called DsRed2-ER. The cells were analysed using laser scanning confocal microscopy (Bio-Rad system) before they were first observed under a fluorescent microscope to assess the transfection efficiency. In HEK293 cells, it was approximately 50-80 % compared to 40-60 % in C2C12 cells however, in HepG2 cells it was only 10-15 %. Therefore, it was decided that the HepG2 cell line would be omitted from this part of the study. The data from this chapter is from C2C12 and HEK293 cell lines and experiments were repeated on separate occasions so that at least 30 transfected cells could be used to analyse colocalisation between the two fluorescent markers. (Please refer to chapter 2.5.3 in methods and materials).

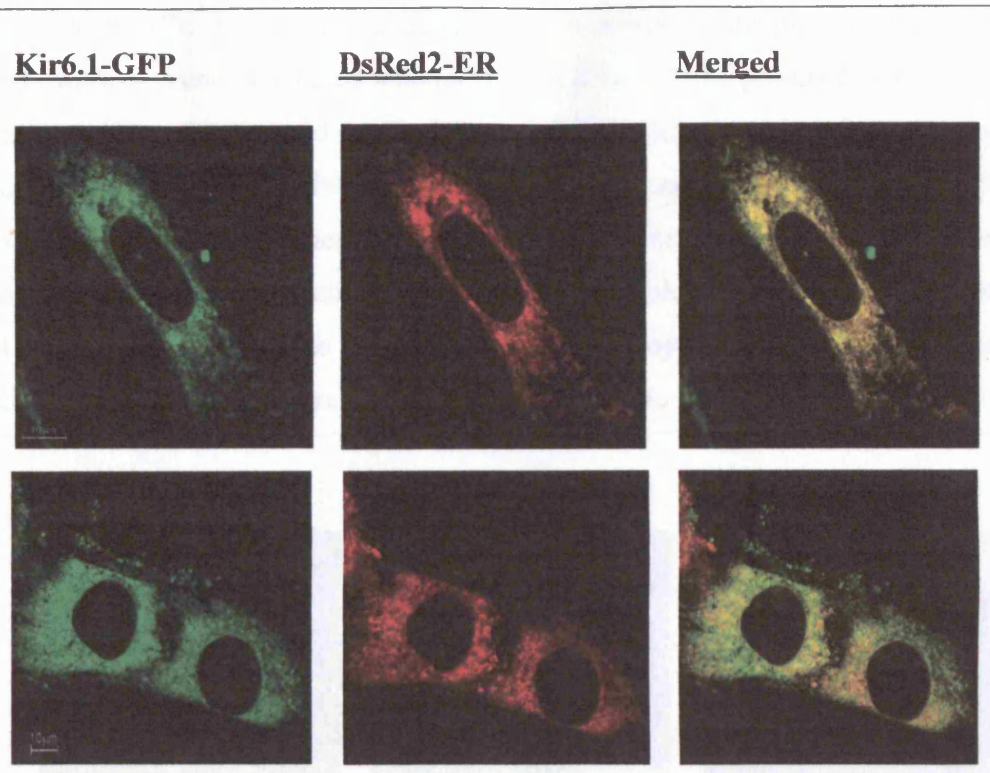

Figure 3.9. Kir6.1 and ER colocalisation in C2C12 cells transfected with Kir6.1-GFP and DsRed2-ER.

Images to show colocalisation between Kir6.1-GFP and DsRed2-ER in C2C12 cells. These were transfected with Kir6.1-GFP and DsRed2-ER. The cells were transfected for 15 hours at 37°C before the transfection mixture was removed and replaced with MEM supplemented with 10 % FCS and 1 % P/S. The cells were used for confocal analysis 36-48 hours later.

Kir6.1-GFP was excited using the 488 nm laser with a 510-530 nm emission filter whereas DsRed2-ER was excited with the 543 nm laser with 560-630 nm emission filter. The fluorophores were images sequentially. The merged image (right) shows the colocalisation between the Kir6.1-GFP and DsRed2-ER. A high proportion of Kir6.1 channel subunit is located in the endoplasmic reticulum.

3.2.1 Kir6.1 is predominantly distributed in the endoplasmic reticulum

In figure 3.9, C2C12 cells were transfected with Kir6.1-GFP and DsRed2-ER. The images show that there was a high proportion of Kir6.1 located in the ER and the majority of the yellow pixels (where there is colocalisation) were located around the

nucleus and ER. However, the signals did not overlap at the plasma membrane. C2C12 cells were also co-transfected with SUR1 but Kir6.1 in the presence of the sulphonylurea receptor was still retained in the ER and not trafficked to the plasma membrane, see figure 3.10. The rationale for transfecting SUR1 and not SUR2A or SUR2B in these experiments is because there is strong evidence to suggest that the SUR subunit of the native mitoK$_{ATP}$ channel could be SUR1. Pharmacological studies carried out by Liu et al concluded that native mitoK$_{ATP}$ channels they isolated closely resembled the Kir6.1/SUR1 channel expressed in HEK293 cells (*Liu et al. 2001*).

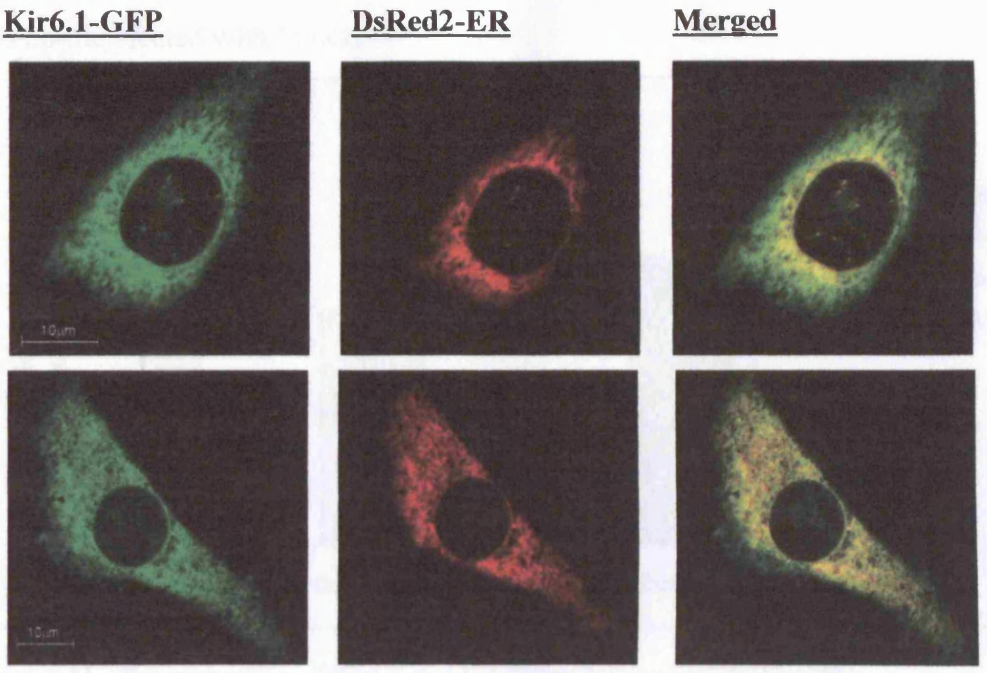

C2C12 Kir6.1-GFP, DsRed2-ER and SUR1

Figure 3.10. Kir6.1 and ER colocalisation in C2C12 cells transfected with Kir6.1-GFP, DsRed2-ER and SUR1.

Images to show the colocalisation between Kir6.1-GFP and DsRed2-ER in C2C12 cells. Cells were transfected with Kir6.1-GFP, DsRed2-ER and SUR1. The cells were prepared as described in figure 3.9. The degree of colocalisation is the same as cells transfected with just Kir6.1-GFP and DsRed2-ER but Kir6.1 is still retained in the endoplasmic reticulum in the presence of SUR1.

The proportion of colocalisation between the two signals was calculated using a program called Laserpix and the results were compared against a theoretical value of zero using a

rank scoring test known as the Mann Whitney test. Results were significant if $p<0.05$ (*). The results for C2C12 cells transfected with Kir6.1-GFP and DsRed2-ER and Kir6.1-GFP, DsRed2-ER and SUR1 are displayed as medians with 25 % and 75 % interquartile ranges in figure 3.11. The graph shows the proportion of Kir6.1-GFP pixels which colocalise with DsRed2-ER pixels and vice versa. The first column (b) represent the data for cells transfected with Kir6.1-GFP and DsRed2-ER where the total number of green pixels (a) which also contain red pixels (c) please refer to the Venn diagram in chapter 2.5.3. The second column shows the total number of red pixels that colocalise with the green. The third and fourth columns show the proportion of colocalisation in cells co-transfected with SUR1.

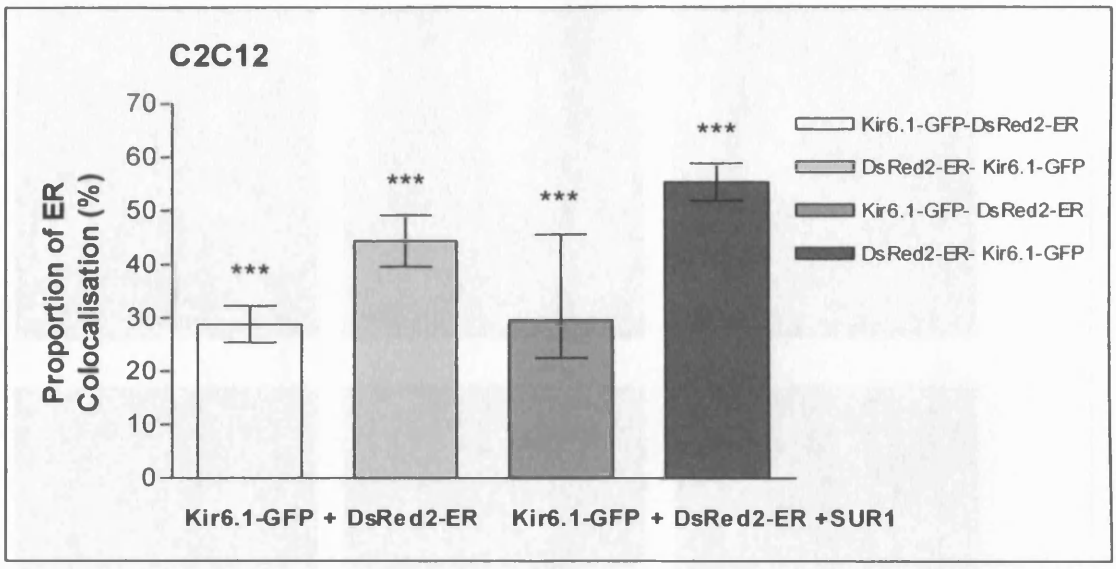

Figure 3.11. The proportion of Kir6.1 and ER colocalisation in C2C12 cells.

A graph to show the proportion of Kir6.1 (Kir6.1-GFP) that colocalises with endoplasmic reticulum (DsRed2-ER) n= 48 and Kir-6.1GFP with DsRed2-ER in C2C12 cells co-transfected with SUR1 n= 32. The first and third column corresponds to the total number of Kir6.1-GFP pixels that colocalise with the red. Statistical analysis showed that the data were highly significant when $p<0.001$ (***). The percentage of colocalisation between the two experiments is almost identical for cells transfected with and without SUR1. SUR1 does not significantly influence the trafficking of Kir6.1 to the plasma membrane.

The first column indicates that 28 % (median value) of Kir6.1 was ER retained and a similar value was observed in cells co-transfected with SUR1 (column three). The second and fourth columns confirm that 45 % and 55 % (SUR1) of the DsRed2-ER

marker colocalises with Kir6.1-GFP. Although a significant proportion of Kir6.1 was located in the ER, there is still a large proportion of Kir6.1 that is unaccounted for. This may be located in other specialised compartments throughout the cell such as mitochondria. The results for C2C12 cells co-transfected with SUR1 show that the sulphonylurea receptor did not significantly influence the transport of Kir6.1 to the plasma membrane because the similar median values were obtained. The null hypothesis (H_o) where '*There is no colocalisation between Kir6.1-GFP and DsRed2-ER signals*' was rejected $p<0.001$ (***).

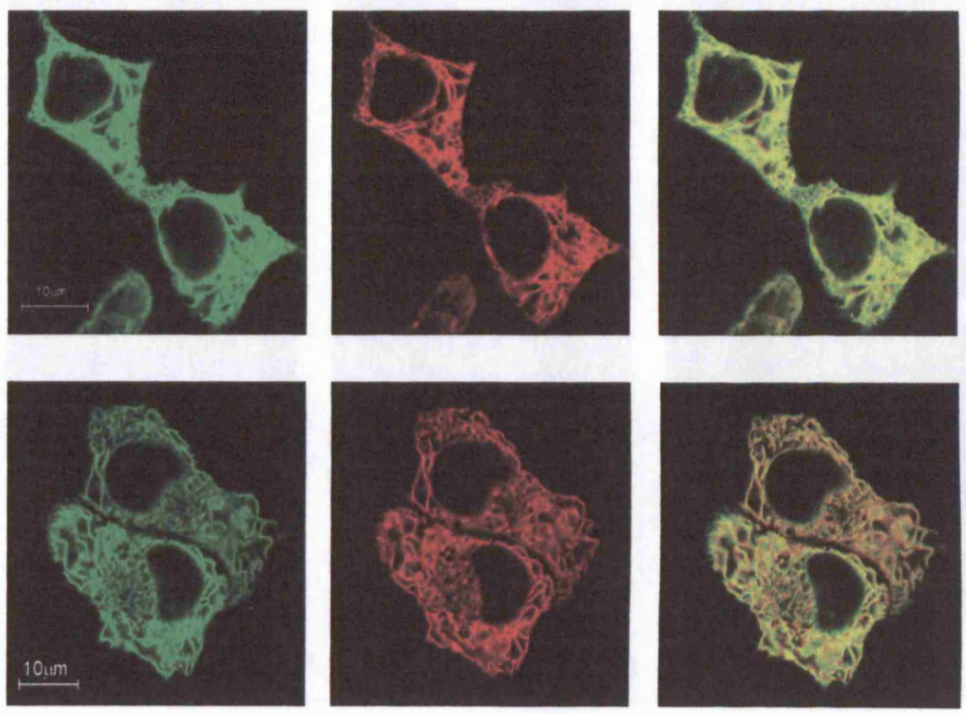

HEK293 Kir6.1-GFP and DsRed2-ER

Figure 3.12. Kir6.1 and ER colocalisation in HEK293 cells transfected with Kir6.1-GFP, and DsRed2-ER.

Images to show the colocalisation of Kir6.1-GFP and DsRed2-ER in HEK293 cell line. Cells were transfected with Kir6.1-GFP and DsRed2-ER. The cells were imaged in the same manner as described in figure 3.2. The images show that a high percentage of Kir6.1 is located in the ER. The ER appears to be more reticular than in C2C12 cells.

The HEK293 cell line was also used to investigate the distribution of Kir6.1. HEK293 cells do not contain endogenous Kir6.1 so transfecting Kir6.1-GFP would be useful in determining where the Kir6.1 protein may be distributed in the cell (*Cui et al. 2001*). Figure 3.12 shows the images for HEK293 cells transfected with Kir6.1-GFP and DsRed2-ER. A higher percentage of Kir6.1-GFP pixels overlap with the DsRed2-ER pixels. The merged images show that there was a significant proportion of Kir6.1 in the ER, most of Kir6.1 appeared to be cytoplasmic and ER retained with some strong colocalisation on the nuclear envelope.

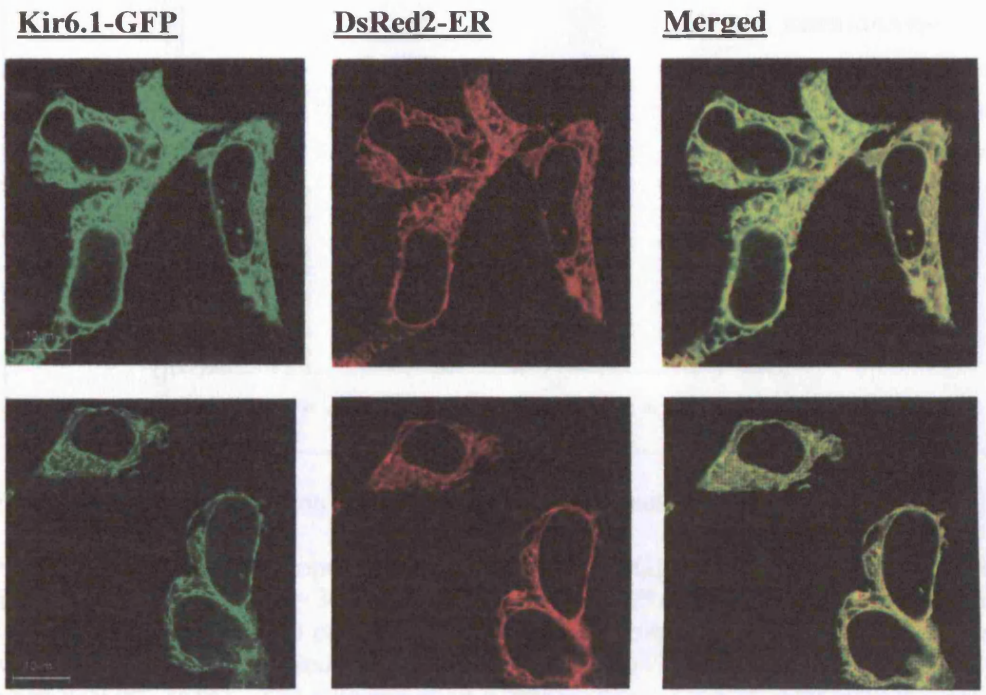

Figure 3.13. Kir6.1 and ER colocalisation in HEK293 cells transfected with Kir6.1-GFP, DsRed2-ER and SUR1.

Images to show the colocalisation of Kir6.1-GFP and DsRed2-ER in HEK293 cells. Cells were transfected with Kir6.1-GFP, DsRed2-ER and SUR1. The cells were imaged in the same manner as described in figure 3.2.1. Kir6.1 is predominantly located in the endoplasmic reticulum and nuclear envelope, even in the presence of the sulphonylurea receptor, SUR1.

In figure 3.13, the proportion of Kir6.1 that was trafficked to the plasma membrane in the presence of SUR1 was expected to be significantly higher but the proportion of ER colocalisation remained the same in the cells without the sulphonylurea receptor, see figure 3.12. I would expect less Kir6.1 to be ER retained because Kir6.1 should form an octameric complex with SUR1. The ER retention motif (RKR) on both subunits would be masked promoting exit from the ER followed by translocation to the cell surface to form functional K_{ATP} channels (*Zerangue et al. 1999*).

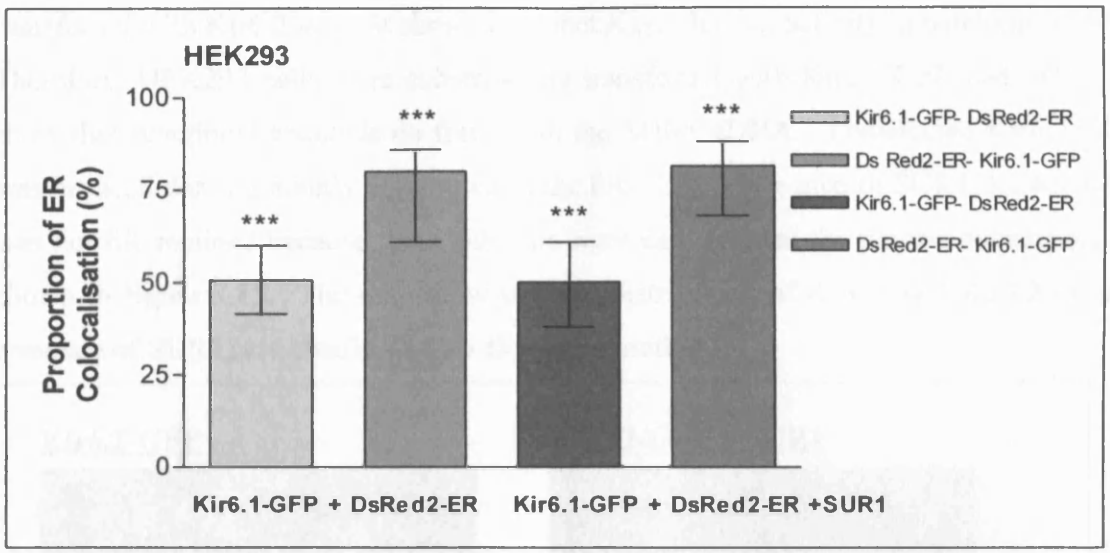

Figure 3.14. The proportion of Kir6.1 and ER colocalisation in HEK293 cells.

A graph to show the proportion of Kir6.1 (Kir6.1-GFP) that colocalises with endoplasmic reticulum (DsRed2-ER) n= 34 and Kir6.1-GFP with DsRed2-ER in the presence of SUR1 n= 48. The first and third column corresponds to the total number of Kir6.1-GFP pixels that colocalise with DsRed2-ER pixels. Statistical analyses showed that both sets of data were highly significant when $p<0.001$ (***). The colocalisation between the two signals was almost identical for cells transfected with and without the sulphonylurea receptor.

HEK293 cells contained a greater proportion of transfected Kir6.1 in the ER compared to the C2C12 cell line, see figure 3.14. In cells transfected with just Kir6.1-GFP and DsRed2-ER, the median value showed that 50 % of Kir6.1 was ER retained (first column). The other 50 % of Kir6.1 as discussed previously could be located in other intracellular compartments such as the mitochondria. The results for cells co-transfected with SUR1 are the same because SUR1 does not influence the trafficking of Kir6.1 to the plasma membrane. The proportion of colocalisation between Kir6.1-GFP and DsRed2-ER is significant $p<0.001$ (***).

From this colocalisation study, transfecting SUR1 did not significantly affect the distribution of Kir6.1. However, SUR1 will form functional K_{ATP} channels with Kir6.2 as found in pancreatic β-cells (*Ashcroft & Gribble 1998*). Liu's study demonstrated that Kir6.1/SUR1 formed distinct membrane currents similar for native mitoK_{ATP} channels. One can argue that as the SUR1 cDNA used was not fluorescently tagged it would difficult to establish whether it was transfected successfully into the cell lines I used. However, previous observations in our laboratory showed that our SUR1 cDNA co-transfected with Kir6.2 subunit showed distinct K_{ATP} channel activity in patching studies. Therefore, HEK293 cells were subsequently transfected with Kir6.2-GFP and SUR1 to show that functional channels do form with the SUR1 cDNA. Transfected Kir6.2-GFP was intracellular and mainly distributed in the ER. In the presence of SUR1, Kir6.2-GFP was not ER retained because these subunits were expressed at the plasma membrane, as shown in figure 3.15. The data show that the distribution of Kir6.1 and Kir6.2 (in the presence of SUR1) are clearly distinct from one another.

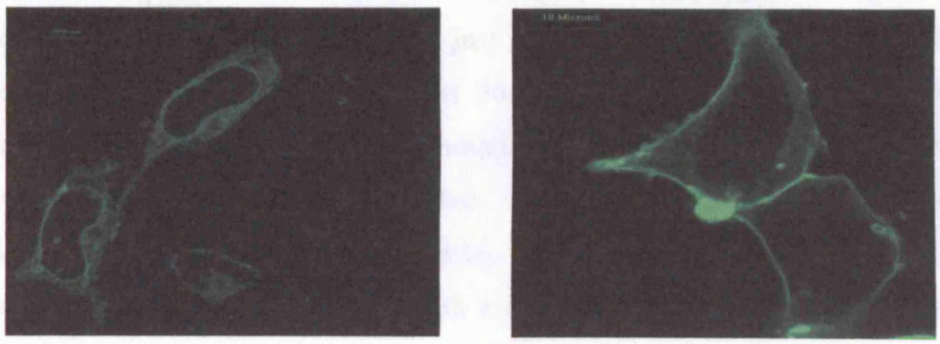

Figure 3.15. HEK293 cells transfected with Kir6.2 GFP and SUR1.

On the right, the image show that Kir6.2-GFP alone is retained in the ER whereas co-transfection with SUR1 (right) allows the two K_{ATP} subunits form a protein complex and exit the ER to localise to the plasma membrane.

3.2.2 Kir6.1 may be localised in mitochondria

This part of the colocalisation study has shown that Kir6.1 is predominantly distributed in the ER however, it is not trafficked to the plasma membrane when co-transfected with SUR1. Although the data have shown that the Kir6.1 is mostly expressed in the ER, there was also a significant proportion of Kir6.1 that may be located elsewhere. For example, Kir6.1 may exist in subcellular compartments such as the mitochondria. The identity of the mitoK_{ATP} channel is under debate but I decided to examine if Kir6.1 exists in mitochondria by continuing the colocalisation studies using mitochondrial specific dyes and probes. I examined the distribution of Kir6.1 in mitochondria using three different approaches. i). Mito DsRed ii). TMRE and iii). MitoTracker Red. See figure 3.16.

In figure 3.16A, the mito DsRed probe was transfected alone to label the mitochondria but this caused problems because the probe produced significant green background fluorescence in cells transfected with just MitoDs-Red. This occurred regularly in cells which were transfected for less than 36 hours as MitoDs-Red existed as the green fluorescent product which was the immature form of the protein. Therefore, it was not possible to co-transfect Mito DsRed with Kir6.1-GFP this into these cells for colocalisation experiments. This overlap of the signals complicated the colocalisation analysis and was pursued further with a mitochondrial membrane potential dye called TMRE. C2C12 and HEK293 cells were first loaded with TMRE to ensure that there was no crosstalk between the two fluorophores during imaging Kir6.1-GFP, see figure 3.16B. In figure 3.16C, C2C12 and HEK293 cells were then transfected with Kir6.1-GFP before they were loaded with TMRE. Cells were also transfected with either Kir6.1-GFP or Kir6.1-GFP and SUR1. C2C12 and HEK293 cells were packed with mitochondria after loading with 50 nM TMRE with mitochondria observed as thin structures. TMRE is a membrane potential sensitive dye and Kir6.1 overexpression may have caused mitochondrial depolarisation decreasing TMRE fluorescence which in effect would be a problem when interpreting data.

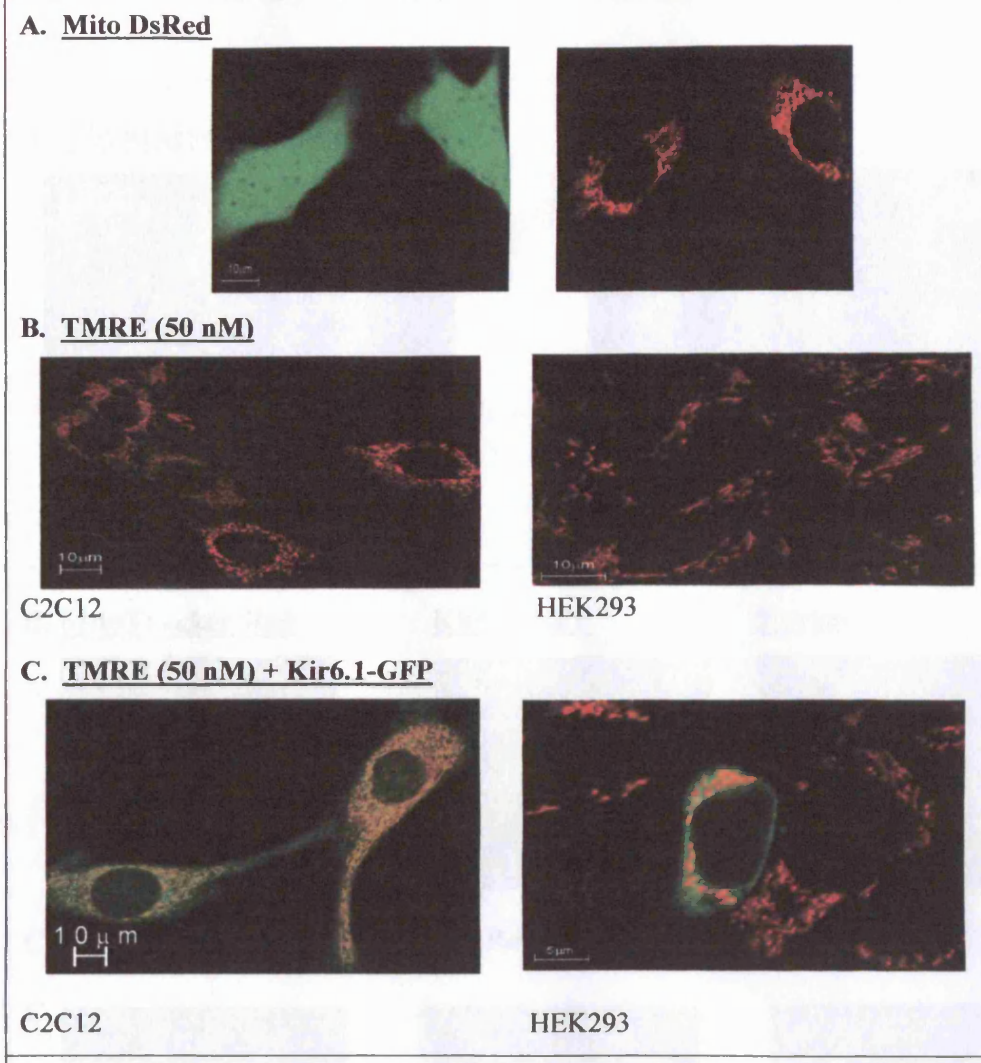

Figure 3.16. Investigating the distribution of Kir6.1 in mitochondria.

A. C2C12 cells were also transfected with just Mito DsRed probe; this was not a stable probe to use as Mito Ds-Red also fluoresced in the green channel if it was imaged less than 36 hours after transfection (left image). The green product is the immature form of the protein. The red product was visible between 36-48 hours (right image).
B. HEK293 and C2C12 cells were loaded with 50 nM TMRE for 30 minutes at 37°C before confocal analysis. The mitochondria appear as small distinct structures.
C. C2C12 cells were transfected with Kir6.1-GFP prior loading with 50 nM TMRE. There is a small amount of colocalisation in mitochondria. However, there is very little overlap of signals in HEK293 cells

Using TMRE was technically difficult and labelling mitochondria was not always successful because they appeared to depolarise, therefore the next approach was to use to

another mitochondrial probe called MitoTracker Red to examine this further. See figure 3.17.

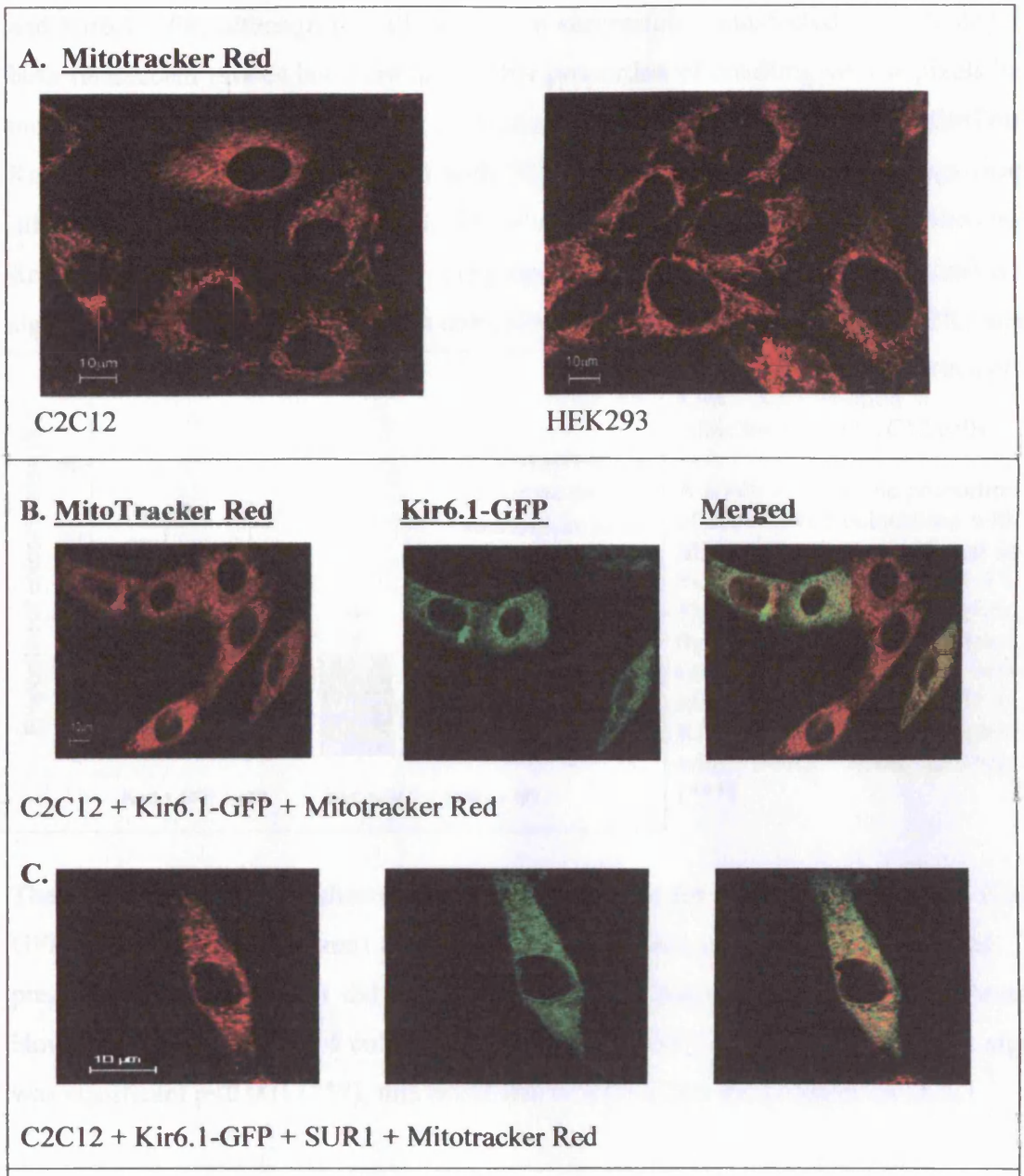

Figure 3.17. Investigating the distribution of Kir6.1 using mitotracker red.

A. HEK293 and C2C12 cells were loaded with 150 nM Mitotracker Red for 30 minutes at 37°C before confocal analysis. B. C2C12 cells were transfected with Kir6.1-GFP prior to loading with Mitotracker Red. The signals show little overlap and the same overlap of signals is observed in cells transfected with SUR1 in C. where C2C12 cells were co-transfected with SUR1 before they were loaded with Mitotracker Red.

In figure 3.17A, the mitochondria in C2C12 and HEK293 cells were loaded with 150 nM. The images in figure 3.17B show that there was some overlap between MitoTracker Red and Kir6.1-GFP, although not all cells were successfully transfected and labelled with both fluorescent probes but there is a higher proportion of resulting yellow pixels in the merged images. The proportion of colocalisation between Kir6.1-GFP and MitoTracker Red signals in cells co-transfected with SUR1 in figure 3.17C were not significantly different to the cells in figure 3.17B. Therefore, these results obtained using MitoTracker Red were analysed. In comparison, the proportion of colocalisation in mitochondria was significantly lower in comparison to colocalisation experiments with DsRed2-ER marker.

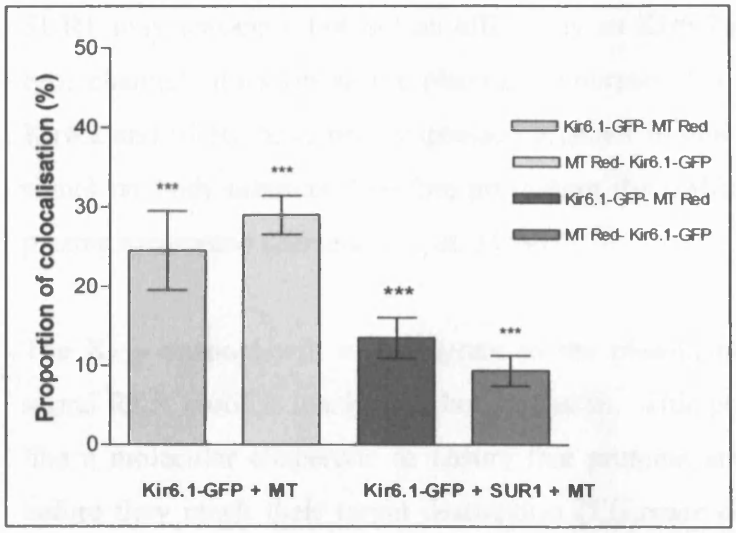

Figure 3.18. The proportion of Kir6.1 colocalisation in mitochondria in C2C12 cells.

A graph to show the proportion of Kir6.1 that colocalises with Mitotracker Red n= 36 and in the presence of SUR1 n= 17. The statistical analysis showed that the data were significant for Kir6.1-GFP and Mitotracker Red and when Kir6.1-GFP was co-transfected with SUR1 when $p<0.001$ (***)

The graph in figure 3.18 shows that the median value for cells transfected with Kir6.1-GFP was 25 % (first column) and 14 % in the presence of SUR1 (third column). The presence of SUR1 subunit did not promote the distribution of Kir6.1 to mitochondria. However, the proportion of colocalisation between Kir6.1-GFP and DsRed2-ER signals was significant $p<0.001$ (***), this result was unaffected by the presence of SUR1.

The distribution of Kir6.1 was investigated using transient transfections in C2C12 and HEK293 cell lines. Kir6.1 was evenly distributed in both cell lines but predominately expressed in the ER. About 28 % of Kir6.1 was retained in C2C12 cells whilst in HEK293 cells; it was higher at 50 %. One explanation for this difference may be because HEK293 cells contain very little endogenous Kir6.1 so the transfected protein would be evenly distributed throughout the cell. My data also indicate that Kir6.1 could be present in other subcellular compartments such as mitochondria or perhaps nuclear membrane. In the presence of SUR1, Kir6.1 was perhaps expected to translocate to the plasma membrane. However, both cell lines showed no clear membrane staining. Kir6.1 and SUR1 may associate but not as efficiently as Kir6.2 and SUR1 because Kir6.1/SUR1 type channels do form as the plasma membrane (*Liu et al 2001*). In addition to this, Kir6.2 and SUR1 have been expressed together in one study to mask the RKR retention signal on both subunits therefore promoting the trafficking of the K_{ATP} channel to the plasma membrane (*Zerangue et al. 1999*).

The K_{ATP} channel will only migrate to the plasma membrane when the ER retention signal RKR motif is masked on both subunits. This process is important because it acts like a molecular chaperone to ensure that proteins are correctly folded and assembled before they reach their target destination *(Klausner & Sitia 1990)*. My colocalisation studies showed that co-transfection with SUR1 did not significantly change the results. However, staining for natively expressed SUR1 has also been completed in our laboratory with this particular plasmid. The HEK293 and C2C12 cell lines co-transfected with Kir6.1-GFP and SUR1 showed that the same proportion of Kir6.1 is still retained in the ER. Furthermore, our group were able to carry out some studies in HEK293 cells expressing Kir6.2-GFP and SUR1 and this was trafficked to the cell membrane and not ER retained with distinct membrane currents (*Cui & Tinker, unpublished observations*). See Figure 3.19. This also showed that Kir6.1 fluorescently tagged to GFP did not affect the trafficking of mature K_{ATP} channel to the plasma membrane.

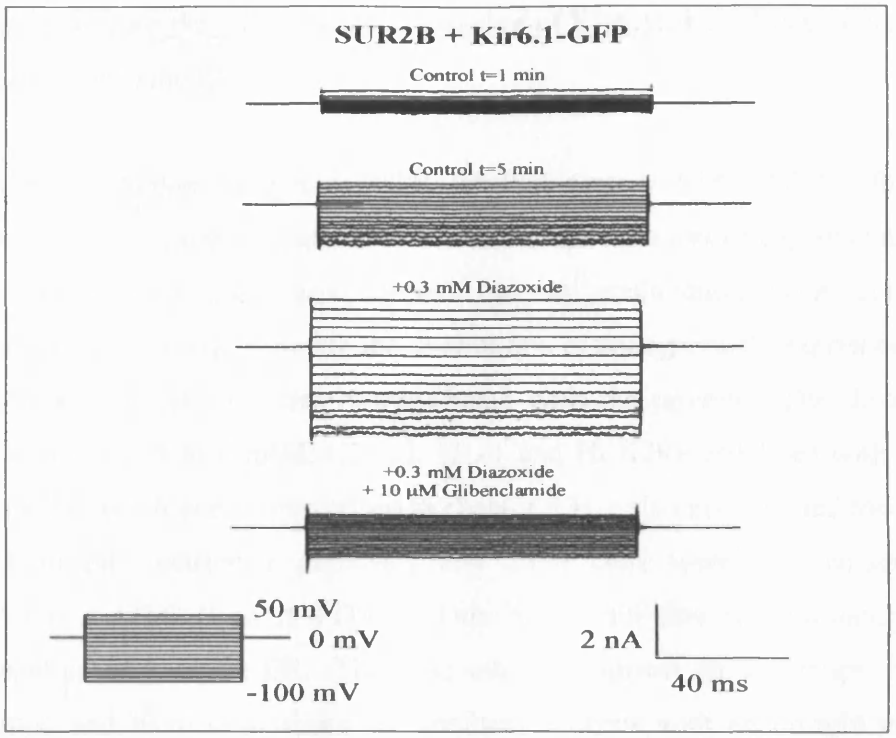

Figure 3.19. K_{ATP} channel activity in HEK293 cells transfected with Kir6.1-GFPand SUR2B.

Cells were stimulated with 0.3 mM diazoxide and channel activity was inhibited with 10 μM glibenclamide. (The data was kindly provided by Professor Andrew Tinker).

The investigation was taken one step further to examine if Kir6.1 was present in mitochondria as suggested by several investigators (*Zhou et al 2005*; *Lacza et al 2003a, 2003b; Suzuki et al 1997*). After preliminary work, MitoTracker Red was used for colocalisation studies because in my hands, using the Mito DsRed probe in our cell lines along with Kir6.1-GFP was problematic. Transfecting cells with just mitoDs Red alone produced green fluorescence in control cells without Kir6.1-GFP. With MitoTracker Red it diffuses readily across the plasma membrane readily and accumulates in active respiring mitochondria, which oxidises the dye into a fluorescent conjugate. This produced better images and was technically an easier probe to use than TMRE. After statistical analysis, my results showed that a small but significant proportion of Kir6.1 may exist in mitochondria. Given these observations, the next step was to examine the distribution of natively expressed Kir6.1 in immortalised cell lines in chapter 3.3.

3.3 Investigating the endogenous expression of Kir6.1: Kir6.1 is predominantly expressed in the ER

To investigate whether exogenous GFP labelled protein Kir6.1-GFP influences the distribution of Kir6.1, it was essential to determine the endogenous expression of Kir6.1. Immunofluorescent staining was carried out in conjunction with colocalisation experiments so that I could compare the distribution of endogenously expressed Kir6.1 in native cells and in cells transiently transfected with the protein. The distribution of Kir6.1 was examined in HepG2, C2C12, HL-1 and HEK293 cell lines with the Kir6.1 MBP antibody, which was characterised in chapter 3.1. I also investigated the expression of Kir6.1 in rat ventricular myocytes and these cells were also co-stained with Concanavalin A-FITC (Con A FITC). This is a lectin that predominantly binds to glycosylated proteins in the ER. The cells were first grown on coverslips, before they were stained and fixed onto slides for confocal analysis with an upright microscope. Please refer to chapter 2.8.

3.3.1 Kir6.1 is endogenously expressed in cardiac, liver and skeletal muscle cells

Control experiments were set up using wild type HEK293 cells and the stable line HEK Kir6.1/SUR2B to determine the sensitivity of MBP-Kir6.1C (93A) antibody. Kir6.1 was detected with a rhodamine conjugated goat anti rabbit secondary antibody, see figure 3.20. As expected, the stable cell line Kir6.1/SUR2B showed a significant amount of natively expressed Kir6.1. From my observations, Concanavalin A staining appeared to be membrane associated in the stable cell lines. As expected, the antibody did not detect endogenous Kir6.1 in wild type HEK293 cells. HEK293 cells are an important cell line to use in this part of the study because in our hands (Tinker group), immunofluorescence studies showed that HEK293 cells do not express endogenous Kir6.1 (and Kir6.2) (*Cui et al 2001*).

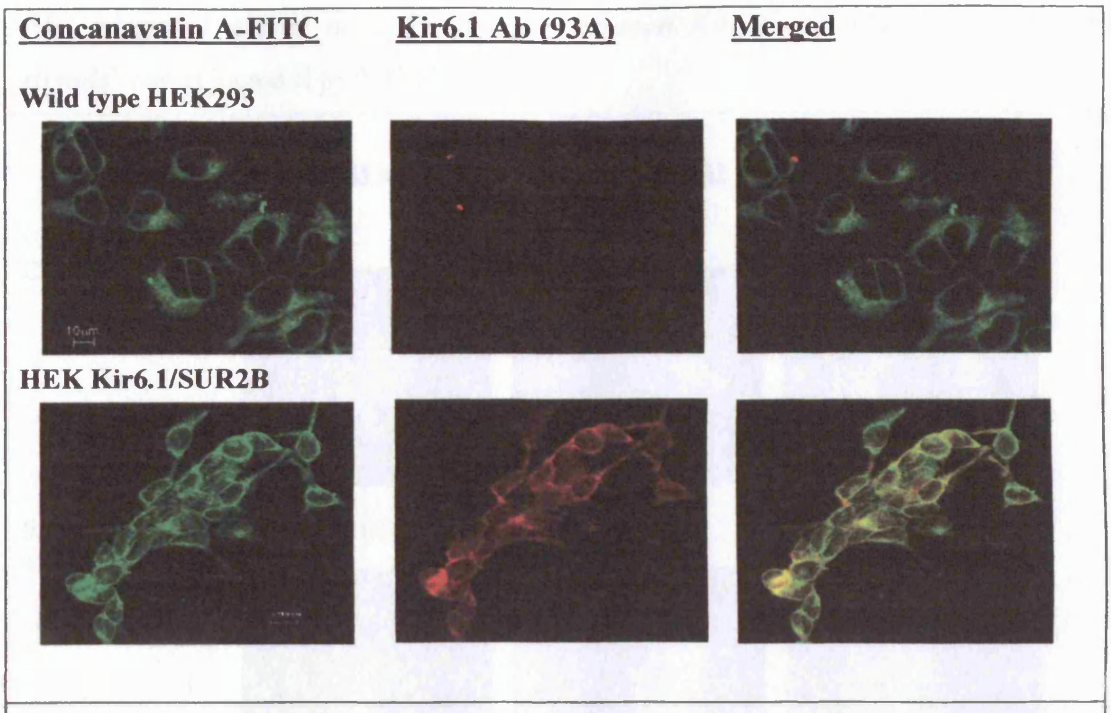

Figure 3.20. The distribution of Kir6.1 in HEK293 and Kir6.1/SUR2B cells.

HEK293 and HEK Kir6.1/SUR2B cell lines were used to act as controls for the MBP Kir6.1C antibody (93A). The cells were analysed using confocal microscopy using the same settings for colocalisation experiments in chapter four.

Wild type HEK293 cells contain very little endogenous Kir6.1. The stable line HEK Kir6.1/SUR2B was processed at the same time as HEK293 cells and the antibody detected Kir6.1. Endogenous Kir6.1 was detected with a rhodamine conjugated antibody. The staining for Concanavalin A FITC is the same for both cell lines. Concanavalin A staining in the stable cell line is more membrane associated; this may be the results of stably tranfecting K_{ATP} channel subunits.

C2C12 cells contain an abundant amount of endogenous Kir6.1 and this was evenly distributed throughout the cell, see figure 3.21. The pre-immune sample and the 93A antibody fused to the MBP fusion protein were used as controls where no endogenous Kir6.1 was detected in both control experiments. The images also show that C2C12 cells stained well with Concanavalin A FITC. The graph in figure 3.22 suggests that 38 % (Median value) of Kir6.1 was located in the ER (second column). However, there is still a significant amount of Kir6.1 that may be located in other intracellular compartments such as mitochondria; this was previously discussed in chapter 3.2. The null hypothesis

(H_o) where '*There is no colocalisation between Kir6.1 and Concanavalin A FITC signals*' was rejected if $p<0.05$ (*).

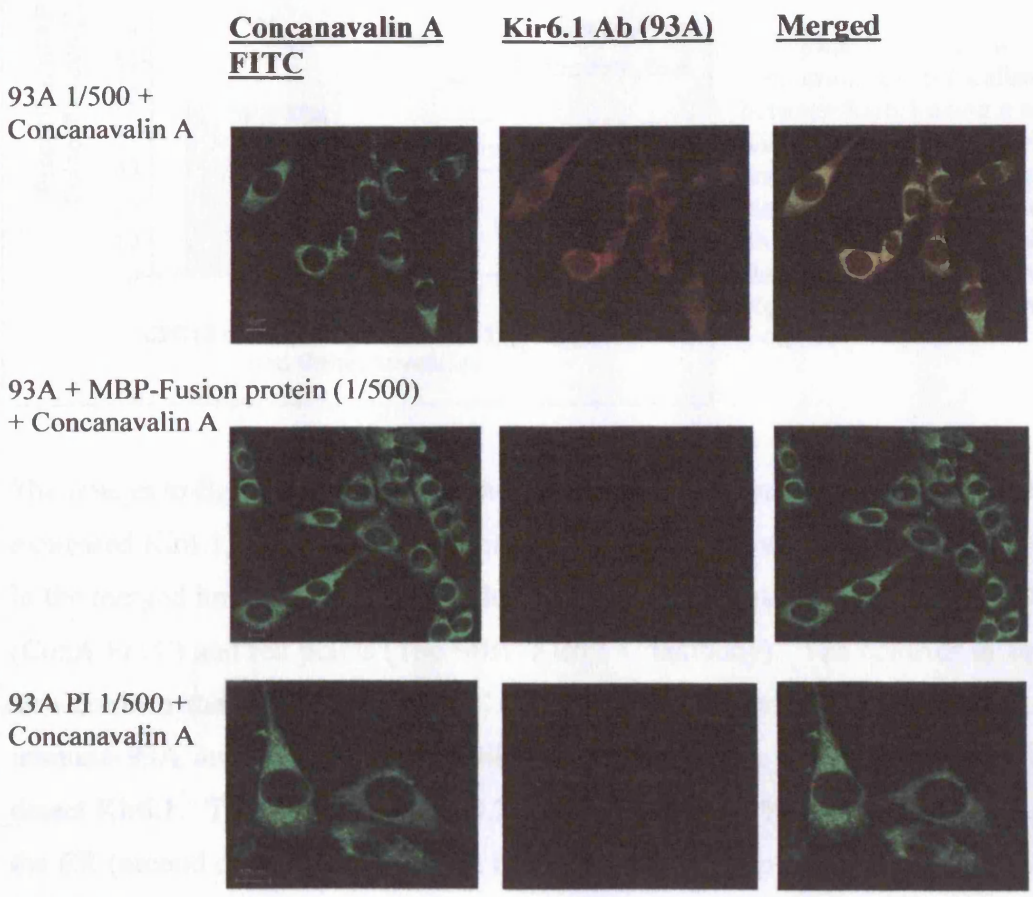

Figure 3.21. The distribution of Kir6.1 in C2C12 cells.

Images to show the endogenous distribution of Kir6.1 in C2C12 cell line using MBP-Kir6.1C antibody (93A) and ER marker, Concanavalin A FITC. The controls used were pre-immune sample and MBP-fusion protein bound to the antibody.

The images show that the C2C12 cells contain endogenous Kir6.1; Kir6.1 is predominately located in the ER. The controls show no Kir6.1 staining with 93A pre-immune sample and 93A + MBP-fusion protein, whereas staining with Concanavalin A FITC is consistent in all of the experiments.

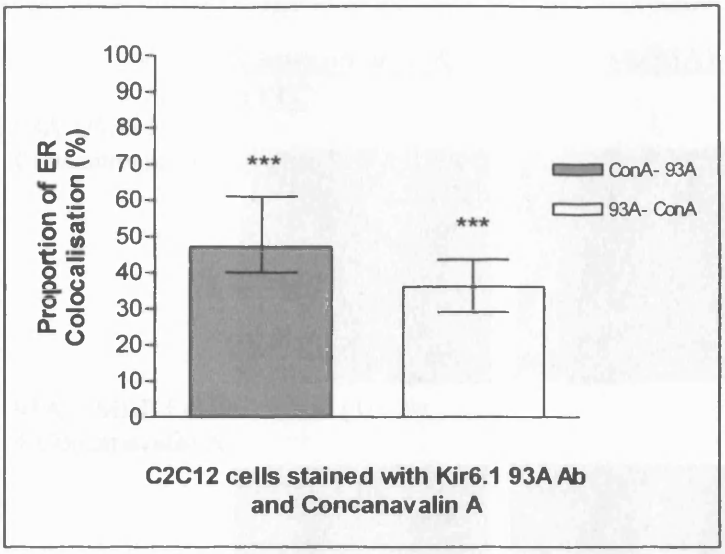

Figure 3.22. The proportion of Kir6.1 and ER colocalisation in C2C12 cells.

A graph to show the proportion of colocalisation between Kir6.1 using a MBP Kir6.1 C antibody (93A) and endoplasmic reticulum marker Con A FITC in n= 25. Statistical analysis showed that the data were highly significant when $p<0.001$ (***)

The images in figure 3.23 show that the HepG2 cell line contains higher levels of natively expressed Kir6.1, the staining for Concanavalin A FITC is similar to the C2C12 cell line. In the merged image, there is a significant proportion of colocalisation between the green (ConA FITC) and red pixels (The MBP-Kir6.1 C antibody). The controls in figure 3.23 also confirm that the MBP-Kir6.1 C antibody is sensitive for Kir6.1 because the pre-immune 93A and MBP-Kir6.1C antibody incubated with MBP-fusion protein did not detect Kir6.1. The graph in figure 3.24 indicates that 48 % of Kir6.1 was expressed in the ER (second column). This result is highly significant $p<0.001$ (***) confirming that a large amount of Kir6.1 does exist in the ER in liver cells

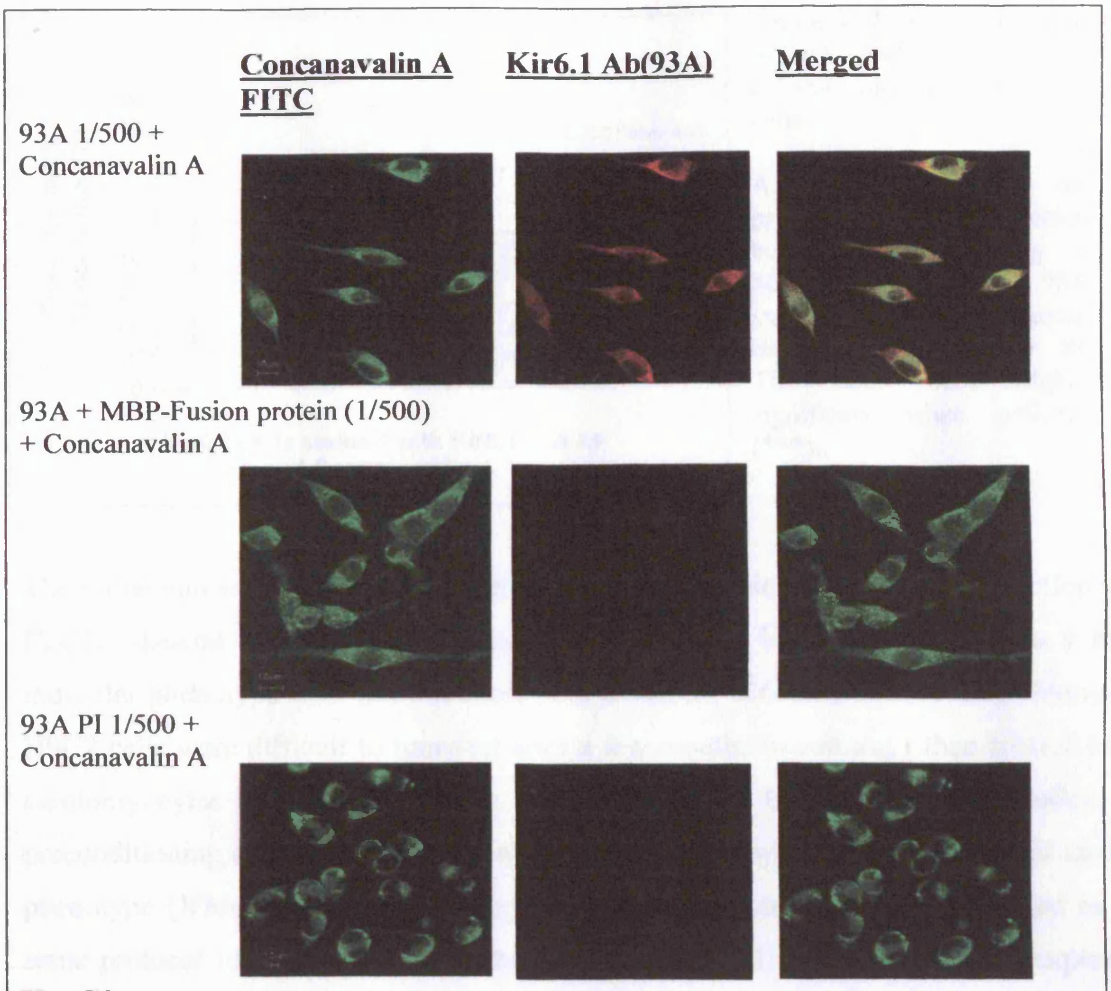

Figure 3.23. The distribution of Kir6.1 in HepG2 cells.

Images showing the endogenous distribution of Kir6.1 in HepG2 cell line using MBP Kir6.1C antibody (93A) and endoplasmic reticulum marker Concanavalin A FITC. The same controls were used here as in figure 3.21.

The HepG2 cell line contains high levels of endogenous Kir6.1 which colocalises with the ER marker in the merged image. The controls show that no Kir6.1 was detected with the 93A pre-immune sample and 93A + MBP-fusion protein. The staining with Concanavalin A FITC is consistent in all experiments.

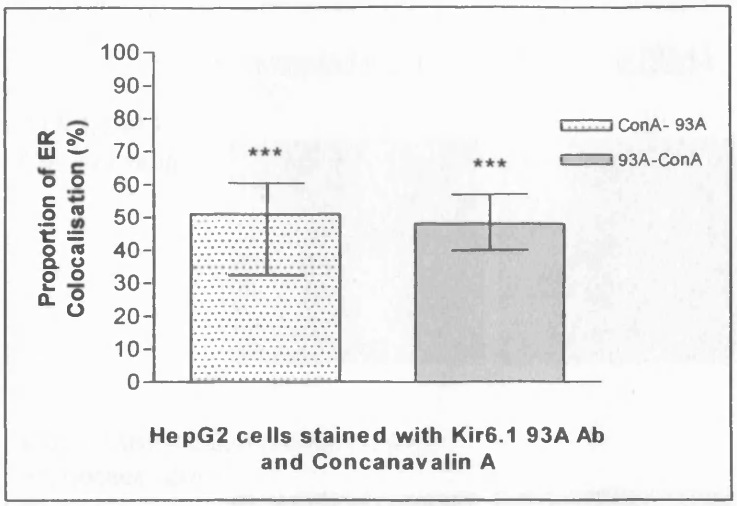

Figure 3.24. The proportion of Kir6.1 and ER colocalisation in HepG2 cells.

A graph to show the proportion of colocalisation between Kir6.1 using a MBP-Kir6.1 C antibody 93A and endoplasmic reticulum using Con A FITC n= 30. The data were highly significant when $p<0.001$ (***).

The initial aim was to stain H9C2 (derived from embryonic rat heart) in conjunction with C2C12 skeletal muscle cells because they could also be differentiated into a more muscular phenotype with *trans* retinoic acid treatment (*Menard et al. 1999*). However, H9C2 cells were difficult to transfect after a few months in culture; I then studied HL-1 cardiomyocytes because these cells were reported to be good cellular models for preconditioning and were able to spontaneously contract whilst maintaining their cardiac phenotype (*White et al. 2004*). The HL-1 cardiomyocytes were also subjected to the same protocol to examine whether they contained Kir6.1. I found that they expressed high levels of Kir6.1, which was evenly distributed throughout the cell, see figure 3.25. The merged image shows that there was also a significant proportion of colocalisation between Kir6.1 and Concanavalin A FITC pixels. The yellow pixels exist in the ER but as the images suggests, a small proportion of Kir6.1 may be located elsewhere, perhaps at the plasma membrane as well. I found that the pre-immune sample for 93A and 93A incubated with the MBP fusion protein did not detect any Kir6.1 in HL-1 cardiomyocytes. The graph in figure 3.26 suggests that the degree of colocalisation between the two signals is high $p<0.001$ (***). This is reflected in the statistics because the median value showed that 46 % of the ER pixels colocalise with Kir6.1 pixels (see first column).

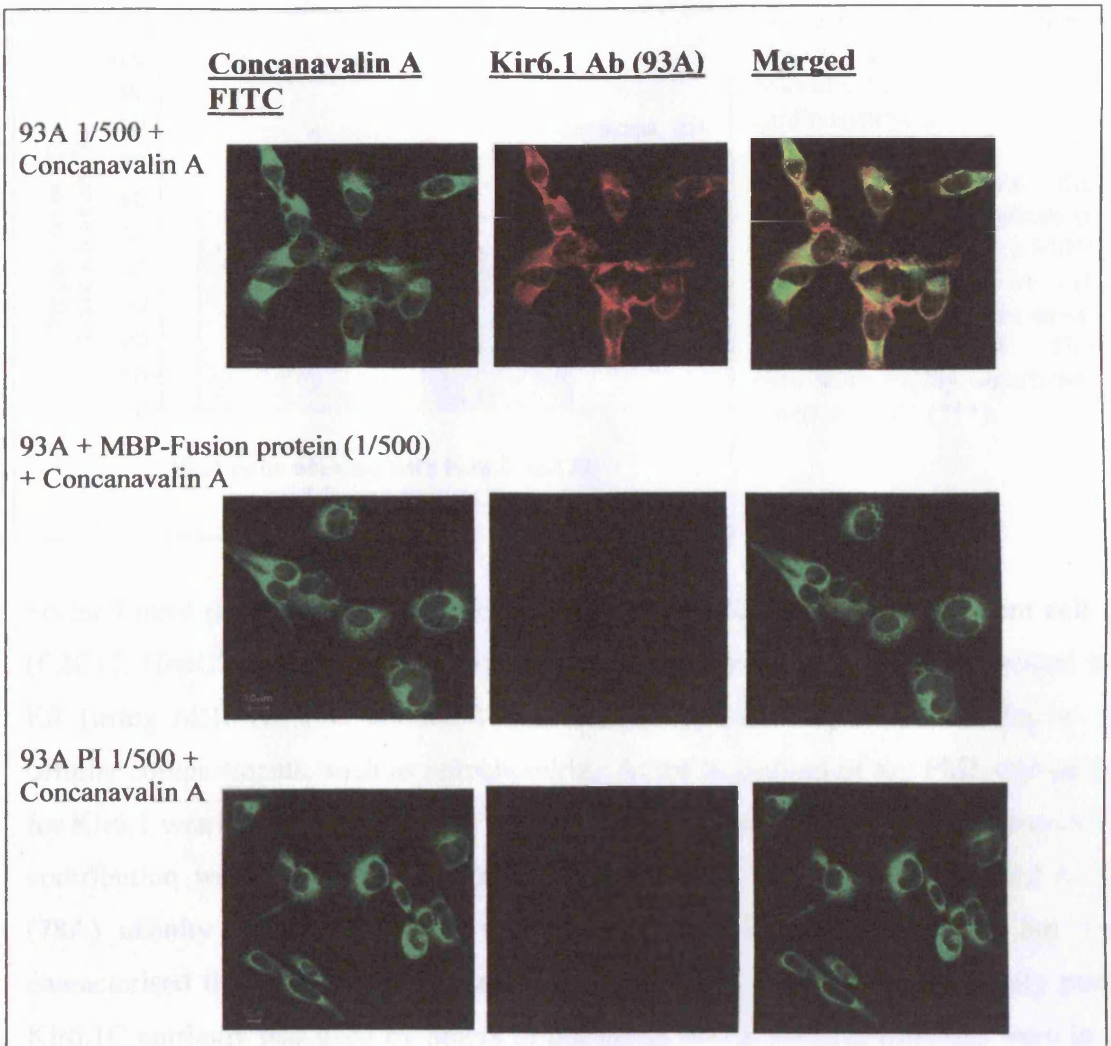

Figure 3.25. The distribution of Kir6.1 in HL-1 cardiomyocytes.

Images showing the endogenous distribution of Kir6.1 in HL-1 cardiomyocytes using Kir6.1 antibody (93A) and endoplasmic reticulum marker Concanavalin A FITC. The same controls were used here as in figure 3.20

The images show that the HL-1 cardiomyocytes contain endogenous Kir6.1 as in the HepG2 cell line and this channel subunit does colocalise with the endoplasmic reticulum marker. The controls show no Kir6.1 staining was observed with the 93A pre-immune sample and 93A + MBP-fusion protein, staining with Concanavalin A FITC remains the same.

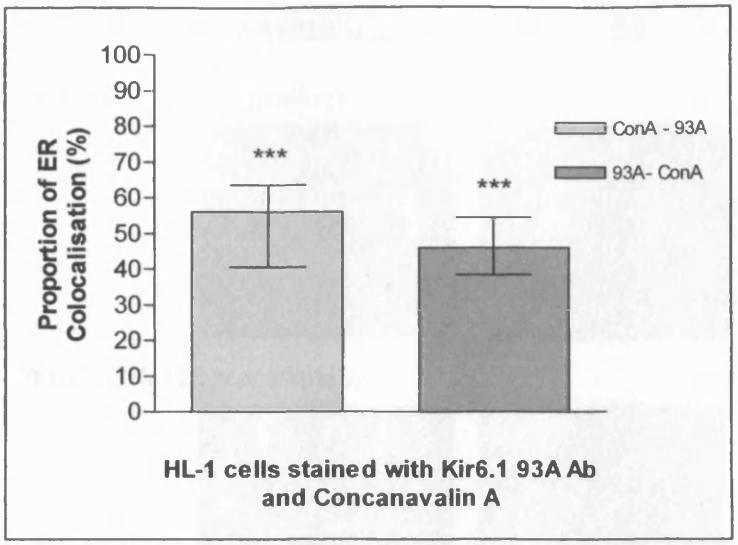

Figure 3.26. The proportion of Kir6.1 and ER colocalisation in HL-1 cardiomyocytes.

A graph to show the proportion of colocalisation between Kir6.1 using a MBP Kir6.1 C antibody 93A and endoplasmic reticulum using Con A FITC n= 28. The data were highly significant when $p<0.001$ (***).

So far I have detected the endogenous distribution of Kir6.1 in three different cell lines (C2C12, HepG2 and HL-1 cardiomyocytes). The majority of Kir6.1 was located in the ER (using MBP-Kir6.1C antibody) with a small proportion perhaps existing in other cellular compartments, such as mitochondria. At the beginning of my PhD, one antibody for Kir6.1 was already available for me to perform my colocalisation studies but my own contribution was the purification of the MBP-Kir6.1C antibody (93A). The Kir6.1C (78A) affinity purified antibody was previously purified in our group but I also characterised this antibody as described in chapter 3.1. However, the affinity purified Kir6.1C antibody was used by others in our group hence the acid fractions were in very short supply. Therefore the MBP-Kir6.1C antibody (93A) (which was purified and characterised by me) was used throughout this chapter to detect native Kir6.1 as I managed to purify a significant amount of this antibody.

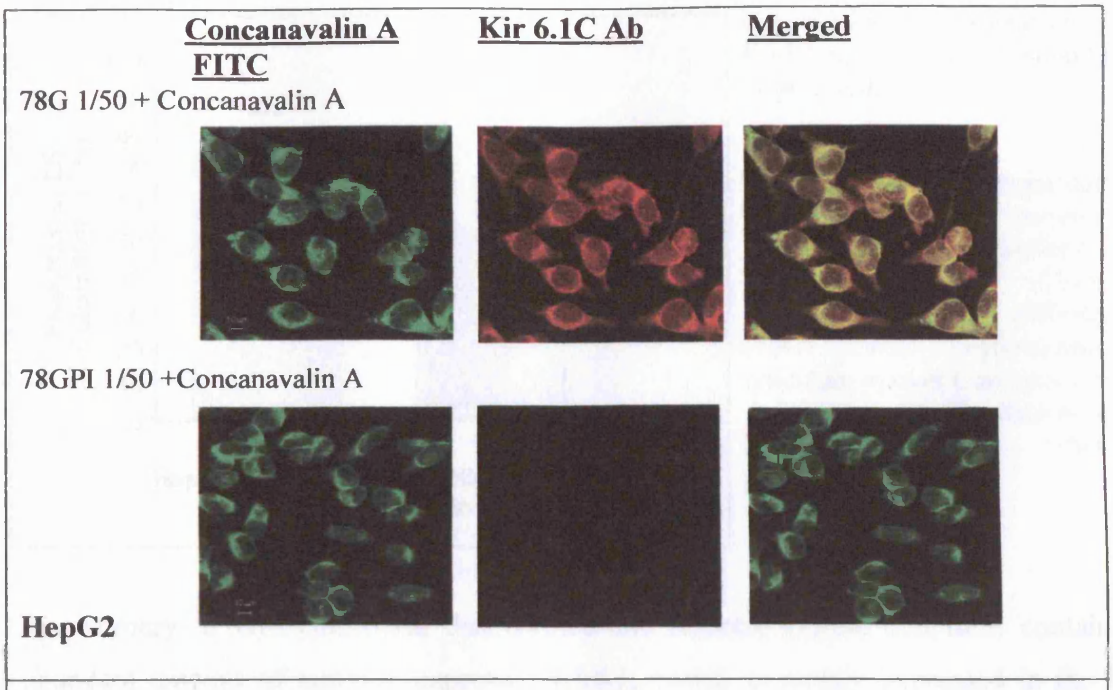

Figure 3.27. The distribution of Kir6.1 in HepG2 cells.

Images to show the endogenous distribution of Kir6.1 in HepG2 cell line using Kir6.1C (Affinity purified) antibody 78G and Concanavalin A FITC. The 78G pre-immune sample was used as the control and slides were analysed as described in figure 3.20. This second antibody confirms that there is endogenous Kir6.1 in the HepG2 cell line.

During the purification process, the antibody is usually present in acidic fractions but there is also a possibility it is present in the guanidine fractions (which was also stored). The concentration of this antibody would be lower in the guanidine fractions so a higher concentration of the Kir6.1C (78A) affinity purified antibody was used to detect natively expressed Kir6.1. This antibody was able to detect a significant amount of Kir6.1 in HepG2 cells, see figure 3.27. In addition to this, the control experiment show that Kir6.1 was not detected with the pre-immune sample (78PI). The statistics in figure 3.28 indicates that there was significant colocalisation between Kir6.1 and ER pixels $p<0.001$ (***). About 50 % of Kir6.1 was expressed in the ER.

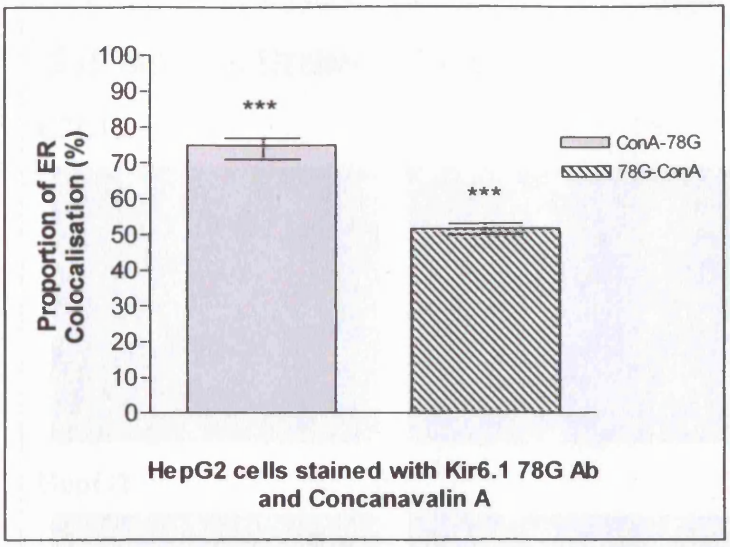

Figure 3.28. The proportion of Kir6.1 and ER colocalisation in HepG2 cells.

A graph to show the proportion of colocalisation between Kir6.1 and the endoplasmic reticulum using a affinity purified Kir6.1C antibody (78G) and endoplasmic reticulum marker Concanavalin A FITC n= 29. The data were highly significant when $p<0.001$ (***).

In summary, I have confirmed that cardiac and skeletal muscle cell lines contain an abundant amount of natively expressed Kir6.1, which is mostly expressed in the ER. Despite this observation, there is a small but rather significant proportion of Kir6.1 that is unaccounted for which may be located in other intracellular compartments such as the mitochondria. I then decided to explore this further by using a marker for mitochondria called as cytochrome C oxidase (complex IV) as this is a component of the electron transport chain involved in oxidative phosphorylation. The MBP-Kir6.1C antibody (93A) is a reliable tool as I had previously set up suitable controls to detect Kir6.1. However, I decided for this particular experiment to also use the affinity purified antibody Kir6.1C (78G) to stain for Kir6.1. In my hands, this antibody was more specific than the MBP-Kir6.1C antibody because it only detected a 48 kDa band corresponding to the molecular weight of Kir6.1 (see chapter 3.1). The endogenous expression of Kir6.1 and cytochrome oxidase in skeletal muscle and liver cell lines is shown in figure 3.29.

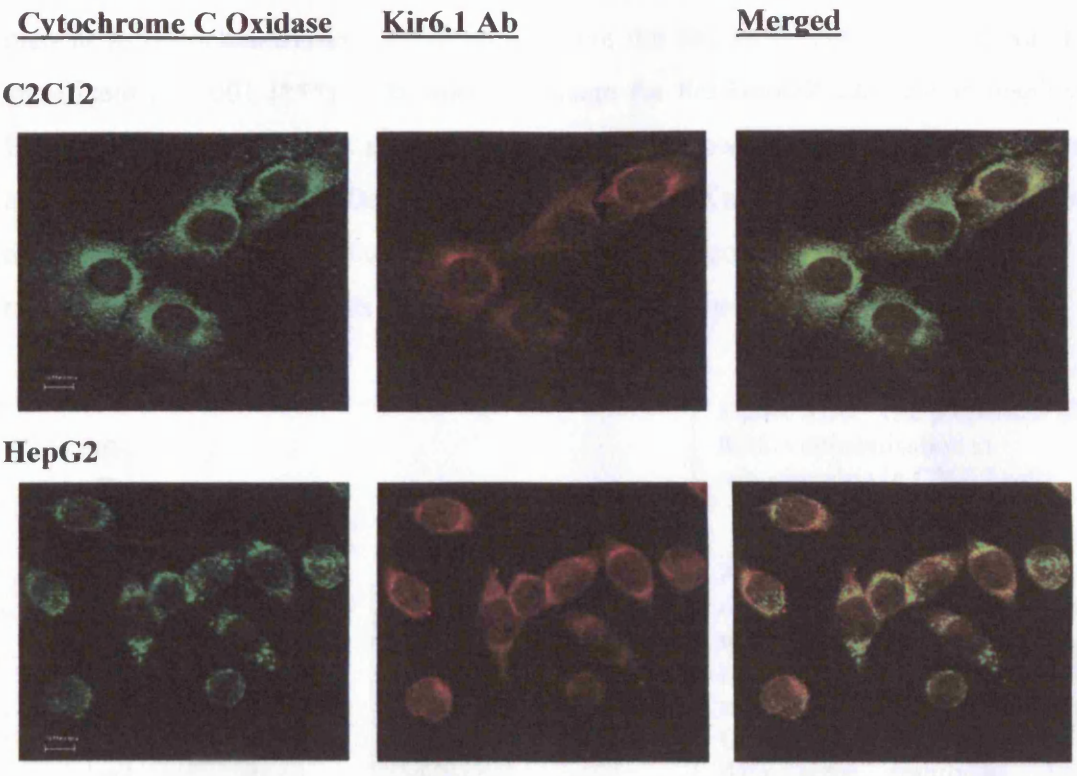

Figure 3.29. The distribution of Kir6.1 in mitochondria.

Images to show the endogenous expression of Kir6.1 and cytochrome C oxidase in C2C12 and HepG2 cell line. I used Kir6.1C (78G) antibody and mouse monoclonal cytochrome C oxidase as the marker for mitochondria. The secondary antibody used to identify Kir6.1 was a rhodamine conjugated goat anti-rabbit antibody and a FITC conjugated donkey anti-mouse antibody was used to detect cytochrome C oxidase.

The liver and skeletal muscle cell lines stained for cytochrome C oxidase in particular, the protein in C2C12 cell line is evenly distributed throughout the cell whereas in HepG2 cells, the signal for cytochrome C oxidase is more granular and randomly distributed throughout the cytoplasm. The proportion of colocalised yellow pixels in the C2C12 cell line is high as shown in the merged image. HepG2 cells are active cells and contain lots of mitochondria and interestingly; the mitoK_{ATP} channel was originally isolated from mitochondria in this cell line (*Inoue et al. 1991*). The proportion of colocalisation between Kir6.1 (red) and cytochrome C oxidase pixels (green) was significant for both

cell lines. The results in figure 3.30 show that about 65 % (second column) of Kir6.1 was present in mitochondria in C2C12 cells where the degree of colocalisation was highly significant $p<0.001$ (***). The merged image for the HepG2 cell line is displayed in figure 3.28 and shows that a fraction of Kir6.1 does not colocalise in the mitochondria and remains cytoplasmic. Despite this, about 30 % of Kir6.1 pixels exist in mitochondria as indicated by the second column in figure 3.31. The colocalisation between Kir6.1 and mitochondria in HepG2 cells was also significant when $p<0.001$ (***).

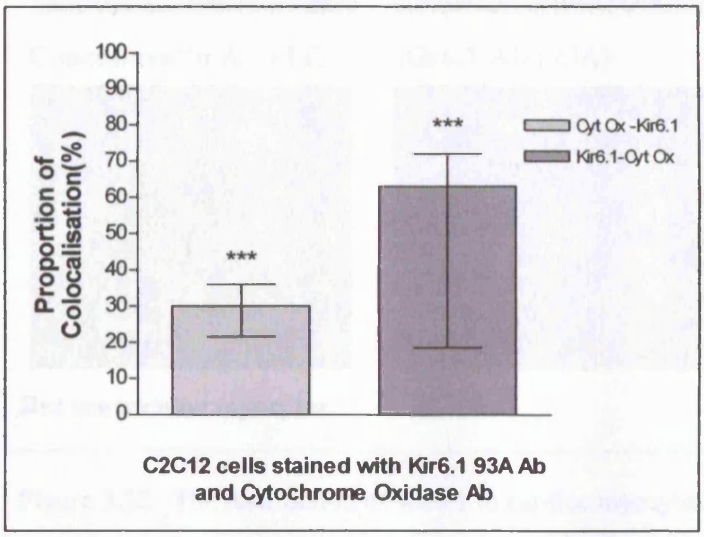

Figure 3.30. The proportion of Kir6.1 colocalisation in mitochondria in C2C12 cells.

A graph to show the proportion of colocalisation between mitochondria and Kir6.1 using a affinity purified Kir6.1C antibody (93A) and cytochrome C oxidase antibody n= 17. The data were significant when $p<0.001$ (***).

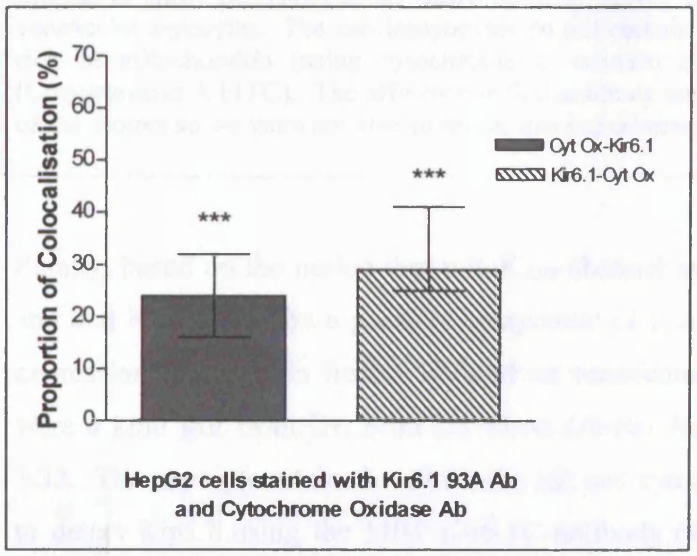

Figure 3.31. The proportion of Kir6.1 colocalisation in mitochondria in HepG2 cells.

C. A graph to show the proportion of colocalisation between mitochondria and Kir6.1 using a affinity purified Kir6.1C antibody (93A) and cytochrome C oxidase antibody n= 22. The data were significant when $p<0.001$ (***).

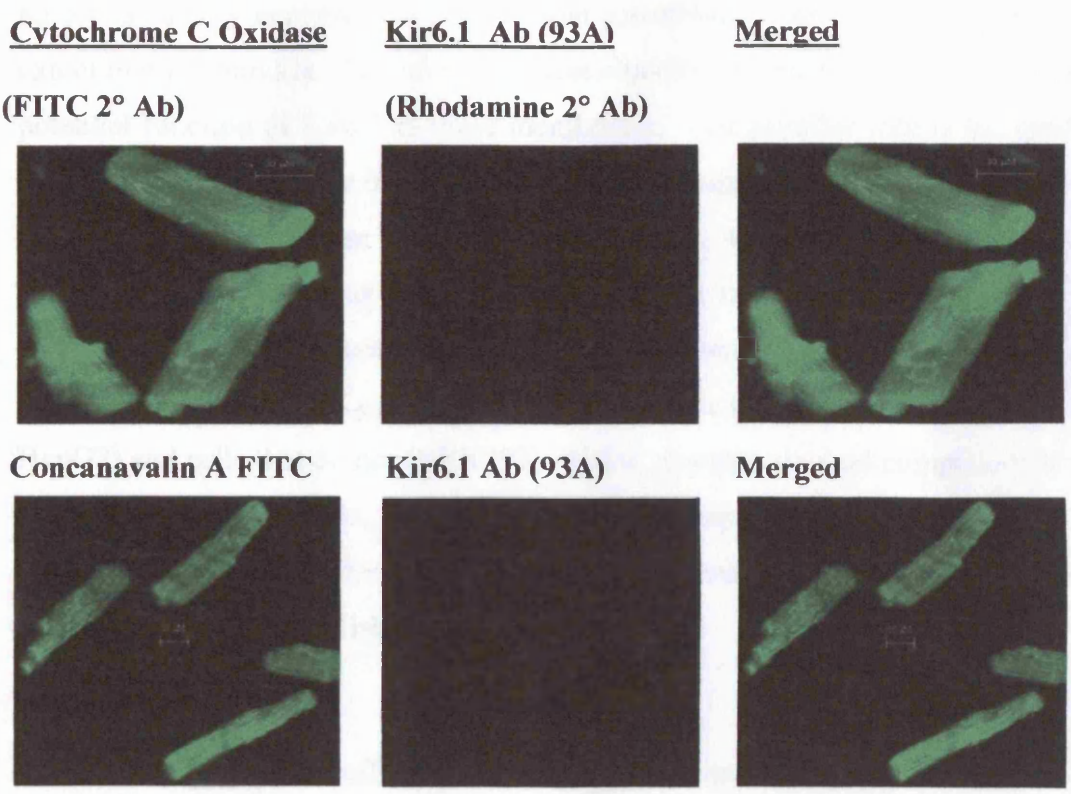

Figure 3.32. The distribution of Kir6.1 in cardiac myocytes.

Images to show the endogenous distribution of Kir6.1 using MBP-Kir6.1C (93A) in rat ventricular myocytes. The cardiomyocytes do not contain Kir6.1. However, these cells are rich in mitochondria (using cytochrome C oxidase as the marker) and contain ER (Concanavalin A FITC). The affinity purified antibody was no longer available at this stage of the project so we were not able to repeat this experiment with this tool.

Finally, based on the notion that mitoK_{ATP} channel may be involved in cardioprotection and that Kir6.1 may be a possible component of this channel, I decided to examine the expression of Kir6.1 in freshly isolated rat ventricular myocytes. These cells were also were a kind gift from Dr. Sean Davidson (*Hatter institute, UCL, London*). See figure 3.32. The myocytes stained well for the ER and cytochrome C oxidase but I was unable to detect Kir6.1 using the MBP-Kir6.1C antibody (93A) this could be because Kir6.1 expression may be below detectable levels. Although this antibody could not detect Kir6.1 in rat myocytes, earlier, I was able to detect Kir6.1 in rat HL-1 cardiomyocytes.

3.4 Investigating reactive oxygen species production in immortalised cell lines

Kir6.1 is mainly expressed in intracellular membranes such as the ER and to some extent in mitochondria. Therefore, the next objective of this thesis was to examine the potential function of Kir6.1 in these membranes. One possible role is the production of ROS as a consequence of mitoK_{ATP} channel opening during IPC. The mechanisms conferring protection are poorly understood but the general consensus is that mitoK_{ATP} channel opening promotes mitochondrial matrix swelling, conserves ATP reserves and ROS production. It is therefore essential to establish whether ROS production is linked to K_{ATP} channel activity in cells that express Kir6.1 (C2C12 and HepG2) and cells that do not (HEK293). Using pharmacological compounds to assess the role of K_{ATP} channels, the ROS assay was set up to examine whether diazoxide could increase ROS production in these immortalised cell lines and whether glibenclamide could abolish this response.

3.4.1 Investigating the effect of diazoxide and glibenclamide on ROS production

Three experimental conditions were set up to measure ROS production. In the control experiment, a placebo consisting of DMSO and PBS was administered at 1 and 3 minutes. The control experiment was set up to demonstrate that the basal medium and drug solvents did not modulate the activity of K_{ATP} channels; therefore, there should be no significant changes in ROS production. ROS production was then examined in the presence of 50 μM diazoxide and 10 μM glibenclamide. I also investigated the effect of 100 μM diazoxide to assess whether ROS production was dose dependent. Each experimental condition was carried out at least three times. Please refer to chapter 2.9 for methods.

The focus of this chapter was to establish whether ROS production is related to the expression of Kir6.1. This was carried out by suppressing Kir6.1 protein expression to probe for differences, if any, in ROS production in response to diazoxide and glibenclamide with molecular tools such as DN and siRNA of Kir6.1. In figure 3.33, a typical trace measuring the changes in ROS fluorescence from each condition is shown for HepG2 cells. The raw data for each cell line and different experimental

condition were not displayed as means ± SEM because if the whole data set for each condition were averaged, this would obscure the results with large error bars which would make it difficult to observe any trends in response to the drugs.

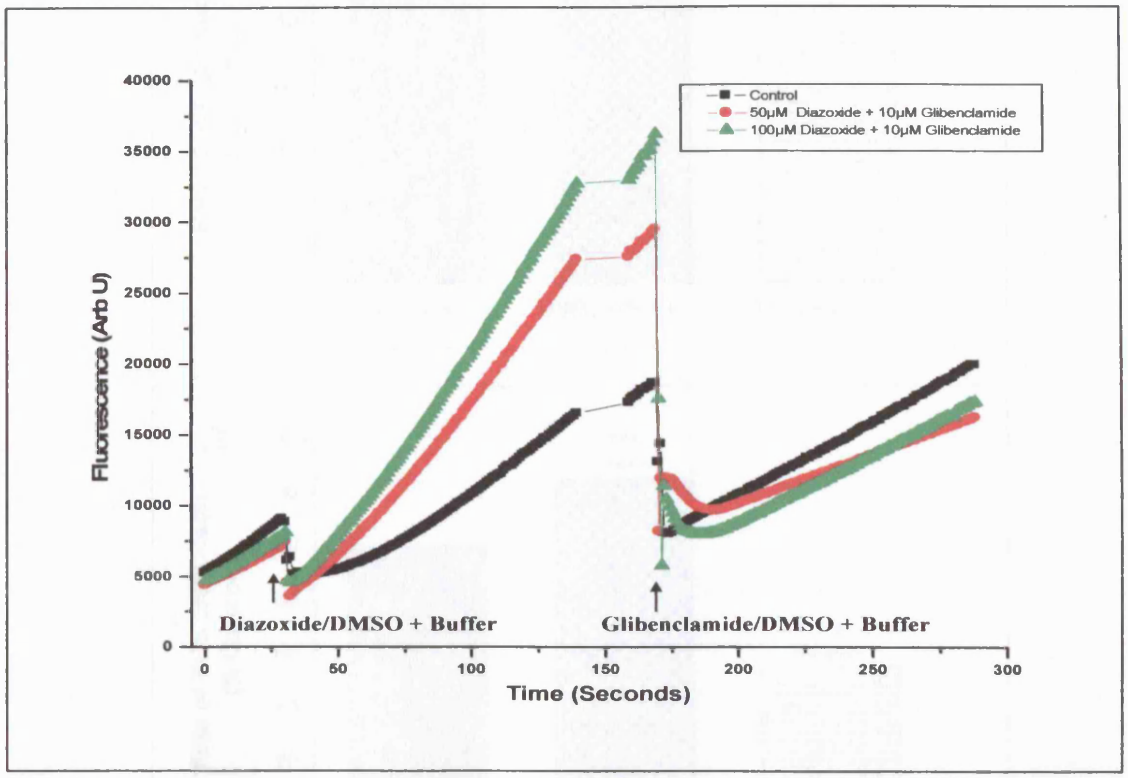

Figure 3.33. A graph to show the raw data for HepG2 cells loaded with DCF-DA.

Three different conditions were set up and the cells were either treated with DMSO + buffer or diazoxide (50 μM or 100 μM) followed by 10 μM glibenclamide. The fluorescence (arbitrary units) was measured every second.

To analyse the effect of interventions, the alteration of the rate was compared to the control value for each experiment using a paired t-test. The p values that were <0.05 were considered significant. For graphical display, the control values are set to 100 %, and changes are observed as percentage (%) increase or decrease. The data for ROS production is displayed in figure 3.34. Statistical analyses were carried out between the two concentrations of diazoxide as well as differences between control cells and cells without Kir6.1. Please refer to tables 3.6 and 3.7 (end of chapter).

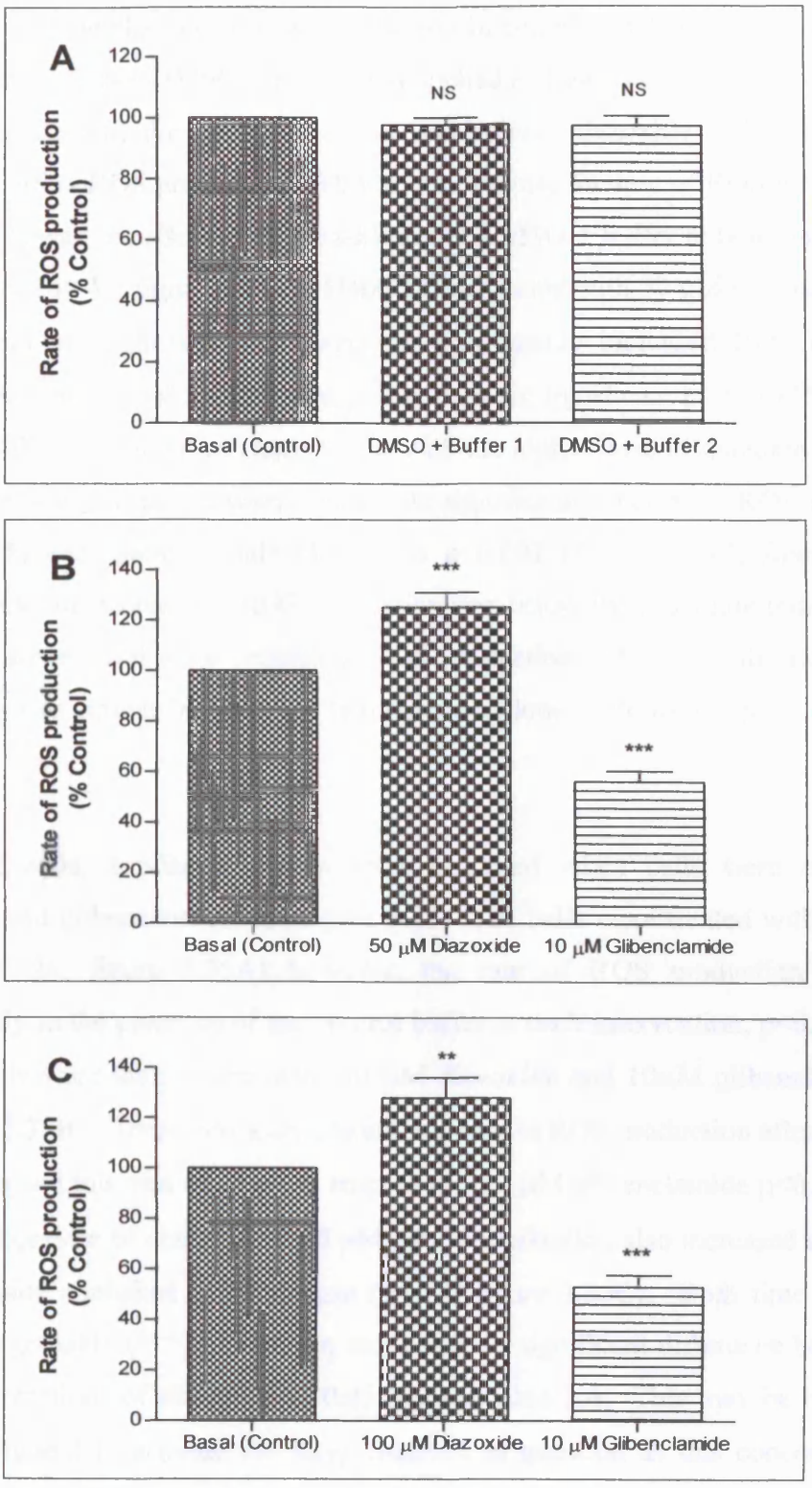

Figure 3.34. Data for ROS production in HepG2 cells.

A. A graph to show the rate of ROS production in HepG2 cells (n= 47).
B. A graph to show the rate of ROS production in the presence of 50 μM diazoxide and 10 μM glibenclamide in HepG2 cells (n= 48).
C. A graph to show the rate of ROS production in the presence of 100 μM diazoxide and 10 μM glibenclamide in HepG2 cells (n= 41).

Figure 3.34 shows the rate of ROS production in control HepG2 cells. The carriage medium consisting of DMSO + buffer was applied at 1 and 3 minutes. It is important to demonstrate that the DMSO used to reconstitute diazoxide and glibenclamide would not affect ROS production. This is true because the rate of ROS production in HepG2 cells was not affected by the addition of DMSO + buffer at both interventions $p>0.05$ (NS) (n= 47, figure 3.34A). HepG2 cells treated with 50 μM diazoxide and 10 μM glibenclamide showed that diazoxide significantly increased ROS production with glibenclamide abolishing this response, both are significant $p<0.01$ (***) (n= 48, figure 3.34B). Treatment of HepG2 cells with the higher dose of diazoxide (100μM) showed the same response where diazoxide significantly increased ROS production $p<0.01$ (**) and glibenclamide blocked it $p<0.001$ (***) (n= 41, figure 3.34C). Interestingly, the decrease in ROS production was below the basal rate indicating that there was some basal K_{ATP} dependent ROS production. However, the rate of ROS production was similar between the two concentrations of diazoxide $p>0.05$ (†). See table 3.6.

In C2C12 cells, similar responses were observed when cells were exposed to diazoxide and glibenclamide, see figure 3.35. The cells were treated with DMSO + buffer (n= 24, figure 3.35A) however, the rate of ROS production decreased significantly in the presence of the control buffer at each intervention, $p<0.001$ (***). C2C12 cells were then treated with 50 μM diazoxide and 10μM glibenclamide (n= 24, figure 3.35B). There was a significant increase in ROS production after diazoxide application and this was reversed in response to 10 μM glibenclamide $p<0.001$ (***). At the higher dose of diazoxide (100 μM), ROS production also increased and 10 μM glibenclamide abolished this response (n= 24, figure 3.35C). Both time points are significant $p<0.001$ (***). However, there was no significant difference between the two concentrations of diazoxide $p>0.05$ (€), see table 3.6. This may be because 50 μM is sufficient to activate the K_{ATP} channels in question as this concentration of diazoxide reached the top of the dose response curve and increasing the concentration of diazoxide would therefore not have any further effect on ROS production.

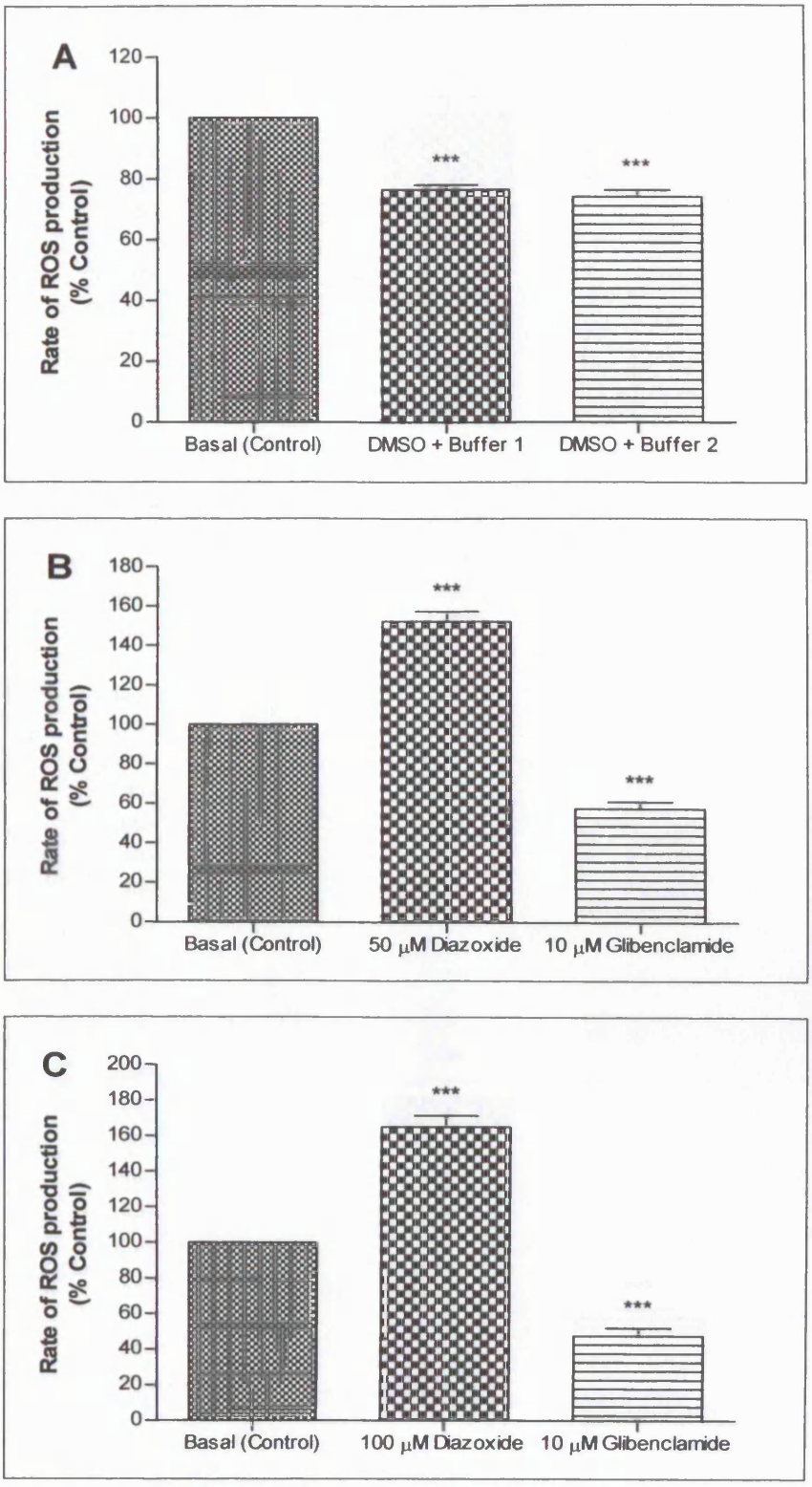

Figure 3.35. Data for ROS production in C2C12 cells.

A. A graph to show the rate of ROS production in C2C12 cells (n= 24).
B. A graph to show the rate of ROS production in the presence of 50 μM diazoxide and 10 μM glibenclamide in C2C12 cells (n= 24).
C. A graph to show the rate of ROS production in the presence of 100 μM diazoxide and 10 μM glibenclamide in C2C12 cells (n= 24).

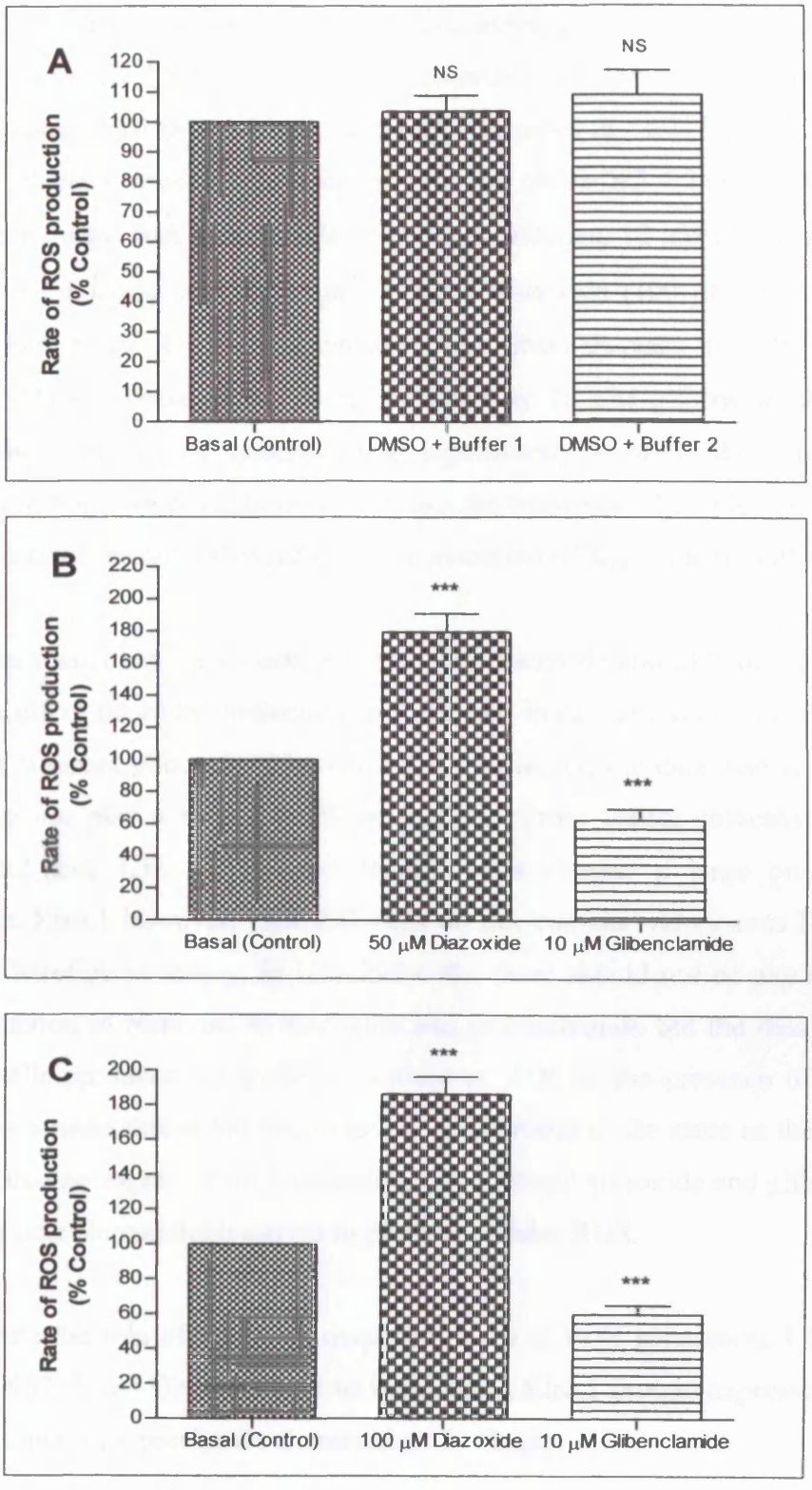

Figure 3.36. Data for ROS production in HEK293 cells.

A. A graph to show the rate of ROS production in HEK293 cells (n= 59).
B. A graph to show the rate of ROS production in the presence of 50 μM diazoxide and 10 μM glibenclamide in HEK293 cells (n= 53).
C. A graph to show the rate of ROS production in the presence of when 100 μM diazoxide and 10 μM glibenclamide in HEK293 cells (n= 51).

The HEK293 cell line which does not express endogenous Kir6.1 was also used for this assay (*Cui et al. 2001*). HEK293 cells recorded a steady rate of ROS production in the presence of DMSO + buffer at 1 and 3 minutes (n= 59, figure 3.36A). No significant changes were observed in the presence of DMSO + buffer $p>0.05$ (NS). HEK293 cells were then treated with 50 μM diazoxide and 10 μM glibenclamide (n= 51, figure 3.36B), and with the higher dose of diazoxide (100 μM) (n= 53, figure 3.36C). Both doses of diazoxide caused a significant increase in ROS production $p<0.001$ (***) and these effects were abolished by 10 μM glibenclamide $p<0.001$ (***). The presence of glibenclamide significantly reduced the rate of ROS production in both experiments i.e. lower than the basal rate. In table 3.6, the rate of ROS production was not affected by the concentration of diazoxide $p>0.05$ (‡).

These experiments have demonstrated that both diazoxide and glibenclamide have a significant effect on ROS production in these cell lines. Diazoxide increased ROS production whereas glibenclamide reduced it. However, the data also suggests that Kir6.1 may not play a role in ROS production. From earlier colocalisation work (chapter 3.2 and 3.3), C2C12 and HepG2 cells express a large proportion of endogenous Kir6.1 however; HEK293 cells do not contain endogenous Kir6.1 (and Kir6.2). Therefore in theory, in HEK293 cells, there should not be any changes in ROS production in response to diazoxide and glibenclamide but the data show that HEK293 cells produced a significant amount of ROS in the presence of diazoxide with glibenclamide abolishing this response. This result is the same as the other two cells lines that do express Kir6.1 indicating that perhaps diazoxide and glibenclamide may act on other intracellular targets to produce cellular ROS.

To determine the role of Kir6.1 in diazoxide induced ROS generation, I treated my cells with siRNA and DN for Kir6.1 to knockdown Kir6.1 protein expression. These molecular tools were previously characterised in chapter 3.1.

The human form of siRNA for Kir6.1 was transiently transfected into HepG2 and HEK293 cell lines whilst 61siRNA duplex 2 (from rat) was transfected into the C2C12 cell line. A parallel experiment was set up where cells were co-transfected with eGFP so that the transfection efficiencies could be assessed, see figure 3.37. The transfected cells were visualised with a UV microscope 24 hours after transfection. The transfection efficiency for HepG2 cells would be higher than 30 % after 48 hours, however, I did not want the cells to become too confluent as this would affect the cell density and may obscure the results. The transfected cells were examined again after 36 hours before the plate containing cells transfected with just 61siRNA (without eGFP) were loaded with the ROS indicator, DCF-DA. The logic for not using cells transfected with both 61siRNA and eGFP is because the fluorophore would also be excited by the 488 nm laser which is intended for the DCF-DA dye.

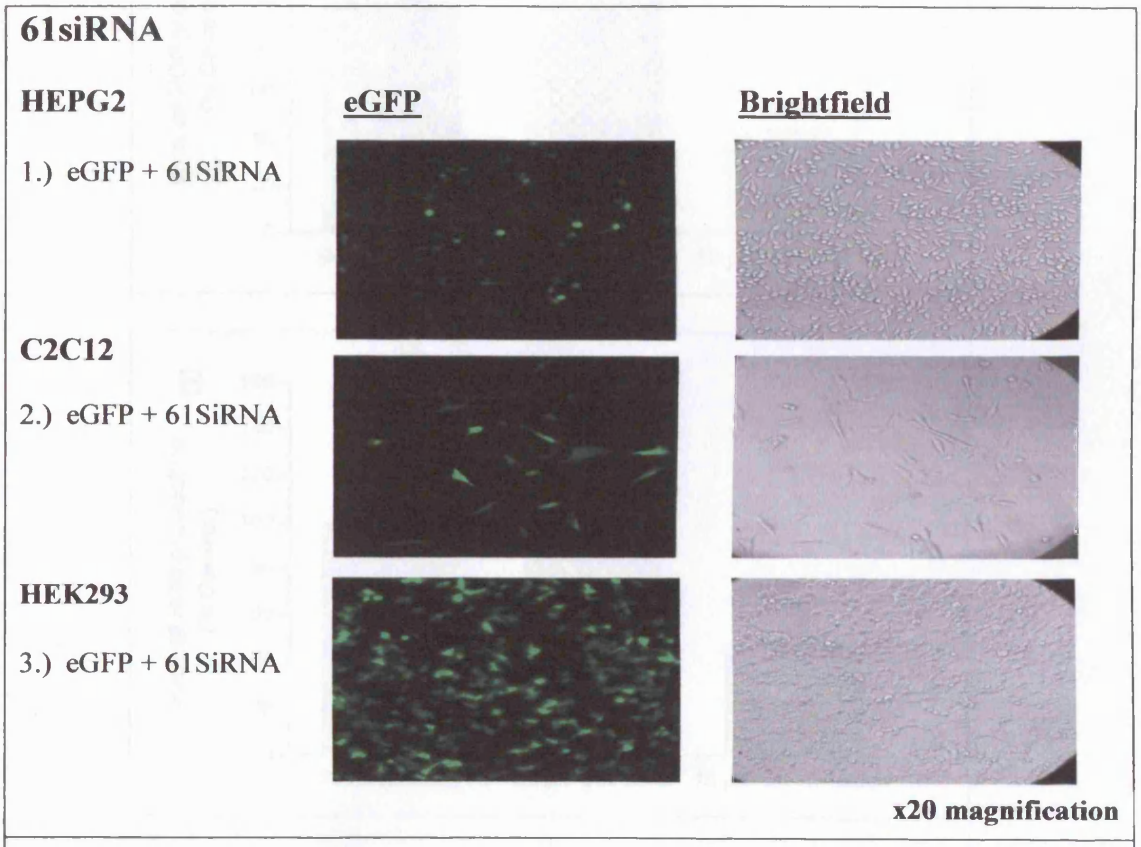

Figure 3.37. Images to show the cells used for ROS assay were transfected efficiently with siRNA for potassium channel subunit Kir6.1.
1.) HepG2 cells were transfected with eGFP and 61siRNA; these cells had a transfection efficiency of about 30-40 %. The cells were healthy and alive after transfection, see brightfield image. 2.) C2C12 cells had a transfection efficiency of 40 %. 3.) HEK293 cells were also transfected with eGFP and 61SiRNA but had 90 % transfection efficiency.

To explore the possible role of Kir6.1 in ROS production, HepG2 cells were transfected with the human form of siRNA61, see figure 3.38. These cells were treated with 50 μM or 100 μM diazoxide and 10 μM glibenclamide (both n= 24). In figure 3.38A, there was an increase in ROS production from basal levels in response to 50 μM diazoxide $p<0.05$ (*) with glibenclamide blocking this response $p<0.001$ (***). In figure 3.38B, 100 μM diazoxide also increased ROS production and glibenclamide significantly decreased ROS production $p<0.001$ (***). Statistical analysis showed that there was no significant difference between the two concentrations of diazoxide (††), see table 3.6.

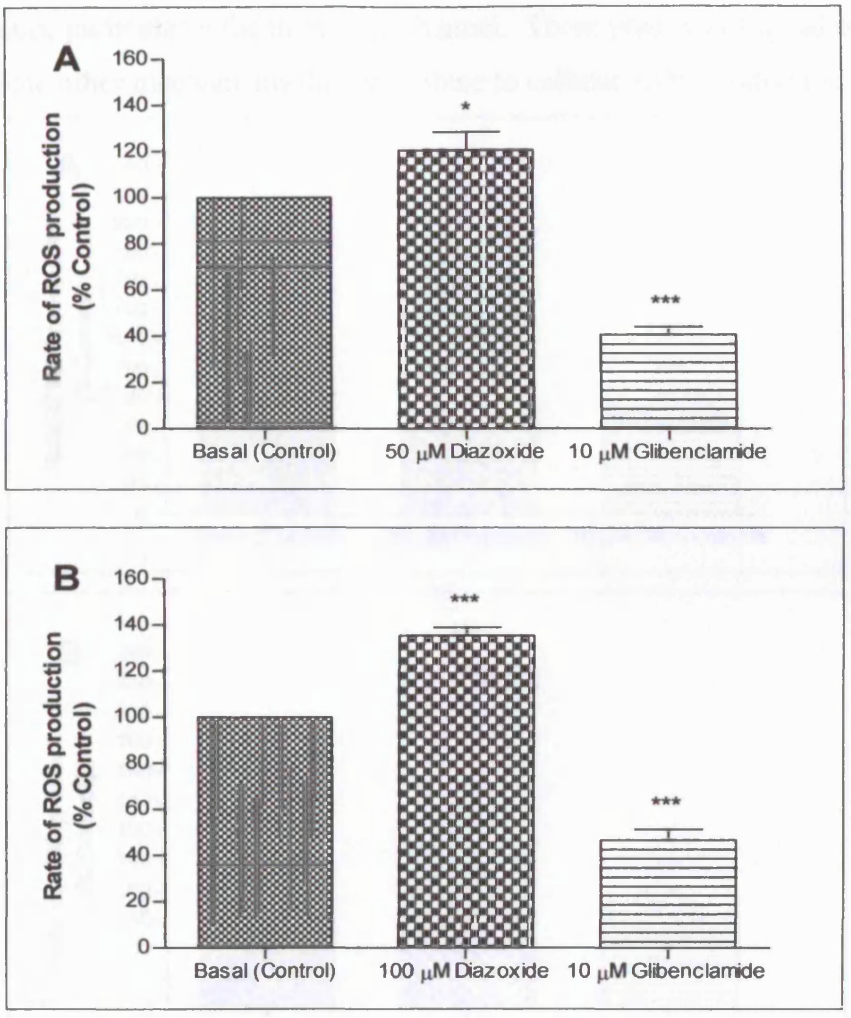

Figure 3.38. Data for ROS production in HepG2 cells without Kir6.1.

A. A graph to show the rate of ROS production in HepG2 cells transfected with siRNA for Kir6.1 in the presence of 50 μM diazoxide and 10 μM glibenclamide (n= 24).
B. A graph to show the rate of ROS production in HepG2 cells transfected with siRNA for Kir6.1 in the presence of 100 μM diazoxide and 10 μM glibenclamide (n= 24).

The effects of diazoxide and glibenclamide were also examined in C2C12 cells transfected with 61siRNA duplex 2 (both n= 24, figure 3.39). In figure 3.39A, 50 μM diazoxide significantly increased ROS production with glibenclamide abolishing this response $p<0.001$ (***). This is a big increase compared to control C2C12 cells which contain Kir6.1, see figure 3.35. The higher dose of diazoxide (100 μM) in figure 3.39B also increased ROS production but this was similar to the lower dose of diazoxide (50 μM) (€€), see table 3.6. In figure 3.39B, glibenclamide reversed diazoxide induced ROS production $p<0.001$ (***). The data suggest that the absence of Kir6.1 may increase the cells' sensitivity to diazoxide but also questions the role of K_{ATP} channels, particularly the mitoK_{ATP} channel. These pharmacological compounds may modulate other mechanisms that contribute to cellular ROS production.

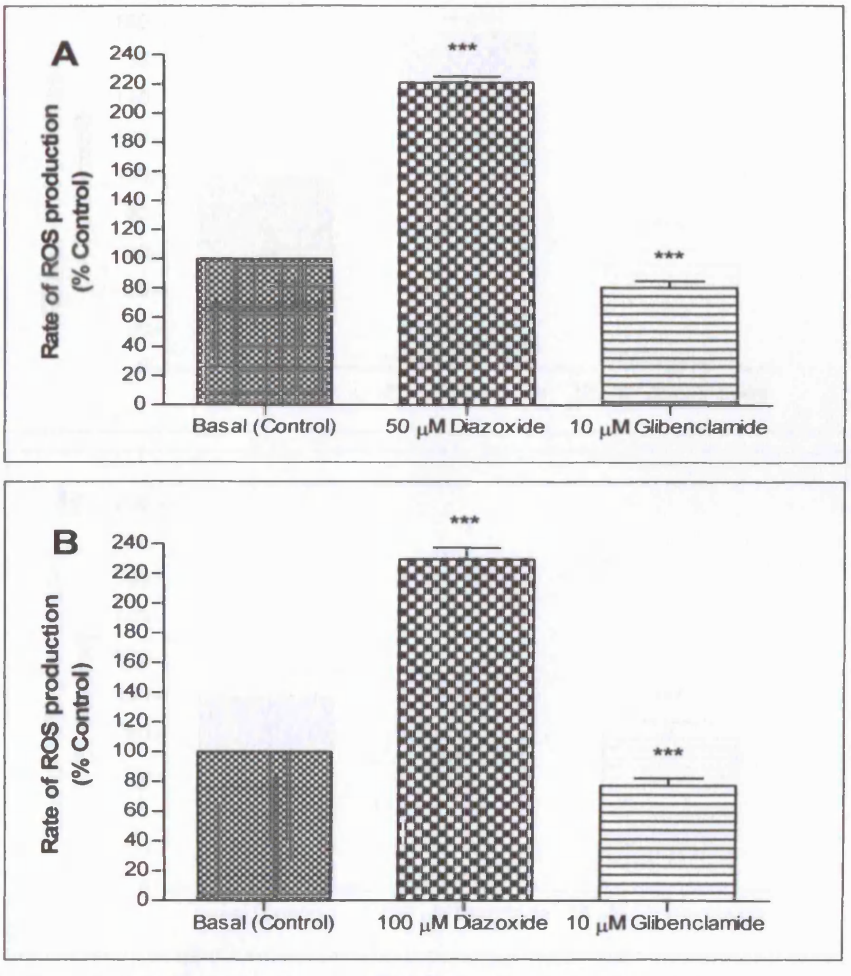

Figure 3.39. Data for ROS production in C2C12 cells without Kir6.1.

A. A graph to show the rate of ROS production in C2C12 cells transfected with siRNA for Kir6.1 in the presence of 50 μM diazoxide and 10 μM glibenclamide (n= 24).
B. A graph to show the rate of ROS production in C2C12 cells transfected with siRNA for Kir6.1 in the presence of 100 μM diazoxide and 10 μM glibenclamide (n= 24).

The previous data in HEK293 cells suggested that these pharmacological compounds have a significant effect on ROS production which is independent of K_{ATP} channels. HEK293 cells were also transfected with human 61siRNA, see figure 3.40. HEK293 cells treated with 50 μM diazoxide significantly increased ROS production and 10 μM glibenclamide abolished this effect $p<0.001$ (***) (n= 24, figure 3.40A). The higher dose of diazoxide showed a similar response (n= 24, figure 3.40B). The addition 10 μM glibenclamide significantly reduced ROS production $p<0.001$ (***). However, the rate of ROS production was not affected by the two concentrations of diazoxide (‡‡), see table 3.6.

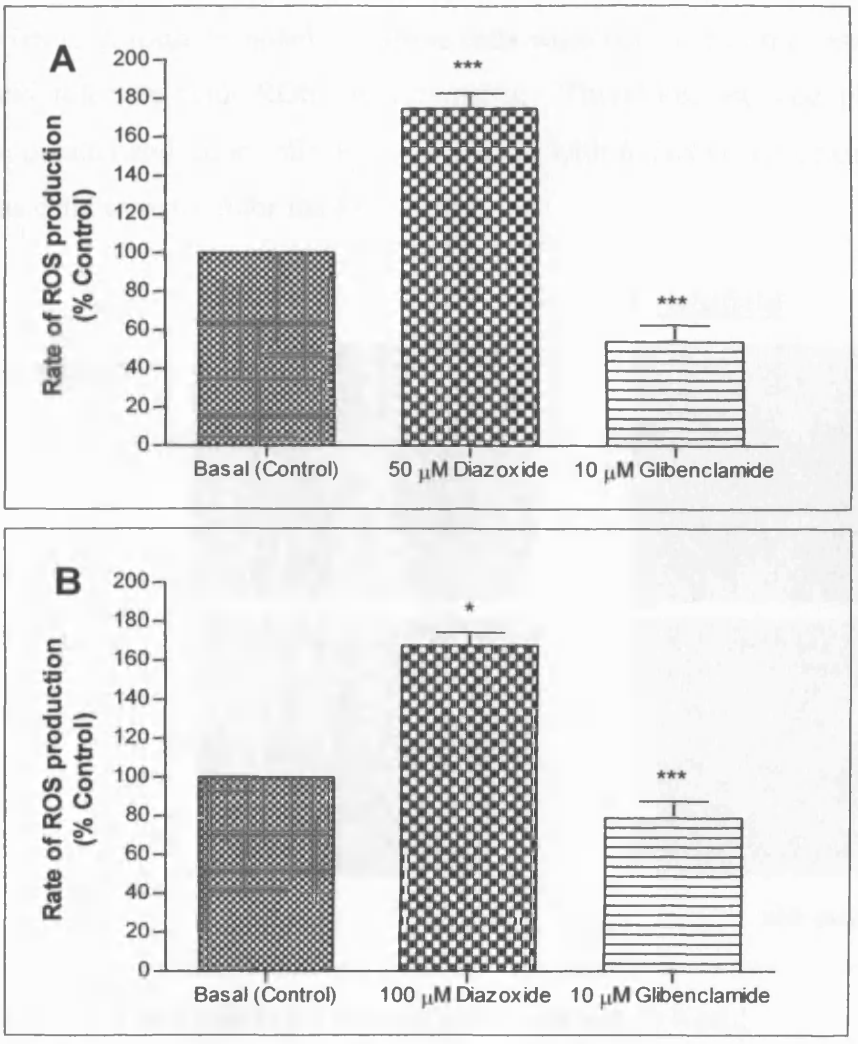

Figure 3.40. Data for ROS production in HEK293 cells without Kir6.1.

A. A graph to show the rate of ROS production in HEK293 cells transfected with siRNA for Kir6.1 in the presence of 50 μM diazoxide and 10 μM glibenclamide (n=24).
B. A graph to show the rate of ROS production in HEK293 cells transfected with siRNA for Kir6.1 in the presence of 100 μM diazoxide and 10 μM glibenclamide (n=24).

The data show that diazoxide promoted ROS production whereas glibenclamide inhibited this response. HEK293 cells do not contain endogenous Kir6.1 but showed a response to diazoxide suggesting that Kir6.1 probably does not have a role in ROS production. Moreover, the absence of Kir6.1 in cells transfected with 61siRNA did not affect the rate of ROS production. These results show that the responses observed in cells transfected with 61siRNA were independent of Kir6.1 and diazoxide-induced ROS production may involve other cellular mechanisms. To confirm this finding, C2C12 cells were transfected with DN forms of Kir6.1, called 61DN G→A or 61DN G→S. These were co-transfected with eGFP so that the transfection efficiency could be quantified. Figure 3.41 contains examples of these transfections with the DN forms of Kir6.1. It must be noted that these cells were not used in the assay because eGFP would interfere with ROS measurements. Therefore, separate plates were prepared in parallel and these cells were transfected with 61DN G→A or 61DN G→S only. These cells were used for the ROS assay.

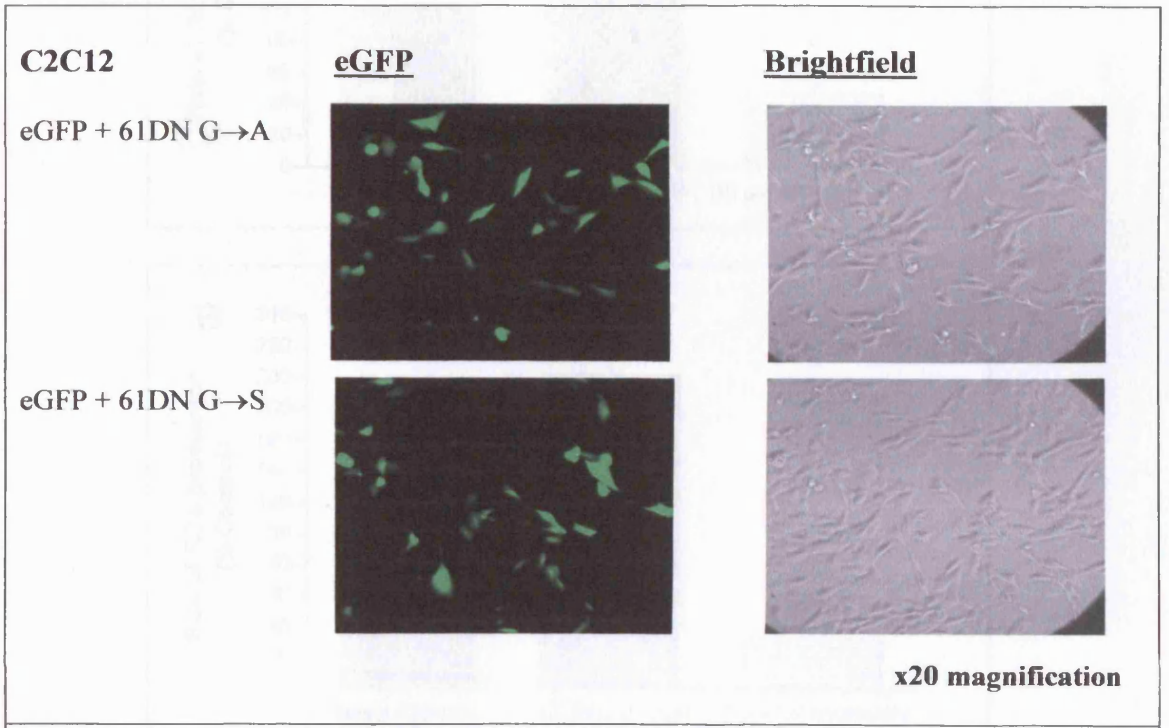

Figure 3.41. C2C12 cells transfected with dominant negatives for Kir6.1

Images to show the C2C12 cell were transfected efficiently with dominant negative for potassium channel subunit Kir6.1. The brightfield images show that the cells were healthy after transfection. C2C12 cells transfected with eGFP and DN for Kir6.1 G→A substitution and Kir6.1 G→S substitution. The transfection efficiency was approximately 50%.

In figure 3.42, C2C12 cells were transfected with 61DNG→A before they were treated with 50 μM or 100 μM diazoxide and 10 μM glibenclamide. The lower dose of diazoxide (50 μM) caused a significant increase in ROS production (100 %) $p<0.001$ (***) with 10 μM glibenclamide abolishing this effect $p<0.01$ (*) (n= 19, figure 3.42A). C2C12 cells treated with the higher dose of diazoxide (100 μM) also showed the same response (n= 17, figure 3.42B). The addition of both drugs were highly significant $p<0.001$ (***). In table 3.6, the stimulatory effect of diazoxide was not dose dependent (#) but both experiments show that the inhibitory effect of glibenclamide reduced ROS production below basal levels.

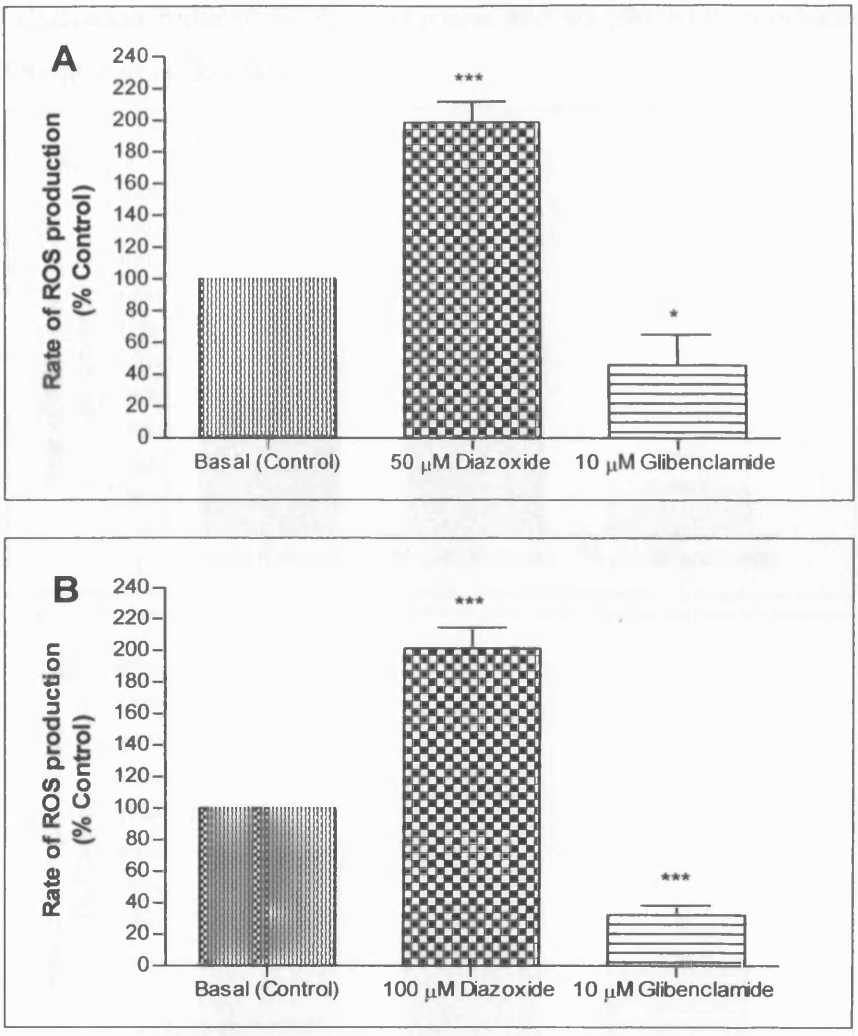

Figure 3.42. Data for ROS production in C2C12 cells transfected with dominant negatives for Kir6.1.

A. A graph to show the rate of ROS production in C2C12 cells transfected with transfected with 61DNG→A in the presence of 50 μM diazoxide and 10 μM glibenclamide (n= 19).
B. A graph to show the rate of ROS production in C2C12 cells transfected with transfected with 61DNG→A in the presence of 100 μM diazoxide and 10 μM glibenclamide (n= 17).

In figure 3.43, C2C12 cells treated with 61DN G→S also showed the same response to diazoxide and glibenclamide. Both concentrations of diazoxide (50 μM and 100 μM) significantly increased the rate of ROS production with 10 μM glibenclamide inhibiting the stimulatory effects of diazoxide $p<0.001$ (***) (n= 16, figure 3.43A and n= 17, figure 3.43B). The concentration of diazoxide did not affect the rate of ROS production (¶), see table 3.6. These experiments show that Kir6.1 is not involved in mediated ROS production as suppressing Kir6.1 protein expression did not alter the cells' response to these compounds. The results in this chapter are summarised in table 3.6. Statistical analyses were carried out to test for significant differences in i) the rate of diazoxide induced ROS production and ii) and ROS production in cells with and without Kir6.1, see table 3.7.

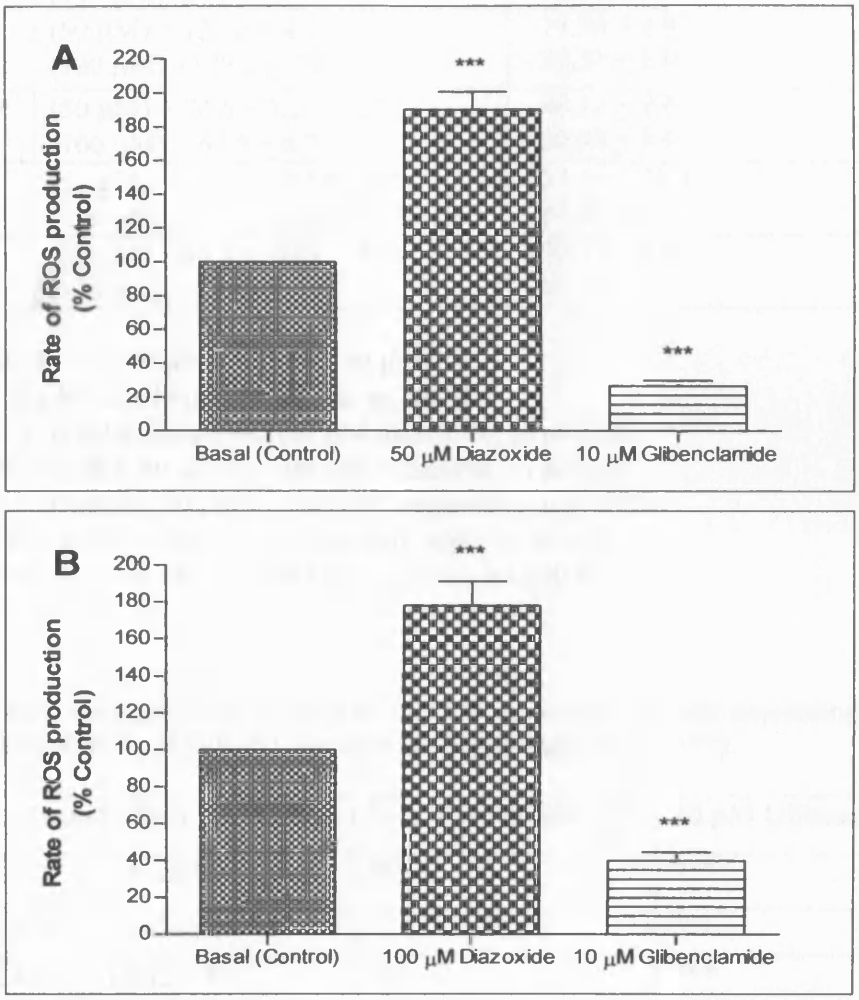

Figure 3.43. Data for ROS production in C2C12 cells transfected with dominant negatives for Kir6.1.
A. A graph to show the rate of ROS production in C2C12 cells transfected with transfected with 61DNG→S in the presence of 50 μM diazoxide and 10 μM glibenclamide (n= 16).
B. A graph to show the rate of ROS production in C2C12 cells transfected with transfected with 61DNG→S in the presence of 100 μM diazoxide and 10 μM glibenclamide (n= 17).

Table 3.6.

A table to summarise the average % increase or decrease in ROS production in the presence of 50 μM or 100 μM diazoxide and 10μM glibenclamide in control and transfected C2C12, HepG2 and HEK293 cells. The results are presented as means ± SEM.

Cell Type	**Average % increase in ROS production in the presence of 50 μM or 100 μM diazoxide**	**Average % decrease in ROS production in the presence of 10 μM glibenclamide**
HepG2	(50 μM) + 25.0 ± 5.9 † (100 μM) + 27.9 ± 8.0	- 44.0 ± 4.2 - 46.87 ± 4.6
C2C12	(50 μM) + 52.3 + 5.0 € (100 μM) + 65.3 + 6.3	- 42.45 + 3.5 - 52.03 + 4.3
HEK293	(50 μM) + 79.4 ± 11.5 ‡ (100 μM) + 86.3 ± 10.1	- 37.44 ± 6.7 - 40.15 ± 5.4
HepG2 + 61siRNA	(50 μM) 120.6 ± 7.9 †† (100 μM) 135.5 ± 3.7	- 59.35 ± 3.5 - 53.27 ± 4.6
C2C12 + 61siRNA	(50 μM) + 121.2 ± 4.1 €€ (100 μM) +129.7 ± 7.8	- 19.50 ± 4.9 - 22.51 ± 5.0
HEK293 + 61siRNA	(50 μM) + 74.6 ± 8.2 ‡‡ (100 μM) + 67.8 ± 6.7	- 46.12 ± 8.6 - 20.92 ± 8.6
C2C12 + DNG→A	(50 μM) + 98.7 ± 13.1 # (100 μM) + 101.6 ± 10.5	- 54.14 ± 19.1 - 67.57 ± 6.0
C2C12 + DNG→S	(50 μM) + 90.1 ± 10.5 ¶ (100 μM) + 78.1 ± 13.3	- 73.23 ± 3.0 - 60.11 ± 4.7

† HepG2 50 μM vs. 100 μM diazoxide, ns $p>0.05$.
‡ HEK293 50 μM vs. 100 μM diazoxide, ns $p>0.05$.
†† HepG2 + 61siRNA 50 μM vs. 100 μM diazoxide, ns $p>0.05$.
€€ C2C12 + 61siRNA 50 μM vs. 100 μM diazoxide, ns $p>0.05$.
‡‡ HEK293 + 61siRNA 50 μM vs. 100 μM diazoxide, ns $p>0.05$.
# C2C12 + DNG→A 50 μM vs. 100 μM diazoxide, ns $p>0.05$.
¶ C2C12 + DNG→S 50 μM vs. 100 μM diazoxide, ns $p>0.05$.

Table 3.7.

A table to show the significant differences in ROS production in cells expressing Kir6.1 and in cells without Kir6.1. If $p<0.001$, the data are highly significant (***).

Control vs. transfected cells	**50 μM Diazoxide**	**10 μM Glibenclamide**
C2C12 vs. C2C12 +61siRNA	***	***
C2C12 vs. C2C12 DNG→A	***	NS
C2C12 vs. C2C12 DNG→S	***	***
HepG2 vs. HepG2 + 61siRNA	NS	*
HEK293 vs. HEK293 + 61siRNA	NS	NS

To summarise, I have demonstrated that the KCO diazoxide increased ROS production and inhibitor glibenclamide abolished this effect in C2C12, HepG2 and HEK293 cell lines. Diazoxide increased ROS production at both concentrations however; there were no significant differences between the two concentrations of diazoxide. In C2C12 cells transfected with siRNA and DN for Kir6.1, the stimulatory effect of diazoxide and inhibitory effect of glibenclamide were pronounced compared to control C2C12 (apart from DNG→A, where the response of both transfected and non transfected C2C12 cells to 10 μM glibenclamide were similar). For HEK293 and HepG2 cells, the stimulating effect of diazoxide on ROS production was the same in cells expressing Kir6.1 and in cells without Kir6.1. HepG2 cells lacking Kir6.1 were more sensitive to glibenclamide but the response was similar in HEK293 cells.

The data suggest that these pharmacological compounds will modulate other mechanisms that may lead to ROS production. The mitoK_{ATP} channel has been hypothesised to be involved in preconditioning by generating protective levels of intracellular ROS, which act as messengers that trigger other pathways leading to protection. My results show that Kir6.1 is not involved in ROS production in immortalised cells lines suggesting that the responses were independent of Kir6.1. While Kir6.1 may not be accountable for the changes in ROS levels, my cell lines may contain K_{ATP} channels composed of Kir6.2. However, there is no concrete evidence to suggest that ROS production is linked to sarcK_{ATP} channels and Kir6.2 had not been put forward as a component of the mitoK_{ATP} channel. The likely explanation for these results is that both diazoxide and glibenclamide possess K_{ATP} channel independent effects that can modulate ROS production.

3.5 Investigating the changes in mitochondrial redox state and mitochondrial membrane potential ($\Delta\psi_m$) in C2C12 cells and rat ventricular myocytes

The ATP-sensitive potassium subunit Kir6.1 is predominantly distributed in the ER in cardiac and skeletal muscle cell lines with a small but significant proportion in mitochondria. In my hands, I was not able to detect endogenous Kir6.1 in rat isolated ventricular myocytes. The objective of this chapter was to examine the effects of KCOs and inhibitors on mitochondria in these cells. Using confocal analysis, I examined mitochondrial function by measuring the changes in flavoprotein and NADH autofluorescence and mitochondrial membrane potential ($\Delta\psi_m$) in C2C12 cells and rat ventricular myocytes. The myocytes were generously provided by Dr. Sean Davidson (*Hatter Institute, UCL, London*). These primary cells were used for this study, as it would be interesting to compare differences in mitochondrial function, if any, between acutely dissociated cells and immortalised cell lines.

Recently, a multiprotein complex with mitoK_{ATP} channel activity was identified in mitochondrial fractions. This consisted of SDH but Kir6.1 was reported to be absent from this complex (*Ardehali et al. 2004*). This protein complex also exhibited K_{ATP} channel activity upon the addition of 100 μM diazoxide and was inhibited with 500 μM 5-HD, 10 μM glibenclamide or 2 mM ATP. Three-nitroproprionic acid (3-NPA), an inhibitor of SDH, activated this channel with 5-HD abolishing this response. Preliminary experiments in our group showed that primary cardiomyocytes treated with 1 mM 3-NPA and 30 μM diazoxide exhibited an increase in flavoprotein oxidation, which could not be observed with 3-NPA or diazoxide alone (*Duchen, unpublished observations*). Therefore, I decided to test this phenomenon further to examine flavoprotein oxidation in the presence of 3-NPA and diazoxide and whether this response could be reversed by glibenclamide.

For mitochondrial redox state measurements, cells were assessed fluorimetrically by measuring NADH (blue autofluorescence), excited by the 364 nm laser and FAD^{2+} (green autofluorescence) which was excited by the 458 nm laser using the Zeiss LSM510 confocal system. A fully reduced state is induced by NaCN, and fully oxidised state by FCCP. The two variables will change reciprocally. The cells were first calibrated with NaCN to the reduced state, indicated by an increase in blue autofluorescence and a decrease in green autofluorescence. NaCN was washed out and the addition of FCCP stimulated respiration producing maximal oxidation, indicated by an increase in green autofluorescence and decrease in blue autofluorescence. Calibrations were carried out so that specific redox signals were measured. The images presented in 3.5.1 with the two variables will be shown as a merged image. The data from this chapter will not include results from HEK293 and HepG2 cells because in preliminary experiments, the signal could not be detected making it technically difficult to take measurements from these cells.

The $\Delta\psi_m$ was examined using a mitochondrial dye called TMRM. For each set of experiments, a region of interest (ROI) was selected from each cell in the field and data for NADH and FAD^{2+} (and TMRM) fluorescence were saved as text files before they were imported into Origin 6.0 for further analysis. From here, the data was normalised and averaged so any changes in the fluorescence would be expressed as a percentage and changes could be quantified from the basal level (arbitrary units). The data for mitochondrial redox state and TMRM fluorescence are presented as means $\pm$ SEM. One-way ANOVA with Dunnetts post test was used to analyse the changes in NADH, FAD^{2+} and TMRM where each drug application was compared to the basal value. Examples of each experimental condition are displayed in 3.5.1 and 3.5.2 with the total number of experiments indicated in brackets. The experiments were carried out at least three times using different cell preparations.

3.5.1 Mitochondrial redox state

In figure 3.44 (n= 3, total cells = 10), myocytes were treated with 100 μM diazoxide and 10 μM glibenclamide. In figure 3.44A, NADH and flavoprotein autofluorescence did not change throughout the whole experiment (the time in minutes are shown in brackets). These observations are supported by the graph in figure 3.44B. The statistical analysis in figure 3.44C and figure 3.44D show that the diazoxide and glibenclamide did not significantly alter these variables $p>0.05$ (NS). The conclusion is that diazoxide and glibenclamide have no apparent effect on mitochondrial function because there were no changes in NADH and FAD^{2+} autofluorescence. However, other groups reported an increase in flavoprotein autofluorescence in the presence of 100 μM diazoxide (*Sato et al 2000; Liu et al 1998*). It must be noted that these groups did not study flavoprotein and NADH autofluorescence simultaneously.

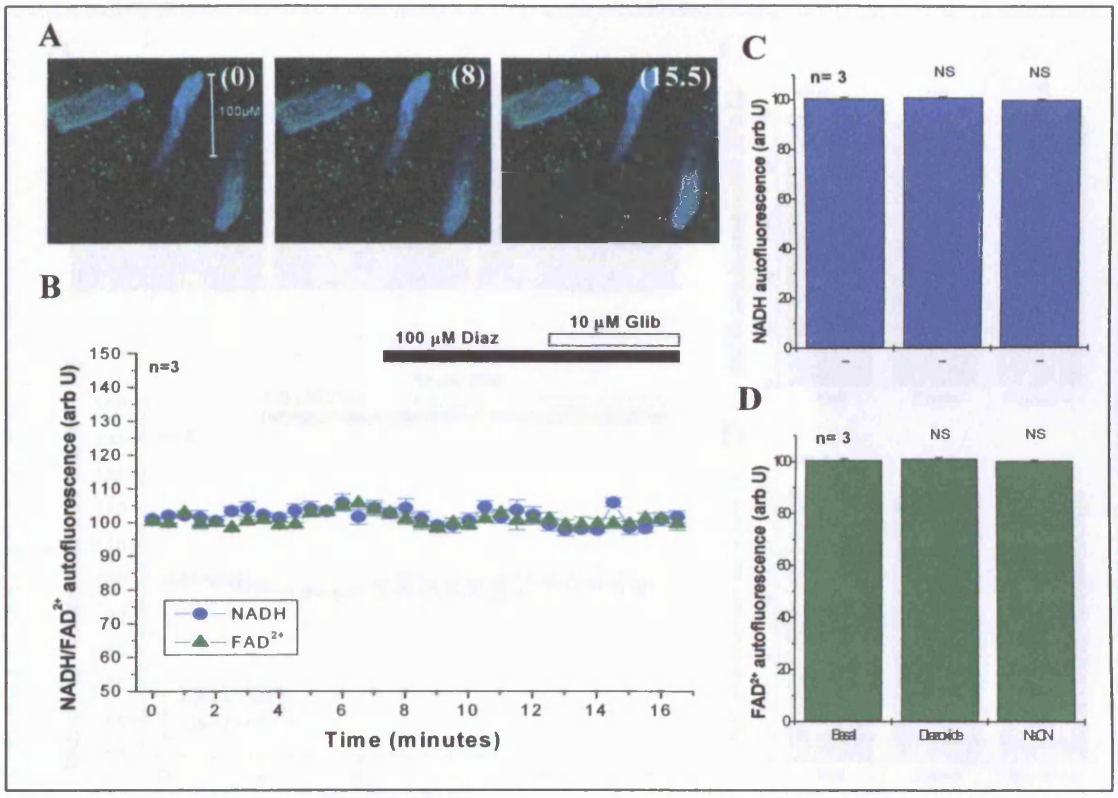

Figure 3.44. The changes in mitochondrial redox state in rat myocytes treated with 100 μM diazoxide and 10 μM glibenclamide (n= 3).

A. A set of images to show the redox state of the myocytes. B. A graph to show the changes in $NADH/FAD^{2+}$ autofluorescence (arbitrary units). The data were normalised, averaged and presented as percentage means ± SEM. C. A graph to show the changes in NADH autofluorescence. Statistical analyses were carried out using One-way ANOVA. D. A graph to show the changes in FAD^{2+} autofluorescence.

In my hands, Kir6.1 was not detected in rat myocytes. Diazoxide and glibenclamide had no effects on these cells; therefore, I decided to test the same compounds on C2C12 cells, which do express native Kir6.1. The data are summarised in figure 3.45 (n= 4, total cells = 11) where C2C12 cells were exposed to 100 μM diazoxide and 10 μM glibenclamide. Despite the presence of Kir6.1 in this cell line, 100 μM diazoxide and 10 μM glibenclamide did not significantly alter mitochondrial redox state, see figure 3.45A and figure 3.45B. There were no significant changes in flavoprotein and NADH autofluorescence p >0.05 (NS), see figure 3.45C and figure 3.45D. The results obtained so far suggest that diazoxide and glibenclamide had no effects on the redox state, hence mitochondrial function in immortalised and primary cell lines. The next step was to examine the maximal oxidised and reduced state of the cells with FCCP and NaCN to ensure that signals could be calibrated to provide specific redox signals that could be measured.

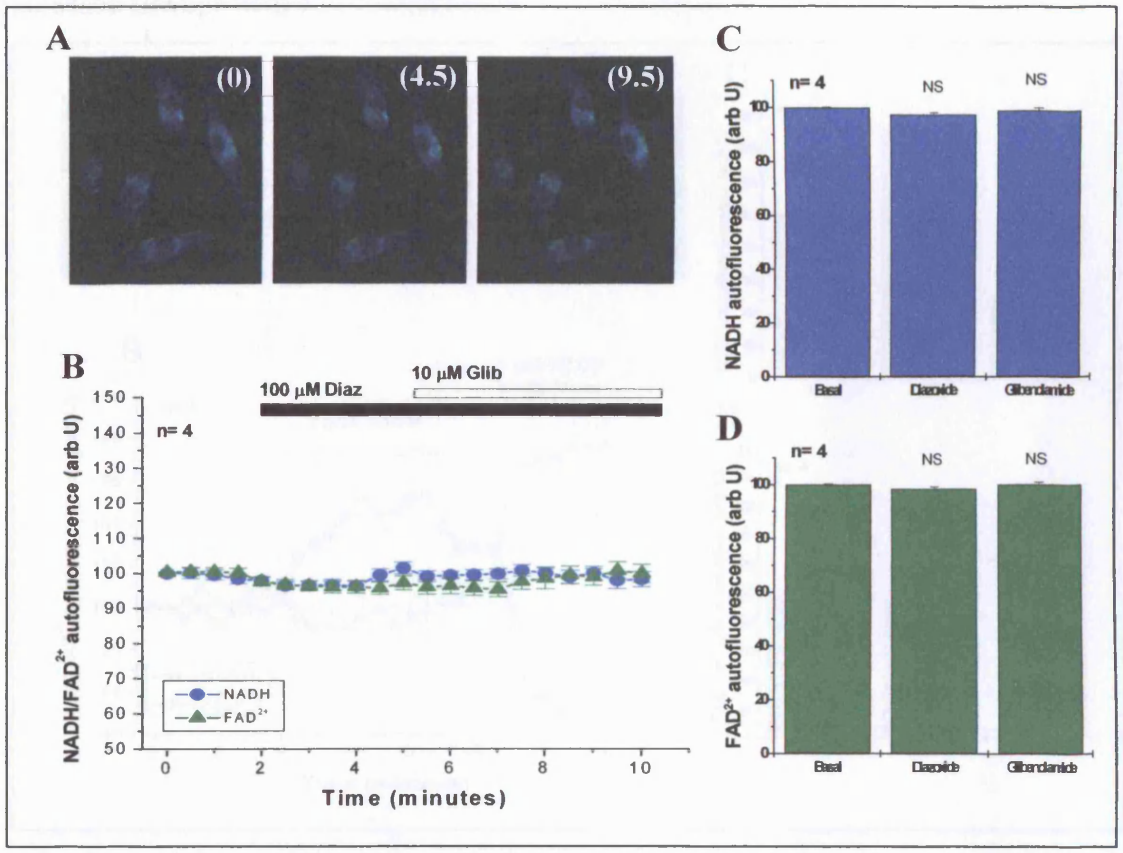

Figure 3.45. An experiment to show the changes in mitochondrial redox state in C2C12 cells treated with 100 μM diazoxide and 10 μM glibenclamide (n= 4).

A. A set of images to show the redox state of C2C12 cells. B. A graph to show the changes in NADH/FAD^{2+} autofluorescence (arbitrary units). C. A graph to show the changes in NADH autofluorescence. D. A graph to show the changes in FAD^{2+} autofluorescence.

In figure 3.46 (n= 4, total cells = 10), C2C12 cells were calibrated with 2 mM NaCN and 1 μM FCCP. Calibration with NaCN and FCCP is an important step because it gives an indication of the cell's resting redox state. NaCN was used to inhibit complex IV of the respiratory chain as this impairs oxidative phosphorylation and NADH cannot be oxidised resulting in a build up of fluorescent NADH, see figure 3.46A. This was observed as an increase in NADH autofluorescence and decrease in flavoprotein autofluorescence, see figure 3.46B. Interestingly, NADPH is also fluorescent because it has similar spectral properties to NADH. Both forms are present in mitochondrial and cytosolic compartments, I assumed the NADH measurements were mitochondrial because it is more abundant than cytosolic NADH and only mitochondrial NADH will change with FCCP (*Duchen et al. 2003, 2001*). The recording medium was replaced with fresh solution to allow cells to recover from NaCN application before FCCP was then applied. This stimulated respiration and increased flavoprotein autofluorescence.

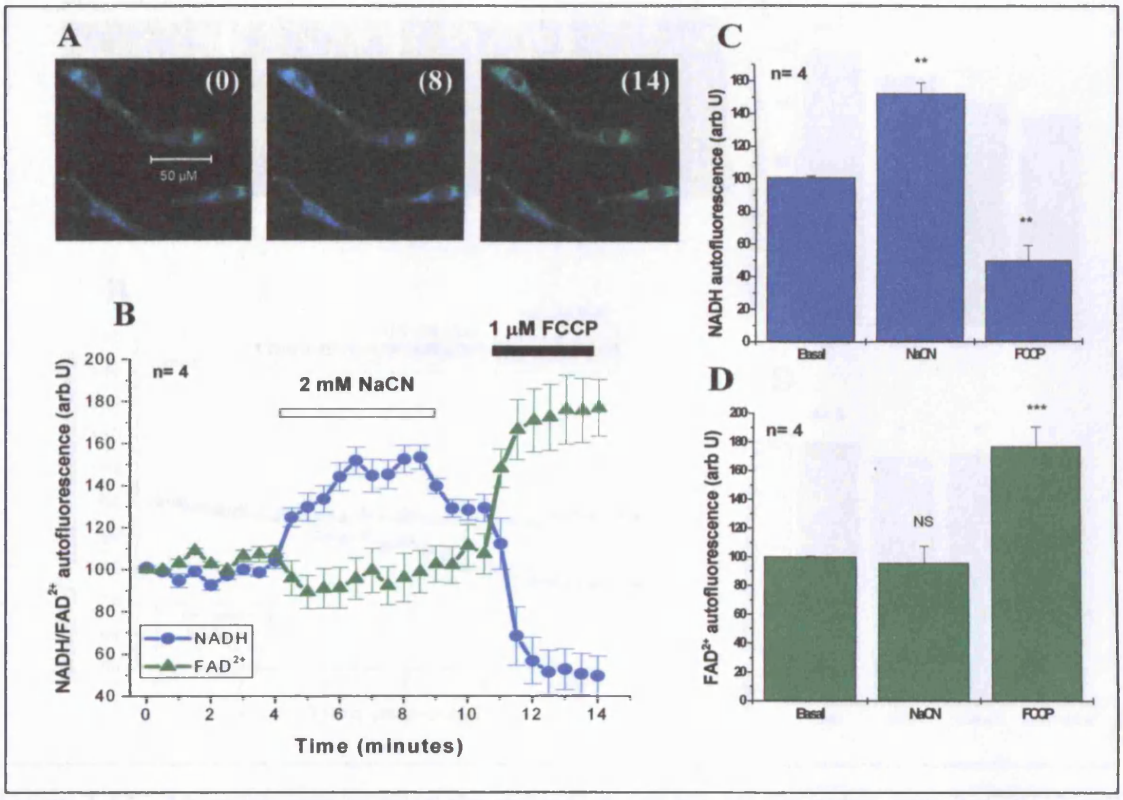

Figure 3.46. A calibration experiment using 20 mM NaCN and 1 μM FCCP to show the maximally reduced and oxidised state in C2C12 cell line.

A. A set of images to show the redox state of C2C12 cells used in this experiment (n= 4). B. A graph to show the changes in NADH/FAD^{2+} autofluorescence (arbitrary units). C. A graph to show the changes in NADH autofluorescence. D. A graph to show the changes in FAD^{2+} autofluorescence.

In figure 3.46C, NaCN significantly increased the NADH autofluorescence by 50 % (100-150) $p<0.01$ (**) but flavoprotein autofluorescence at this time point was not significant $p>0.05$ (NS) (figure 3.46D). During the washout period, NADH and flavoprotein autofluorescence returned to basal levels. FCCP (1 μM) was then applied which caused a substantial reduction in NADH fluorescence by 100 % (150-50) $p<0.01$ (**), this was followed by an increase in flavoprotein autofluorescence by almost 80 % (100-180) $p<0.001$ (***). The previous experiment showed that C2C12 cells did not respond to diazoxide and glibenclamide, the signal in these cells could be calibrated with NaCN and FCCP. Therefore, the next step was to test the combination of 3-NPA and diazoxide and observe whether respiration would be stimulated as demonstrated in the pilot experiments (*Duchen, unpublished observations*). C2C12 cells were treated with 1 mM 3-NPA, 100 μM diazoxide and 10 μM glibenclamide. The data for this experiment is displayed in figure 3.47 (n= 5, total cells = 13).

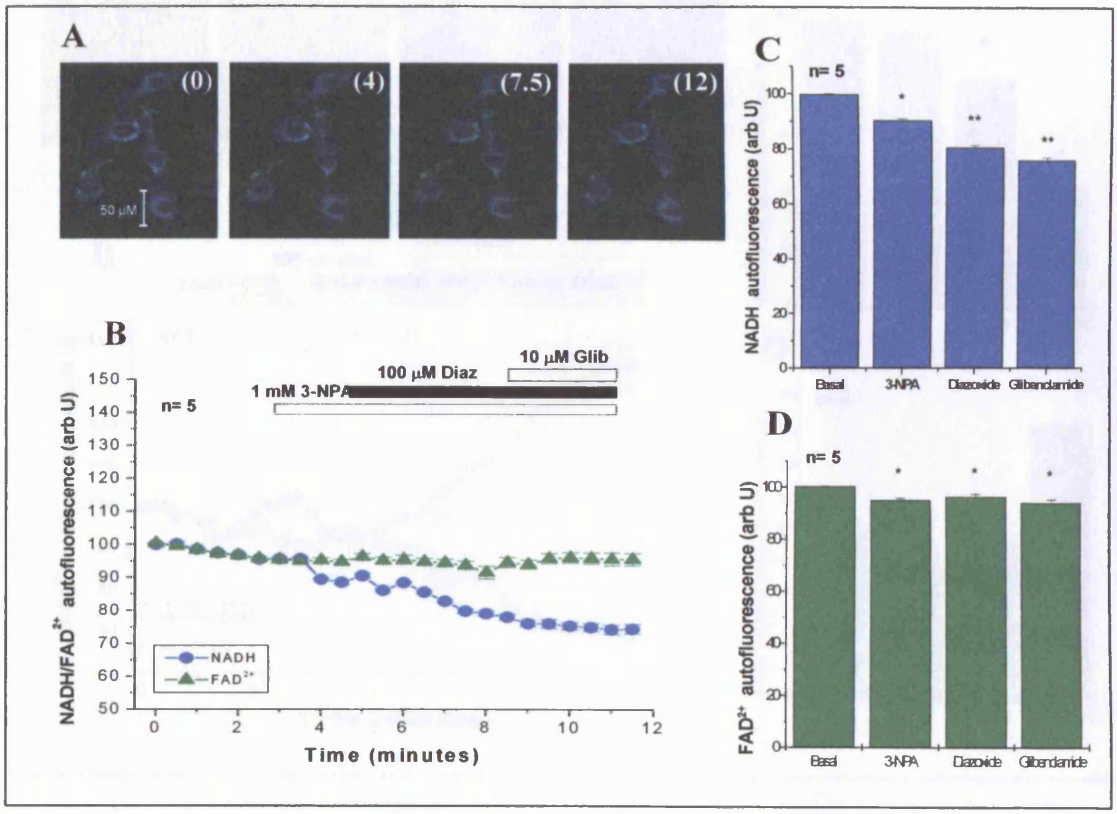

Figure 3.47. An experiment to show the changes in mitochondrial redox state in C2C12 cell treated with 1 mM 3-NPA, 100 μM diazoxide and 10 μM glibenclamide.

A. A set of images to show the redox state of C2C12 cells used in this experiment (n= 5). B. A line graph to show the changes in $NADH/FAD^{2+}$ autofluorescence (arbitrary units).C. A graph to show the changes in NADH autofluorescence. D. A graph to show the changes in FAD^{2+} autofluorescence.

On closer inspection, the graph in figure 3.47C shows that NADH autofluorescence decreased in the presence of 3-NPA $p<0.05$ (*), diazoxide and glibenclamide $p<0.01$ (**). Flavoprotein autofluorescence decreased after 3-NPA application $p<0.05$ (*) and continued to decrease in the presence of diazoxide and glibenclamide $p<0.05$ (*), see figure 3.47D. C2C12 cells showed small but significant changes in NADH autofluorescence in the presence of 1 mM 3-NPA, 100 μM diazoxide and 10 μM glibenclamide. However, the decrease in NADH autofluorescence was not followed by the reciprocal increase in flavoprotein autofluorescence. These compounds were then tested on rat ventricular myocytes to compare responses. In figure 3.48, myocytes were treated with 1 mM 3-NPA, 100 μM diazoxide and 10 μM glibenclamide, (n= 4, total cells = 12).

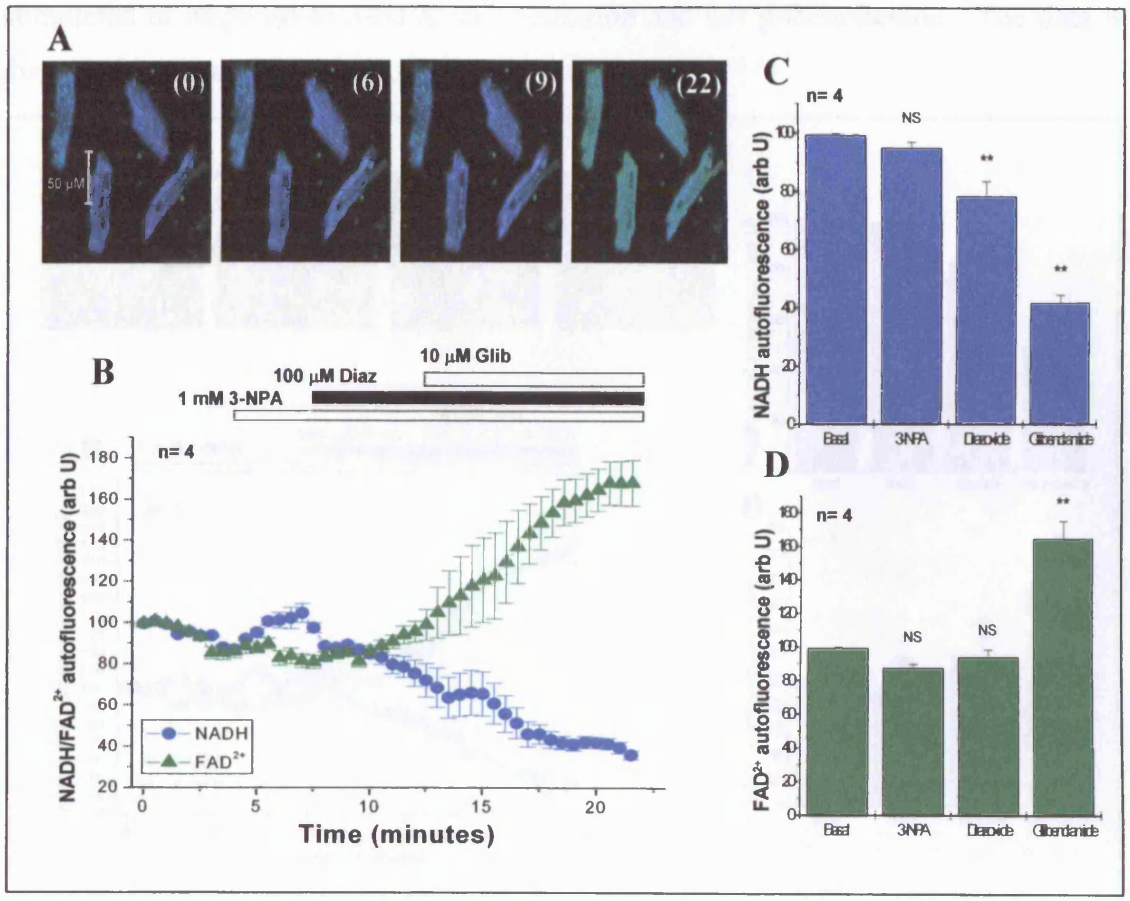

Figure 3.48. An experiment to show the changes in mitochondrial redox state in rat ventricular myocytes treated with 1 mM 3-NPA, 100 μM diazoxide and 10 μM glibenclamide.

A. A set of images to show the redox state of rat myocytes used in this experiment (n= 4). B. A graph to show the changes in NADH/FAD^{2+} fluorescence (arbitrary units). C. A graph to show the changes in NADH autofluorescence. D. A graph to show the changes in FAD^{2+} autofluorescence.

In figure 3.48A, the combination of 3-NPA, diazoxide and glibenclamide increased flavoprotein oxidation; this was similar to the response induced by uncoupler FCCP. These changes in NADH and flavoprotein autofluorescence are shown in figure 3.48B. It is important to note that individual cells in each field respond to the drugs at different times, some cells become more oxidised than others, which may have influenced the statistical analysis. NADH autofluorescence decreased upon diazoxide application and this response continued in the presence of glibenclamide $p < 0.01$ (**), (figure 3.48C). Flavoprotein autofluorescence was not affected by 3-NPA and diazoxide $p > 0.05$ (NS) but in the presence of glibenclamide, respiration was stimulated and flavoprotein autofluorescence increased significantly by 60 % $p < 0.01$ (**). The next experiment was designed to confirm that flavoprotein oxidation was stimulated in response to 3-NPA and diazoxide and not glibenclamide. The data is displayed in figure 3.49 (n= 3, total cells = 14).

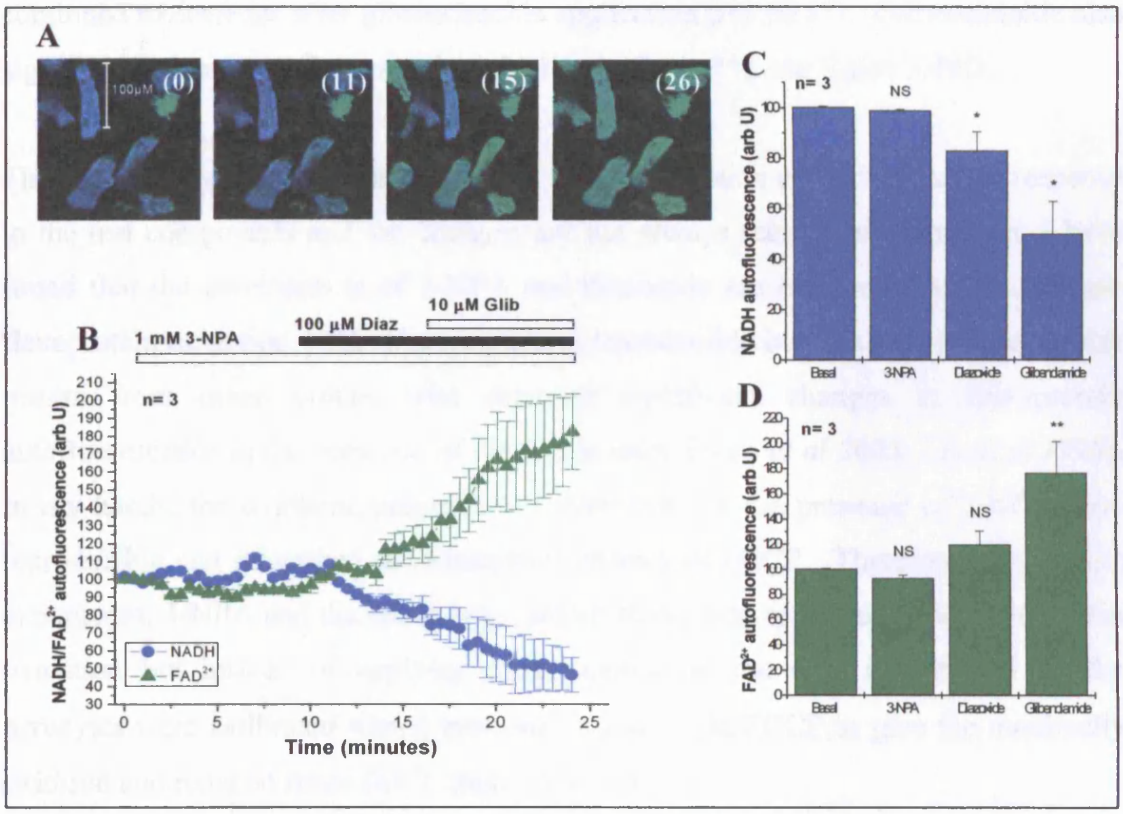

Figure 3.49. An experiment to show the changes in mitochondrial redox state in rat ventricular myocytes treated with 1 mM 3-NPA, 100 µM diazoxide and 10 µM glibenclamide.

A. A set of images to show the redox state of cardiomyocytes used in this experiment (n= 3). B. A graph to show the changes in $NADH/FAD^{2+}$ autofluorescence (arbitrary units). C. A graph to show the changes in NADH autofluorescence. D. A graph to show the changes in FAD^{2+} autofluorescence.

This time, the drugs were administered in the same order but with longer time intervals in between each application to show the effect of each compound on mitochondrial redox state. Myocytes are quite robust cells so it was possible to extend the duration of this experiment to prove this point. In figure 3.49A and figure 3.49B, the myocytes were unaffected by 3-NPA and flavoprotein autofluorescence only started to increase after diazoxide application. There was also a 10-minute gap before diazoxide was administered to show that 3-NPA alone did not affect redox state. After glibenclamide application, the increase in flavoprotein autofluorescence and decrease in NADH autofluorescence continued. The statistical analysis in figure 3.49C and figure 3.49D reflects these changes and shows that 3-NPA itself did not have any effects on redox state $p>0.05$ (NS). Diazoxide decreased NADH autofluorescence $p<0.05$ (*) but it did not increase flavoprotein autofluorescence at this point $p>0.05$ (NS). In figure 3.49C, NADH autofluorescence decreased and continued to decrease after glibenclamide application $p<0.05$ (*). Glibenclamide also significantly increased flavoprotein oxidation $p<0.01$ (**), see figure 3.49D.

The data suggests that the rate of NADH and flavoprotein oxidation vary in response to the test compounds and the changes are not always reciprocal. However, I have found that the combination of 3-NPA and diazoxide are both required to stimulate flavoprotein oxidation. This phenomenon is reproducible but this does not agree with results from other groups who reported significant changes in flavoprotein autofluorescence in the presence of diazoxide alone (*Sato et al 2000; Liu et al 1998*). In my hands, the oxidising properties of diazoxide (in the presence of 3-NPA) was reproducible and mimicked the stimulatory effects of FCCP. Therefore, in the final experiment, 3-NPA and diazoxide were administered first to demonstrate flavoprotein oxidation but instead of applying glibenclamide at the end, in figure 3.50, the myocytes were calibrated with 2 mM NaCN and 1 μM FCCP to give the maximally oxidised and reduced states (n= 2, total cells = 9).

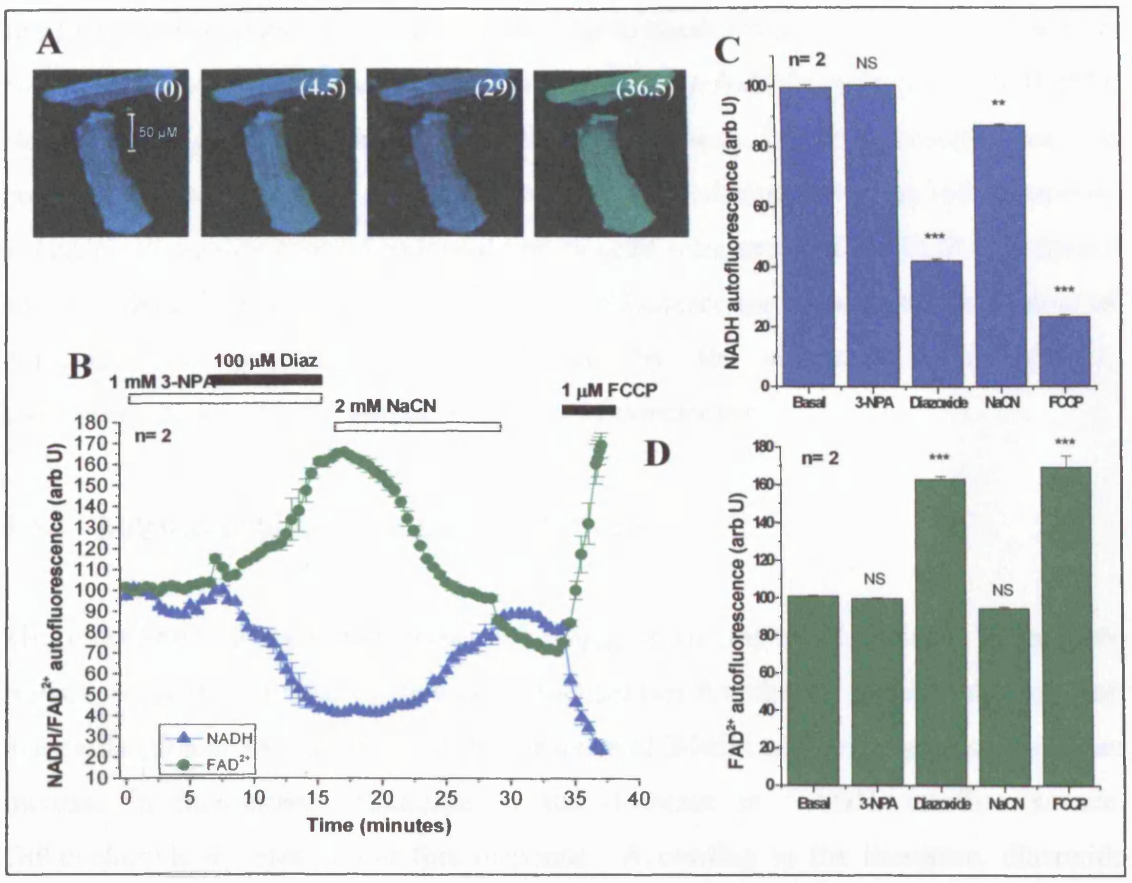

Figure 3.50. An experiment to show the changes in mitochondrial redox state in rat ventricular myocytes treated with 1 mM 3-NPA, 100 µM diazoxide, 20 mM NaCN and 1 µM FCCP.

A. A set of images to show the redox state of cardiomyocytes used in this experiment (n= 2). B. A graph to show the changes in NADH/FAD^{2+} autofluorescence (arbitrary units). C. A graph to show the changes in NADH autofluorescence. D. A graph to show the changes in FAD^{2+} autofluorescence.

Figure 3.50A and figure 3.50B show that the application of 3-NPA and diazoxide caused an increase in flavoprotein autofluorescence and a decrease in NADH autofluorescence. Mitochondrial redox state did not change immediately but only after a time delay of 5-10 minutes. Diazoxide, in the presence of 3-NPA can somehow induce cells to their fully oxidised state; the degree of oxidation is similar to FCCP and was very significant $p<0.001$ (***). There was an increase in flavoprotein autofluorescence and decrease in NADH fluorescence, see figure 3.50C and figure 3.50D. NaCN addition to these myocytes show that diazoxide stimulated respiration could be reversed, this response took about 10 minutes but is a reversible effect and must be due to some non-specific target in mitochondria. Inhibiting respiration restored NADH and flavoprotein autofluorescence to near basal levels. Flavoprotein

autofluorescence at this time point was similar to basal levels $p>0.05$ (NS). However, NADH autofluorescence had not recovered fully from NaCN application $p<0.01$ (**). NaCN would normally inhibit respiration immediately but it is possible that the presence of the other drugs in the solution may have slowed down the cell's response to NaCN. A washout period followed before cells were exposed to FCCP, this caused an immediate increase in flavoprotein autofluorescence, producing the maximal oxidised state $p<0.001$ (***), indicated by the increase in flavoprotein autofluorescence and decrease in NADH autofluorescence.

3.5.2 Mitochondrial membrane potential ($\Delta\psi_m$)

The mitochondrial membrane potential ($\Delta\psi_m$) is an important variable to measure because it provides further insight on mitochondrial function. I have established that diazoxide stimulated respiration in the presence of 3-NPA and this was observed as an increase in flavoprotein fluorescence and decrease in NADH autofluorescence. Glibenclamide did not inhibit this response. According to the literature, diazoxide will activate the mitoK$_{ATP}$ channel and cause mitochondrial depolarisation promoting respiration and the oxidation of flavoproteins and NADH. This in turn allows the influx of K^+ ions into the matrix, which will be driven by an equal rate of H^+ ejection by the electron transport chain. The increase in H^+ current would lower the $\Delta\psi_m$ (*Garlid 2000*). If K^+ influx capacity is large, part of the H^+ gradient that is used to export K^+ ions via K^+/H^+ exchanger will prevent mitochondrial swelling and lysis. Closing the mitoK$_{ATP}$ channel with glibenclamide would cause repolarisation and recovery of the $\Delta\psi_m$.

The $\Delta\psi_m$ was measured with Tetramethyl rhodamine methyl ester (TMRM) (see materials and methods 2.5.4). C2C12 cells were loaded with 20 nM TMRM for 30 minutes at 37 °C whereas myocytes were loaded for one hour, as this was required for these cells to equilibrate and reach a steady state. The dye distributes in the compartments according to the Nernst equation. When mitochondria become depolarised, the dye redistributes and moves from mitochondria to cytosol. Therefore, mitochondrial TMRM fluorescence decreases whereas cytosolic TMRM fluorescence increases (*Voronina et al. 2004, Duchen et al. 2003*). In preliminary

experiments, I observed diazoxide induced flavoprotein and NADH oxidation (in the presence of 3-NPA) in myocytes but not in C2C12 skeletal muscle cells therefore, it would be relevant to examine if the responses in $\Delta\psi_m$ are different in these two cellular models.

In figure 3.51 (n = 3, total cells = 11). C2C12 cells were loaded with 20 nM TMRM and treated with 100 μM diazoxide, 10 μM glibenclamide and 1 μM FCCP. Three ROIs were selected from each cell and are shown as different coloured traces in figure 3.51B. Diazoxide caused a small decrease in TMRM fluorescence. The application of glibenclamide caused a slight spike in the data but this was due to the addition of the drug, see figure 3.51A.

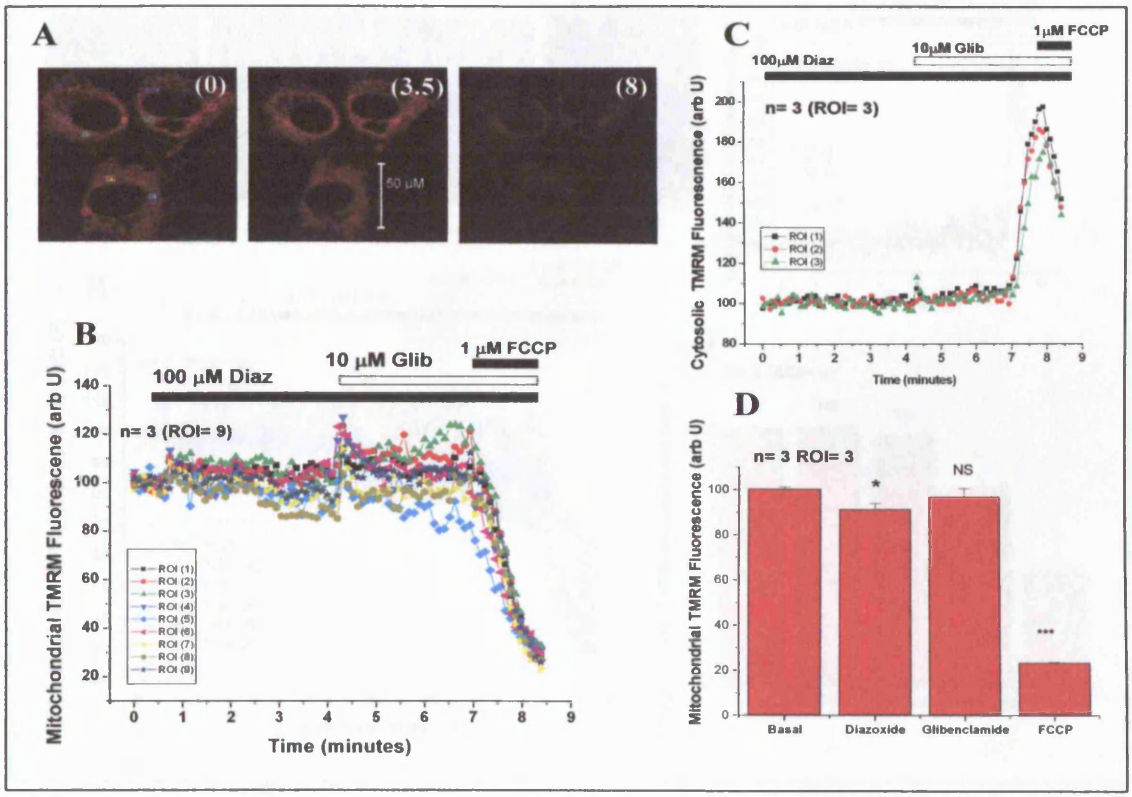

Figure 3.51. An experiment to show the changes in $\Delta\psi_m$ in C2C12 cells loaded with 20 nM TMRM. The cells were treated with 100 μM diazoxide, 10 μM glibenclamide and 1 μM FCCP.

A. A set of images to show the changes in overall TMRM fluorescence during the experiment (n=3 ROIs = 9). B. A graph to show the changes in mitochondrial TMRM fluorescence (arbitrary units). The results were normalised before they were averaged and are presented as percentage means ± SEM. C. An image to show the three ROIs which were taken for cytosolic TMRM fluorescence measurements. D. A graph to show the changes in cytosolic TMRM fluorescence in the ROIs highlighted in C. Statistical analyses were carried out using One-way ANOVA, the time points were taken at the end of each drug application.

When FCCP was administered, the mitochondria depolarised immediately allowing the dye to exit the mitochondria and enter the cytosol, see figure 3.51C. This observation was confirmed by measuring the increase in cytosolic TMRM fluorescence. In figure 3.51D, diazoxide caused mitochondrial depolarisation $p<0.05$ (*), there were no significant changes in $\Delta\psi_m$ in response to glibenclamide but the collapse of the $\Delta\psi_m$ in response to FCCP was observed as a significant drop in TMRM fluorescence by almost 80 % (100-20) $p<0.001$ (***). The next step was to explore the effects of 1 mM 3-NPA, 100 µM diazoxide and 10 µM glibenclamide on $\Delta\psi_m$ in rat myocytes because the combination of 3-NPA and diazoxide significantly increased flavoprotein autofluorescence. See figure 3.52 (n= 3, total cells = 10).

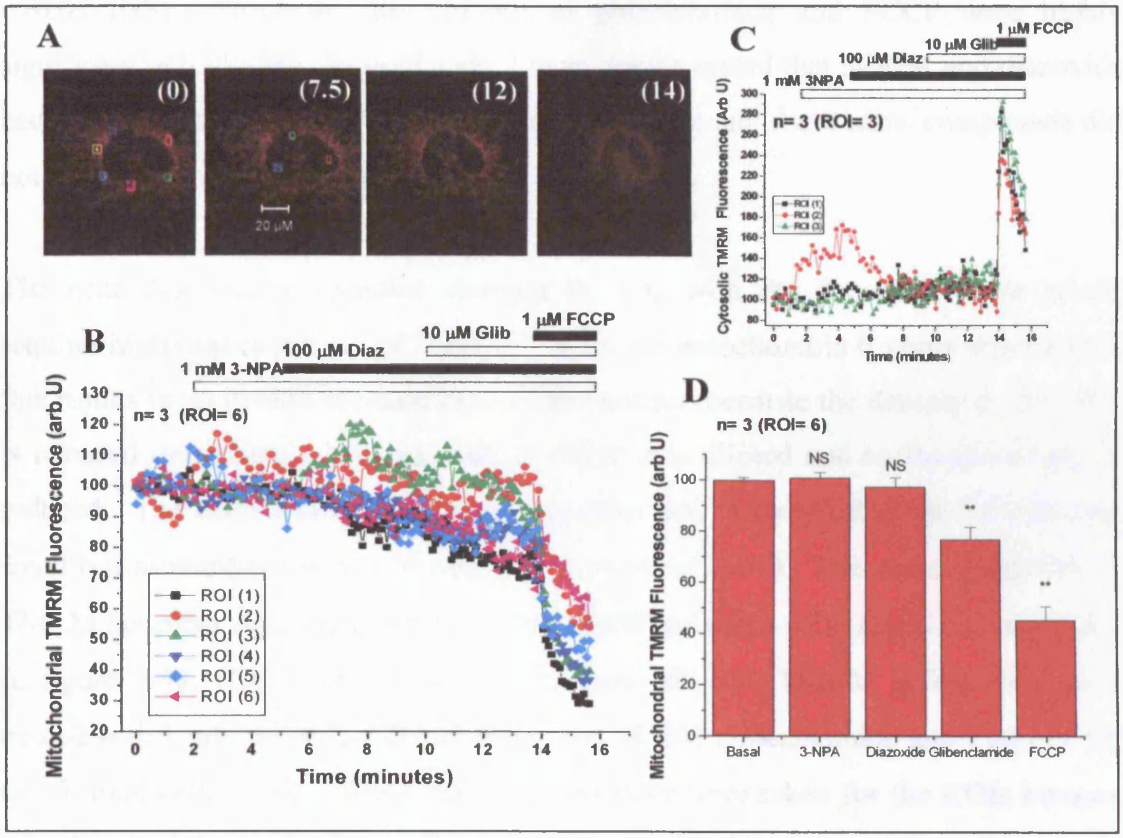

Figure 3.52. An experiment to show the changes in $\Delta\psi_m$ in C2C12 cells loaded with 20 nM TMRM. The cells were treated with 1 mM 3-NPA, 100 µM diazoxide, 10 µM glibenclamide and 1 µM FCCP.

A. A set of images to show the changes in overall TMRM fluorescence during the experiment (n= 3). B. A graph to show the changes in mitochondrial TMRM fluorescence. C. A graph to show the changes in cytosolic TMRM fluorescence in the ROIs highlighted in A. D. A graph to compare the changes in $\Delta\psi_m$ in response to the different compounds.

Two ROIs were selected for each cell and the traces are displayed as six coloured traces in figure 3.52B. The data show that mitochondria did not depolarise in response to diazoxide (and 3-NPA) and mitochondrial depolarisation occurred after glibenclamide application. The rate of depolarisation increased when FCCP was administered as this resulted in an immediate decrease in mitochondrial TMRM fluorescence and increase in cytosolic TMRM fluorescence. In figure 3.52A, three ROIs were selected for cytosolic TMRM fluorescence measurements in figure 3.52C. The addition of FCCP caused a prominent 'spike' at 14 minutes where the dye moved from mitochondria to the cytosol. Statistical analysis in figure 3.52D showed that mitochondrial TMRM fluorescence was not influenced by 3-NPA and diazoxide $p>0.05$ (NS). However, the addition of glibenclamide and FCCP were highly significant $p<0.01$ (**). In my hands, I have demonstrated that 3-NPA and diazoxide had no significant effect on mitochondrial redox state and these same compounds did not have major effects on $\Delta\psi_m$ in C2C12 cells either.

The next step was to examine changes in $\Delta\psi_m$ with the dequench mode which requires high concentrations of TMRM. When the mitochondria become depolarised, this results in an overall increase in cell fluorescence because the densely packed dye is released immediately into the cytosol where it is diluted and so the quenching is reduced. The dequench mode is more sensitive and is more effective for detecting small but substantial changes in $\Delta\psi_m$ (*Voronina et al 2004*). This not only applies to TMRM but other $\Delta\psi_m$ dyes such as TMRE and Rhodamine 123 (*Duchen et al. 2001*). In figure 3.53, C2C12 cells were loaded with 400 nM TMRM before they were treated with 1 mM 3-NPA, 100 μM diazoxide, 10 μM glibenclamide and 1 μM FCCP (n= 5, total cells = 14). Whole cell measurements were taken for the ROIs because mitochondrial depolarisation in these cells loaded with this concentration of dye could be observed as an increase in overall cell fluorescence.

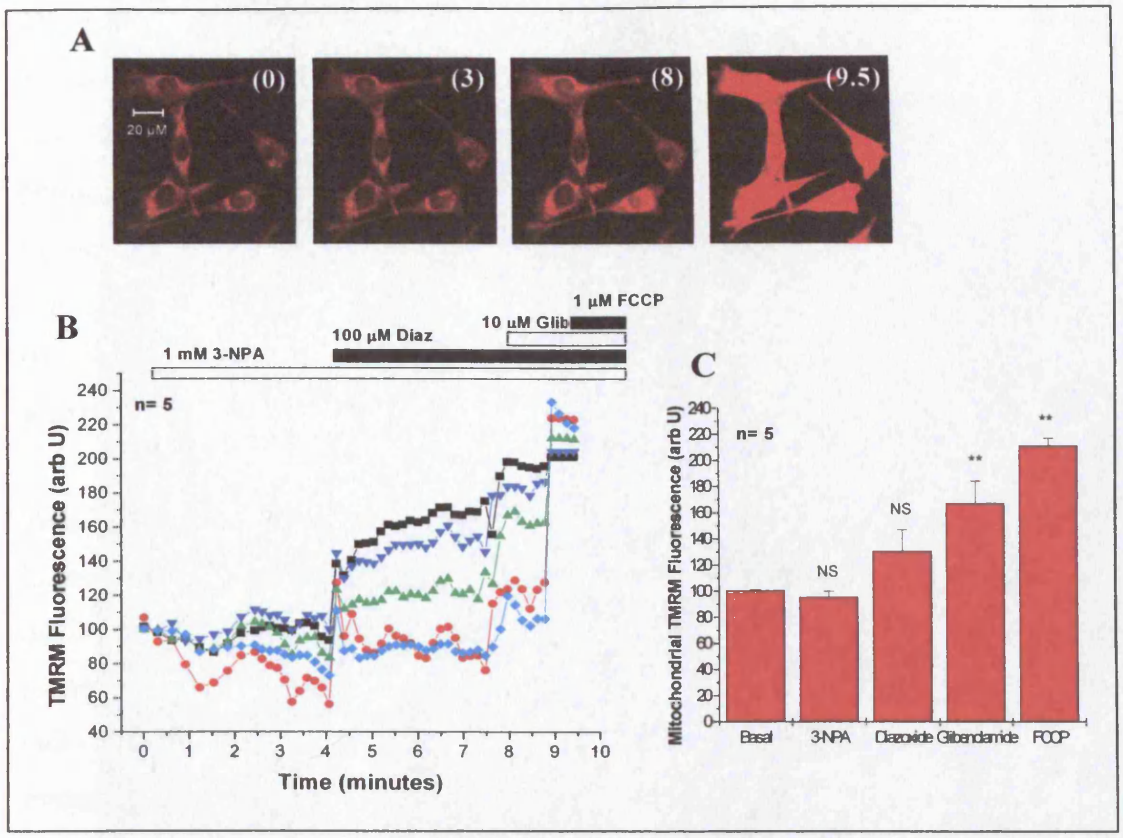

Figure 3.53. An experiment to show the changes in $\Delta\psi_m$ in C2C12 cells loaded with 400 nM TMRM. The cells were treated with 1 mM 3-NPA, 100 µM diazoxide, 10 µM glibenclamide and 1 µM FCCP.

A. A set of images to show the changes in overall TMRM fluorescence during the experiment (n=5). B. A graph to show the changes in mitochondrial TMRM fluorescence (arbitrary units). C. A graph to show changes in $\Delta\psi_m$ fluorescence during the experiment.

The images in figure 3.53A suggest that were no changes in TMRM fluorescence in response to 3-NPA and diazoxide. However, glibenclamide and FCCP induced mitochondrial depolarisation, contributing to the increase in cell fluorescence. The changes in mitochondrial TMRM fluorescence are displayed in figure 3.53B where five separate traces are shown for each cell in the field. The results show that mitochondria did not respond to 3-NPA or diazoxide $p>0.05$ (NS) but in figure 3.53 C, mitochondria started to depolarise in the presence of glibenclamide $p<0.01$ (**). The application of FCCP continued to dissipate the $\Delta\psi_m$ $p<0.05$ (**). This is an interesting result because previously I was not able to measure any changes in mitochondrial redox state with the same compounds in this cell line. This suggests that the changes in redox state and $\Delta\psi_m$ are not necessarily associated with the changes in mitochondrial redox state.

The experiments with myocytes have not been included in this chapter because these experiments were technically difficult to perform within the timescale available. I also found that mitochondria depolarised rapidly because the laser used had phototoxic properties. The dye would 'leak' from the cells, an indication that the myocytes were not capable of maintaining their $\Delta\psi_m$, which in turn caused the myocytes to shorten with no relaxation. On the other hand, the lasers used to measure the changes in flavoprotein and NADH autofluorescence in these same cells were not accompanied with shortening.

To summarise, the KCO diazoxide has significant effects on mitochondrial redox state in myocytes however; this response was not observed in C2C12 cells. Diazoxide, in the presence of 3-NPA stimulated flavoprotein oxidation, which was observed as in increase in flavoprotein autofluorescence and decrease in NADH autofluorescence. Glibenclamide did not attenuate this response. Using two different methods to evaluate $\Delta\psi_m$, I found that mitochondria in C2C2 cells depolarised in response to diazoxide but there were no significant changes in $\Delta\psi_m$ with 3-NPA and diazoxide. These results suggest that the changes in mitochondrial redox state may not be linked to diazoxide induced K_{ATP} channel opening but more likely that these pharmacological agents have non-specific effects, which are independent of their K_{ATP} channel opening properties.

3.6 Investigating the function of Kir6.1 in calcium signalling

3.6.1 Ca^{2+} signalling

I have examined the intracellular localisation of the ATP-sensitive potassium channel subunit Kir6.1 in immortalised cell lines. Both endogenous and recombinant transfected Kir6.1 are predominantly located in the ER with a small proportion in mitochondria. The ER is involved in Ca^{2+} handling. Given these observations, the next step was to establish whether this localisation may have a function in the regulation of Ca^{2+}.release and sequestration in cardiac or skeletal muscle. Ca^{2+} is a universal intracellular messenger responsible for controlling a diverse range of cellular processes and it has a major function when its concentration is elevated in the cytosolic compartment. The release of Ca^{2+} from intracellular stores is mediated by several types of messenger activated channels.

Mammalian Ca^{2+} pumps fall into two main classes of enzymes: The plasma membrane Ca^{2+}-ATPase (PMCA) pumps Ca^{2+} from the cell to regulate the supply of intracellular Ca^{2+} via the plasma membrane, while sarco/endoplasmic Ca^{2+} ATPases (SERCAs) sequester Ca^{2+} within intracellular organelles such as the sarcoplasmic reticulum (SR) in muscle or the ER in non-muscle cells (*Bootman et al. 2001; Guerini et al. 1998*). The threshold of activation of SERCAs by Ca^{2+} is of the order of 100-200nM, so that they set the resting level of cytoplasmic Ca^{2+}. In fast-twitch muscle such as skeletal muscle, the SERCA1 isoform is expressed at high levels. SERCA2 is found in slow twitch muscle, SERCA2A is expressed in the heart whereas SERCA3 is widely expressed in some blood cells and purkinje neurons. There are exchangers such as the Na^{+}/Ca^{2+} exchanger (NCX) that use the Na^{+} electrochemical gradient to diffuse down its concentration gradient across the plasma membrane in exchange for Ca^{2+}. Mitochondria also play a significant role in modulating cytosolic Ca^{2+} as they possess a low affinity, but high capacity Ca^{2+} uniporter that can reduce high local Ca^{2+} concentrations and can act as a spatial Ca^{2+} buffer (*Duchen 2000; 1999).* The entry of Ca^{2+} into mitochondria is driven by the highly polarised membrane potential and this feature of mitochondria is important because Ca^{2+} accumulation can lead to mitochondrial Ca^{2+} overload in response to pathophysiological events such as ischaemia, ischaemic reperfusion injury, apoptosis and necrosis (*Zucchi et al. 2001*).

The contraction and relaxation of muscle is regulated by the ionised Ca^{2+} content of the sarcoplasm. In resting muscle fibres, Ca^{2+} is stored in the SR and muscle contraction is initiated by the release of Ca^{2+} from the intracellular stores. This can happen in two ways. In cardiac myocytes, Ca^{2+} is released from the SR after the entry of Ca^{2+} via the L-type Ca^{2+} channels whilst in skeletal muscle, Ca^{2+} release is caused by the electrochemical coupling between the surface membrane and the RyR. Relaxation of the muscle occurs when Ca^{2+} is pumped back to the SR via the Ca^{2+} ATPase. There are also Ca^{2+} binding proteins such as calreticulin and calsequesterin that will sequester excess Ca^{2+} (*MacLennan & Wong 1971*). Calsequesterin is unique to SR and is a high-capacity, low-affinity Ca^{2+} binding protein which is hydrophobically bonded onto the interior of these vesicles. However, in non-striated and smooth muscle cells, Ca^{2+} release can be mediated by receptor mediated mechanisms such as purinergic signalling.

The P2 Purinergic receptors are classed into two major groups P2X and P2Y receptors. P2X are ligand-gated ion channels (P2X) and P2Y are G-protein-coupled receptors (GPCRs) (*Erb et al. 2006; Abbracchio & Burnstock 1994*). P2Y receptors are activated by purine and pyrimidine nucleotides and consist of an extracellular N terminus with N-glycosylation sites and intracellular C terminus with phosphorylation sites. P2X receptors have two transmembrane domains with intracellular N and C terminus, consensus phosphorylation sites and the extracellular loop that contains an ATP binding site. P2Y receptors are vital for regulating cellular processes such as cell proliferation, differentiation, apoptosis and metabolism. The P2X receptors have an important role in generating nerve impulses and muscle contraction. They are essentially ATP-gated ion channels that upon activation by extracellular ATP, the P2X receptor subunit opens and allow the movement of cations across the plasma membrane depolarise the cell (*Erb et al. 2006*). P2X receptors mediate Na^+ influx, K^+ efflux, and to some degree Ca^{2+} influx which leads to membrane depolarisation (*Dubyak & El-Moatassim 1993; Bean 1992*). The events that follow are more poorly understood but the net influx of extracellular cations and membrane depolarisation is believed to activate voltage-sensitive Ca^{2+} channels and Ca^{2+} channel, which in turn, leads to additional Ca^{2+} influx and a further increase in cytosolic Ca^{2+} levels. Their activation increases intracellular Ca^{2+} ($[Ca^{2+}]_i$) levels which is responsible for the activation of a number of intracellular signalling molecules.

3.6.2 Ca^{2+} release from the ER/SR in C2C12 cells and rat ventricular myocytes

The skeletal muscle cell line C2C12 was used for this study as these cells can grow indefinitely in culture as undifferentiated myoblasts. However, they can also be induced to form well-defined myotubes by growth to confluence followed with serum deprivation (*Challet et al. 2001*). In muscle development, the ER develops into the specialised SR and is characterised by specific receptors responsible for Ca^{2+} release called ryanodine receptors (RyR). RyR are structurally similar to IP_3 receptors and are predominantly expressed in excitable cells such as striated muscle as they are crucial components of the cascade leading to muscle contraction. The RyR is activated by the plant alkaloid ryanodine at low concentrations (1-10 μM) and irreversibly inhibited at higher concentrations (100 μM). The receptor can also be activated by caffeine (in mM range) as this also increases the sensitivity of RyR to Ca^{2+} ions.

Cells were loaded with 5 μM Fura 2AM and 0.005 % pluronic acid in a HEPES-buffered salt solution (HBSS) for 30 minutes before the medium was replaced with fresh recording solution containing 0.5 mM EGTA. EGTA is a Ca^{2+} chelator which binds to free Ca^{2+} ions in solution. If a Ca^{2+} response was observed in the presence of caffeine or ATP, the source of the Ca^{2+} can be derived from intracellular ER/SR stores or extracellularly. Therefore if a Ca^{2+} transient is observed, the source of Ca^{2+} must be from internal stores. This can be through P2Y IP_3 receptor mediated pathway or via RyR. The cells were imaged using the cooled CCD imaging system and the results are presented as the ratio of excitation at 340 and 380 nm, both with emission at >515 nm. The data presented is from one coverslip (one experiment) but experiments were carried out at least five times from four different cell preparations.

In figure 3.54 (n= 26, total n= 114) non-differentiated C2C12 cells were treated with 10 μM ATP to induce Ca^{2+} release from internal stores. External ATP activates the ligand gated P2Y receptor-mediated pathway; which generates IP_3 which binds to IP_3 receptors on the ER to release Ca^{2+}.

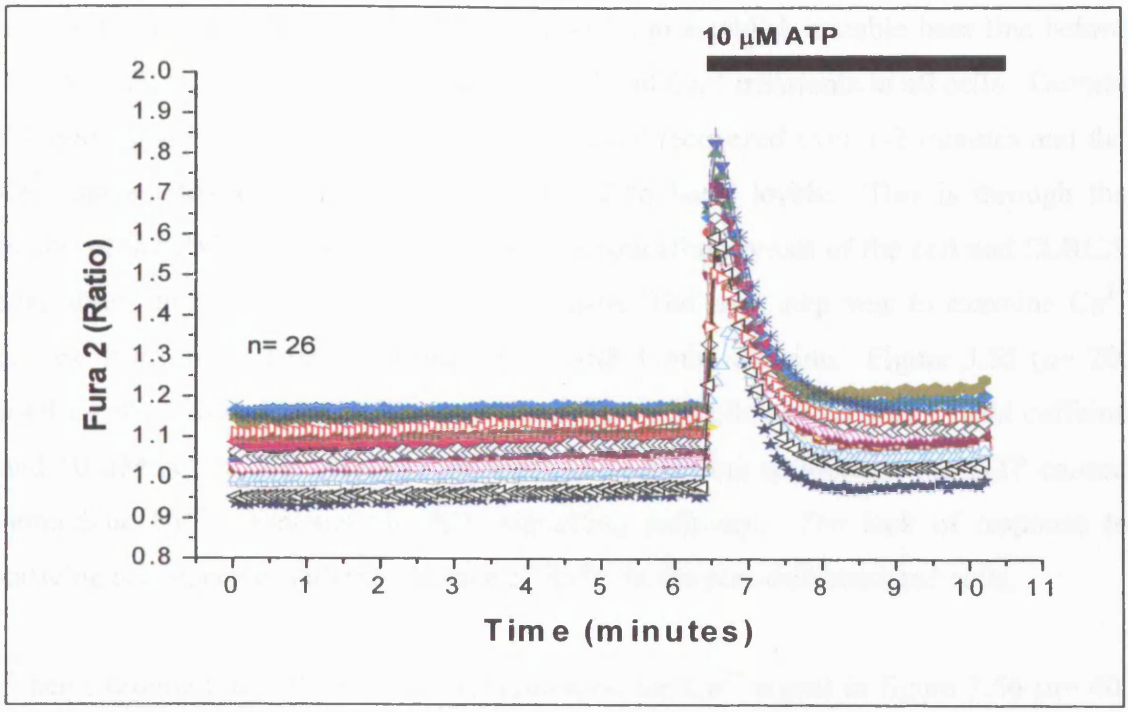

Figure 3.54. A graph to show the Ca^{2+} transients in C2C12 cells stimulated with just 10 μM ATP (n= 26).

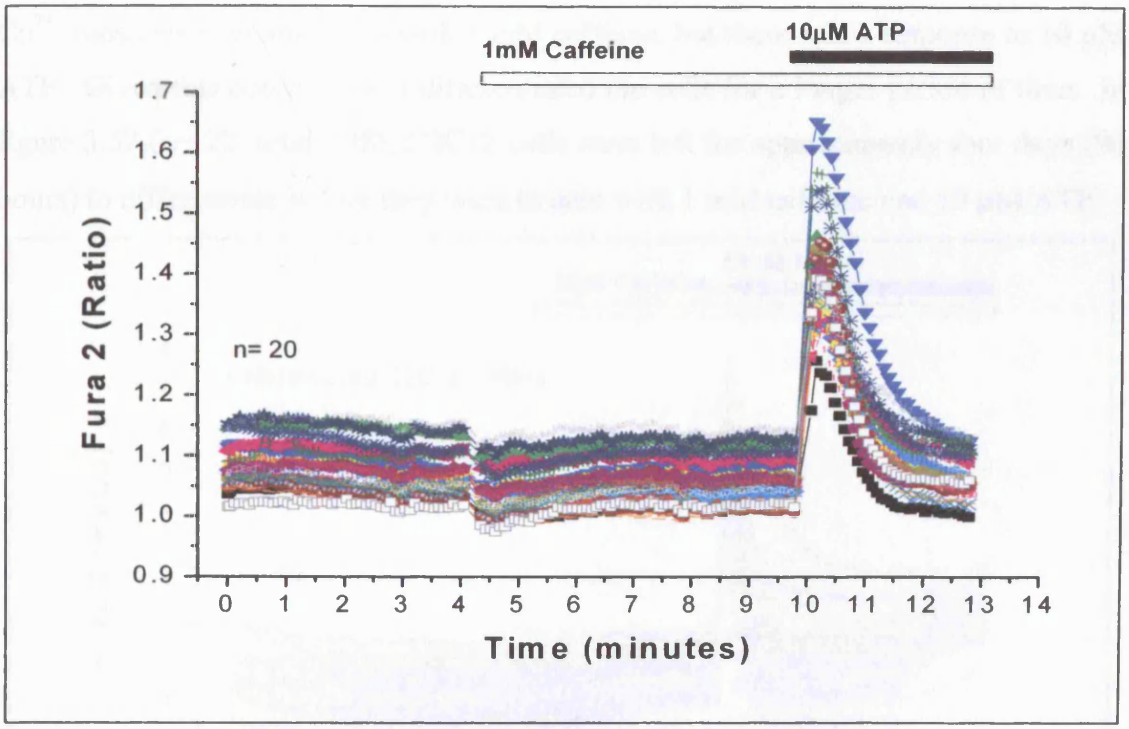

Figure 3.55. A graph to show the Ca^{2+} transients in C2C12 cells stimulated with 1 mM caffeine and 10 μM ATP (n= 20). The cells did not respond to caffeine.

A longer time interval was established between caffeine and ATP application so that when 10 μM ATP was applied, all cells elicited a Ca^{2+} response.

The cells were left for approximately 6 minutes to establish a stable base line before 10 μM ATP was applied which caused significant Ca^{2+} transients in all cells. Despite the maintained presence of ATP, the Ca^{2+} signal recovered over 1-2 minutes and the Ca^{2+} spikes disappeared and $[Ca^{2+}]_i$ returned to basal levels. This is through the action of the PMCA which can pump Ca^{2+} extracellularly out of the cell and SERCA that allow internal stores to start filling again. The next step was to examine Ca^{2+} release from internal stores through RyR with 1 mM caffeine. Figure 3.55 (n= 20, total n= 96) shows the individual traces for C2C12 cells treated with 1 mM caffeine and 10 μM ATP. The cells did not respond to caffeine application but ATP caused immediate Ca^{2+} transients via P2Y signalling pathway. The lack of response to caffeine is consistent with the absence of RyRs in the non-differentiated cells.

I then examined the effect of differentiation on the Ca^{2+} signal in figure 3.56 (n= 40, total n= 88). C2C12 cells were differentiated for 48 hours with 2 % horse serum and visualised under a light microscope to ensure that distinct myotubes were present. No Ca^{2+} transients were observed with 1 mM caffeine, but there was a response to 10 μM ATP. Given this observation, I differentiated the cells for a longer period of time. In figure 3.57 (n= 22, total= 98), C2C12 cells were left for approximately four days (96 hours) to differentiate before they were treated with 1 mM caffeine and 10 μM ATP.

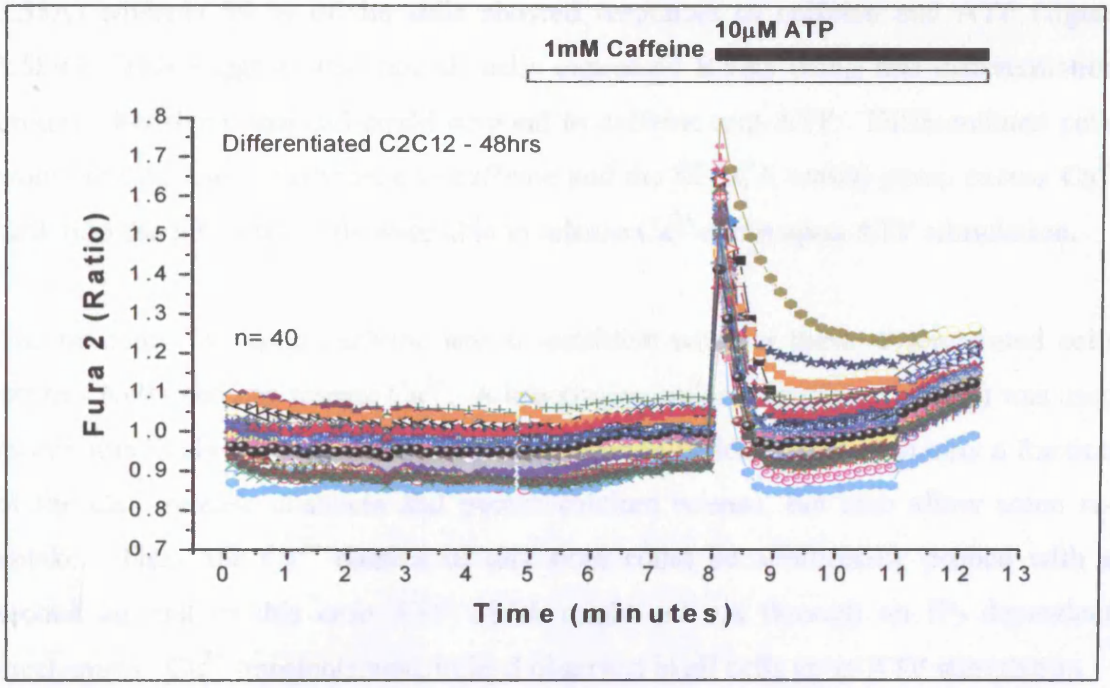

Figure 3.56. A graph to show the Ca^{2+} transients in differentiated C2C12 cells (48 hours). The cells were stimulated with 1 mM caffeine and 10 μM ATP (n= 40).

The cells showed Ca^{2+} transients in response to both caffeine and ATP, however it is possible to deduce the proportion of cells responding to each agonist therefore it was necessary to separate the traces, see figure 3.58.

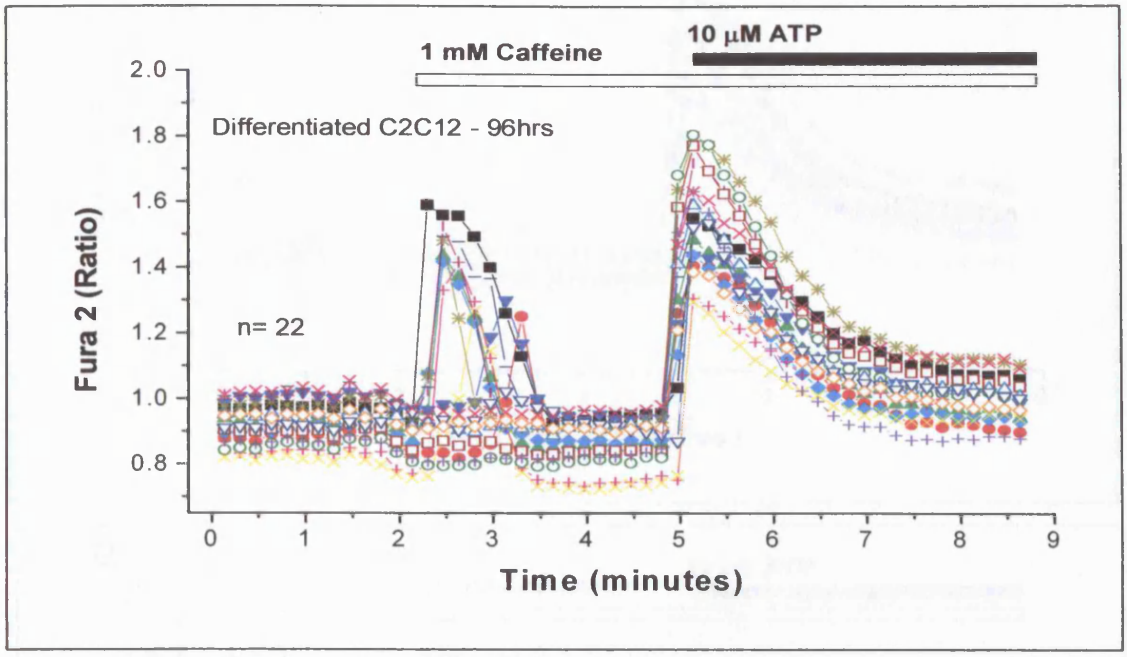

Figure 3.57. A graph to show the Ca^{2+} transients in differentiated C2C12 cells (96 hours). The cells were stimulated with 1 mM caffeine followed by 10 μM ATP (n= 22). The cells showed a response to both caffeine and ATP.

On closer inspection, 41 % of cells only showed ATP induced Ca^{2+} transients (figure 3.58A) whereas 59 % of the cells showed responses to caffeine and ATP (figure 3.58B). This suggests that not all cells expressed RYRs using this differentiation protocol but those that did could respond to caffeine and ATP. Differentiated cells would release Ca^{2+} in response to caffeine and the SERCA would pump excess Ca^{2+} back into the SR so the cells were able to release Ca^{2+} again upon ATP stimulation.

The rationale for using caffeine was to establish whether these differentiated cells express RyRs and can release Ca^{2+}. A low concentration of caffeine (1 mM) was used as this was likely to be a sub-optimal concentration which would open only a fraction of the Ca^{2+} release channels and permit calcium release, but also allow some re-uptake. Thus, the Ca^{2+} content of this store could be additionally probed with a second agonist in this case ATP which might act via through an IP_3 dependent mechanism. Ca^{2+} transients were indeed observed in all cells upon ATP stimulation.

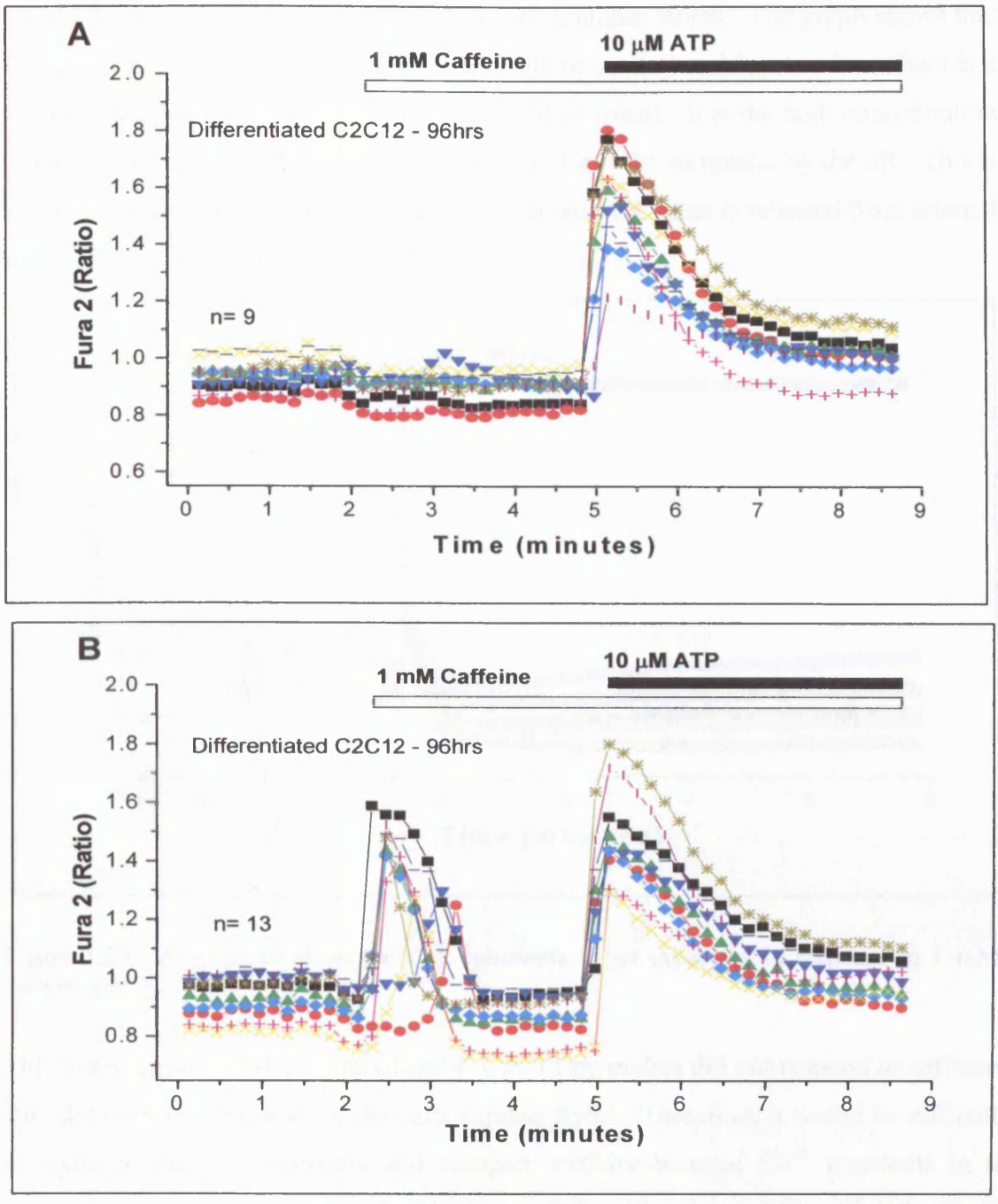

Figure 3.58. The Ca^{2+} transients in figure 3.57 were separated according to their response. A. A graph to show the Ca^{2+} transients in C2C12 cells in response to 10 µM ATP (n= 9). B. A graph to show the Ca^{2+} transients in C2C12 cells response to 1 mM caffeine and 10 µM ATP (n= 13). The response to caffeine was at different times.

To confirm that C2C12 cells did not respond to caffeine because they did not express the RyR and it was not a technical issue, I carried out experiments with rat ventricular myocytes. Myocytes express the cardiac RyR2 and therefore release Ca^{2+} into the cytosol in response to caffeine (*Taur & Frishman 2005*). In figure 3.59, rat ventricular myocytes (n= 7, total= 48) were stimulated with 1 mM caffeine which

caused the immediate release of Ca^{2+} from intracellular stores. The graph shows that the rate of recovery is fast, when $[Ca^{2+}]_i$ levels return to basal levels where there is a slight 'undershoot' in cells (apart from the yellow trace). It is the high concentration of Ca^{2+} in the cytosol which creates the driving force for its uptake by the SR. This is a characteristic response observed in myocytes with Ca^{2+} that is released from internal stores (*Baro et al 1993*).

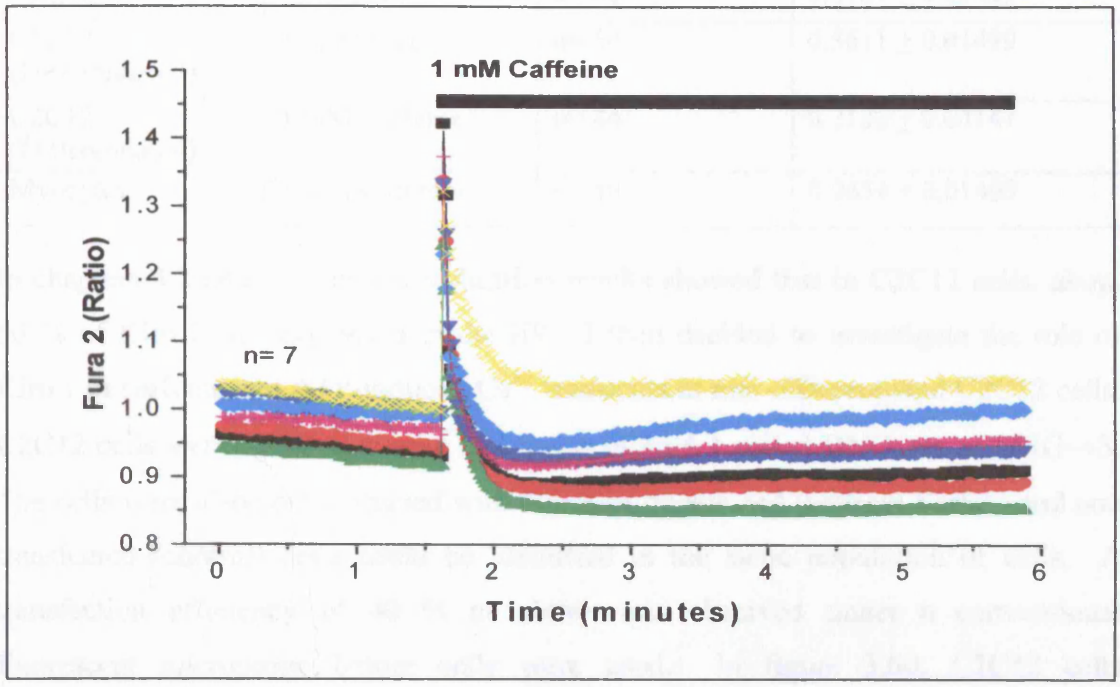

Figure 3.59. A graph to show the Ca^{2+} transients in rat myocytes in response to 1 mM caffeine (n= 7).

The data suggest that the 'differentiated' C2C12 myotubes did not respond to caffeine stimulation because not all of the cells express RyRs. Therefore, it would be difficult to continue these experiments and compare caffeine-induced Ca^{2+} transients in a population of cells that consisted of both non-differentiated and differentiated cells if only a certain percentage of cells respond to caffeine. The data accumulated so far are summarised in table 3.8.

Table 3.8.

A table to summarise the relative increase in intracellular Ca^{2+} levels in experiments carried out throughout this chapter. The results are presented as means ± SEM.

Cell Type and experiment	**Agonist**	**Number of cells**	**Ca^{2+} transient (Fura-2 ratio relative increase)**
C2C12	1 mM Caffeine	n= 66	No response
C2C12	10 μM ATP	n= 66	0.4189 ± 0.03483
C2C12 (Differentiated)	10 μM ATP	n= 54	0.5611 ± 0.01499
C2C12 (Differentiated)	1 mM Caffeine	n= 44	0.2139 ± 0.04141
Myocytes	1 mM Caffeine	n= 48	0.2654 ± 0.01409

In chapters 3.2 and 3.3, the colocalisation results showed that in C2C12 cells, about 50 % of Kir6.1 was expressed in the ER. I then decided to investigate the role of Kir6.1 in caffeine and ATP-induced Ca^{2+} transients in non-differentiated C2C12 cells. C2C12 cells were transfected with DN forms of Kir6.1 called DNG→A or DNG→S. The cells were also co-transfected with eGFP so transfected (without Kir6.1) and non transfected (control) cells could be identified in the same population of cells. A transfection efficiency of 40 % or above was observed under a conventional fluorescent microscope before cells were used. In figure 3.60, C2C12 cells transfected with DNG→A were treated with 1mM caffeine and 10 μM ATP (Control n= 7, total= 41; transfected n= 6, total= 39).

As expected, 1 mM caffeine did not induce a response in these non-differentiated cells whereas ATP elicited immediate Ca^{2+} transients, $[Ca^{2+}]_i$ returned to basal levels in under 2 minutes. However, the magnitude of the Ca^{2+} transient is smaller in the transfected cells, which suggests that Kir6.1 may have a role in Ca^{2+} release from internal stores. Although the amplitude of the Ca^{2+} transients in transfected cells were smaller than in non transfected cells, it is apparent from figure 3.60 that the presence of eGFP altered Fura-2 measurements.

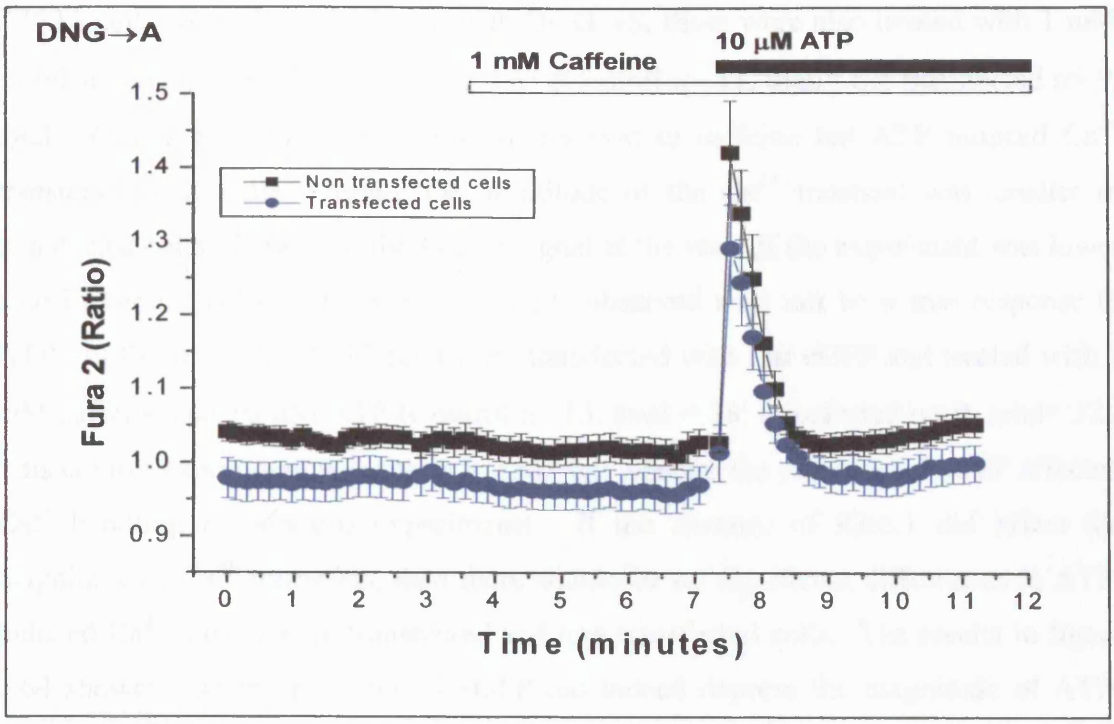

Figure 3.60. A graph to show the Ca^{2+} transients in C2C12 cells transfected with DNG→A, these were stimulated with 1 mM caffeine and 10 μM ATP. (Non transfected cells = 7, transfected cells = 6).

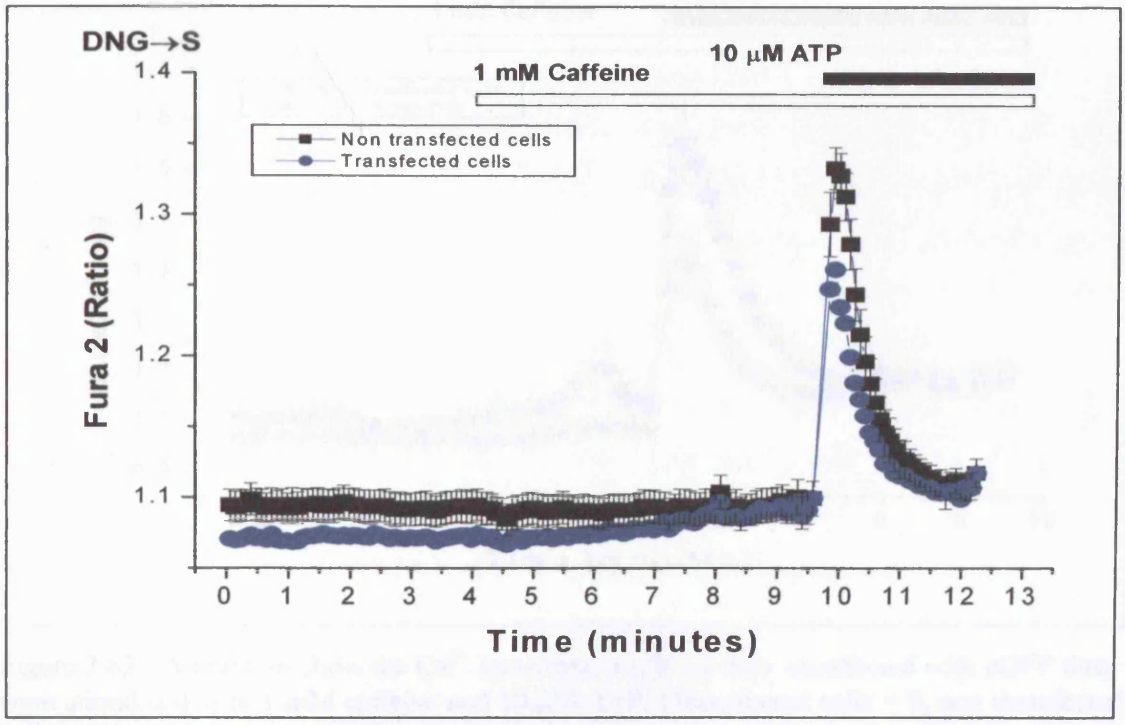

Figure 3.61. A graph to show the Ca^{2+} transients in C2C12 cells transfected with DNG→S, these were stimulated with 1 mM caffeine and 10 μM ATP. (Transfected cells = 9, non transfected cells = 11).

C2C12 cells were also transfected with DNG→S, these were also treated with 1 mM caffeine and 10 μM ATP, see figure 3.61 (Control n= 11, total= 61; transfected n= 9, total= 43). Again, these cells did not respond to caffeine but ATP induced Ca^{2+} transients in all cells. Again, the amplitude of the Ca^{2+} transient was smaller in transfected cells. However, the Fura-2 signal at the start of the experiment was lower than in control cells so the Ca^{2+} transients observed may not be a true response to ATP. In figure 3.62, C2C12 cells were transfected with just eGFP and treated with 1 mM caffeine and 10 μM ATP (Control n= 13, total = 38; transfected n= 9, total= 32). This control experiment was set up to examine whether the presence of eGFP affected Ca^{2+} handling in previous experiments. If the absence of Kir6.1 did affect the magnitude of Ca^{2+} transients, then there should be no significant differences in ATP-induced Ca^{2+} transients in transfected and non transfected cells. The results in figure 3.64 showed that the presence of eGFP did indeed depress the magnitude of ATP-induced Ca^{2+} transients. This suggests that silencing Kir6.1 may not influence Ca^{2+} handling in the ER because the presence of eGFP perturbs the Fura-2 signal.

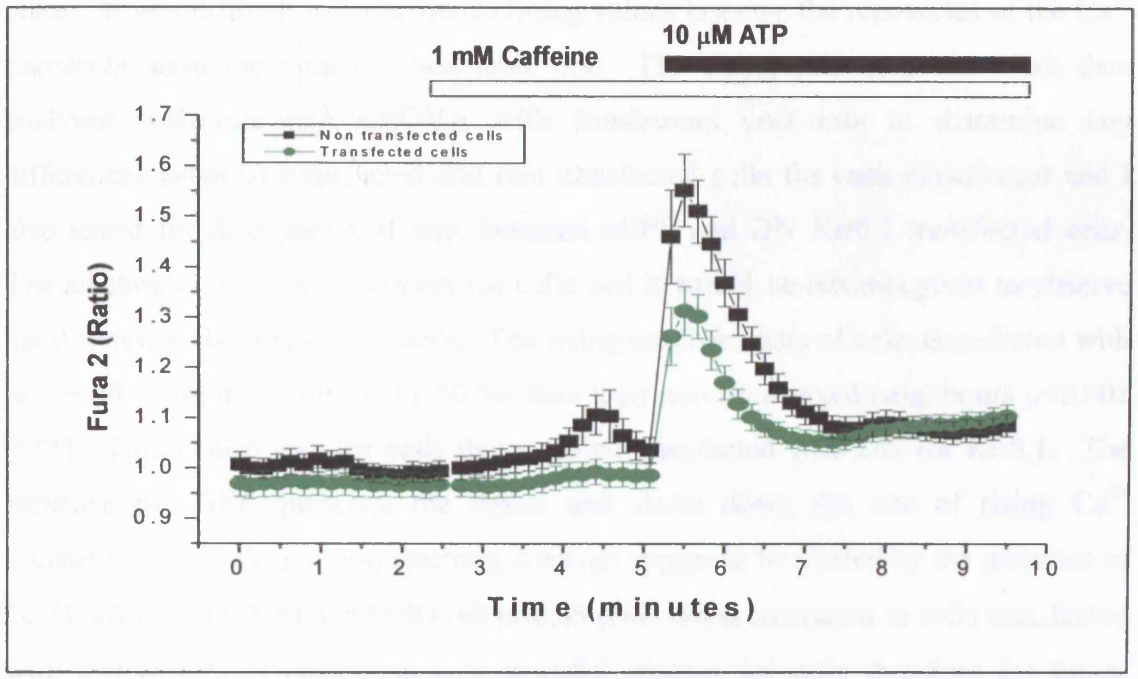

Figure 3.62. A graph to show the Ca^{2+} transients in C2C12 cells transfected with eGFP these were stimulated with 1 mM caffeine and 10 μM ATP. (Transfected cells = 9, non transfected cells = 13).

The rationale for using a ratiometric fluorochrome such as Fura-2 and not single wavelength dyes such as Fluo-4 was that Ca^{2+} measurements would be less affected by considerations such as dye leakage from the cell and other factors that would affect absolute signal levels. However, eGFP is excited at UV wavelengths and so would contribute to an increased background signal in my experiments. Furthermore, the presence of eGFP has been shown subsequently to significantly depress Fura-2 signals (*Bolsover et al. 2001*). Therefore, it would be difficult to compare fluorescence signal intensities as eGFP affects the magnitude of ATP induced Ca^{2+} transients. Because of this observation, I measured the kinetics of this response which may be less affected by eGFP to test for differences, if any, between control cells, cells transfected with eGFP only and those transfected with eGFP and DN for Kir6.1 to examine whether Kir6.1 expression does indeed modulate Ca^{2+} dynamics.

The rising rate constants of ATP induced Ca^{2+} transients were measured in these three experiments by calculating the largest rate between successive data points in this rapid phase. It was difficult to compare declining values because the recoveries of the Ca^{2+} transients were incomplete. See table 3.9. The rising rate constants were then analysed with one-way ANOVA with Bonferonni post-tests to determine any differences between transfected and non transfected cells for each experiment and I also tested for differences, if any, between eGFP and DN Kir6.1 transfected cells. Transfection is a stressful process for cells and it would be advantageous to observe the differences between these cells. The rising rate constants of cells transfected with just eGFP were much lower (by 50 %) than their non transfected neighbours $p<0.001$ (***). This is also true for cells that were co-transfected with DN for Kir6.1. The presence of eGFP quenches the signal and slows down the rate of rising Ca^{2+} transients but the degree of quenching does not appear to be altered by the presence of DNG→A $p>0.05$ (NS) and DNG→S $p>0.05$ (NS) when compared to cells transfected with just eGFP. Transfection is a stressful process for cells therefore for future experiments, it would advisable to transfect cells with lipofectamine alone or with an inert protein for a control experiment. Please refer to chapter 4.0 for further discussion on the limitations in this experiment.

Table 3.9.

A table to summarise the rate of rise and recovery of ATP induced Ca^{2+} transients in C2C12 cells transfected with eGFP, eGFP + DNG→A and eGFP + DN→GS. The results are presented as means ± SEM. (C)= control, (TF)= transfected.

Experiment (C2C12 cells)	**Rising rate constant min^{-1}**	**Reference**
eGFP only	2.15 ± 0.26 (C) † 1.07 ± 0.21 (TF)	Figure 3.62
eGFP + DNG→A	1.02 ± 0.14 (C) ‡ 0.61 ± 0.11 (TF)	Figure 3.60
eGFP + DNG→S	0.54 ± 0.06 (C) ¶ 0.32 ± 0.06 (TF)	Figure 3.61

† Rise: eGFP (C) vs. (TF) $p<0.001$ (***).
‡ Rise: eGFP + DNGA (C) vs. (TF) $p>0.05$ (NS)
¶ Rise: eGFP + DNGS (C) vs. (TF) $p>0.05$ (NS)

Rise eGFP (TF) vs. eGFP + DNGA (TF)
Rise eGFP (TF) vs. eGFP + DNGS (TF)

4.0 Discussion

4.1 The distribution of Kir6.1 in immortalised cells lines:

The main focus of this thesis was to investigate the subcellular distribution of ATP-sensitive potassium subunit Kir6.1 in immortalised cell lines. Using transient transfections, I found that a large proportion of Kir6.1 was expressed in the ER however, in the presence of its receptor SUR1, there was very little membrane staining and the majority of the signal remained intracellular. In addition to this, immunofluorescent staining results support the fact that native Kir6.1 is expressed in the ER to some extent in mitochondria. The latter is an important observation as Kir6.1 may be a component of the mitoK$_{ATP}$ channel that is hypothesised to be involved in IPC (*Suzuki et al. 1997).* Using two different approaches: i) the overexpression of proteins and ii) staining for endogenous protein, approximately 35-55 % of Kir6.1 was distributed in the ER with 20-25 % expressed in mitochondria in immortalised cell lines.

4.2 The evidence for Kir6.1 in mitochondria

In my hands, I showed that Kir6.1 is present in the ER and mitochondria in cardiac, skeletal muscle and liver cell lines. I did not investigate the trafficking of Kir6.1 in primary cells because of the timescale available and the fact that they are notoriously difficult to transfect. Transient transfections and staining for native Kir6.1 showed that a small but significant proportion of Kir6.1 exists in mitochondria in these cell lines. Using the immunofluorescent staining approach, I then co-stained these cells with the Kir6.1 antibody and cytochrome C oxidase, a classic marker for mitochondria and detected a small proportion of Kir6.1 in mitochondria. My antibody also detected Kir6.1 in HL-1 cardiomyocytes which is a rat cell line however; I was not able to detect natively expressed Kir6.1 in freshly dissociated rat ventricular myocytes.

Based on the fact that sarcK_{ATP} and mitoK_{ATP} channels are very similar, it has been suggested that mitoK_{ATP} channels would also consist of Kir6.0 and SUR subunits. Suzuki et al suggested that Kir6.1 was located in mitochondria based on the immunoblot analysis of mitochondrial fractions from rat skeletal muscle and liver from isolated plasma membrane vesicles. Their antibodies detected Kir6.1 as a 51 and 47 kDa protein. My Kir6.1 antibody also detected a band of a similar size (48 kDa) which is consistent for the molecular weight of Kir6.1. Furthermore, Garlid's group later identified two proteins at 55 and 63 kDa with mitoK_{ATP} activity in mitochondrial fractions (*Bajar et al. 2001; Paucek et al. 1992*). The 63 kDa protein was proposed to be the SUR subunit whilst the 55 kDa protein was the pore forming subunit of the channel. The 63 kDa protein from rat brain was bound to fluorescent glibenclamide and the authors suggested that this may be the SUR subunit of the mitoK_{ATP} channel. Recent studies using different cell types have confirmed that Kir6.1 is expressed in mitochondria *(Lacza et al 2003a, 2003b*).

It has been reported that Kir6.1 mRNA and not Kir6.2 or SUR2A is only elevated in cardiomyocytes during metabolic stress such as ischaemia (*Akao et al. 1997*). Interestingly, one group have reported the clear expression of Kir6.1 and SUR1 in cardiac ventricular myocytes with their antibodies (*Morrissey et al. 2005*). On the other hand, Kir6.1, Kir6.2 and SUR2 proteins were also expressed in mitochondria using Western blot analysis (*Cuong et al. 2005*). The authors showed that the SUR subunit, which was identified using green fluorescent probe glibenclamide-BODIPY colocalised with mitotracker red in rat myocytes and mitochondria but SUR1 was not present in mitochondria. The SUR2A gene is expressed abundantly in cardiac muscle so the presence of SUR1 may indicate that the mitoK_{ATP} channel does consist of Kir6.1/SUR1 as Liu et al originally suggested (*Liu et al. 2001*). It is possible that a small proportion Kir6.1 and SUR1 may form K_{ATP} channels but I was unable to detect Kir6.1 at the plasma membrane because expression levels were too low.

In agreement with my results, the subcellular distribution of Kir6.1 was reported to be expressed strongly in mitochondrial and microsome fractions but weakly on the plasma membrane (*Zhou et al. 2005*). Interestingly, Kir6.2 was also expressed in the microsome fraction but weakly at the plasma membrane and mitochondria. This is in line with my findings as I was not able to detect any membrane staining in cells transfected with Kir6.1-GFP and SUR1. Furthermore, Kir6.2-GFP did not localise in mitochondria in HEK293 cells which implies that Kir6.2 is not part of the mitoK$_{ATP}$ channel (*Hu et al. 1999*). Kir6.1 has also been identified in rat ventricular myocytes and were localised with a mitochondrial marker called MitoFluor red, and anti-Kir6.1 antibodies recognised a polypeptide of 48 kDa in mitochondrial membrane fractions SUR1 and SUR2 were absent in heart mitochondria, which suggest that if Kir6.1 is part of the mitoK$_{ATP}$ channel, it may coassemble with a different sulphonylurea like subunit (*Singh et al. 2003*). According to the literature, this can either be a SUR1 or even a SUR2 like protein (*Liu et al 1999*). There is more evidence to support the fact that Kir6.1 and not Kir6.2 is the possible component of the mitoK$_{ATP}$ channel though I am not in the position to speculate the exact identity of its sulphonylurea receptor. Kir6.1 may be expressed in mitochondria, it but does not imply that it is part of the mitoK$_{ATP}$ channel.

4.3 The evidence against Kir6.1 in mitochondria

There are studies that support the hypothesis that Kir6.1 exists in mitochondria, whether it is part of the mitoK$_{ATP}$ channel remains controversial. In the last eight years, this field has taken a new direction as there are now studies that question the existence of mitoK$_{ATP}$ channels. My data suggests that a significant amount of Kir6.1 is expressed in the ER with a small proportion of Kir6.1 in mitochondria. Previous studies have suggested that Kir6.1/SUR1 K$_{ATP}$ channel subunits transfected in HEK293 cells most resembled the native mitoK$_{ATP}$ channel in rabbit myocytes with such channel activity and pharmacology (*Liu et al. 2001*). The presence of SUR1 did not significantly alter the distribution of Kir6.1 at the plasma membrane or mitochondria. Another group reported that GFP-tagged Kir6.1, alone or co-expressed with various splice forms of SUR1 did not target to mitochondria at all (*Hambrock et al. 2002*). However, our group has been able to detect

channel activity in HEK293 cells transfected with Kir6.2-GFP and SUR1. The mitoK$_{ATP}$ channels may not exist or may be composed of entirely different subunits which imply that Kir6.1 and SUR1 may not form functional channels naturally.

One study examined the molecular composition of K$_{ATP}$ channels with adenoviral gene transfer expressing wild-type and dominant-negative constructs of Kir6.1 and 6.2 in rabbit ventricular myocytes (*Seharaseyon et al. 2000*). Kir6.1 and Kir6.2 constructs did not affect mitoK$_{ATP}$ channel activity, as assayed by measuring the changes in flavoprotein autofluorescence. These results contradict the earlier proposal based on subcellular antibody localisation that Kir6.1 may be part of the mitoK$_{ATP}$ channel (*Suzuki et al. 1997*). The authors did not rule out that Kir6.1 may exist in mitochondria but it may not heterodimerize with the dominant negative forms. This may be true for with my results as Kir6.1 was detected in mitochondria using transfected Kir6.1 which may not co-assemble with SUR1. Recent studies have also suggested that neither Kir6.1 nor Kir6.2 are part of the mitoK$_{ATP}$ channel in mitochondria isolated from rabbit and mouse heart (*Miki et al 2002; Suzuki et al 2002*). Furthermore, Kir6.1 knockout mice were shown to die from sudden cardiac death associated with vasopasm but mitoK$_{ATP}$ channel opening was not affected by the absence of this K$_{ATP}$ subunit (*Miki et al. 2002*).

The original study which used the immunogold labelling technique to investigate the distribution of Kir6.1 was novel at the time (*Suzuki et al. 1997*). However, a review by Grover and Garlid disputed the reliability of the Kir6.1 antibody used in this study because there was a possibility that it could bind to other unidentified proteins in the sample (*Grover & Garlid 2000*). Other Kir6.1 antibodies in different studies have been used to identify the location of Kir6.1 but recent reviews have recognised potential flaws in their data. For example, the technical aspect of Lacza's study was questioned by Hanley and Daut's recent review because the mitochondrial samples used were enriched by a factor of 8 in Western blots increasing the chances of contamination because the antibodies could cross react with other proteins. Kir6.1 and Kir6.2 also contained mitochondrial targeting sequences which Hanley and Daut were not able to verify

(*Hanley & Daut 2005*). Suitable measures and controls were set up in my experiments to ensure that the endogenous expression of Kir6.1 in the immortalised were accurate.

Ardehali's prominent study in 2004 questioned the existence of mitoK$_{ATP}$ channels. The authors' findings added further controversy to the identity of the mitoK$_{ATP}$ channel because this multiprotein complex that conferred mitoK$_{ATP}$ activity consisted of five different mitochondrial proteins including SDH *(Ardehali et al. 2004)*. These proteins were detected via Western blotting however, Kir6.1 was not detected. This group later examined this multiprotein complex further and postulated that perhaps this complex could act upstream and modulate the mitoK$_{ATP}$ channel (*Ardehali & O'Rourke 2005*).

4.4 Putting colocalisation and immunofluorescent staining data together

Kir6.1 is expressed in tissues such as in cardiac muscle, skeletal muscle, liver and pancreas (*Inagaki et al. 1995c*). I examined the distribution of Kir6.1 in skeletal muscle (C2C12), liver (HepG2) and cardiac (HL-1) cell lines. The results showed that Kir6.1 was predominantly located in the ER with a small proportion located in mitochondria. In cells transfected with Kir6.1-GFP and SUR1, Kir6.1 was expected to translocate to the membrane because RKR retention motif is masked on both subunits, which promotes exit from the ER. However, Kir6.1 was still ER retained and there was no clear membrane staining. The rationale for transfecting Kir6.1-GFP with SUR1 in my experiments was because in Liu's study, it was reported that the Kir6.1/SUR1 channel closely resembled native mitoK$_{ATP}$ channels with such pharmacology and single channel conductance at the plasma membrane (*Liu et al. 2001*). These results are in line with another group where the Kir6.1/SUR1 type channel does exist and exhibited channel activity in HEK293 cells. In these cells, K$_{ATP}$ channel currents were activated in the presence of diazoxide and inhibited by tolbutamide or glibenclamide (*Ammala et al. 1996a; 1996b*).

A plausible explanation for these observations may be that overexpressing Kir6.1 would lead to a higher proportion of Kir6.1 being ER retained as there are sufficient functional K$_{ATP}$ channels already on the plasma membrane. Most post-translational processes occur

on the ER it is the site where excess proteins are retained before they are registered for degradation (*Klausner & Sitia 1990*). However, it is likely that Kir6.1 does not normally associate with SUR1 therefore the RKR motif is not masked causing Kir6.1 to be retained in the ER. If I had chosen SUR2A or SUR2B, there may be some translocation to the plasma membrane or possibly mitochondria as we know these combinations of K_{ATP} channel subunits exist in different tissues. On a technical note, the GFP tag on the Kir6.1 subunit could interfere with the assembly of the K_{ATP} channel causing Kir6.1 to accumulate in the ER. Furthermore, our group have previously shown that HEK293 cells co-transfected with Kir6.1-GFP and SUR2B can form functional channels with distinct channel activity at the plasma membrane (*Cui & Tinker, unpublished observations*). This was not the case because HEK293 cells transfected with Kir6.2-GFP alone did not exit the ER but co-transfection with SUR1 showed prominent membrane staining and which suggests that the Kir6.1/SUR1 isoform does not exist and form functional channels. For example, Cuong et al did not detect SUR1 in their samples and it is likely more evidence to suggest that if Kir6.1 is part of the mitoK_{ATP} channel, it would associate would a SUR2 like protein (*Lacza et al. 2003, Cuong et al 2005*).

Despite this observation, Kir6.1 may exist in other intracellular membranes for example; functional K_{ATP} channels have been identified on the nuclear membrane of pancreatic β cells (*Quesada et al. 2002*). The majority of Kir6.1 was distributed in the ER and I was able to detect a small proportion of Kir6.1 in mitochondria. The immunofluorescent staining data confirmed that Kir6.1 was natively expressed in these immortalised cell lines. Concanavalin A FITC mainly stains the ER but it may also stain proteins that contain lectins, namely internal and non-reducing terminal alpha-mannosyl groups therefore it must be taken into consideration that the results obtained in chapter 3.3 that show prominent ER staining may also stain parts of the Golgi body. Kir6.1 is also expressed in mitochondria. However, its distribution was not altered in the presence of SUR1. It is possible that there was a small amount of Kir6.1 at the plasma membrane which I could not detect and Kir6.1 may reside in the ER before it is redistributed to the plasma membrane. Although there is now emerging evidence to suggest that a SUR2 like protein is more likely to be closely associated with Kir6.1, my colocalisation studies were

carried out based on the fact that Kir6.1/SUR1 subunits express distinct membrane currents as reported by Liu et al (*Liu et al 2001*). Its pharmacology is almost identical to native mitoK_{ATP} channels in this paper indicate that SUR1 may be part of the mitoK_{ATP} channel. For example, this channel was activated by diazoxide and this is an important observation because SUR2A containing channels do not respond to diazoxide. In addition to this, 5-HD only blocked channel activity in SUR1 containing channels. P-1075 did not activate mitoK_{ATP} and Kir6.1/SUR1 channels.

From these observations, Kir6.1 does not appear to be part of the mitoK_{ATP} channel and the channel in question may be composed of entirely different subunits. The distribution of Kir6.1 in these organelles may have important functional roles. In the ER, Kir6.1 may modulate Ca^{2+} handling and the small proportion in mitochondria may modulate mitochondrial function. I then examined the functional consequences of this subcellular distribution using siRNA and dominant negatives for Kir6.1.

4.5 The role of Kir6.1 and K_{ATP} channels in ROS production

The aim of chapter 3.4 was to examine whether K_{ATP} channel opening would lead to ROS production and in particular, whether K_{ATP} channel subunit Kir6.1 may have a functional role in mediating ROS production. I predicted that the addition of diazoxide would cause a significant increase in ROS production due to the opening of K_{ATP} channels and glibenclamide would inhibit this response. The data showed that diazoxide induced the oxidation of the ROS indicator dye dichlorohydrofluorescein (H_2DCF), hence an increase in ROS production in HepG2 and C2C12 cell lines which contain an abundant amount of endogenous Kir6.1. In addition to this, I observed the inhibitory effects of glibenclamide on ROS production, which also implies the involvement of K_{ATP} channels. In agreement with my findings, the results of another study showed that diazoxide increased H_2DCF oxidation in rat ventricular myocytes with 5-HD attenuating this response (*Forbes et al 2001*). On the other hand, a similar study using rabbit cardiomyocytes showed no changes in fluorescence in response to diazoxide (*Cone & Liu 2001*).

HEK293 cells do not contain endogenous Kir6.1 (or Kir6.2) therefore it is unlikely that functional K_{ATP} channels would exist in this cell line (*Cui et al. 2001*). Given this observation, I did not anticipate changes in ROS production in response to diazoxide and glibenclamide in this cell line. However, diazoxide was able to increase ROS production and glibenclamide abolished this effect. These observations suggest that these pharmacological agents have K_{ATP} channel independent effects. Furthermore, the lack of functional K_{ATP} channels in HEK293 cells imply that the responses observed in C2C12 and HepG2 cell lines may not result from K_{ATP} channel activity or Kir6.1 expression but rather the indirect effects of diazoxide and glibenclamide. The absence of Kir6.1 did not alter diazoxide-induced ROS production in HepG2 and HEK293 cells. The stimulatory effect of diazoxide and inhibitory effect of glibenclamide were more pronounced in C2C12 cells lacking Kir6.1 which imply that these compounds do possess indirect effects. If Kir6.1 is a component of the mitoK_{ATP} channel then the source of ROS must be derived from elsewhere such as the respiratory chain or perhaps a mitoK_{ATP} channel composed of entirely different subunits may be involved in mediating ROS production and protection (*Ardehali et al. 2004*). My results also showed that ROS production was unrelated to Kir6.1 expression.

In support of my findings, one recent study has confirmed that K_{ATP} channels are not responsible for diazoxide induced ROS production (*Dröse et al. 2006*). In isolated liver and heart mitochondria, diazoxide-induced ROS production and 5-HD abolished this response. Dröse et al were able to exclude the complete involvement of K_{ATP} channels because diazoxide could still stimulate ROS production K^+ free medium and absence of ATP. In theory, mitoK_{ATP} channels should be opened in the absence of ATP and K^+ (*Garlid & Paucek 2003*). Furthermore, the protective doses of diazoxide stimulated mitochondrial respiration and increased ROS generation with 5-HD attenuating this response (*Minners et al. 2007*). Protection was independent of mitoK_{ATP} channel activity and the data showed that inhibiting mitochondrial respiration was a key step in ROS signalling. The authors suggested an alternate hypothesis that mitochondrial respiratory inhibition rather than mitoK_{ATP} channel opening was the mediating event in diazoxide induced protection.

Diazoxide is considered a protective agent because it opens the mitoK$_{ATP}$ channel which activates a number of intracellular messengers that lead to protection. It has been reported that at high doses, diazoxide can act as a weak protonophoric uncoupler rather than a KCO (*Holmuhamedov et al. 2004; Kowaltowski et al. 2001; Portenhauser et al. 1971*). Diazoxide and pinacidil are lipophilic and facilitate the transfer of protons across the mitochondrial inner membrane; this is consistent with the fact that a high $\Delta\psi_m$ will enhance ROS production (*Holmuhamedov et al. 2004*). This may also explain the results where a burst of ROS was observed perhaps due to the uncoupling rather than channel opening properties of diazoxide. In addition to this, the uncoupler DNP was shown to protect hearts from ischaemia which strongly supports the notion that protonophoric uncoupling is another mechanism that can precondition the heart which is independent of K$_{ATP}$ channels (*Minners et al. 2000*). However the list of non specific effects such as the ability to enhance mitochondrial swelling, substrate oxidation and cause changes in fatty acid metabolism and ROS production suggests that it may not act directly on mitoK$_{ATP}$ channels. Garlid originally reported that diazoxide was a specific and potent activator of mitoK$_{ATP}$ channels with half-maximal effect (EC50) at <3 μM (*Garlid et al. 1996*). The foundation for using glibenclamide instead of 5-HD in my experiments was because 5-HD is a known substrate for the β-oxidation pathway and possess many other channel independent actions (*Dröse et al. 2006; Hanley et al. 2002, 2003*). However, these pharmacological compounds are not always truly 'selective' for K$_{ATP}$ channels and their cardioprotective mechanism can be attributed by other mechanisms.

My data showed that diazoxide and glibenclamide had significant effects on ROS production. The source of ROS is cellular, I cannot confirm whether it is mitochondrial but it can be derived from other intracellular sources such as xanthine oxidase, NADPH oxidase or the respiratory chain. Given more time, further experiments would be carried out in the presence of specific inhibitors for these enzymes to determine their involvement in ROS production. For NADPH oxidase, diphenylene iodonium (DPI) would be used to inhibit NADPH oxidase activity whereas xanthine oxidase would be inhibited using oxypurinol; this is a metabolite of allopurinol and has preferential binding to the reduced form of xanthine oxidase. If the source of ROS is derived from the

respiratory chain, the presence of these inhibitors should not affect diazoxide induced ROS production. However, DPI is known to inhibit the respiratory chain, NADPH oxidases and xanthine oxidase (*Li & Trush 1998, O'Donnell et al 1994*). To conclude, diazoxide induced ROS production was abolished by glibenclamide however, there is no link between diazoxide mediated ROS production and Kir6.1 expression.

4.6 The effects of pharmacological agents on mitochondrial redox state

Kir6.1 does not have role in ROS production and diazoxide and glibenclamide possess non specific effects that are independent of K_{ATP} channels. Despite this conclusion, K_{ATP} channels may still exist in mitochondria and their activity can be modulated by these pharmacological compounds.

Table 4.1. A table to show the studies that measured the changes in flavoprotein fluorescence and the effects of potassium channel opener diazoxide and inhibitor glibenclamide on mitochondrial redox state.

Journal	Cell type	Diazoxide (100 μM)	Glibenclamide (10 μM)	Other pharmacological agents	Reference
Circulation	Rabbit Ventricular myocytes	Oxidised flavoproteins	No effect (but may promote further uncoupling of mitochondria)	500 μM 5-HD blocked diazoxide induced flavoprotein oxidation	Liu et al. 1998
Annals of the New York Academy of Sciences	Rabbit Ventricular myocytes	Oxidised flavoproteins (P-1075 also produced the same effect)	n/a	500 μM 5-HD blocked diazoxide induced flavoprotein oxidation	Liu et al. 1999
Circulation	Rabbit Ventricular myocytes	Oxidised flavoproteins	n/a	500 μM 5-HD blocked diazoxide induced flavoprotein oxidation, 30 μM HMR1098 did not	Sato et al. 2000
British Journal of Pharmacology	Rat ventricular myocytes	No effect	n/a	n/a	Lawrence et al. 2001
Journal of Physiology	Guinea Pig ventricular myocytes	No effect	n/a	n/a	Hanley et al. 2002

The opening of mitoK$_{ATP}$ channels would alter the $\Delta\psi_m$ and uncouple mitochondria. Such dissipation will enhance electron transfer within the respiratory chain leading to the net oxidation of the mitochondrial matrix which can be detected by measuring an increase in flavoprotein autofluorescence. This technique is routinely used as an indicator of mitoK$_{ATP}$ channel activity and many groups have used this method to evaluate the relationship between mitoK$_{ATP}$ channel activity and pharmacological agents (*O'Rourke 2004*; *Garlid 1996*). The studies of interest are highlighted in table 4.1. In my hands, a small amount of Kir6.1 was expressed in mitochondria. Given this observation, I investigated the possible effects of diazoxide and glibenclamide on mitochondria by measuring the changes in mitochondrial redox state.

My data showed that 100 μM diazoxide and 10 μM glibenclamide had no significant effect on mitochondrial redox state in C2C12 cells and rat ventricular myocytes. Despite these initial observations, diazoxide significantly increased flavoprotein oxidation when myocytes were pre-treated with 1 mM 3-NPA. This increase in flavoprotein oxidation (observed as an increase in flavoprotein autofluorescence and reciprocal decrease in NADH autofluorescence) was completely diazoxide dependent. Glibenclamide did not block this response. However, I could not reproduce this phenomenon in C2C12 cells. My results oppose previously published work because Marban's group were able to initiate flavoprotein oxidation with 100 μM diazoxide (*Liu et al. 1998*). The authors investigated the effects of diazoxide and 5-HD on mitochondrial redox state and sarcK$_{ATP}$ current in rabbit ventricular myocytes. These variables were measured simultaneously where 100 μM diazoxide increased flavoprotein autofluorescence but failed to activate sarcolemmal currents, confirming the existence of mitoK$_{ATP}$ channels. The selective mitoK$_{ATP}$ blocker 5-HD abolished the redox changes induced by diazoxide.

In my hands, the inhibition of SDH by 3-NPA was vital for diazoxide induced flavoprotein oxidation. My results are in line with two similar studies where 100 μM diazoxide alone did not promote flavoprotein oxidation in rat and guinea pig myocytes (*Hanley et al 2002; Lawrence et al. 2001*) but disagree with the original findings of Marban's group (*Liu et al 1998*). Subsequent studies conducted by Marban's group were

able to replicate diazoxide-induced flavoprotein oxidation in rabbit ventricular myocytes (*Sato et al 2000; Sasaki et al. 2000; Liu et al. 1999*). It is important to note that the recordings from Marban's group were obtained from myocytes isolated in M199 medium but experiments were performed in glucose-free physiological salt solution which may have enhanced the cells' ability to consume more substrates when respiration was stimulated with pharmacological agents. The myocytes used in my experiments were not substrate starved which may account for the difference in results. The variation between the studies highlighted in table 4.1 may be linked to experimental conditions or possibly even species differences.

My data also showed that 3-NPA alone did not affect flavoprotein oxidation. The inhibition of SDH by 3-NPA may not be necessary to dissipate the $\Delta\psi_m$ because electrons will continue to pass from complex I to III, which may explain why no change in flavoprotein autofluorescence was observed in the presence of 3-NPA. However, 3-NPA pre-treatment was essential for diazoxide to stimulate respiration. Previous work carried out in our laboratory showed that 1 mM 3-NPA and 30 μM diazoxide induced flavoprotein oxidation (*Duchen lab, unpublished observations*). In my hands, it was not possible to induce flavoprotein oxidation unless 100 μM diazoxide was administered. Glibenclamide was administered after diazoxide application based on the assumption that it would inhibit flavoprotein oxidation by closing the mitoK_{ATP} channel but my data showed that it did not reverse flavoprotein oxidation. Furthermore, glibenclamide has been shown to uncouple mitochondria significantly (*Garlid et al. 1997; Szewczyk et al. 1997*). These experiments have shown that 3-NPA and diazoxide were responsible for flavoprotein oxidation but this phenomenon does not confirm the involvement of Kir6.1 nor mitoK_{ATP} channels. To add further fuel to this controversy, Ardehali's study found that their multiprotein complex was sensitive to KCOs and inhibitors but also to SDH inhibitors such as 3-NPA which promoted mitoK_{ATP} channel activity and K^+ transport (*Ardehali et al 2004*).

4.6 The effect of pharmacological agents on $\Delta\psi_m$

The $\Delta\psi_m$ is an important factor to measure because the dissipation of $\Delta\psi_m$ is thought to lead to an increase in flavoprotein oxidation. My data showed that 100 μM diazoxide caused mitochondrial depolarisation in C2C12 cells, whereas glibenclamide had no effect. Similar effects of KCOs have been reported in isolated rat skeletal muscle mitochondria and intact L6 skeletal myoblasts (*Debska et al. 2002*). In other studies, C2C12 myoblasts subjected to diazoxide or adenosine treatment resulted in mild uncoupling, assayed by the increase in oxygen consumption, small decrease in $\Delta\psi_m$, and reduction of cellular ATP levels (*Minners et al. 2000*). The authors also reported that diazoxide and nicorandil caused significant mitochondrial depolarisation which was followed by an increase in oxygen consumption in a dose dependent manner; this effect was completely inhibited by glibenclamide but partially by 5-HD. However, the $\Delta\psi_m$. did not change in the presence of 3-NPA and diazoxide (which caused significant flavoprotein oxidation) but there was some uncoupling effect upon glibenclamide addition. The presence of 3-NPA has been confirmed by others to not affect the $\Delta\psi_m$ whereas in Ardenhali's study, 3-NPA was able to activate mitoK_{ATP} currents in lipid bilayers (*Busija et al. 2005*, *Ardehali et al. 2004*).

Table 4.2. A table to show the studies that examined the changes in mitochondrial membrane potential ($\Delta\psi_m$) in the presence of potassium channel opener diazoxide.

Journal	Cell type	Diazoxide (100 μM)	Glibenclamide (10 μM)	Other compound	Reference
British Journal of Pharmacology	Rat Ventricular myocytes	No changes in $\Delta\psi_m$	n/a	1 μM FCCP collapsed $\Delta\psi_m$	Lawrence et al. 2001
Journal of Physiology	Rabbit Ventricular myocytes	No changes in $\Delta\psi_m$	n/a	100 μM DNP collapsed $\Delta\psi_m$	Hanley et al. 2002

The data suggest that the changes in flavoprotein autofluorescence are not associated with the changes in $\Delta\psi_m$. I was not able to examine the effects of 3-NPA, diazoxide and glibenclamide in rat ventricular myocytes. The phototoxicity effect of the laser caused

significant depolarisation followed by cell shortening which affected the cells and proved difficult to take accurate measurements. The studies of interest are highlighted in table 4.2. In my hands, the addition of 1 mM 3-NPA and 100 μM diazoxide did not alter $\Delta\psi_m$ in C2C12 cells, perhaps, the combination of 3-NPA and diazoxide increased respiration significantly (observed as an increase in flavoprotein autofluorescence) to restore the $\Delta\psi_m$ so the changes in $\Delta\psi_m$ could not detected. The complete dissipation of the $\Delta\psi_m$ was only observed in response to the protonophore FCCP. Hanley et al's data agrees with my results as they also observed no changes in $\Delta\psi_m$ with 100 μM diazoxide (and 100 μM pinacidil) in guinea pig ventricular myocytes (*Hanley et al 2002*). These findings are also in agreement with another group where $\Delta\psi_m$ was not affected by the presence of 100 μM diazoxide (*Lawrence et al. 2001*).

4.7 The non-specific effects of K_{ATP} channel openers and inhibitors

The decision to use diazoxide and glibenclamide in these experiments was based on their specificity and ability to modulate the mitoK_{ATP} channel. Garlid reported that diazoxide had a potency for mitoK_{ATP} channel about 2000-fold higher than the sarcK_{ATP} channel (*Garlid et al. 1996*). Studies in the 1970's demonstrated the coupling effects of diazoxide in heart and liver mitochondria where 150 μM diazoxide caused 60 % inhibition of SDH and a decrease in pyruvate and fatty acid oxidation (*Schafer et al. 1971*). Therefore, diazoxide may act either to open the mitoK_{ATP} channel or inhibit SDH depending on the concentration used. My functional data showed that these compounds possess non-specific and toxic effects that are independent of K_{ATP} channels.

In preliminary studies, I was not able to induce flavoprotein oxidation with a low dose of diazoxide (50 μM) (***unpublished observations***). Liu's study showed that the increase in flavoprotein autofluorescence in rabbit myocytes was due to 100 μM diazoxide (*Liu et al 1998*). The increase in flavoprotein autofluorescence was interpreted as mitoK_{ATP} channel opening and was a consequence of mitochondrial depolarisation. This is an interesting result because it is the low concentration of diazoxide (30 μM) that is reported to confer protection in isolated hearts. However, the increase in flavoprotein oxidation in

rat myocytes occurred only in the presence of 1 mM 3-NPA and 100 μM diazoxide. My data (and studies) discussed here show that only the higher dose of diazoxide will promote flavoprotein oxidation which is not consistent with these observations. Furthermore, Garlid stressed that a high dose of diazoxide (100 μM) was higher than required to open K_{ATP} channels in Liu's study to observe changes in flavoprotein oxidation. Therefore the results may not be a direct response to mitoK_{ATP} opening because in addition, there was a significant time delay of 10-12 minutes between the administration of diazoxide and the start of the signal (*Garlid 2000*). This specific time delay is also true for my data but diazoxide alone could not increase flavoprotein oxidation unless the cells were pre-treated with 3-NPA.

One advantage of my work is that I was able to measure the changes in flavoprotein and NADH autofluorescence simultaneously. My results are in agreement with Hanley's study where they also observed no effect of 100 μM diazoxide on flavoprotein autofluorescence in guinea pig ventricular myocytes. They also stated that the inhibition of SDH was important for flavoprotein oxidation which operates independently of mitoK_{ATP} channels (*Hanley et al. 2002*). A recent study examining the crystal structure of avian complex II protein showed that 3-NPA irreversibly inactivates complex II upon oxidation by forming permanent covalent bonds to modify its catalytic machinery (*Huang et al. 2006*). This supports the hypothesis that SDH may modulate mitoK_{ATP} channels because when SDH is inhibited, the addition of diazoxide may still activate a mitoK_{ATP} channel or act independently on neighbouring proteins to activate signal transduction pathways that increase rate of respiration (*Ardehali & O'Rourke 2005*).

Glibenclamide significantly reduced diazoxide induced ROS production which initially suggested the involvement of K_{ATP} channels. Glibenclamide had no major effects on mitochondrial redox state in C2C12 cells but in rat myocytes, glibenclamide did not block the rate of flavoprotein oxidation which suggests that it may not act on mitochondrial redox state. Gibenclamide has non-specific effects; it is a potent inhibitor of carnitine palmitoyltransferase which reduces the rate of fatty acid oxidation perhaps contributing to increased flavoprotein oxidation (*Cook 1987*). This may explain why

glibenclamide did not block flavoprotein autofluorescence in my rat myocytes and this is also true of Liu's original study in rabbit myocytes because the rate of flavoprotein oxidation was maintained (*Liu et al. 1998*). However, at higher concentrations, glibenclamide can inhibit other members of the ABC family of transport proteins and chloride channels (*Payen et al. 2001; Rabe et al. 1995*). The uncoupling effects of glibenclamide may not be due to enhanced H^+ pumping to maintain the ψ_m but rather the increase in permeability to Cl^- which results in K^+ influx (*Fernandes et al. 2004*).

In Liu's study, the data showed that 5-HD abolished diazoxide induced flavoprotein autofluorescence but this was not used for my experiments because of its many and non-specific side effects. Various groups have reported 5-HD to affect sarcK_{ATP} channel currents in myocytes induced by cromakalim and pinacidil whereas glibenclamide abolished this effect (*Sato et al. 1998; McCullough et al. 1991*). Furthermore, Notsu and co-workers showed 5-HD could also block K_{ATP} channel activity in cardiomyocytes subjected to metabolic inhibition; this suggests that it is not particularly selective for the mitoK_{ATP} channel (*Notsu et al. 1992a and b*). Like all fatty acids, 5-HD is catalysed by acyl-CoA synthethase to 5-HD CoA which can be further metabolised in rat mitochondria (*Lim et al. 2002*). This questions the reliability of their data because 5-HD in substrate free conditions is metabolised by the β-oxidation pathway and fatty acid oxidation can induce flavoprotein oxidation (*Hanley et al. 2002; 2003; Vuorinen et al. 1995*).

4.8 The controversies surrounding the mitoK_{ATP} channel

In this section, I will aim to examine my data and discuss the evidence for the mitoK_{ATP} channel. The pharmacological compounds used to probe the function of Kir6.1 are not always selective for K_{ATP} channels. In particular, my data question the assumption that sensitivity to diazoxide and glibenclamide implies the involvement of mitoK_{ATP} channels. Diazoxide is a cardioprotective agent because it initiates mitochondrial depolarisation, conserves cellular ATP and limits Ca^{2+} uptake (*Holmuhamedov et al 1999*). Marban's earlier studies showed that diazoxide increased mitochondrial oxidation and this piece of evidence was interpreted as mitoK_{ATP} channel opening. Once the $\Delta\Psi_m$ dissipates, there is

an increase in mitochondrial oxidation to re-establish the $\Delta\Psi_m$ and maintain ATP production. However, the relationship between mitochondrial uncoupling, $\Delta\Psi_m$ and flavoprotein oxidation are not always related because it is possible to cause oxidation without depolarisation. This has been demonstrated with my work because my data showed that the changes in flavoprotein oxidation and $\Delta\psi_m$ do not go hand in hand and it is unclear whether these two variables are closely linked.

In support of my findings, Brennan and colleagues showed that low concentrations of FCCP (100 nM) caused flavoprotein oxidation without mitochondrial depolarisation whereas higher concentrations of FCCP (300 nM) caused significant depolarisation which can be detrimental (*Brennan et al. 2006b*). Furthermore this group showed that FCCP was able to promote protection and protection was dependent on ROS but independent of K_{ATP} channels. The evidence for this showed that the sarcK_{ATP} channel was not activated and protection was not abolished by glibenclamide and 5-HD. Myocytes can oppose mitochondrial depolarisation by increasing electron transport through the respiratory chain by depleting creatine phosphate (*Brennan et al. 2006a*).

The opening of the mitoK_{ATP} channels has been reported to have little effect on respiration, ψ_m, or Ca^{2+} uptake but had pronounced effects on matrix and intermembrane space volumes (*Kowaltowski et al. 2001*). The influx and magnitude of K^+ was too small to influence respiration and $\Delta\psi_m$. Since pharmacological preconditioning with diazoxide is usually credited with mitoK_{ATP} channel opening, an alternative explanation for the cardioprotective effect of these drugs was required. One school of thought is that the potential role of mitoK_{ATP} channels is its direct interaction with the components of the electron transport chain. For example, the inhibition of respiratory chain enzyme SDH may induce a conformational change in the protein complex that is accompanied by mitochondrial swelling; this mechanism may protect mitochondria from metabolic stress and offer protection by conserving energy and ATP stores.

These observations lead investigators to believe that inhibiting respiration rather than K_{ATP} channel activation may be the underlying mechanism responsible in preconditioning

(*Hanley et al. 2002; Lim et al. 2002*). Diazoxide at high concentrations is also capable of inhibiting SDH but SDH inhibitors such as 3-NPA and malonate have been reported to attenuate metabolic stress and promote cardioprotection in the heart (*Horiguchi et al. 2003; Ozcan et al. 2002; Ockaili et al. 2001*). Recently, one study reported diazoxide inhibited succinate supported respiration which promoted ROS production in C2C12 myotubes. Interestingly, this response was achieved independently of mitoK_{ATP} channels (*Minners et al 2007*). In support of my data, the recent study published by *Dröse* et al questioned the protective role of diazoxide in cardioprotection (*Dröse et al. 2006*). Diazoxide induced ROS production in isolated liver and heart mitochondria but this response was still observed in the absence of ATP and K^+ which strongly suggests that ROS production was not the result of K_{ATP} channel opening.

Diazoxide at cardioprotective concentrations may not induce mitochondrial oxidation or depolarisation. (*Lawrence et al .2001*). The other mechanisms may be linked to the changes in mitochondrial matrix volume or the generation of ROS rather than mitoK_{ATP} channel opening (*Pain et al 2000*). In addition, Hanley et al showed diazoxide had K_{ATP} channel independent targets in the heart and it may be the partial inhibition of the respiratory chain that leads to an increase in ROS production (*Hanley et al. 2002*). In light of my results, diazoxide will stimulate respiration in cells pre-treated with 3-NPA. However, the changes in flavoprotein autofluorescence and $\Delta\psi_m$ did not correlate which suggest that these compounds had no effect on the mitoK_{ATP} channel. Despite these observations, the partial inhibition of the respiratory chain may increase the transfer of electrons which was detected as increase in flavoprotein oxidation. Another possibility is that the channel may already be opened but the influx of K^+ into the matrix was too small to influence $\Delta\psi_m$ but instead promote the close interaction between components of the electron transport chain such as SDH and mitoK_{ATP} channel. These results suggest that the changes in $\Delta\psi_m$ and flavoprotein oxidation are not inevitable consequences of diazoxide application in intact cardiac myocytes, and that the mitoK_{ATP} channel may not be the essential component of the mechanism that provides protection. The evidence from my studies suggests that these pharmacological compounds may offer protection via a different mechanism that is independent of K_{ATP} channels.

4.9 Ca^{2+} signalling and K_{ATP} channels-what is the connection?

Kir6.1 is expressed in the ER of cardiac and skeletal muscle as well as liver cell lines. I investigated the possible role of Kir6.1 in Ca^{2+} handling with the ratiometric Ca^{2+} indicator Fura-2 in C2C12 cells. I also examined Ca^{2+} release in rat myocytes because these cells express RYR and elicit Ca^{2+} transients in response to caffeine. Ca^{2+} is important for controlling a number of cellular processes and $[Ca^{2+}]_i$ is regulated by the entry of external Ca^{2+} (influx) and its release from internal stores. Once Ca^{2+} has carried out its signalling functions, the high concentration of Ca^{2+} is rapidly restored by the Ca^{2+} pumps, PMCA and SERCAs as well as secondary active transporters such as NCX. The opening of a K_{ATP} channel in intracellular membranes such as the ER/SR and mitochondria may have a significant impact on cytosolic Ca^{2+} levels. K^+ is vital for the normal electrical activity of cardiac muscle as the K^+ gradient is responsible for maintaining the resting membrane potential and is critical for the repolarisation of the cell membrane when an action potential has been elicted. The role of K^+ in excitation-contraction (EC) coupling is unclear but there are K^+ channels in the cardiac SR membrane similar to those in the sarcolemma (*Hill et al. 1989*). However, there is no evidence for K_{ATP} channel expression in the ER/SR.

Ca^{2+} overload has been linked to the damage caused by ischaemic reperfusion and mechanisms that reduce the rate of Ca^{2+} release or deplete Ca^{2+} stores are cardioprotective. One such mechanism involves the opening of K_{ATP} channels in the SR which may promote Ca^{2+} release and change Ca^{2+} transients that can prevent SR Ca^{2+} accumulation during cytosolic Ca^{2+} overload. More importantly, it has been shown that cytosolic Ca^{2+} overload occurs during myocardial ischaemic injury (*Gettes et al. 1991*). In cardiac tissue, the release of Ca^{2+} from the SR will interfere with the transmembrane potential which can inhibit its own release and prevent muscle contraction. It has been suggested that the opening of the SR K_{ATP} channel allows K^+ moves in the opposite direction to Ca^{2+} across the SR membrane during the uptake and release of Ca^{2+} by the

SR to prevent the development of large charge imbalances which could inhibit Ca^{2+} movement. This mechanism is based on the 'charge compensation' theory mediated by the movement of K^+ and Cl^- in the SR which maintains electroneutrality (*Kourie et al. 1997; Tinker et al 1992; Labarca et al. 1980*). IPC is often associated with decreased calcium release from the SR regulating contractility. One study showed that preconditioning still occurred when the SR was unable to accumulate Ca^{2+} (by using a low dose of ryanodine to block the channel). These observations suggested that the changes in SR calcium release are not essential in the mechanism of preconditioning (*Cave & Garlick 2000*). Furthermore, K_{ATP} channels had no defined role in contractility and Ca^{2+} release in voltage clamped cells (*Tokuno et al 1999*).

Many studies have shown that ATP can stimulate the release of Ca^{2+} specifically from intracellular stores (*El-Moatassim et al. 1992; Inscho et al. 1996*). My C2C12 cells showed a robust response to 10 μM ATP with significant Ca^{2+} transients. EGTA was included in low Ca^{2+} extracellular solutions so that the Ca^{2+} responses observed would be derived from internal stores presumably via purinergic P2Y signalling pathway. However, caffeine did not induce Ca^{2+} transients in these cells. The next step was to differentiate the cells into distinct myotubes to express RYR. Caffeine should then elicit significant Ca^{2+} transients by activating RYR however, this was not the case. The population of cells were differentiated for five days but caffeine-induced Ca^{2+} transients were only observed in 51 % of cells. The Ca^{2+} stores were partially emptied using this low concentration of caffeine and so it was possible for re-uptake into the SR. The rationale for using 1 mM caffeine as opposed to 10 mM was because I did not want to deplete stores and additional stimulation with ATP would elicit further Ca^{2+} release.

For future experiments, staining the 'differentiated' cells for RyRs may help determine if the myotubes in my study had expressed mature and sufficient RyRs. To confirm that caffeine dependent RYR Ca^{2+} release could be measured, rat myocytes were also treated with the same caffeine stock solution and all cells responded immediately by eliciting Ca^{2+} transients. The next step was to examine if Kir6.1 expression was related to Ca^{2+} release therefore C2C12 cells were co-transfected with DN for Kir6.1 and eGFP to

identify transfected cells. However, there were limitations with these experiments. Fura-2 was excited by UV light (340/380 nm) whereas blue light would predominantly excite eGFP. The initial results showed that Kir6.1 may play a small role in modulating ATP-induced Ca^{2+} release from the ER/SR because smaller Ca^{2+} transients were observed in cells without Kir6.1. However, the magnitude of Ca^{2+} transients in cells transfected with just eGFP were also affected. The Fura-2 ratio in the resting state was lower in eGFP-expressing cells than in their non expressing neighbours. This was an important observation because it showed that the presence of eGFP affected $[Ca^{2+}]_i$ measurements and made it difficult to determine if transfection itself alter Ca^{2+} transients.

It has been reported that eGFP can seriously contaminate Ca^{2+} (Fura-2) measurements (*Bolsover et al. 2001*). According to the authors, the excitation and emission spectra of GFP and its variants are very broad, contributing to cross-talk between the fluorescence signals from GFP and the fluorescent Ca^{2+} indicator. The excitation spectra of both Fura-2 and eGFP were measured and a small but rather significant short wavelength tail of eGFP excitation spectrum (350 nm) was present and so the molecule would be excited by the 380 nm UV light used to excite Fura-2. The light that is emitted from eGFP would thus reduce the 340/380 Ratio. Therefore the $[Ca^{2+}]_i$ measured was lower than expected. Given this observation, I then examined the kinetics of the Ca^{2+} transients in eGFP containing cells and found that the signal was quenched and the rising rate constants were significantly lower than their non-transfected counterparts. It was not possible to measure the falling rate constants because Ca^{2+} transients did not make a full recovery. Statistical analysis showed that the Ca^{2+} transients in cells transfected with DNs and eGFP were similar and knocking out Kir6.1 protein expression did not prevent ATP induced Ca^{2+} transients and co-transfection with eGFP did not affect the cell's ability to release Ca^{2+}. However, transfection itself is a stressful procedure and it would have been advantageous to include a control experiment (with just lipofectamine or an inert protein) to demonstrate that it had not affected the Ca^{2+} transients.

In conclusion, I have demonstrated that eGFP alone does contaminate the Fura-2 ratio therefore direct comparisons could not be made between the two cell populations. To

conclude, ATP can stimulate the P2Y receptor to increase $[Ca^{2+}]_i$ in C2C12 cells but in my hands, I was not able to demonstrate whether Kir6.1 plays a prominent role in modulating Ca^{2+} dynamics. I cannot deduce if Kir6.1 has a modulatory role in Ca^{2+} release from internal stores though it is also possible that Kir6.1 may still have a function in the ER. Given the opportunity, to facilitate the measurement of rate constants, I would increase the sampling rate and use other dyes where there is no detectable contamination of the Ca^{2+} indicator signal by the fluorescent protein. For example, blue fluorescent protein could be used with the Ca^{2+} indicator Fura Red and eGFP could be used with the Ca^{2+} indicator X-Rhod 1.

4.10 Overall conclusion

The ATP-sensitive potassium channel subunit Kir6.1 is predominantly distributed in intracellular organelles such as the ER and to some extent in mitochondria. Kir6.1 was overexpressed in immortalised cell lines and colocalisation studies showed that the majority of Kir6.1 was located in the ER. However, the presence of SUR1 did not affect the distribution of Kir6.1 and its translocation to the plasma membrane. It is possible that overexpressing Kir6.1 in these cell lines would cause excess Kir6.1 to be ER retained, as there are functional K_{ATP} channels already present at the membrane. Kir6.1 has been proposed to be a major component of the controversial mitoK_{ATP} channel. Although the molecular identity of this channel still remains elusive, immunofluorescent staining in cardiac, skeletal muscle and liver cell lines showed that Kir6.1 was present in the ER with a small but significant amount in mitochondria. In addition, several groups have identified endogenous Kir6.1 in primary cardiomyocytes but I was not able to detect natively expressed Kir6.1 in rat myocytes.

The localisation of Kir6.1 is hypothesised to be central to its role in cardioprotection and may modulate cellular respiration and Ca^{2+} handling. Since 1997, several publications in this field have implicated that mitoK_{ATP} channel opening is a crucial step in ischaemic preconditioning. I showed that a small proportion of Kir6.1 was expressed in mitochondria but this data alone was not sufficient to confirm that Kir6.1 was part of the

mitoK$_{ATP}$ channel. The potential role of Kir6.1 was also examined in immortalised cell lines and in rat ventricular myocytes. Firstly, I measured the changes in ROS levels in C2C12 and HepG2 cell lines which express native Kir6.1. The data initially suggested that K$_{ATP}$ channels were involved because diazoxide significantly increased ROS production whereas glibenclamide abolished this effect. However, in the absence of Kir6.1 using siRNA and DNs for Kir6.1 and in HEK293 cells that do not express Kir6.1, the same responses were observed. These results revealed that these pharmacological compounds may have other intracellular targets that may influence cellular ROS production. Furthermore, it has been demonstrated recently that diazoxide induced ROS production is not related to K$_{ATP}$ channels.

The effects of diazoxide and glibenclamide were also examined on mitochondrial function by measuring the changes in mitochondrial redox state and $\Delta\psi_m$. The results showed that 3-NPA pre-treatment (and SDH inhibition) was an essential step for diazoxide to stimulate flavoprotein oxidation in rat ventricular myocytes. In my hands, Kir6.1 was absent in these myocytes whereas the C2C12 cell line expressed Kir6.1. However, these cells showed no changes in flavoprotein oxidation and $\Delta\psi_m$ in response to 3-NPA and diazoxide. Despite these observations, the changes in $\Delta\psi_m$ did not correlate with the changes in flavoprotein oxidation which suggested that these variables were not linked and the effects observed were independent of K$_{ATP}$ channels. Diazoxide may offer protection by partially inhibiting the respiratory chain which may alter mitochondrial function. Recently, emerging evidence has added further fuel to the identity of the mitoK$_{ATP}$ channel by identifying a multiprotein complex which exhibited mitoK$_{ATP}$ channel activity. This complex did not contain Kir6.1. MitoK$_{ATP}$ channel opening may facilitate the influx of K^+ into the matrix and induce mitochondrial swelling to promote the close interaction of proteins in the electron transport chain such as SDH and mitoK$_{ATP}$ channel to initiate protection.

Finally, as the majority of Kir6.1 resides in the ER, Kir6.1 was postulated to have a vital role in Ca^{2+} handling. In C2C12 cells, ATP induced Ca^{2+} release from the ER. In the absence of Kir6.1, the magnitude of ATP induced Ca^{2+} transients were smaller but on

closer inspection, it was revealed that the presence of eGFP that was used to assess the transfection efficiency seriously contaminated the Ca^{2+} (Fura 2) signal. The presence of eGFP altered the emission spectrum and the entire Fura-2 ratio. Suppressing Kir6.1 expression did not affect the cell's ability to release Ca^{2+} but I cannot deduce a conclusion from these results. From my observations, the potassium channel subunit Kir6.1 is predominantly distributed in the ER but also exists in mitochondria. Pharmacological agents such as diazoxide and glibenclamide have non-specific effects and my data show that Kir6.1 does not appear to have a role in ROS production or mitochondrial function which suggests that it may not be a component of the mitoK_{ATP} channel.

5.0 REFERENCES

Abbracchio, M.P. & Burnstock, G. (1994). Purinonergic receptors: are these families of P2X and P2Y purinoergic receptors? Pharmacological Therapeutics 64: 445-475.

Aguilar-Bryan, L., & Bryan, J. (1999). Molecular biology of adenosine triphosphate-sensitive potassium channels. Endocrine Reviews 20: 101-135.

Aguilar-Bryan, L., Clement IV, J. P., Gonzalez, G., Kunjilwar, K., Babenko, A., & Bryan, J. (1998). Toward Understanding the Assembly and Structure of K_{ATP} Channels. Physiological Reviews 78(1): 227-245.

Aguilar-Bryan, L., Nichols, C.G., Wechesler, S.W., Clement IV, J.P., Boyd III A.E., Gonzalez, G., Herrera-Sosa, H., Nguy, K., Bryan, J. & Nelson, D.A. (1995). Cloning of the beta cell high-affinity sulfonylurea receptor: a regulator of insulin secretion. Science. 268: 423-426.

Akao, M., Otani, H., Horie, M., Takano, M., Kuniyasu, A., Nakayama, H., Kouchi, I., Murakami, T. & Sasayama, S. (1997). Myocardial ischemia induces differential regulation of K_{ATP} channel gene expression in rat hearts. Journal of Clinical Investigation 100: 3053-3059.

Albert, C.J. & Ford, D.A. (1999). Protein kinase C translocation and PKC-dependent protein phosphorylation during myocardial ischemia. American Journal of Physiology 276(2 Pt 2):H642-H650.

Ammala, C., Moorhouse, A., Gribble, F., Ashfield, R., Proks, P., Smith, P.A., Sakura, H., Coles, B., Ashcroft, S.J. & Ashcroft F.M. (1996a). Promiscuous coupling between the sulphonylurea receptor and inwardly rectifying potassium channels. Nature 379: 545-548.

Ammala, C., Moorhouse, A. & Ashcroft, F.M. (1996b). The sulphonylurea receptor confers diazoxide sensitivity on the inwardly rectifying K^+ channel Kir6.1 expressed in human embryonic kidney cells. Journal of Physiology 494: 709-714.

Ardehali, H & O'Rourke, B. (2005). Mitochondrial K_{ATP} channels in cell survival and death. Journal of Molecular and Cellular Cardiology 39: 7-16.

Ardehali, H., Chen, Z., Ko, Y., Mejia-Alvarez, R., & Marban, E. (2004). Multiprotein complex containing succinate dehydrogenase confers mitochondrial ATP sensitive K^+ channel activity. Proceedings National Academy of Sciences 101: 11880-11885.

Armstrong, S.C. (2004). Protein kinase activation and myocardial ischemia/reperfusion in contracting isolated ventricular myocytes via protein kinase C activation. Journal of Molecular and Cellular Cardiology 37: 579-591.

Armstrong, S.C., Hoover, D.B., Delacey, M.H., & Ganote, C.E. (1996). Translocation of PKC, protein phosphatase inhibition and preconditioning of rabbit cardiomyocytes. Journal of Molecular and Cellular Cardiology 28: 1479-1492.

Ashcroft, F.M. & Gribble F.M. (2000). New windows on the mechanism of action of K_{ATP} channel openers. Trends in Pharmacological Science 21(11): 439-445.

Ashcroft, F.M. & Gribble, F.M. (1998). Correlating structure and function in ATP-sensitive K^+ channels. Trends in Neuroscience 21(7): 288-294.

Ashcroft, S.J.H. & Ashcroft, F.M. (1990). Properties and functions for ATP-sensitive K-channels. Cellular Signaling 2(3): 197-214.

Auchampach, J.A., Maruyama, M., Cavero, I. & Gross, G.J. (1991). The new K^+ channel opener aprikalim (RP 52891) reduced experimental infarct size in dogs in the absence of hemodynamic changes. Journal of Pharmacological and Experimental Therapeutics. 259: 961-967.

Babenko, A.P., Aguilar-Bryan, L. & Bryan, J. (1998a). A view of SUR/KirX, KATP channels. Annual Reviews in Physiology 60: 667-687.

Babenko, A.P., Gonzalez, G.C., Aguilar-Bryan, L. & Bryan, J. (1998b). Reconstituted human cardiac KATP channels: functional identity wit the native channels from the sarcolemma of human ventricular cells. Circulation Research 83: 1132-1143.

Baines, C.P., Zhang, J., Wang, G.W., Zheng, Y.T., Xiu. J.X., Cardwell, E.M., Bolli, R. & Ping, P. (2002). Mitochondrial PKCepsilon and MAPK form signalling modules in the murine heart: enhanced mitochondrial PKCepsilon-MAPK interactions and differential MAPK activation in PKCepsilon-induced cardioprotection. Circulation Research 90(4): 390-7.

Baines, C.P., Goto, M. & Downey, J.M. (1997). Oxygen radicals released during ischemic preconditioning contribute to cardioprotection in the rabbit myocardium. Journal of Molecular and Cellular Cardiology 29: 207-216.

Baird, A., Sleph, P., Dzwonczyk, S., Behling, R., Malone, H. & Grover, G. (1996). Effect of the K_{ATP} opener BMS-180448 on ischemic/reperfused myocardial function and energetics (abstract). FASEB J. 10: A319.

Bajgar, R., Seetharaman, S., Kowaltowski, A.J., Garlid, K.D. & Paucek, P. (2001). Identification and properties of a novel intracellular (mitochondrial) ATP-sensitive potassium channel in brain. Journal of Biological Chemistry 276: 33369-33374.

Baro, I., O'Neill, S.C. & Eisner, D.A. (1993). Changes of intracellular $[Ca^{2+}]$ during refilling of sarcoplasmic reticulum in rat ventricular and vascular smooth muscle. Journal of Physiology 465: 21-41.

Bean, B.P. (1992). Pharmacology and electrophysiology of ATP-activated ion channels. Trends in Pharmacological Sciences 13: 87-90.

Beavis, A.D., Lu, Y. & Garlid, K.D. (1993). On the regulation of K^+ uniport in intact mitochondria by adenine nucleotides and nucleotide analogs. Journal of Biological Chemistry 268(2): 997-1004.

Beavis, A.D., Brannan, R.D., Garlid, K.D. (1985). Swelling and contraction of the mitochondrial matrix. I. A structural interpretation of the relationship between light scattering and matrix volume. Journal of Biological Chemistry 260(25): 13424-13433.

Beech, D.J., Zhang, H., Nakao, K. & Bolton, T.B. (1993). K channel activation by nucleotide diphosphates and its inhibition by glibenclamide in vascular smooth muscle cells. British Journal of Pharmacology 110(2): 573-582.

Bernardi, H., De Weille, J.R., Epelbaum, J., Mourre, C., Amoroso, S., Slama, A., Fosset, M. & Lazdunski, M. (1993). ATP modulated K^+ channels sensitive to antidiabetic sulfonyureas are present in adenohypophysics and are involved in growth hormone release. Proceedings National Academy of Science USA 90: 1340-1344.

Bicher, D., Haass, F. A., & Jan, L.J. (2003). Merging functional studies with structures of inward-rectifier K^+ channels. Nature: Reviews in Neuroscience 4: 957-967.

Bienengraeber, M., Olson, T.M., Selivanov, V.A., Kathmann, E.C., O'Cochlain, F., Gao, F., Karger, A.B., Ballew, J.D., Hodgson, D.M., Zingman, L.V., Pang, Y.P, Alekseev, A.E. & Terzic, A. (2004). ABCC9 mutations identified in human dilated cardiomyopathy disrupt catalytic K_{ATP} channel gating. Nature Genetics 36(4): 382-387.

Bolli, R. (2000). The late phase of preconditioning. Circulation Research. 87: 972-983.

Bolsover, S., Ibrahim, O., O'luanaigh, N., Williams, H. & Cockcroft, S. (2001). Use of fluorescent Ca^{2+} dyes with green fluorescent protein and its variants: problems and solutions. Biochemical Journal 356(Pt 2): 345-52.

Bootman, M.D., Collins, T.J., Peppiatt, C.M., Prothero, L.S., MacKenzie, L., De Smet. P., Travers, M., Tovey, S.C., Seo, J.T., Berridge, M.J., Ciccolini. F. & Lipp, P. (2001). Calcium signalling-an overview. Seminars in Cell and Developmental Biology 12: 3-10.

Brennan, J.P., Southworth, R., Medina, R.A., Davidson, S.M., Duchen, M.R. & Shattock, M.J. (2006a). Mitochondrial uncoupling with low concentration FCCP, induces ROS-dependent cardioprotection independent of K_{ATP} channel activation. Cardiovascular Research 72: 313-321.

Brennan, J.P., Berry, R.G., Baghai, M., Duchen, M.R. and Shattock, M.J. (2006b). FCCP is cardioprotective at concentrations that cause mitochondrial oxidation without detectable depolarisation. Cardiovascular Research 72: 322-330.

Brierley, G.P. (1974). Passive permeability and energy-linked ion movements in isolated heart mitochondria. Annals of the New York Academy of Science 227: 398-411.

Bryan, J. & Aguilar-Bryan, L. (2003). Sulfonylurea receptors: ABC transporters that regulate ATP-sensitive K^+ channels. Biochimica et Biophysica Acta 1461 (2): 285-303.

Busija, D.W., Katakam, P., Rajapakse, N.C., Kis, B., Grover, G., Domoki, F. & Bari, F. (2005). Effects of ATP-sensitive potassium channel activators diazoxide and BMS-191095 on membrane potential and reactive oxygen species production in isolated piglet mitochondria. Brain Research Bulletin 66(2): 85-90.

Carrasco, A.J., Dzeja, P.P, Alekseev, A.E., Pucar, D., Zingman, L.V., Abraham, M.R. Hodgson, D., Bienengraeber, M., Puceat, M., Janseen, E., Wieringa, B. & Terzic, A. (2003). Adenylate kinase phosphotransfer communicates cellular energetic signals to ATP-sensitive potassium channels. Proceedings National Academy of Science USA 98: 7623-7628.

Cave, A.C & Garlick, P.B (2000). Is a functional sarcoplasmic reticulum necessary for preconditioning? Journal of Molecular and Cellular Cardiology 32(3): 415-427.

Challet, C., Maechler, P., Wollheim, C.B. & Ruegg, U.T. (2001). Mitochondrial calcium oscillations in C2C12 myotubes. Journal of Biological Chemistry 276(6): 3791-3797.

Chandy, K.G. & Gutman., G.A. (1993). Nomenclature for mammalian potassium channel genes. Trends in Pharmacological Science 14: 434.

Chen, W., Gabel, S., Steenbergen, C. & Murphy, E. (1995). A redox-based mechanism for cardioprotection induced by ischemic preconditioning in perfused rat heart. Circulation Research 77: 424-429.

Chutkow, W.A., Samuel, V., Hansen, P.A., Pu, J., Valdivia, C.R., Makielski, J.C. & Burant, C.F. (2001). Disruption of Sur2-containing K(ATP) channels enhances insulin-stimulated glucose uptake in skeletal muscle. Proceedings of National Academy of Science USA 98 (20): 11760-11764.

Chutkow, W.A., Simon, M.C., Le Beau, M.M. & Burant C.F. (1996). Cloning tissue expression and chromosomal localization of SUR2, the putative drug-binding subunit of cardiac muscle. Diabetes 45: 1439-1445.

Clapp, L.H. & Gurney, A.M. (1992). ATP-sensitive K^+ channels regulate resting potential of pulmonary arterial smooth muscle cells. American Journal of Physiology 262: H916-920.

Clement, J.P., Kunjilwar, K., Gonzalez, G., Schwanstecher, M., Panten, U., Aguilar-Bryan, L. & Bryan, J. (1997). Association and stoichiometry of K(ATP) channel subunits. Neuron 18: 827-838.

Cochrane, J., Williams, B.T., Banerjee, A., Harken, A.H., Burke, T.J., Cairns, C.B. & Shapiro, J.I. (1999). Ischemic preconditioning attenuates functional, metabolic, and morphologic injury from ischemic acute renal failure in the rat. Renal Failure 21(2): 135-145.

Cohen, M.V. (2004). Ions and channels: new answers to old questions. Journal of Molecular and Cellular Cardiology 37(2): 473-475.

Cohen, M.V., Yang, X.M., Liu, G.S., Heusch, G. & Downey, J.M. (2001). Acetylcholine, bradykinin, opioids, and phenylephrine, but not adenosine, trigger preconditioning by generating free radicals and opening mitochondrial K(ATP) channels. Circulation Research 89(3): 273-278.

Cohen, M.C., Baines, C.P. & Downey, J.M. (2000). Ischemic Preconditioning: From Adenosine Receptor to K_{ATP} Channel. Annual Reviews in Physiology 62: 79-109.

Cole, W.C., Mcpherson, C.D. & Songtag. D. (1991). ATP-regulated K^+ channels protect the myocardium against ischemia/reperfusion damage. Circulation Research 69: 571-581.

Cone, J & Liu Y. (2001). No evidence of mitoK_{ATP} channel-mediated elevation of reactive oxygen species in isolated rabbit ventricular myocytes (abstract). Journal of Molecular and Cellular Cardiology 33: A23.

Conti, L.R., Radeke, C.M., Shyng, S.L. & Vandenberg, C.A. (2001). Transmembrane topology of the sulphonylurea receptor, SUR1. Journal of Biological Chemistry 276 (44): 41270-41278.

Cook, G.A. (1987). The hypoglycemic sulfonylureas glyburide and tolbutamide inhibit fatty acid oxidation by inhibiting carnitine palmitoyltransferase. Journal of Biological Chemistry 262(11): 4968-4972.

Cook, D.L. & Hales, N. (1984). Intracellular ATP directly blocks K^+ channels in pancreatic ß cells. Nature 312: 446-488.

Cui, Y., Giblin, J.P., Clapp, L.H. & Tinker, A. (2001). A mechanism for ATP-sensitive potassium channel diversity: Functional coassembly of two pore-forming subunits. Proceedings National Academy of Science USA 98: 729-734.

Cuong, D.V., Kim, N., Joo, H., Youm, J.B., Chung, J.Y., Lee, Y., Park, W.S., Kim, E., Park, Y.S. & Han, J. (2005). Subunit composition of ATP-sensitive potassium channels in mitochondria of rat hearts. Mitochondrion 5: 121-133.

Das, M., Parker, J.E. & Halestrap A.P. (2003). Matrix volume measurements challenge the existence of diazoxide/glibencamide-sensitive K_{ATP} channels in rat mitochondria. Journal of Physiology. 547(Pt 3): 893-902.

Das, D.K., Engelman, R.M. & Maulik, N. (1999). Oxygen free radical signalling in ischaemic preconditioning. Annuals New York Academy of Science 874: 49-65.

Debska, G., Kicinska, A., Skalska, J., Szewczyk, A., May, R., Elger, C.E. & Kunz, W.S. (2002). Opening of potassium channels modulates mitochondrial function in rat skeletal muscle. Biochimica et Biophysica Acta 1556(2-3): 97-105.

Dröse, S., Brandt, U. & Hanley, P.J. (2006). K^+-independent actions of diazoxide question the role of inner membrane K_{ATP} channels in mitochondrial cytoprotective signalling. Journal of Biological Chemistry 281(33): 23733-23739.

Dubyak, G.R & el-Moatassim, C. (1993). Signal transduction via P2-purinergic receptors for extracellular ATP and other nucleotides. American Journal of Physiology 265: C577-C606.

Duchen, M.R., Surin, A. & Jacobson, J. (2003). Imaging mitochondrial function in intact cells. Methods in Enzymology 361: 353-389.

Duchen, M.R., Jacobson, J., Keelan, J., Mojet, M.H. & Vergun, O. (2001). Functional imaging of mitochondria within cells. Methods of Cellular Imaging 88-111.

Duchen, M.R. (2000). Mitochondria and calcium: from cell signalling to cell death. Journal of Physiology 529(Pt 1):57-68.

Duchen, M.R. (1999). Contributions of mitochondria to animal physiology: from homeostatic sensor to calcium signalling and cell death. Journal of Physiology 516 (Pt 1): 1-17.

Dzeja, P.P., Holmuhamedov, E.L., Ozcan, C., Pucar, D., Jahangir, A. & Terzic, A. (2001). Mitochondria: gateway for cytoprotection. Circulation Research 89(9): 744-746.

El-Moatassim, C., Dornand, J. & Mani, J.C. (1992). Extracellular ATP and cell signalling. Biochimica et Biophysica Acta 1134: 31–45

Erb, L., Liao, L. Seye, C.I. and Weisman, G.A. (2006). P2 receptors: intracellular signalling. Pflugers Arch 452(5): 552-562.

Favre, I., Sun, Y.M. & Moczydlowski, E. (1999). Reconstitution of native and cloned channels into planar bilayers. Methods in Enzymology 294: 287-304.

Fernandes, M.A., Santos, M.S., Moreno, A.J., Duburs, G. Oliveira, C.R. & Vicente, J.R. (2004). Glibenclamide interferes with mitochondrial bioenergetics by inducing changes on membrane ion permeability. Journal of Biochemical and Molecular Toxicology 18(3): 162-169.

Ferrier, C.P., Kurtz, A., Lehner, P., Shaw, S.G., Pusteria, C., Saxenhofer, H., & Weidmann, P. (1989). Stimulation of rennin secretion by potassium channel activation with cromakalim. European Journal of Clinical Pharmacology 26: 443-447.

Findlay, I. (1994). The ATP-sensitive K^+ channel of cardiac muscle and the action potential shortening during metabolic stress. Cardiovascular Research 28 (6): 760-761.

Flagg, T.P., & Nichols, C.G. (2001). Sarcolemmal K(ATP) channels in the heart: molecular mechanisms brought to light, but physiologic consequences still in the dark. Journal of Cardiovascular Electrophysiology. 12: 1195-1198.

Forbes, R.A., Steenbergen, C. & Murphy, E. (2001). Diazoxide-induced cardioprotection requires signalling through a redox-sensitive mechanism. Circulation Research 88(8): 802-809.

Fryer, R.M., Hsu, A.K. & Gross, G.J. (2001a). Mitochondrial K(ATP) channel opening is important during index ischemia and following myocardial reperfusion in ischemic preconditioned rat hearts. Journal of Molecular and Cellular Cardiology 33(4): 831-834.

Fryer, R.M., Pratt, P.F., Hsu, A.K. & Gross, G.J. (2001b). Differential activation of extracellular signal regulated kinase isoforms in preconditioning and opioid-induced cardioprotection. Journal of Pharmacological and Experimental Therapeutics 296(2): 642-649.

Fujita, K. & Kurachi, Y. (2000). Molecular aspects of ATP-sensitive K^+ channels in the cardiovascular system and K^+ channel openers. Pharmacology and Therapeutics 85: 39-53.

Garlid, K.D., Dos Santos, P., Xie, Z.J., Costa, A.D. & Paucek, P. (2003). Mitochondrial potassium transport: the role of the mitochondrial ATP-sensitive $K(^+)$ channel in cardiac function and cardioprotection. Biochimica et Biophysica Acta 1606 (1-3): 1-21.

Garlid, K.D. & Paucek, P. (2003). Mitochondrial potassium transport: the K(+) cycle. Biochimica et Biophysica Acta 1606(1-3): 23-41.

Garlid, K. D. (2000). Opening mitochondrial K_{ATP} in the heart- what happens and what does not happen. Basic Research in Cardiology 95: 275-279.

Garlid, K.D., Jaburek, M. Yarov-Yarovoy, V. & Paucek, P. (1997a) Sulphonylurea receptor-K^+ channel coupling in the mitochondrial K_{ATP} channels. Biophysical Journal 72: A39.

Garlid, K.D., Paucek, P. Yarov-Yaravoy. B., Murray, H.N.M., Darbenzio. R.B., D'Alonzo, A.J., Lodge, N.J. Smith, M.A. & Grover, G.J. (1997b). Cardioprotective effect of diazoxide and its interaction with mitochondrial ATP-sensitive potassium channels: possible mechanism of cardioprotection. Circulation research 81: 1072-1082.

Garlid, K.D., Paucek, P., Yarov-Yarovoy, V., Sun, X., & Schindler, P.A. (1996). The mitochondrial K_{ATP} channel as a receptor for potassium channel openers. Journal of Biological Chemistry 271(15): 8796-8799.

Garlid, K.D (1988). Sodium/proton antiporters in the mitochondrial inner membrane. Advances in Experimental Medicine and Biology 232: 37-46.

Garrino, M.G., Plant, T.D. & Henquin, J.C. (1989). Effects of putative activators of K^+ channels in mouse pancreatic β cells. British Journal of Pharmacology. 98: 957-965.

Gettes, L.S., Cascio, W.E., Johnson, T., & Fleet, W.F. (1991). Local myocardial biochemical and ionic alterations during myocardial ischaemia and reperfusion. Drugs. 42(1): 7-13.

Glaser, B., Kesavan, P., Heyman, M., Davis, E., Cuesta, A., Buchs, A., Stanley, C.A., Thornton, P.S., Permutt, M.A., Matschinsky, F.M. & Herold, K.C. (1998). Familial hyperinsulinism caused by an activating glucokinase mutation. New England Journal of Medicine 338(4): 226-230.

Giblin, J.P., Cui, Y., Clapp, L.H. & Tinker, A. (2002). Assembly limits the pharmacological complexity of ATP-sensitive potassium channels. Journal of Biological Chemistry 277(16): 13717-13723.

Goglia, F. & Skulachev, V.P. (2003). A function for novel uncoupling proteins: antioxidant defence of mitochondrial matrix by translocating fatty acid peroxides from the inner to the outer membrane leaflet. FASEB Journal 17: 1585-1591.

Graham, F.L. & Van der Eb, A.J. (1973). A new technique for the assay of infectivity of human adenovirus 5 DNA. Virology. 52(2): 456-467.

Gray, M.O., Karliner, J.S. & Mochly-Rosen, D. (1997). A selective epsilon-protein kinase C antagonist inhibits protection of cardiac myocytes from hypoxia-induced cell death. Journal of Biological Chemistry 272: 30945-30951.

Gribble, F.M. Tucker, S.J., Seino, S. & Ashcroft, F.M. (1998). Tissue specificity of sulphonylureas: Studies on cloned cardiac and beta-cell K_{ATP} channels. Diabetes 47(9): 1412-1418.

Gribble, F.M., Tucker, S.J. & Ashcroft, F.M. (1997). The essential role of Walker A motifs of SUR1 in K-ATP channel activation by Mg-ADP and diazoxide. EMBO Journal 16: 1145-1152.

Gribkoff, V.K., Lum-Ragan, J.T., Boissard, C.G., Post-Munson, D.J., Meanwell, N.A., Starrett, J.E. Jr, Kozlowski, E.S., Romine, J.L., Trojnacki, J.T., Mckay, M.C., Zhong, J., & Dworetzky, S.I. (1996). Effects of channel modulators on cloned large-conductance calcium-activated potassium channels. Molecular Pharmacology 50(1): 206-217.

Grimmsman, T. & Rustenbeck, I. (1998). Direct effects of diazoxide on mitochondria in pancreatic B-cells and on isolated liver mitochondria. British Journal of Pharmacology 123: 781-788.

Gross, G.J. (2003). Selective ATP-sensitive potassium channel openers: fact or fiction. Journal of Molecular and Cellular Cardiology 35: 1005-1007.

Gross, G.J & Peart, J.N. (2003). K_{ATP} channels and myocardial preconditioning: an update. American Journal of Physiology Heart and Circulatory Physiology 285(3): H921-H930.

Gross, G.J & Fryer, R.M. (1999). Sarcolemmal versus mitochondrial ATP-sensitive K^+ channels and myocardial preconditioning. Circulation Research 84: 973-979.

Gross, G.J. & Auchampach, J.A. (1992). Blockage of ATP-sensitive potassium channels prevents myocardial preconditioning in dogs. Circulation Research 70(2): 223-233.

Grover, G.J. & Atwal, K.S. (2002). Pharmacological profile of the selective mitochondrial K(ATP) opener with no peripheral vasodilator or cardiac action potential shortening activity. Journal of Pharmacological Experimental Therapeutics 297: 1184-1192.

Grover, G.J., D'Alonzo, A.J., Garlid, K.D., Bajgar, R., Lodge, N.J., Sleph, P.G., Darbenzio, R.B., Hess, T.A., Smith, M.A., Paucek, P., & Atwal, K.S. (2001). Pharmacologic characterization of BMS-191095, a mitochondrial K(ATP) opener with no peripheral vasodilator or cardiac action potential shortening activity. Journal of Pharmacological Experimental Therapeutics 297(3): 1184-1192.

Grover, G. & Garlid, K.D. (2000). ATP-Sensitive Potassium Channels: A Review of their Cardioprotective Pharmacology. Journal of Cell Cardiology 32: 677-695.

Grover, G.J., D'Alonzo, A.J., Dzwonczyk, S., Parham, C.S. & Darbenzio, R.B. (1996). Preconditioning is not abolished by the delayed rectifier K^+ blocker dofetilide. American Journal of Physiology 271(3 Pt 2):H1207-H1214.

Grover, G.J., D'Alonzo, A.J, Parham, C.S. & Darbenzio, R.B. (1995). Cardioprotection with K_{ATP} channel opener cromakalim is not correlated with ischemic myocardial action potential duration. Journal of Cardiovascular Pharmacology 26: 145-152.

Grover, G.J., Sleph, P.G. & Dzwonczyk, S. (1992). Role of myocardial ATP-sensitive potassium channels in mediating preconditioning in the dog heart and their possible interaction with adenosine A1-receptors. Circulation 86: 1310-1316.

Grover, G.J., Dzwonczyk, S., Parham, C.S. & Sleph, P.G. (1990a). The protective effects of cromakalim and pinacidil on reperfusion function and infarct size in isolated perfused rat hearts and anesthetized dogs. Cardiovascular Drugs and Therapy 4: 465-474.

Grover, G.J., Dzwonczyk, S. & Sleph, P.G. (1990b). Reduction of ischemic damage in isolated rat hearts by the potassium channel opener, RP 52891. European Journal of Pharmacology 191: 11-18.

Grover, G.J., McCullough, J.R., Henry, D.E., Conder, M.L. & Sleph, P.G. (1989). Anti-ischemic effects of the potassium channel activators pinacidil and cromakalim and the reversal of these effects with the potassium channel blocker glyburide. The Journal of Pharmacology and Experimental Therapeutics 251(1): 98-104.

Grynkiewicz, G., Poenie, M. and Tsien, R.Y. (1985). A new generation of Ca^{2+} indicators with greatly improved fluorescence properties Journal of Biological Chemistry 260: 3440-3450.

Guerini, D., Garcia-Martin, E., Zecca, A., Guidi, F. & Carafoli, E. (1998). The calcium pump of the plasma membrane: membrane targeting, calcium binding sites, tissue-specific isoform expression. Acta Physiologica Scandinavica Supplementum 643: 265-273.

Gumina, R.J., Pucar, D., Bast, P., Hodgson, D.M., Kurtz, C.E., Dzeja, P.P., Miki, T., Seino, S. & Terzic, A. (2003). Knockout of Kir6.2 negates ischemic preconditioning-induced protection of myocardial energetics. American Journal of Physiology Heart and Circulation Physiology 284: H2106-H2113.

Halestrap, A.P. (1989). The regulation of the matrix volume of mammalian mitochondria in vivo and n vitro and its role in the control of mitochondrial metabolism. Biochimica et Biophysica Acta 973: 355-382.

Hambrock, A., Preisig-Muller, R., Russ, U., Piehl, A., Hanley, P.J., Ray, J., Daut, J., Quast, U. & Derst, C. (2002). Four novel splice variants of sulfonylurea receptor 1. American Journal of Physiology Cell Physiology 283(2): C587-C598.

Hanley, P.J. & Daut, J. (2005). K(ATP) channels and preconditioning: a re-examination of the role of mitochondrial K(ATP) channels and an overview of alternative mechanisms. Journal of Molecular and Cellular Cardiology 39(1): 17-50.

Hanley, P.J., Gopalan, K.V., Lareau R.A., Srivastava D.K., Von Meltzer, M. & Daut, J. (2003). Beta-oxidation of 5-hydroxydecanoate, a putative blocker of mitochondrial ATP-sensitive potassium channels. Journal of Physiology 547: 387-393.

Hanley, P.J., Mickel, M., Loffler, M., Brandt, U. & Daut, J. (2002). K(ATP) channel-independent targets of diazoxide and 5-hydroxydecanoate in the heart. Journal of Physiology 542(3): 735-741.

Herskowitz, I. (1987). Functional inactivation of genes by dominant negative mutations. Nature 329: 219-222.

Higgins, C.F. (1992). ABC transporters: from microorganisms to man. Annual Reviews in Cell Biology 8: 67-113.

Hill, J.A., Corondo, R. & Strauss. H.C. (1989). Potassium channel of cardiac sarcoplasmic reticulum is a multi-ion channel. Biophysical Journal 55: 34-46.

Hille, B. (1992). Ionic Channels of Excitable Membranes (Second Edition). Sinauer Associates, Sunderland, MA.

Ho, K., Nichols, C. G., Lederer, W. J., Lytton, J., Vassilev, P. M., Kanazirska, M. V., & Herbert, S. C. (1993). Cloning and expression of an inwardly rectifying ATP-regulated potassium channel. Nature 362: 31-37.

Holmuhamedov, E.L., Jahangir, A., Oberlin, A., Komarov, A., Colombini, M. & Terzic, A. (2004). Potassium channel openers are uncoupling protonophores: implication in cardioprotection. FEBS Letters 568(1-3): 167-170.

Holmuhamedov, E.L., Wang, L. & Terzic, A. (1999). ATP-sensitive K^+ channel openers prevent Ca^{2+} overload in rat cardiac mitochondria. The Journal of Physiology 519: 347-360.

Holmuhamedov, E.L., Jovanovimc S., Dzeja, P.P., Jovanovic, A. & Terzic, A. (1998). Mitochondrial ATP-sensitive K^+ channels modulate cardiac mitochondrial function. American Journal of Physiology 275(5 part 2): 567-576.

Hu, H., Sato, T., Seharaseyson, J., O'Rourke, B. & Marban, E. (1999). Pharmacological and histochemical distinctions between molecularly defined sarcolemmal K_{ATP} channels and native cardiac mitochondrial K_{ATP} channels. Molecular Pharmacology 55: 1000-1005.

Hu, K., Duan. D., Li, G.R. & Nattel, S. (1996). Protein kinase C activates ATP-sensitive K^+ currents in human and rabbit ventricular myocytes. Circulation Research 78: 492-498.

Huang, L.S., Sun, G., Cobessi, D., Wang, A.C., Shen, J.T., Tung, E.Y., Anderson, V.E., & Berry, E.A. (2006). 3-nitropropionic acid is a suicide inhibitor of mitochondrial respiration that, upon oxidation by complex II, forms a covalent adduct with a catalytic base arginine in the active site of the enzyme. Journal of Biological Chemistry 281: 5965-5972.

Imamura, Y., Tomoike, H., Narishige, T., Takahashi, T., Kasuya, H. & Takeshita, A. (1992). Glibenclamide decreases basal coronary blood flow in anesthetized dogs. American Journal of Physiology 263: H399-H404.

Inagaki, N., Gonoi, T. & Seino, S. (1997). Subunit stoichiometry of the pancreatic beta-cell ATP-sensitive K^+ channel. FEBS letters 409 (2): 232-236.

Inagaki, N., Gonoi, T., Clement IV, J. P., Wang, C. Z., Aguilar-Bryan, L., Bryan, J., & Seino, S. (1996). A family of sulfonylurea receptors determines the pharmacological properties of ATP-sensitive K^+ channels. Neuron 16(5): 1011-1017.

Inagaki, N., Inazawa, J. & Seino, S. (1995a). cDNA sequence, gene structure and chromosomal localization of the human ATP-sensitive potassium channel, uKATP-1, gene (KCNJ8). Genomics 30(1): 102-104.

Inagaki, N., Gonoi, T., Clement IV, J. P., Namba, N., Inazawa, J., Gonzalez, G., Aguilar-Bryan, L., Seino, S. & Bryan, J. (1995b). Reconstitution of IKATP: An inward rectifier subunit plus the sulphonylurea receptor. Science 270: 1166-1170.

Inagaki, N., Tsuura, Y., Namba, N., Masuda, K., Gonoi, T., Horie, M., Seino, Y., Mizuta, M., & Seino, S. (1995c). Cloning and functional characterization of a novel ATP-sensitive potassium channel ubiquitously expressed in rat tissues, including pancreatic islets, pituitary, skeletal muscle, and heart. Journal of Biological Chemistry 270(11): 5691-5694.

Inoue, I., Nagase, H., Kishi, K., & Higuti, T. (1991). ATP-sensitive K^+ channel in the mitochondrial inner membrane. Nature 352: 244-247.

Inscho, E.W., Belott, T.P., Mason, M.J., Smith, J.B. & Navar, L.G. (1996). Extracellular ATP increases cytosolic calcium in cultured rat renal arterial smooth muscle cells. Clinical and Experimental Pharmacology and Physiology 23(6-7): 503-507.

Isomoto, S., Kondo, C., & Kurachi, Y. (1997). Inwardly rectifying potassium channels: Their molecular heterogeneity and function. Japanese Journal of Physiology 47: 11-39.

Isomoto, S., Kondo, C., Yamada, M., Matsumoto, S., Higashiguchi, Y., Horio, Y., Matsuzawa, Y. & Kurachi, Y. (1996). A novel sulphonyurea receptor forms with BIR (Kir6.2) a smooth muscle type ATP-sensitive K^+ channel. Journal of Biological Chemistry 271: 24321-24324.

Jaburek, M., Yarov-Yarovoy, V., Paucek, P., & Garlid, K. D. (1998). State-dependent inhibition of the mitochondrial K_{ATP} channel by glyburide and 5-hydroxydecanoate. Journal of Biological Chemistry 272 (22): 13578-13582.

Jacobson, J. & Duchen M.R. (2004). Interplay between mitochondria and cellular calcium signalling. Molecular and Cellular Biochemistry 256-257: 209-218.

Jaeschke, H. (2003). Molecular mechanisms of hepatic ischemia-reperfusion injury and preconditioning. American Journal of Gastrointestinal and Liver Physiology 284(1): G15-G26.

Javadov, S.A., Clarke, S., Das, M., Griffiths, E.J., Lim, K.H. & Halestrap, A.P. (2003). Ischaemic preconditioning inhibits opening of mitochondrial permeability transition pores in the reperfused rat heart. Journal of Physiology 549(Pt 2):513- 524.

Jovanovic, A., Jovanovic, S., Lorenz, E. & Terzic, A. (1998). Recombinant cardiac ATP-sensitive K^+ channel subunits confer resistance to chemical hypoxia-reoxygenation injury. Circulation 98: 1548-1555.

Jovanovic, N., Jovanovic, S., Jovanovic, A. & Terzic, A. (1999). Gene delivery of Kir6.2/SUR2A in conjunction with pinacidil handles intracellular Ca^{2+} homeostasis under metabolic stress. FASEB 13: 923-929.

Kakei, M., Noma, A. & Shibasaki, T. (1985). Properties of adenosine triphosphate regulated potassium channel in guinea pig ventricular cells. Journal of Physiology 363: 441-462.

Kane, C., Shepherd, R.M., Squires, P.E., Johnson, P.R., James, R.F., Milla, P.J., Aynsley-Green, A., Lindley, K.J. & Dunne, M.J. (1996). Loss of functional K_{ATP} channels in pancreatic beta-cells causes persistent hyperinsulinemic hypoglycaemia of infancy. Nature Medicine 2: 1344-1347.

Katz, B. (1949). Les constantes électriques de la membrane du muscle. Archives of Scientific Physiology 3: 285–299.

Kayano, T., Kakei, M., Nakashima, N., Yoshinaga, M., Matsuoka, T. & Tanaka, H. (1993). ATP-regulated K^+ channels are modulated by intracellular H^+ guinea-pig ventricular cells. Journal of Physiology 462: 747-766.

Kenyon, J.L., McKemy, D.D., Airey, J.A., & Sutko, J.L. (1995). Interaction between ryanodine receptor function and sarcolemmal Ca^{2+} currents. American Journal of Physiology 269: C334-C340.

Kirsch, G.E., Codina, J., Birnbaumer, L. & Brown, A.M. (1990). Coupling of ATP-sensitive K^+ channels to A_1 receptors by G proteins in rat ventricular myoctyes. American Journal of Physiology 259: H820-H826.

Klausner, K. D. & Sitia, R. (1990). Protein degradation in the endoplasmic reticulum. Cell 62 (4): 611-614.

Korge, P., Honda, H.M. & Weiss, J.N. (2005). K^+-dependent regulation of matrix volume improves mitochondrial function under conditions mimicking ischemia-reperfusion. American Journal of Physiology Heart and Circulatory Physiology 289(1): H66-H77.

Koster, J.C., Sha, Q., & Nichols, C.G. (1999). Sulfonylurea and K^+-channel opener sensitivity of K_{ATP} channels: Functional coupling of Kir6.2 and SUR1 Subunits. Journal of General Physiology 114(2): 203-213.

Kourie, J.I. (1997). ATP-sensitive voltage- and calcium-dependent chloride channels in sarcoplasmic reticulum vesicles from rabbit skeletal muscle. Journal of Membrane Biology 151(1): 39-51.

Kowaltowski, A.J., Seetharaman, S., Paucek, P. & Garlid, K.D. (2001). Bioenergetic consequences of opening the ATP-sensitive K(+) channel of heart mitochondria. American Journal of Physiology Heart and Circulatory Physiology 280: H649-H657.

Kubo, Y., Baldwin, T. J., Jan, Y. N., & Jan, L. Y. (1993). Primary structure and functional expression of a mouse inward rectifier potassium channel. Nature 362: 127-133.

Kuo, A., Gulbis, J. M., Antcliff, J. F., Rahman, T., Lowe, E. D., Zimmer, J., Cuthbertson, J., Ashcroft, F. M., Ezaki, T., & Doyle, D. A. (2003). Crystal structure of the potassium channel KirBac1.1 in the closed state. Science 300 (5627): 1922-1926.

Labarca, P., Coronado, R. & Miller, C. (1980). Thermodynamic and kinetic studies of the gating behaviour of a K^+- selective channel from the sarcoplasmic reticulum membrane. The Journal of General Physiology 76: 397-324.

Lacza, Z., Snipes, J.A., Miller, A.W., Szabo, C., Grover, G. & Busija, D.W. (2003a) Heart mitochondria contain functional ATP-dependent K^+ channels. Journal of Molecular Cell Cardiology 35: 1339-1347.

Lacza, Z., Snipes, J.A., Kis, B., Szabo, C., Grover, G. & Busija, D.W. (2003b) Investigation of the subunit composition and the pharmacology of the mitochondrial ATP-dependent K^+ channel in the brain. Brain Research 994: 27-36.

Lawrence, C.L., Billups, B., Rodrigo G.C. & Standen, N.B. (2001). The K_{ATP} channel opener diazoxide protects cardiac myocytes during metabolic inhibition without causing mitochondrial depolarisation or flavoprotein oxidation. British Journal of Pharmacology 134: 535-542.

Lebuffe, G., Schumacker, P.T., Shao, Z.H., Anderson, T., Iwase, H. & Vanden Hoek, T.L. (2003). ROS and NO trigger early preconditioning: relationship to mitochondrial K_{ATP} channel. American Journal of Physiology Heart and Circulatory Physiology 284(1): H299-H308.

Lesnefsky, E.J., Chen, Q., Slabe, T.J., Stoll, M.S., Minkler, P.E., Hassan, M.O., Tandler, B. & Hoppel, C.L. (2004). Ischemia, rather than reperfusion, inhibits respiration through cytochrome oxidase in the isolated, perfused rabbit heart: role of cardiolipin. American Journal of Physiology Heart and Circulatory Physiology 287(1): H258-H267.

Li, Y. & Trush, M.A. (1998). Diphenyliodonium, an NADPH oxidase inhibitor, also potently inhibits mitochondrial reactive oxygen species production. Biochemical and Biophysical Research Communications 253: 295–299.

Light, P.E., Kanjo, H.D., Fox, J.E. & French, R.J. (2001). Distinct myoprotective roles of cardiac sarcolemmal and mitochondrial K_{ATP} channels during metabolic inhibition and recovery. FASAB Journal 15: 2586-2594.

Lim, K.H., Javadov, S.A. Das, M., Clarke, S.J., Suleiman, M.S. & Halestrap, A.P. (2002). The effects of ischaemic preconditioning diazoxide and 5-hydroxydecanoate on rat heart mitochondrial volume and respiration. Journal of Physiology 545: 961-974.

Liss, B. & Roeper, J. (2001a). ATP-sensitive potassium channels in dopaminergic neurons: transducers of mitochondrial dysfunction. News Physiological Science 16: 214-217.

Liss, B., & Roeper, J. (2001b). Molecular physiology of neuronal K-ATP channels (Review). Molecular Membrane Biology 18: 117-127.

Liu, G.S., Cohen, M.V., Mochly-Rosen, D. & Downey, J.M. (1999) Protein kinase C-epsilon is responsible for the protection of preconditioning in rabbit cardiomyocytes. Journal of Molecular and Cellular Cardiology 31(10):1937-1948.

Liu, Y. & O'Rourke, B. (2003). Opening of mitochondrial K_{ATP} channels triggers cardioprotection-are reactive oxygen species involved? Circulation Research 88: 750-752.

Liu, Y., Ren, G., O'Rourke, B., Marban, E., & Seharaseyon, J. (2001). Pharmacological comparison of native mitochondrial K_{ATP} channels with molecularly defined surface K_{ATP} channels. Molecular Pharmacology 59: 225-230.

Liu, Y., Sato, T., Seheraseyon, J., Szewczyk, A., O'Rourke, B., Marban, E. (1999). Mitochondrial ATP-dependent potassium channels: Viable candidate effectors of ischemic preconditioning. Annals of New York Academy of Science 874: 27-37.

Liu, Y., Sato, T., O'Rourke, B., & Marban, E. (1998). Mitochondrial ATP-dependent potassium channels: novel effectors of cardioprotection? Circulation 97: 2463-2469.

Liu, Y., Ytrehus, K. & Downey, J.M. (1994). Evidence that translocation of protein kinase C is a key event during ischemic preconditioning of rabbit myocardium. Journal of Molecular Cellular Cardiology 26: 661-668.

Lochner, A., Genade, S., Tromp, E., Podzuweit, T. & Moolman, J.A. (1999). Ischemic preconditioning and the beta-adrenergic signal transduction pathway. Circulation 100(9): 958-966.

MacLennan., D.H. & Wong, P.T.S. (1971). Isolation of a calcium-sequestering protein from sarcoplasmic reticulum. Proceedings National Academy of Sciences 68 (6): 1231-1235.

McCullough, J.R., Normandin, D.E., Conder, M.L., Sleph, P.G., Dzwonczyk, S. & Grover, G.J. (1991). Specific block of the anti-ischemic actions of cromakalim by sodium 5-hydroxydecanoate. Circulation Research 69(4): 949-958.

McPherson, C.D., Pierce, G. N. & Cole, W.C. (1993). Ischemic cardioprotection by ATP-sensitive K^+ channels involves high-energy phosphate preservation. American Journal of Physiology Heart and Circulatory Physiology 265: H1809-H1818.

Menard, C., Pupier, S., Mornet, D., Kitzmann, M., Nargeot, J. & Lory, P. (1999). Modulation of L-type calcium channel expression during retinoic acid-induced differentiation of H9C2 cardiac cells. Journal of Biological Chemistry 274(41): 29063-29070.

Miki, T., Suzuki, M., Shibasaki, T., Uemura, H., Sato, T., Yamaguchi, K., Koseki, H., Iwanaga, T., Nakaya, H. & Seino, S. (2002). Mouse model of Prinzmetal angina by disruption angina by disruption of the inward rectifier, Kir6.1. Nature Medicine 8: 466-472.

Miki, T., Nagashima, K., Tashiro, F., Kotake, K., Yoshitomi, H., Tamamoto, A., Gonoi, T., Imwanaga, T., Miyazaki, J. & Seino, S. (1998). Defective insulin secretion and enhanced insulin action in K_{ATP} channel deficient mice. Proceedings National Academy of Science USA 95: 10402-10406.

Miki, T., Cohen, M.V. & Downey, J.M. (1998). Opioid receptor contributes to ischemic preconditioning through protein kinase C activation in rabbits. Molecular and Cellular Biochemistry 186(1-2): 3-12.

Minners, J., Lacerda, L., Yellon, D.M., Opie, L.H., McLeod, C.J. & Sack, M.N. (2007). Diazoxide-induced respiratory inhibition - a putative mitochondrial K(ATP) channel independent mechanism of pharmacological preconditioning. Molecular and Cellular Biochemistry 294(1-2): 11-8.

Minners, J., Lacerda, L., McCarthy, J. Meiring, J.J., Yellon, D.M. & Sack, M.N. (2001). Ischaemic and pharmacological preconditioning in Girardi cells and C2C12 myotubes induce mitochondrial uncoupling. Circulation Research 89: 787-792.

Minners, J., van den Bos, E.J., Yellon, D.M., Schwalb, H., Opie, L.H. & Sack, M.N. (2000). Dinitrophenol, cyclosporin A, and trimetazidine modulate preconditioning in the isolated rat heart: support for a mitochondrial role in cardioprotection. Cardiovascular Research 47: 68-73.

Mitchell, P. (1961). Coupling of phosphorylation to electron and hydrogen transfer by a chemiosmotic type of mechanism. Nature 191: 144-148.

Mizumura, T., Nithipatikom, K. & Gross, G.J. (1995). Bimakalim, an ATP-sensitive potassium channel opener, mimics the effects of ischemic preconditioning to reduce infarct size, adenosine release, and neutrophil function in dogs. Ciculation 92 (5): 1236-1245.

Morrissey, A., Rosner, E., Lanning, J., Parachuru, L., Dhar Chowdhury, P., Han, S., Lopez, G., Tong, X., Yoshida, H., Nakamura, T.Y., Artman, M., Giblin, J.P., Tinker, A. & Coetzee, W.A. (2005). Immunolocalization of K_{ATP} channel subunits in mouse and rat cardiac myocytes and the coronary vasculature. BMC Physiology (5):1

Morrissey, A., Rosner, E., Lanning, J., Parachuru, L., Dhar Chowdhury, P., Han, S., Lopez, G., Tong, X., Yoshida, H., Nakamura, T.Y., Artman, M., Giblin, J.P., Tinker, A. & Coetzee, W.A. (2005). Immunolocalisation of K_{ATP} channel subunits in mouse and rat cardiac myocytes and the coronary vasculature. BMC Physiology 12 5(1): 1.

Muller, M., Brockhaus, J. & Ballanyi, K. (2002). ATP-independent anoxic activation of ATP-sensitive K^+ channels in dorsal vagal neurons of juvenile mice in situ. Neuroscience 109: 313-328

Murry, C.E., Jennings, R.B. & Reiner, K.A. (1986). Preconditioning with ischaemia: a delay of lethal cell injury in ischemic myocardium. Circulation 74: 1124-1136.

Nakayama, K., Fan, Z., Marumo, F. & Hiraoka, M. (1990). Interrelation between pinacidil and intracellular ATP concentrations on activation of the ATP-sensitive K^+ current in guinea pig ventricular myocytes. Circulation Research 67: 1124-1133.

Nestorowicz, A., Inagaki, N., Gonoi, T., Schoor, K.P., Wilson, B.A., Glaser, B., Landau, H., Stanley, C.A., Thornton, P.S., Seino, S. & Permutt, M.A. (1997). A nonsense mutation in the inward rectifier potassium channel gene, Kir6.2, is associated with familial hyperinsulinism. Diabetes 46 (11): 1743-1748.

Nichols, C.G. & Lederer, W.J. (1991). Adenosine triphosphate-sensitive potassium channels in the cardiovascular system. American Journal of Physiology 261: H1675-H1686.

Noma, A. (1983). ATP-regulated K^+ channels in cardiac muscle. Nature 305: 147-148.

Notsu, T., Tanaka, I., Takano, M. & Noma, A. (1992a). Blockade of the ATP-sensitive K^+ channel by 5-hydroxydecanoate in guinea pig ventricular myocytes. The Journal of Pharmacology and Experimental Therapeutics 260: 702-708.

Notsu, T., Ohhashi, K., Tanaka, I., Ishikawa, H., Niho, T., Fukutake, K. & Mizota M (1992b). 5-Hydroxydecanoate inhibits ATP-sensitive K^+ channel currents in guinea-pig single ventricular myocytes. European Journal of Pharmacology 220: 35-41.

Novalija, E., Kevin, L.G., Camara, A.K., Bosnjak, Z.J., Kampine, J.P. & Stowe, D.F. (2003). Reactive oxygen species precede the epsilon isoform of protein kinase C in the anaesthetic preconditioning signalling cascade. Anaesthesiology 99(2): 421-428.

Ockaili, R.A. Bharagava, P. & Kukreja, R.C. (2001). Chemical preconditioning with 3-nitropropionic acid in hearts: role of mitochondrial K(ATP) channel. American Journal of Physiology Heart Circulation Physiology 280: H2406-2411.

O'Donnell, V.B., Smith, G.C.M. & Jones, O.T.G. (1994). Involvement of phenyl radicals in iodonium compound inhibition of flavoprotein enzymes. Molecular Pharmacology 46: 778–785.

Oldenburg, O. Yang X.M., Krieg, T. Garlid, K.D. Cohen, M.V., Grover, G.J. & Downey, J.M. (2003a). P1075 opens mitochondrial K(ATP) channels and generates reactive oxygen species resulting in cardioprotection of rabbit hearts. Journal of Molecular and Cellular Cardiology 35: 1035-42.

Oldenburg, O., Cohen, M.V. & Downey, J.M. (2003b). Mitochondrial K(ATP) channels in preconditioning. Journal of Molecular and Cellular Cardiology 35:569-575.

O'Rourke, B. (2003) Myocardial K_{ATP} Channels in Preconditioning. Circulation Research 87 (10): 845-855.

O'Rourke, B. (2004) Evidence for mitochondrial K^+ channels and their role in cardioprotection. Circulation Research 94: 420-432.

Ovide Bordeaux, S., Ventura-Clapier, R., & Veksler, V. (2000). Do modulators of the mitochondrial K_{ATP} channel change the function of mitochondria in situ? Journal of Biological Chemistry 275: 37291-37295.

Ozcan, C., Bienengraber, M., Dzija, P.P. & Terzic, A. (2002). Potassium channel openers protect cardiac mitochondria by attenuating oxidant stress at reoxygenation. American Journal of Physiology- Heart and Circulatory Physiology 282: H531-H539.

Pagano, J.S. & McCutchan, J.H. (1969). Enhancement of viral infectivity with DEAE-dextran: application to development of vaccines. Progress in Immunobiological Standardisation 3: 152-158.

Pain, T., Yang, X. M., Critz, S. D., Yue, Y., Nakano, A., Liu, G. S., Heusch, G., Cohen, M. V., & Downey, J. M. (2000). Opening of mitochondrial K(ATP) channels triggers the preconditioned state by generating free radicals. Circulation Research 87 (6): 431-433.

Pang, C.Y., Neligan, P., Zhong, A., He, W., Xu, H. & Forrest, C.R. (1997). Effector mechanism of adenosine in acute ischemic preconditioning of skeletal muscle against infarction. American Journal of Physiology 273(3 Pt 2): R887-R895.

Patel, H.H., Ludwig, L.M., Fryer, R.M., Hsu, A.K., Warltier, D.C. & Gross, G.J. (2002). Delta opioid agonists and volatile anesthetics facilitate cardioprotection via potentiation of K(ATP) channel opening. FASEB Journal 16(11): 1468-1470.

Paucek, P., Yarov-Yarovoy, V., Sun, X., & Garlid, K.D. (1996). Inhibition of the mitochondrial K_{ATP} channel by long-chain acyl-CoA esters and activation by guanine nucleotides. Journal of Biological Chemistry 271(50): 32084-32088.

Paucek, P., Mironova, G., Mahdi, F., Beavis, A.D., Woldegiorgis, G. & Garlid, K.D. (1992) Reconstitution and partial purification of the glibenclamide-sensitive, ATP-dependent K^+ channel from rat liver and beef heart mitochondria. Journal of Biological Chemistry 267: 26062-26069.

Payen, L., Delugin, L., Courtois, A., Trinquart, Y., Guillouzo, A. & Fardel O (2001). The sulphonylurea glibenclamide inhibits multidrug resistance protein (MRP1) activity in human lung cancer cells. British Journal of Pharmacology 132 (3): 778-784.

Peart, J.N. & Gross,G.J. (2002). Sarcolemmal and mitochondrial K_{ATP} channels and myocardial ischaemic preconditioning. Journal of Cellular and Molecular Medicine 6(4): 453-464.

Petrosillo, G., Ruggiero, F.M., Di Venosa, N. & Paradies, G. (2003). Decreased complex III activity in mitochondria isolated from rat heart subjected to ischemia and reperfusion: role of reactive oxygen species and cardiolipin. FASEB Journal 17(6):714-716.

Ping, P., Zhang, J., Qiu, Y., Tang, X.L., Manchikalapudi, S., Cao, X. & Bolli, R. (1997). Ischemic preconditioning induces selective translocation of protein kinase C isoforms epsilon and eta in the heart of conscious rabbits without subcellular redistribution of total protein kinase C activity. Circulation research 81(3): 404-414.

Portenhauser, R., Schafer, G. & Trolp, R. (1971). Inhibition of mitochondrial metabolism by the diabetogenic thiadiazine diazoxide. II. Interaction with energy conservation and ion transport. Biochemical Pharmacology 10: 2623-32.

Quasthoff S, Spuler A, Spittelmeister W, Lehmann-Horn F & Grafe P (1990). K+ channel openers suppress myotonic activity of human skeletal muscle in vitro. European Journal of Pharmacology 186(1):125-8.

Quayle, J.M. Nelson, M.T. & Standen, N.B. (1997). ATP-sensitive and inwardly rectifying potassium channels in smooth muscle. Physiological Reviews 77: 1165-1232.

Quayle, J.M., Bonev, A.D., Brayden J.E. & Nelson, M.T. (1995). Pharmacology of ATP sensitive K^+ currents in smooth muscle cells from rabbit mesenteric artery. American Journal of Physiology 269 (38): C1112-C1118.

Quayle, J.M., Bonev, A.D., Brayden J.E. & Nelson, M.T. (1994). Calcitonin gene-related peptide activated ATP-sensitive K^+ currents in rabbit arterial smooth muscle via protein kinase a. Journal of Physiology 471(1): 9-13.

Quesada, I., Rovira, J. M., Martin, F., Roche, E., Nadal, A., & Soria, B. (2002). Nuclear K_{ATP} channels trigger nuclear Ca^{2+} transients that modulate nuclear function. Proceedings National Academy of Sciences 99(14): 9544-9549.

Quinn, K.V., Cui, Y., Giblin, J.P., Clapp, L.H. & Tinker, A. (2003). Do anionic phospholipids serve as cofactors or second messengers for the regulation of activity of cloned ATP-sensitive K^+ channels? Circulation Research 93: 646–655.

Rabe, A., Disser, J. & Fromter, E. (1995). Cl^- channel inhibition by glibenclamide is not specific for the CFTR-type Cl^- channel. Pflügers Archiv European Journal of Physiology 429(5): 659-652.

Rajashree, R., Koster, J.C., Markova, K.P., Nichols, C.G., & Hofmann, P.A. (2002). Contractility and ischemic response of hearts from transgenic mice with altered sarcolemmal K(ATP) channels. Journal of Physiology Heart Circulation Physiology 283: H584-H590.

Reinmann, F., Dabroski, M., Jones, P., Gribble, F.M & Ashcroft, F.M. (2003). Analysis of the differential modulation of sulphonylurea block of ß-cell and the cardiac ATP-sensitive K^+ (K_{ATP}) channels by Mg-nucleotides. Journal of Physiology 547: 159-168.

Reinmann, F. & Ashcroft, F. M. (1999). Inward rectifying potassium channels. Current Opinion in Cell Biology 11: 503-508.

Riess, M.L., Stowe, D.F. & Warltier, D.C. (2004). Cardiac pharmacological preconditioning with volatile anesthetics: from bench to bedside? American Journal of Physiology Heart and Circulatory Physiology 286(5): H1603-H1607.

Ribalet, B., Ciani, S. & Eddlestone, G.T. (1989). ATP mediates both activation and inhibition of K_{ATP} channel activity via cAMP-dependent protein kinase in insulin secreting cell lines. Journal of General Physiology 94(4): 693-717.

Rizzuto, R., Brini, M., Pizzo, P., Murgia, M. & Pozzan T. (1995). Chimeric green fluorescent protein as a tool for visualizing subcellular organelles in living cells. Current Biology 5(6): 635-42

Rodrigo, G.C. & Standen, N.B. (2005). ATP-Sensitive potassium channels. Current Pharmaceutical Design 11: 1-18.

Sakura, H., Trapp, S., Liss, B. & Ashcroft, F.M. (1999). Altered functional properties of K_{ATP} channel conferred by a novel splice variant of SUR1. Journal of Physiology 521 (Part 2): 337-350.

Sanada, S., Asanuma, H., Tsukamoto, O., Minamino, T., Node, K., Takashima, S., Fukushima, T., Ogai, A., Shinozaki, Y., Fujita, M., Hirata, A., Okuda, H., Shimokawa, H., Tomoike, H., Hori, M. & Kitakaze, M. (2004). Protein kinase A as another mediator of ischemic preconditioning independent of protein kinase C. Circulation 110(1): 51-57.

Sanchez, J.A., Gonoi, T., Inagaki, N., Katada, T. & Seino, S. (1998). Modulation of reconstituted ATP-sensitive K(+)-channels by GTP-binding proteins in a mammalian cell line. Journal of Physiology 507: 315-324.

Sanger, F., Niklen, S. & Coulson, A.R. (1977). DNA sequencing with chain terminating inhibitors. Proceddings National Academy of Science 74: 5463-5467.

Samaha, F.F., Heineman, F., Ince, J., Fleming, J. & Baraban, R.S. (1992). ATP-sensitive potassium channel is essential to maintain basal coronary vasculartone in vivo. American Journal of Physiology 262: C1220-C1227.

Sanada, S., Kitakaze, M., Asanuma, H., Harada, K., Ogita, H., Node, K., Takashima, S., Sakata, Y., Asakura, M., Shinozaki, Y., Mori, H., Kuzuya, T. & Hori, M. (2001). Role of mitochondrial and sarcolemmal K(ATP) channels in ischemic preconditioning of the canine heart. American Journal of Physiology 280: H256-H263.

Sasaki, N., Sato, T., Ohler, A., O'Rourke, B, & Marban, E. (2000). Activation of mitochondrial ATP-dependent potassium channels by nitric oxide. Circulation 101: 439-445.

Sato, T., Saito, T., Saegusa, N. & Nakaya, H. (2005). Mitochondrial Ca^{2+}-activated K^+ channels in cardiac myocytes: a mechanism of the cardioprotective effect and modulation by protein kinase A. Circulation 111: 198-203.

Sato, T., Sasaki, N., Seharaseyon, J. O'Rourke, B. & Marban, E. (2000). Selective pharmacological agents implicate mitochondrial but not sarcolemmal K(ATP) channels in ischemic cardioprotection. Ciculation 101: 2418-2423.

Sato, T., O'Rourke, B. & Marban, E. (1998). Modulation of mitochondrial ATP dependent K^+ channels by protein kinase C. Circulation Research 83: 110-114.

Schafer, G. Wegener, C. Portenhauser, R. & Bojanovski D. (1969). Diazoxide, an inhibitor of succinate oxidation. Biochemical Pharmacology 18: 2678-2681.

Schafer, G., Portenhauser, R. & Trolp, R. (1971). Inhibition of mitochondrial metabolism by the diabetogenic thiadiazine diazoxide. Biochemical Pharmacology 20: 1271-1280.

Seghers, V., Nakazaki, M., DeMayo, F., Aguilar-Bryan, L. & Bryan, J. (2000). Surl knockout mice. A model for K(ATP) channel-independent regulation of insulin secretion. Journal of Biological Chemistry 275(13): 9270-9277.

Seharaseyon, J., Ohler, A., Sasaki, N., Fraser, H., Sato, T., Johns, D. C., O'Rourke, B. & Marban, E. (2000). Molecular composition of mitochondrial ATP-sensitive potassium channels probed by viral Kir gene transfer. Journal of Molecular and Cellular Cardiology 32: 1923-1930.

Seino, S. & Miki, T. (2003a). Physiological and pathophysiological roles of ATP-sensitive K^+ channels. Progress in Biophysics and Molecular Biology 81: 133-176.

Seino, S. & Miki, T. (2003b). Gene targeting approach to clarification of ion channel function: Studies of Kir6.x null mice. Journal of Physiology 554(2): 295-300.

Shyng, S & Nichols, C.G. (1997). Octameric stoichiometry of the KATP channel complex. Journal of General Physiology 110(6): 655-664.

Shyng, S., Ferrigni, T. & Nichols, C.G. (1997). Control of rectification and gating of cloned KATP channels by Kir6.2 subunit. Journal of General Physiology 116 (5): 599-608.

Simkhovich, B.Z., Przyklenk, K. & Kloner, R.A. (1998). Role of protein kinase C as a cellular mediator of ischemic preconditioning: a critical review. Circulation Research 40(1): 9-22.

Singh, H., Hudman, D., Lawrence, C.L., Rainbow, R.D., Lodwick, D. & Norman, R.I. (2003). Distribution of Kir6.0 and SUR2 ATP-sensitive potassium channel subunits in isolated ventricular myocytes. Journal of Molecular Cell Cardiology 35(5): 445-459.

Stanley, C.A., Lieu, Y.K., Hsu, B.Y., Burlina, A.B., Greenberg, C.R., Hopwood, N.J., Perlman, K., Rich, B.H., Zammarchi, E. & Poncz, M. (1998). Hyperinsulinism and hyperammonemia in infants with regulatory mutations of the glutamate dehydrogenase gene. New England Journal of Medicine 338(19): 1352-1357.

Suzuki, M., Sasaki, N., Sato, T., Tamagawa, M., Miki, T., Seino, S., & Nakaya, H. (2003). Cardioprotective effects of diazoxide is mediated by activation of sarcolemmel but not mitochondrial ATP-sensitive potassium channels in mice. Circulation 107: 682-685.

Suzuki, M., Sasaki, N., Miki, T., Sakamoto, N., Ohmoto-Sekine, Y., Tamagawa, M., Seino, S., Marban, E., & Nakaya, H. (2002). Role of sarcolemmal K_{ATP} channels in cardioprotection against ischemia/reperfusion injury in mice. Journal of Clinical Investigation 109: 509-516.

Suzuki, M., Li, R. A., Miki, T., Uemura, H., Sakamoto, N., Ohmoto-Sekine, Y., Tamagawa, M., Ogura, T., Seino, S., Marban, E. & Nakaya, H. (2001). Functional roles of cardiac and vascular ATP-sensitive potassium channels clarified by Kir6.2-knockout mice. Circulation Research 88: 570-577.

Suzuki, M., Kotake, K., Fujikura, K., Inagaki, N., Suzuki, T., Gonoi, T., Seino, S., & Takata, K. (1997). Kir6.1: A possible subunit of ATP-sensitive K^+ channels in mitochondria. Biochimical and Biophysical Research Communications 241: 693-697.

Szewcyk, A. & Marban, E. (2003). Mitochondria: a new target for K^+ channel openers? Trends in Pharmacological Sciences 20(4): 157-161.

Szewczk, A., Czyz, A. & Nalecz, M.J. (1997). ATP-regulated potassium channel blocker, glybenclamide, uncouples mitochondria. Polish Journal of Pharmacology 49: 49-52.

Szewczk, A., Wojcik, G. & Nalecz, M.J. (1995). Potassium channel opener, RP 66471, induces membrane depolarization of rat liver mitochondria. Biochemical and Biophysical research communications 207: 126-132.

Tanaka, K. Ludwig, L.M. Kersten, J.R. Pagel, P.S. & Warltier, D.C. (2004). Mechanisms of cardioprotection by volatile anaesthetics. Anaesthesiology. 100(3): 707-721.

Taur, Y. & Frishman, W.H. (2005). The cardiac ryanodine receptor (RyR2) and its role in heart disease. Cardiology in Review 13(3): 142-146.

Thornton, J.D., Thornton, C.S. & Downey, J.M. (1993). Effect of adenosine receptor blockade: preventing protective preconditioning depends on time of initiation. American Journal of Physiology 265(2 Pt 2): H504-H508.

Thomas P.M., Ye, Y. & Lightner, E. (1996). Mutation of the pancreatic islet inward rectifier Kir6.2 also leads to familial persistent hyperinsulinaemic hypoglycemia of infancy. Human molecular Genetics 5 (11): 1809-1812.

Thomas, P.M., Cote, G.J., Wohlik, N., Haddad, B., Mathew, P.M., Rabl, W., Aguilar-Bryan, L., Gagel R.F. & Bryan, J. (1995). Mutations in the sulfonylurea receptor gene in familial persistent hyperinsulinemic hypoglycemia of infancy. Science 268: 426-429.

Tillman, T.S. & Cascio, M. (2003). Effects of membrane lipids on ion channel structure and function. Cell Biochemistry and Biophysics 38(2): 161-190.

Tinker, A., Jan, Y.N. & Jan, L.Y. (1996). Regions responsible for the assembly of inwardly rectifying potassium channels. Cell 87: 857-868.

Tinker, A. Lindsay, A.R. & Williams, A.J. (1992). A model for ionic conduction in the ryanodine receptor channel in sheep cardiac muscle sarcoplasmic reticulum. Journal of General Physiology 100: 495-517.

Tokuno, T., Muraki, K., Watanabe, M. & Imaizumi Y (1999). Effects of K^+ channel modulators on the relationship between action potential duration and Ca^{2+} transients in single ventricular myocytes of the guinea pig. Japan Journal of Pharmacology 80(3): 243-253.

Toller, W.G., Gross, E.R., Kersten, J.R., Pagel, P.S., Gross, G.J. & Warltier, D.C. (2000a). Sarcolemmal and mitochondrial adenosine triphosphate-dependent potassium channels: mechanism of desflurance-induced cardioprotection. Anesthesiology 92: 1731-1739.

Toller, W.G., Kerten, J.R., Gross, E.R. Pagel, P.S. & Warltier, D.C. (2000b). Isoflurane preconditions myocardium against infarction via activation of inhibitory guanine nucleotide binding proteins. Anesthesiology 92: 1400-1407.

Tong, H., Chen, W., London, R.E., Murphy, E. & Steenbergen, C. (2000). Preconditioning enhanced glucose uptake is mediated by p38 MAP kinase not by phosphatidylinositol 3-kinase. Journal of Biological Chemistry 275(16): 11981-11986.

Trube, G. & Heschler, J. (1984). Inward-rectifying channels in isolated patches of heart cell membrane: ATP-dependence and comparison with cell-attached patches. European Journal of Physiology (Pflugers Arch) 401: 178-184.

Tsien, R.Y. (1980). New calcium indicators and buffers with high selectively against magnesium and protons: designs, synthesis and properties of prototype structures. Biochemistry 19: 2396-2404.

Tsuchida, A., Miura, T., Tanno, M., Sakamoto, J., Miki, T., Kuno, A., Matsumoto, T., Ohnuma, Y., Ichikawa, Y. & Shimamoto, K. (2002). Infarct size limitation by nicorandil: roles of mitochondrial K(ATP) channels, sarcolemmal K(ATP) channels, and protein kinase C. Journal of the American College of Cardiology 40: 1523-1530.

Tucker, S. J., Gribble, F. M., Zhao, C., & Ashcroft, F. M. (1997). Truncation of Kir6.2 produces ATP-sensitive K^+ channels in the absence of the sulphonylurea receptor. Nature 387: 179-183.

Turrens, J.F. (1997). Superoxide production by the mitochondrial respiratory chain. Bioscience Reports 17: 30-38.

Ueda, K., Inagaki, N. & Seino, S. (1997). MgADP antagonism to Mg^{2+} independent ATP binding of the sulphonylurea receptor SUR1. Journal of Biological Chemistry 272: 22983-22986.

Vanden Hoek, T., Becker, L.B., Shao, Z.H., Li, C.Q. & Schumacker, P.T. (2000). Preconditioning in cardiomyocytes protects by attenuating oxidant stress at reperfusion. Circulation Research 86(5):541-548.

Vanden Hoek, T.L., Becker, L.B., Shao, Z., Li, C. & Schumacker, P.T. (1998). Reactive oxygen species released from mitochondria during brief hypoxia induce preconditioning in cardiomyocytes. Journal of Biological Chemistry 273(29):18092-18098.

Vuorinen, K.H., Ala-Rami, A., Yan, Y., Ingman, P. & Hassinen, I.E. (1995). Respiratory control in the heart during fatty acid oxidation. Energy state or substrate-level regulation by Ca^{2+}? Journal of Molecular Cardiology 27 (8): 1581-1591.

Walker, J.E. Saraste, M. Runwick, M.J. & Gay N.J. (1982). Distantly related sequences in the A and b subunits of ATP-synthase, myosin, kinases and other ATP-requiring enzymes and a common nucleotide binding fold. EMBO Journal 1: 945-951.

Wang, Y., Haider, H.K., Ahmad, N. & Ashraf, M. (2005). Mechanisms by which K(ATP) channel openers produce acute and delayed cardioprotection. Vascular Pharmacology 42(5-6): 253-64.

Wellman, G.C., Qualye, J.M. & Standen, N.B. (1998). ATP-sensitive K^+ channel activation by calcitonin gene-related peptide and protein kinase A in pig coronary arterial smooth muscle. Journal of Physiology 507(Pt 1): 117-129.

White, S. M., Constanin, P. E. & Claycomb, W. C. (2004). Cardiac physiology at the cellular level: use of cultured HL-1 cardiomyocytes for studies of cardiac muscle cell structure and function. American Journal of Physiology: Heart and Circulation Physiology 286: H823-H829.

Xu, W., Liu, Y., Wang, S., McDonald, T., Van Eyk, J.E., Sidor, A., & O'Rourke, B. (2002). Cytoprotective role of Ca^{2+}- activated K^+ channels in the cardiac inner mitochondrial membrane. Science 298(5595): 1029-1033.

Yamada, M., Isomoto, S., Matsumoto, S., Kondo, C., Shindo, T., Horio, Y. & Kurachi, Y. (1997). Sulphonylurea receptor 2B and Kir6.1 form a sulphonylurea-sensitive but ATP-insensitive K^+ channel. Journal of Physiology 499: 715-720.

Yao, Z., Tong, J., Tan, X., Li, C., Shao, Z., Kim, W.C., Vanden Hoek, T.L., Becker, L.B., Head, C.A. & Schumacker, P.T. (1999). Role of reactive oxygen species in acetylcholine-induced preconditioning in cardiomyocytes. American Journal of Physiology Heart and Circulatory Physiology 277: H2504-H2509.

Yao, Z. & Gross, G.J. (1994a). Effects of the K_{ATP} channel opener bimakalim on coronary blood flow, monophasic action potential duration, and infarct size in dogs. Circulation 4: 1769-1775.

Yao, Z. & Gross, G.J (1994b). Activation of ATP-sensitive potassium channels lowers threshold for ischaemic preconditioning in dogs. American Journal of Physiology 267: H1888-H1894.

Yarov-Yarovoy, V., Paucek, P., Jaburek, M., & Garlid, K.D. (1997). The nucleotide regulatory sites on the mitochondrial KATP channel face the cytosol. Biochimica et Biophysica Acta 1321(2): 128-136.

Yellon, D. M. & Downey, J. M. (2003). Preconditioning the myocardium: From cellular physiology to clinical cardiology. Physiological Reviews 83: 1113-1151.

Yokoshiki, H., Sunagawa, M., Seki, T. & Sperelakis, N. (1998). ATP-sensitive K^+ channels in pancreatic, cardiac and vascular smooth muscle cells. American Journal of Physiology 274: C25-C37.

Yoshida, K., Hirata, T., Akita, Y., Mizukami, Y., Yamaguchi, K., Sorimachi, Y., Ishihara, T. & Kawashiama, S. (1996). Translocation of protein kinase C-alpha, delta and epsilon isoforms in ischemic rat heart. Biochimica et Biophysica Acta 1317(1): 36-44.

Ytrehus, K., Liu, Y. & Downey, J.M. (1994). Preconditioning protects ischemic rabbit heart by protein kinase C activation. American Journal of Physiology 266: H1145–H1152.

Yuan, S.H., Sunahara, F.A. & Sen, A.K. (1987). Tumor-promoting phorbol esters inhibit cardiac functions and induce redistribution of protein kinase C in perfused beating rat heart. Circulation Research 61(3): 372-378.

Zhou, M., Tanaka, O., Sekiguchi, M., He, H.L., Yasuoka, Y., Itoh, H., Kawahara, K. & Abe, H. (2005). ATP-sensitive K^+ channel subunits on the mitochondrial and endoplasmic reticulum of rat cardiomyocytes. Journal of Histochemistry and Cytochemistry 53(12): 1491-1500.

Zerangue, N., Schwappach, B., Jan, Y. N., & Jan, L. Y. (1999). A new ER trafficking signal regulates the subunit stoichiometry of plasma membrane K(ATP) channels. Neuron 3: 537-548.

Zhang, C.L., Miki, T., Shibasaki, T., Yokokura, M., Atsunori, A. & Seino, S. (2006). Identification of characterisation of a novel member of the ATP-sensitive K^+ channel subunit, Kir6.3 in zebrafish. Physiological Genomics 24: 290-297.

Zhang, D.X., Chen, Y.F., Campbell, W.B., Zou, A.P., Gross, G.J., & Li, P.L. (2001). Characteristics and superoxide-induced activation of reconstituted myocardial mitochondrial ATP-sensitive potassium channels. Circulation Research 89: 1177-1183

Zucchi, R., Ronca, F. & Ronca-Testoni, S. (2001). Modulation of sarcoplasmic reticulum function: a new strategy in cardioprotection? Pharmacology and Therapeutics 89(1): 47-65.

Zweier, J.L., Flaherty, J.T. & Weisfeldt, M.L. (1987). Direct measurement of free radical generation following reperfusion of ischemic myocardium. Proceedings of the National Academy of Sciences USA 84: 1404–1407.